Laboratory Analysis of Restrengthening on Simulated Faults

by

Stephen L. Karner

Submitted to the Department of Earth, Atmospheric and Planetary Sciences

in partial fulfillment of the requirements for the degree of

Doctor of Philosophy

at the

MASSACHUSETTS INSTITUTE OF TECHNOLOGY

May 1999

[June 1999]

Author: _____

Department of Earth, Atmospheric and Planetary Sciences

May 1999

Certified by: _____

Chris Marone

Professor

Thesis Supervisor

Accepted by: _____

Ronald Prinn

Department Head

Laboratory Analysis of Restrengthening on Simulated Faults

by

Stephen L. Karner

Submitted to the Department of Earth, Atmospheric and Planetary Sciences
in partial fulfillment of the requirements for the degree of
Doctor of Philosophy

Prof. Chris Marone, Advisor

Abstract

Seismic data show that stress drop increases with the logarithm of earthquake recurrence interval (1-5 MPa per decade time). If stress drop is taken as a proxy for fault strength, then the data suggest that faults restrengthen during the quiescent period of the earthquake cycle. Seismic surveys across natural faults show that seismic velocities increase with elapsed time after an earthquake. These data also indicate that faults lithify and heal during the interseismic period. Hence, this thesis is centered on laboratory research designed to investigate fault restrengthening. Experiments have been conducted to study the factors that effect stick-slip behavior of bare rock surfaces, and healing of simulated fault gouge under a range of physico-chemical conditions.

We have performed experiments to investigate the repetitive stick-slip behavior of initially bare granite surfaces (nominal contact area 25 cm^2). The tests were conducted in a double-direct shear apparatus at room-temperature and humidity, and normal stress was held constant throughout. Shear was induced by controlling the velocity of the loading piston (0.5-300 μm/s). Data from individual stick-slip cycles show that shear stress increases quasi-linearly without considerable displacement across the sliding surface (stick), and sample failure (slip) is accompanied by a rapid stress drop. The amount of stress drop ranges from 0.1 to 3.1 MPa (or 4-49% of the failure strength). Prior to each instability samples exhibit yielding, consistent with previous laboratory observations of premonitory slip. Quasi-periodic instabilities occur repeatedly and we study the effect of loading rate and normal load on stress drop and recurrence interval (the time since the last event). We measure recurrence interval from the time when reloading begins after a slip event to the time that the next instability occurs. At a given loading rate, our data show a positive correlation between stress drop and recurrence interval, indicating healing rates of ~3.5 MPa per decade increase in recurrence time. However, the combined data from all velocities show a lower rate, suggesting an apparent healing rate of ~0.8 MPa per decade increase in recurrence time. We observe a similar velocity-dependent correlation between the peak shear stress prior to failure (a measure of the ultimate strength of the material) and recurrence interval. We find a consistent scaling between different loading rates when the stress drop data are compared to the loadpoint displacement prior to failure. The data for all

velocities delineate a single trend and show larger stress drops for greater amounts of pre-failure displacement. We also observe that pre-failure strength and post-slip stress levels converge with increasing velocities. Our data indicate that post-seismic minimum stress levels (hence, stress drop) depends on loading rate, and point to the existence of a critical velocity marking the transition between stick-slip and stable sliding.

Laboratory friction experiments are important for understanding fault restrengthening (healing) during the interseismic period. To date, attention has focused mainly on time and velocity dependence of friction observed for small perturbations about steady-state conditions. To investigate healing under a wider range of conditions, we vary shear load (τ_{hold}), hold time (t_h), loadpoint velocity (V), and initial gouge layer-thickness (T_0). We shear layers of granular quartz in a biaxial testing apparatus at room temperature and humidity. The experiments are similar to conventional slide-hold-slide (C-SHS) tests except that we rapidly reduce τ_{hold} prior to each hold. Healing ($\Delta\mu$) is defined as the difference between reload static friction and pre-hold sliding friction. For constant t_h (100s), T_0 (3 mm), and V (10 μm/s) we find a systematic increase in $\Delta\mu$ with decreasing τ_{hold} ($\Delta\mu$ ~0.007 for C-SHS tests, to ~0.05 for zero-load SHS tests, i.e. τ_{hold} =0). For zero-load SHS tests our data consistently show decreasing $\Delta\mu$ with increasing t_h (thus time-dependent weakening) and a slight decrease in $\Delta\mu$ with increasing V. We have also performed tests to study the effects of initial layer thickness (0.5-3 mm) on healing. For thicker layers, healing levels increase ($\Delta\mu$ ~0.03 to 0.05) and healing rates become more negative (-0.002 to -0.005 per decade t_h). Data from tests on thin layers (T_0 = 1 and 0.5 mm) show similar healing values and restrengthening rates. We compare our results to data from C-SHS tests on gouge, and zero-load SHS tests on initially bare rock surfaces. We have performed numerical simulations using existing rate and state friction laws. Healing predicted by the Dieterich law mimic the trend of our observed τ_{hold} dependence but not the magnitude. The Ruina law does not match the τ_{hold} dependence shown by our data. Neither law predict our observed healing rates. As applied to earthquakes, our data indicate that coseismic stress drop has an effect on fault healing rates.

We report on experiments to investigate the influence of healing duration and temperature on the strength and healing rate of simulated faults. Layers of μm-sized quartz powder were used to simulate granular fault gouge. Gouge layers were sheared within Sioux quartzite in a triaxial pressure vessel at elevated pressures (P_c=250 MPa), elevated temperatures (230-636 °C), and in the presence of water (P_{H20}=75 MPa). We performed "hold-slide" experiments in which samples were subjected to a period of healing under hydrostatic load, followed by shear deformation. Healing times ranged from a few hundred s to 10^5 s. To isolate the effects of lithification and temperature on friction, we ran two types of hold-slide experiments: 1) samples were subjected to healing and shear deformation at elevated temperature, and 2) following healing at elevated temperature, temperature was reduced prior to shear. We also ran slide-hold-slide experiments in which samples were healed under shear load at elevated temperature (636 °C). Experiments in which deformation was carried out at a lower temperature than healing show that both the static and sliding coefficient of friction increase with heal time. Samples healed and deformed at higher temperature showed lower peak strengths, and within the scatter of our

data, did not exhibit time dependent strengthening. These data are interpreted to result from enhanced lithification rates at elevated temperature. Samples healed under shear load exhibited a log-linear decrease in friction with hold time. Modeling using rate- and state-dependent friction laws indicates velocity strengthening behavior, with friction a-b values of 0.05 to 0.08. The data indicate that at high temperature, the effective state-evolution term b is negative. Moreover, the rate of frictional strengthening varies significantly for hydrostatic and non-hydrostatic load conditions. The measurements of healing are consistent with seismic estimates of fault healing rates, if stress drop is a fraction of the total shear stress and effective fault normal stress is 60 to 100 MPa.

Acknowledgments

There are so many people to whom I owe a debt of gratitude for their guidance and companionship throughout the course of my thesis research. To begin, I must express my heartfelt appreciation to my advisor, Prof. Chris Marone, who had the courage to accept me as his first graduate student. For me, Chris has been the perfect advisor. His keen interest in the Earth Sciences and his close interaction with students was quite agreeable to me (not to mention his interest in "all things Australian"). During my time at MIT, Chris has been an exceptionally supportive advisor at both the academic and personal levels. Whether it was to provide suggestions for courses, to guide my research directions, to expose the scientific community to our work, or to keep tabs on my well-being...Chris has been extremely attentive. Chris has always inspired me to pursue very interesting avenues of study, and his energetic approach easily spurred me on. There have also been several instances where his patience has amazed me. How Chris was able to put up with endless iterations of our publications, I will never know. I have also appreciated the many conversations that we have engaged in, which I always found to be quite encouraging. I am extremely grateful for all that I have learned from Chris over the years. He is certainly an excellent mentor. Combined with his bubbly personality, these traits have made it a pleasure to have worked with him throughout my doctoral studies. May we continue to have such a rapport in the years to come!

Prof. Brian Evans has also been instrumental in my academic development here at MIT. Brian's supervision of my experiments on the triaxial pressure vessel was exemplary. Brian showed enormous faith in me when I razed the older components of the triaxial vessel in order to upgrade the system. For myself, I am only glad that I was able to get everything back in working order (now, where did I put those nuts and bolts that were left over). I have often been astounded by Brian's insights and his ability to wrap his mind around any problem. Brian has an uncanny knack of asking those thought-provoking questions, and because of that I have enjoyed our discussions about my research. I am also very appreciative for his academic and moral support over the years, playing the role of surrogate advisor. Brian's dry sense of humor also appealed to my native upbringing, and could cheer me up when I needed it. It seems inappropriate to use only two words. However, Brian...thank you!

I would not have coped nearly as well if it were not for my family. I am utterly amazed at how my wife, Karen, has coped with me over the years. She has provided a endless supply of psychological and emotional support during my time at MIT, and has enriched my life considerably. Karen has always seen to it that my home-life was as harmonious as it could possible be. She eased the burdens on me by taking on the responsibilities that accompany daily living. To me, this degree belongs as much to Karen as it does me...after all, she certainly has earned it. To my extra-special wife, I now declare that you are no longer a "Ph.D. widow"! My parents, Lois and Garry, have also earned their fair share of this degree. They have always been there for me and Karen...whether we needed a shoulder to lean on, an ear to talk to, some time to relax, or emergency funds. They are

both very special people, and words cannot express how grateful I am to them. I must also thank other members of our immediate family for their high spirits and for keeping "my feet on the ground"...my brother, David; my sister, Paula; and Karen's parents, Joan and Ken. You are all wonderful.

Life in the laboratory would have been considerably more difficult if it were not for the "residents" of the 7th floor. Marie Sénat-André has been fantastic in taking care of all the administrative issues that developed. What would take me days to achieve, Marie can take care of in a matter of hours. I may not have learned the intricacies of MIT bureaucracy, but I *can* fix computer problems faster than Marie! Derek (Jock) Hirst has attended to the technical aspects of the laboratory with incredible prowess. Give the man a piece of paper with scribble on it, and he'll make you a masterpiece. Truly amazing! I am so glad to have had the opportunity to work with several other magnificent people. Gunter Siddiqi taught me the ropes on my arrival and became an extremely valuable friend. He was there whenever I needed someone to talk to, and his humor always cheered me up. After Gunter left, these roles were adopted by Karen Mair. Karen's chirpy nature and efficient work ethics have made research in the laboratory a lot of fun. I have also enjoyed interacting with the other fabulous people in the lab... Javier, Greg, Eliza, Uli, Kevin, Joerg, Wenlu, Gretchen, and Mike. Our discussions have been incredibly stimulating. You folks are great! I have also valued my discussions with Mike Blanpied and Nick Beeler, both at the U.S.G.S. in Menlo Park, California. Whether at conferences, via email, or as reviewers...they have stimulated my mind. I also want to thank Karen, Kevin, and Joerg for their help in the days leading up to my thesis defense and deposition. My gratitude also goes out to my committee members: Brian Evans, Kip Hodges, Tom Jordan, and Chris Scholz. I appreciate their willingness to participate in my thesis defense, and for the thought provoking discussions.

Finally, I must also express a hearty thanks to Kim and Chris Stoll, Mary Herndon and Chris Stipp, and Joe Duggan for their friendships. You all have contributed so much to Karen and my happiness here in the Boston metro area. I am also grateful to you all for providing Karen with a social outlet at times when I was otherwise pre-occupied.

Table of Contents

List of Figures

List of Tables

CHAPTER 1

Introduction

Results from friction studies have received widespread attention from researchers in material science, engineering, physics, soil mechanics, and Earth science. The data have proven useful for investigations of machinery wear, material fatigue, production of composite materials, granular flow, soil stability, and geologic deformation. For the Earth, friction experiments provide key information for understanding fault rheology and the earthquake process. Thus, a major goal of rock friction studies is to determine the physico-chemical factors that influence fault behavior.

Seismic data and geologic observations indicate that fault deformation occurs via a complex interplay between many factors. Fault slip can occur slowly as aseismic creep, or as sudden and discrete events in the form of earthquake rupture. Exactly how slip is accommodated may depend on factors such as the fault zone geology, fluid pressures, the presence of wear material (fault gouge), and fault roughness. Earthquakes are observed to occur in a variety of tectonic settings including those identified as active plate boundaries, intraplate regions, volcanic areas, and where mineralogic phase changes are possible. Seismic observations show that earthquakes can nucleate over a wide range of depths, and that rupture for a given earthquake may involve several faults. During earthquakes, rupture propagation and slip distribution can vary considerably owing to heterogeneities in material strength, fault morphology, and tectonic loading conditions.

Over geologic time, deformation of seismically active faults is accommodated by quasi-periodic recurrence of earthquakes. The magnitude of earthquakes and their frequency of occurrence depend on several factors including tectonic loading rates, state of stress in the Earth, geologic composition of the fault zone, and material properties (such as failure strength). The strength of a fault may relate to earthquake stress drop, which is determined

from seismic moment-magnitude data. Using these estimates and a knowledge of the time between events, it has been observed that the amount of stress drop is greater for earthquakes occurring after longer recurrence intervals. This implies that faults regain their strength with increasing time after an earthquake. Time-dependent restrengthening is also indicated from seismic surveys of faults on which earthquakes have occurred. These data show that seismic velocity increases with time after an earthquake, and may be due to the crack closure in the vicinity of the fault. These observations have provided the impetus for many laboratory studies of rock friction, and form the central motivation for the material presented in this thesis.

It has long been accepted that seismic deformation resembles stick-slip motion observed from laboratory friction studies. For both, intervals of relative quiescence are interrupted by episodes of rapid slip across a (quasi) planar surface. In the next section we present results from experiments on bare granite surfaces that exhibited stick-slip behavior. The tests were designed to determine the effect of loading conditions on the magnitude of slip instabilities and, thus, on fault restrengthening (or healing). The data are analyzed in the context of seismic observations, and indicate that the amount of stress drop during an instability increases with greater fault normal stress and slower loading rates. When cast in terms of recurrence interval, we observe two apparent healing rates that are each a function of normal stress and loading velocity. The data describe a single trend that correlates to the stiffness of the testing apparatus and sample assembly. Measurements of peak stress prior to slip, and post-slip minimum stress, show convergence as loading rate increases. Thus, the data indicate that stick-slip behavior may not be observed for loading rates above a critical velocity. These results may have implications for the earthquake process and the transition to dynamic rupture. For these tests, we did not observe significant accumulations of wear material (gouge) as slip progressed. It has been well documented that faults having greater amounts of accumulated slip also contain thick gouge zones (up to a kilometer thick for mature faults such as the San Andreas). Thus, we ask the questions:

how would the presence of gouge effect rates of fault restrengthening, and what factors would effect healing levels?

Results from previous laboratory friction studies show that the presence of gouge acts to stabilize slip. In this case, experiments can be performed to investigate the dependence of sliding friction on loading rate and time of stationary contact. For tests involving step changes in loading velocity, friction typically increases to a peak value and subsequently decays to a new sliding level. The initial response to the change in loading rate is referred to as the direct-effect, while the slower decay to stable sliding is termed the evolution effect. Of particular interest from these velocity-stepping tests is the difference between sliding friction levels before and after the loading perturbation. When sliding friction is lower for a step increase in loading rate the deforming sample exhibits velocity weakening (conversely for velocity strengthening). Results from these tests show a correlation between the occurrence of instabilities and the observed velocity dependence. Samples exhibiting velocity strengthening slide in a stable manner, while for velocity weakening instability may occur. Thus, the velocity dependence of sliding friction is indicative of stability regimes.

A different style of experiment also incorporates changes in the imposed loading rate. For these, the loading piston is advanced at an initial velocity. The piston is then stopped and its position is held fixed for a finite interval of time, after which loading restarts at the initial rate. These are referred to as slide-hold-slide tests. During holds, friction decays and samples continue to creep forward. When loading restarts, friction increases to a peak value and then decays back to the pre-hold stable sliding level. The peak friction achieved on reloading is considered to be a measure of static strength of the material. Thus, the effect of holding time on frictional strength can be investigated. Results from room-temperature experiments on simulated fault gouge show that static friction increases with the logarithm of holding time (thus, time-dependent strengthening). The rates of increase

in static friction are comparable to fault restrengthening rates observed from seismic stress drop data.

There has been a large volume of data published from velocity-stepping and slide-hold-slide tests conducted under a range of laboratory conditions. An outgrowth of these data has been the development of several constitutive relations that describe friction in terms of the imposed loading rate and a state variable. The state variable collectively describes the nature of the shear zone. The friction laws are formulated on the premise that it is the state variable that determines the evolution effect. In essence, the friction laws use a rate dependent term to describe the direct effect observed for a change in loading velocity, and a state-dependent evolution term that describes the gradual change of friction after the imposed velocity perturbation. Each of the laws that have been proposed incorporate the same description of the rate-dependent term. Thus, the constitutive relations differ only in their description of state evolution. The laws are able to model many aspects of laboratory data, and are increasingly being used in numerical simulations of seismic rupture. With application to laboratory data, these laws predict only subtle differences in frictional behavior. This makes it difficult to determine which of the laws is better suited for modeling fault deformation and seismic rupture. Hence, the goals of laboratory friction studies are to determine the rate and state-variable parameters used to model faults, and to test whether the friction laws are applicable to a broad range of conditions.

With this in mind, and to investigate a wider range of loading conditions, we present results from a suite of experiments on simulated fault gouge in Chapter 3. For this study we adopted the procedure used for slide-hold-slide (SHS) experiments. However, the experiments differ in that shear load was rapidly decreased prior to holding. The data from these tests is analyzed in a manner consistent with previous laboratory investigations of frictional restrengthening. The results indicate that fault strength varies systematically as a function of shear load, loading rate, hold time, and layer thickness. We observe that healing increases with lower shear stress levels for holds. For holds conducted at zero

shear load, we observe lower healing levels for longer hold times, for thinner gouge layers, and for faster loading rates. The most striking observation from our zero-load SHS tests is that of time-dependent weakening associated with positive compaction rates. This contrasts dramatically with the positive rates of healing and compaction observed from conventional SHS tests. Thus, our data indicate that the micro-mechanical processes operative under zero macroscopic shear load differ from those for the slide-hold-slide tests described above. The data are also analyzed using the existing friction laws. We find that the laws cannot describe all of the trends shown by the data. This indicates that the present formulations of the friction laws require modification.

To here, we have only considered factors that effect the strength of materials subjected to room-temperature and room-humidity conditions. These are not the conditions that exist within the Earth. Rocks are subjected to elevated temperatures and pressures at depth, and they contain interstitial fluids (such as water). Under such conditions, how would the strength of faults be effected? Previous results from hydrothermal experiments on geologic materials have shown that the presence of water promotes mineralogic reactions. The type of alteration product formed, and the extent to which diagenesis occurs, may have significant impact on the frictional behavior of faults. The formation of water-bearing clays may serve to lubricate faults, or may reduce permeability by clogging pore throats (thus, promoting fluid overpressure). On the other hand, the generation of silicate cements may act to lithify fault gouge and favor restrengthening. Temperature also plays a critical role in determining the alteration product formed by diagenesis of complex minerals. For example, at low temperatures feldspars alter primarily to clays while at elevated temperatures the formation of zeolites is favored. Laboratory data have also shown that temperature influences the velocity-dependence of frictional sliding. The data show a transition from velocity strengthening to weakening behavior at low temperatures, and a change back to velocity-strengthening for temperatures typical of mid-crustal depths.

Thus, a goal of laboratory research is to investigate rock friction for conditions likely to exist at depth within the Earth.

In Chapter 4 we present results from experiments designed to explore the influence of hydrothermal conditions on fault restrengthening, and to compare the data to predictions using the rate- and state-dependent friction laws. The tests were performed on layers of fine-grained quartz gouge sandwiched between quartzite forcing blocks. This quartz-water binary system avoids the complex reactions that can occur for other minerals. We performed experiments where samples were subjected to elevated temperatures under hydrothermal conditions (healing) for finite intervals of time (holds). Temperature was either held at the healing level for sample deformation, or was lowered prior to deformation. Data from samples deformed at lower temperatures show systematic variations in sample strength with hold time and healing temperature. Peak strength increases with hold time and healing temperature. Samples deformed at the elevated healing temperatures did not show significant time-dependence on the peak strength. Slide-hold-slide tests were also performed at the healing temperature to determine the effect of hold time. For these tests, we did not observe a frictional peak upon reloading after holds. This indicates that at high temperatures the friction coefficient describing the evolution effect is negative. Furthermore, the data show lower sliding friction levels after holds and that the steady-state sliding friction is lower for longer hold times. These results are interesting when compared to our data from room-temperature tests on quartz gouge (Chapter 3), as the data indicate time-dependent weakening for high temperatures.

Thus, this thesis is centered on results from laboratory experiments designed to investigate fault restrengthening. The studies show systematic effects on frictional healing as a function of loading rate, normal and shear load, time of stationary contact, the presence of gouge, gouge layer thickness, the presence of water, and temperature. The results have significance for modeling of the earthquake process and rupture dynamics.

CHAPTER 2

The effects of loading rate and normal stress on stick-slip behavior

Synopsis: Observations from natural faults and seismic data suggest that faults restrengthen during the quiescent period of the earthquake cycle. Seismic data show that stress drop increases with the logarithm of earthquake recurrence interval (1-5 MPa per decade time). We have performed experiments to investigate the repetitive stick-slip behavior of initially bare granite surfaces (nominal contact area 25 cm^2). The tests were conducted in a double-direct shear apparatus at room-temperature and humidity, and normal stress was held constant throughout. Shear was induced by controlling the velocity of the loading piston (0.5-300 μm/s). Data from individual stick-slip cycles show that shear stress increases quasi-linearly without considerable displacement across the sliding surface (stick), and sample failure (slip) is accompanied by a rapid stress drop. The amount of stress drop ranges from 0.1 to 3.1 MPa (or 4-49% of the failure strength). Prior to each instability samples exhibit yielding, consistent with previous laboratory observations of premonitory slip. Quasi-periodic instabilities occur repeatedly and we study the effect of loading rate and normal load on stress drop and recurrence interval (the time since the last event). We measure recurrence interval from the time when reloading begins after a slip event to the time that the next instability occurs. At a given loading rate, our data show a positive correlation between stress drop and recurrence interval, indicating healing rates of ~3.5 MPa per decade increase in recurrence time. However, the combined data from all velocities show a lower rate, suggesting an apparent healing rate of ~0.8 MPa per decade increase in recurrence time. We observe a similar velocity-dependent correlation between the peak shear stress prior to failure (a measure of the ultimate strength of the material) and recurrence interval. We find a consistent scaling between different loading rates when the

stress drop data are compared to the loadpoint displacement prior to failure. The data for all velocities delineate a single trend and show larger stress drops for greater amounts of pre-failure displacement. We also observe that pre-failure strength and post-slip stress levels converge with increasing velocities. Our data indicate that post-seismic minimum stress levels (hence, stress drop) depends on loading rate, and point to the existence of a critical velocity marking the transition between stick-slip and stable sliding.

2.1. Background

Since *Brace and Byerlee* [1966] documented the similarity between natural earthquakes and stick-slip motion observed from friction experiments, considerable attention has focused on determining the factors that effect dynamic instability and the characteristic behavior of repetitive stick-slip motion. These factors include loading rate, normal stress, elastic stiffness of the loading assembly, inertia, temperature, presence of water, presence of wear material (gouge), roughness of the sliding surface, time of stationary contact, and the composition and properties of the material being tested [e.g. *Rabinowicz*, 1958; *Byerlee*, 1967; *Byerlee and Brace*, 1968; *Brace*, 1972, 1974; *Dieterich*, 1972, 1978; *Scholz et al.*, 1972; *Ohnaka*, 1973; *Johnson*, 1981; *Johnson and Scholz*, 1976; *Beeler et al.*, 1989; *Wong and Zhao*, 1990; *Baumberger et al.*, 1994; *Heslot et al.*, 1994; *Berman et al.*, 1996; *Roy and Marone*, 1996; *Nasuno et al.*, 1998].

In their study of earthquakes that occurred on faults from many different tectonic regimes (excluding subduction events), *Kanamori and Allen* [1986] found that earthquakes with longer recurrence times had larger seismic moments, and thus larger coseismic stress drops. Their data show that the amount of stress drop increases by approximately 1-5 MPa per decade change in earthquake recurrence interval. In a similar study of repeating earthquakes occurring on a single patch of the Calaveras Fault (California, USA) *Marone et al.* [1995] determined that stress drop increased by ~3 MPa per decade change in recurrence

time. The observations from these studies suggest that faults restrengthen (or heal) during the interseismic period of the earthquake cycle. Interseismic healing of faults has also been indicated by acoustic velocity measurements across natural faults, and results from laboratory experiments that investigate time-dependent strengthening in rocks. From seismic surveys across a fault that participated in the 1992 Landers earthquake (the Johnson Valley Fault, California), *Li et al.* [1998] observed that the travel times of P- and S-waves decreased by 0.5-1.5% from 1994 to 1996. They interpreted this result in terms of increased crack closure in the vicinity of the fault, indicating that the Johnson Valley Fault was healing over the two-year time period. Their results correlate with observations from laboratory experiments that indicate geologic materials restrengthen with time of stationary contact, temperature, and changes in loading conditions [e.g. *Dieterich*, 1972, 1978; *Chester and Higgs*, 1992; *Fredrich and Evans*, 1992; *Linker and Dieterich*, 1992; *Marone and Kilgore*, 1993; *Beeler et al.*, 1994; *Karner et al.*, 1997; *Nakatani and Mochizuki*, 1996; *Marone*, 1998; *Nakatani*, 1998; *Karner and Marone*, 1998; *Richardson and Marone*, 1998]. However, it is important to understand other factors that may have an influence on stress drop amplitudes.

To investigate the repetitive stick-slip behavior of rock friction, and to study the effects of loading rate and normal stress on fault healing, we have performed experiments on initially bare granite surfaces at room-temperature and humidity. Our results are consistent with those of previous studies, and the data show systematic effects as a function of the variables that were tested. We observe that stress drop increases with greater normal stress and slower loading rates. We also observe two apparent rates of stress drop increase with recurrence interval that are described by the elastic stiffness of the loading assembly. As a function of increasing velocity, the maximum shear stress prior to instability and the post-slip minimum stress converge. This result is consistent with previous studies that have found a critical velocity marking a transition from stick-slip motion to stable sliding.

2.2. The experiments

To investigate stick-slip behavior of initially bare surfaces, we have conducted experiments in a hydraulically driven double-direct shear testing apparatus [described by *Karner and Marone*, 1998; *Mair and Marone*, 1998]. The tests were performed at room-temperature and humidity on Westerly granite. Samples consisted of a triple-block geometry where a central forcing block is sheared between two stationary side blocks. The samples were machined to produce side blocks having height/width/thickness dimensions of 5x5x3 cm^3, and the size of the central sliding block was 5x8x4 cm^3. Thus, the nominal contact area on which shear occurred was 5x5 cm^2. We controlled the roughness of the sliding surfaces by surface-grinding the samples with a #100 grinding wheel.

The parameters that were investigated include loading rate (0.5-300 μm/s) and normal stress (5 or 10 MPa). We monitored the applied forces and displacements at the loadpoint position and data were digitally acquired with sampling rates up to 1000 Hz. To investigate the effect of normal load, we sheared samples at normal stresses of 5 and 10 MPa. For each experiment, normal stress was controlled by using the loadforce signal in a servo-controlled feedback loop. Shear was induced by controlling the velocity of the loading piston, which was achieved via a computer generated command signal. To study the effects of velocity, we imposed step changes in loading rate throughout each test. Owing to the relatively large displacements possible in our testing apparatus (up to 3 cm for the samples used), several hundred stick-slip cycles occur for a given test. We have analyzed over 1500 individual stick-slip events that occurred during our experiments, and these data are discussed below.

2.3. Results

We show a portion of the shear load data for one experiment, including the initial load-up from zero shear stress, in Figure 2.1a. The data are presented as a function of time in order to better distinguish the stick-slip cycles for different loading rates. For this test,

normal stress was held constant throughout (10 MPa) and we varied the loadpoint velocity from 10 to 300 μm/s. For the conditions of our experiments, samples exhibited unstable sliding, with instabilities occurring repeatedly throughout the tests. It is evident from the data that the levels of minimum friction after an instability (τ_{min}) increase slightly with velocity, while the levels of peak friction prior to instability (τ_{max}) may decrease with faster loading rates. Thus, the data indicate that the difference between peak and minimum stress for instabilities (stress drop, $\Delta\tau$) are lower for faster loading rates. Analysis of a single instability shows characteristic stick-slip behavior observed by previous researchers [e.g. *Ohnaka*, 1973; *Engelder et al.*, 1975; *Engelder and Scholz*, 1976; *Johnson and Scholz*, 1976; *Shimamoto and Logan*, 1981; *Teufel and Logan*, 1978; *Wong and Zhao*, 1990]. In Figure 2.1b we plot an enlarged view of several stick-slip cycles. As loading of the sample proceeds, little motion occurs across the sliding surface (stick) and shear stress gradually increases quasi-linearly, indicating an elastic stiffness of the loading column of ~0.065 MPa/μm. As deformation continues, shear stress departs from the quasi-linear trend, consistent with yielding and previous observations of premonitory slip. Shear stress continues to increase until it reaches a peak value (τ_{max}) that corresponds to the traditional definition of static friction. During an instability, the slider block rapidly moves forward (slip) and shear stress decreases to a fraction of the peak strength (τ_{min}). We define stress drop ($\Delta\tau$) as the difference between the pre-slip peak stress (τ_{max}) and the post-slip minimum stress (τ_{min}). With subsequent loading, samples continue to slide in an unstable manner as can be seen by the repeated, quasi-periodic stick-slip cycles.

We have measured the peak and minimum stresses to determine stress drop ($\Delta\tau$), and we compare the data from each stick-slip cycle to the time since the previous slip event (Figure 2.2). Our data show systematic variations as a function of loading rate and normal stress. First, the data show larger τ_{max}, τ_{min}, and stress drops for greater normal stress, consistent with results from previous studies. Second, we observe small but systematic variations in τ_{max} and τ_{min} as a function of loading rate (Figures 2.2a-b). The data in Figure

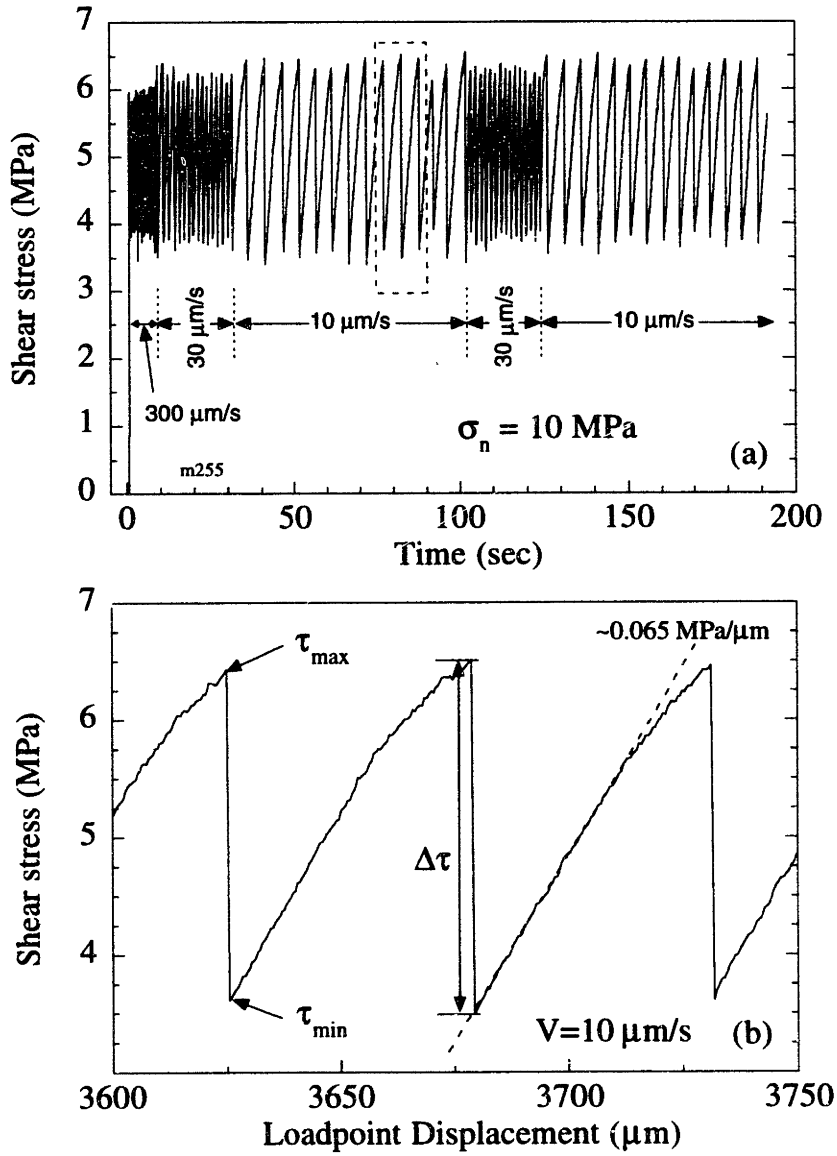

Figure 2.1. Shear stress data from a typical section of an experiment. **a).** Shear stress data plotted as a function of experiment time, for clarity, and includes the initial loading from zero shear stress. Loading velocity was stepped between 10, 30 and 300 μm/s. Data show repeated stick-slip events occurred during the test, and that the amplitude of the instabilities decreases with faster loading rates. **b).** An enlarged view of the section of data within the dashed box in (a), plotted against loadpoint displacement. Loading rate for this section was 10 μm/s. For each instability, data show an initial elastic loading with stiffness of ~0.065 MPa/μm (expressed as shear stress per unit loadpoint displacement). As loading continues, samples exhibit yielding prior to failure. During an instability, shear stress decreases rapidly to a fraction of the pre-failure peak stress level.

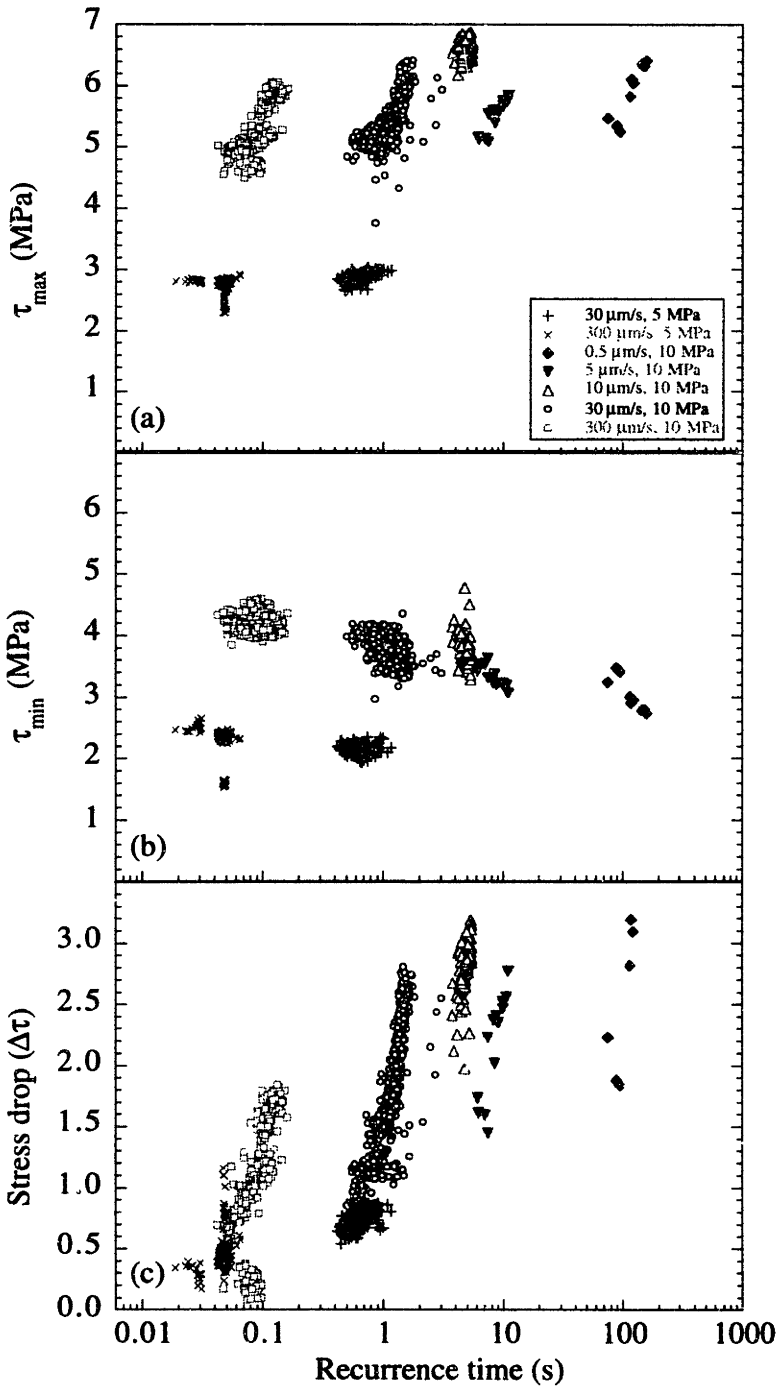

Figure 2.2. Shear stress data plotted as a function of time since the previous instability. Data are from tests with normal stress of 5 to 10 MPa, and loading rates of 0.5-300 µm/s. **a).** Maximum shear stress prior to instability. For a given loading rate, peak stress increases with recurrence interval. For a constant normal load (i.e. including all loading rates), data show little or no dependence of peak stress on recurrence interval. **b).** Minimum stress following a slip event. Data are for the same stick-slip events shown in (a). Minimum stress increases with normal load and loading rate. **c).** The difference between τ_{max} and τ_{min} are calculated as stress drop. Data are for the same events in (a). Stress drop increases with normal load. For a given loading rate, stress drop increases with recurrence interval by ~4MPa per decade time. For a given normal load, data show a different rate of stress drop increase (~1MPa per decade change in time).

2.2a show that the values of τ_{max} are nearly constant as a function of loading rate. We also observe that τ_{min} increases slightly for faster loading rates (Figure 2.2b). These observations are consistent with data from individual stick-slip cycles (as shown in Figure 2.1a). Third, our data indicate that stress drop increases as a function of recurrence interval, but the rate of increase depends on the imposed normal load and loading velocity (Figure 2.2c). For a given normal stress and loading rates from 0.5 to 300 μm/s, we observe that stress drop increases by ~0.75-1 MPa per decade change in recurrence interval. On the other hand, data for a given loading rate show that stress drop increases by ~3.5 to 4 MPa per decade change in time. Thus, the rates of increase in stress drop differ when viewed as a function of either loading rate or normal stress. This discrepancy has relevance for laboratory studies of frictional restrengthening and seismic studies of fault healing. We shall pursue this discussion further in the next section of this manuscript.

2.4. Discussion

The data from our experiments show two distinctly different rates at which stress drop increases with recurrence time, and these are dependent on loading velocity and normal stress (Figure 2.2c). In order to better understand this discrepancy, we have replotted the stress drop data against the loadpoint displacement leading up to each instability (Figure 2.3a). We observe that the stress drop data for all stick-slip cycles describe a single quasi-linear trend as a function of loadpoint displacement. As we are plotting loadpoint displacement and shear stress drop (essentially the change in loadforce), we infer that our data define an effective stiffness. For comparison to our data, we have used the loading stiffness obtained from individual stick-slip cycles (e.g. Figure 2.1b, k=0.065 MPa/μm) to calculate an idealized elastic loading curve (the line in Figure 2.3a). We find that our data plot to the right of this line indicating that the loading piston advanced further than it should have for perfectly elastic loading of the sample. Thus, the excess loading displacement indicates that samples experienced premonitory slip prior to instability, consistent with

observations of yielding (e.g. Figure 2.1b). To investigate the relationship between premonitory slip and stress drop we have removed the linear elastic loading trend from the data (Figure 2.3b). The detrended data do not show any discernible relationship between pre-failure slip and stress drop. Furthermore, the data show no obvious dependence of pre-failure slip on loading rate or normal stress.

In Figure 2.2 we plot shear stress data against recurrence interval in order to permit direct comparison to seismic observations. However, we recognize that neither of these variables are directly controlled in our experiments and, as such, this is reflected in data reproducibility. Furthermore, between each instability we do not control the state of the shearing surfaces. As the population and character (e.g. shape, strength) of contacting asperities is likely to differ for each stick-slip cycle, this would influence the mechanical behavior of the sample. A population of strong asperities would inhibit premonitory slip and samples would exhibit "perfect" elastic loading. On the other hand, premonitory slip owing to gradual deformation of contacting asperities (e.g. by brittle failure) would relieve some of the imposed shear load and result in longer recurrence intervals. This factor may be responsible for some of the data scatter we observe from measurements of τ_{max} (Figure 2.2a). During instabilities, the population and character of asperities (coupled with elastic interactions with the testing apparatus) may influence the level of dynamic overshoot before slip is arrested. This may account for some variability observed from measurements of τ_{min} (Figure 2.2b).

Our data show that stress drop decreases with faster loading rates (Figures 2.1 and 2.2), in agreement with results from previous studies of frictional instability for geologic materials [*Ohnaka*, 1973; *Engelder et al.*, 1975; *Engelder and Scholz*, 1976; *Johnson and Scholz*, 1976; *Shimamoto and Logan*, 1981; *Teufel and Logan*, 1978; *Wong and Zhao*, 1990], for metals [*Rabinowicz*, 1958], and for thin molecular films separating sheets of mica [*Berman et al.*, 1996]. As pointed out by *Cao and Aki* [1986], this correlation between loading rate and stress drop is important in the context of fault healing inferred

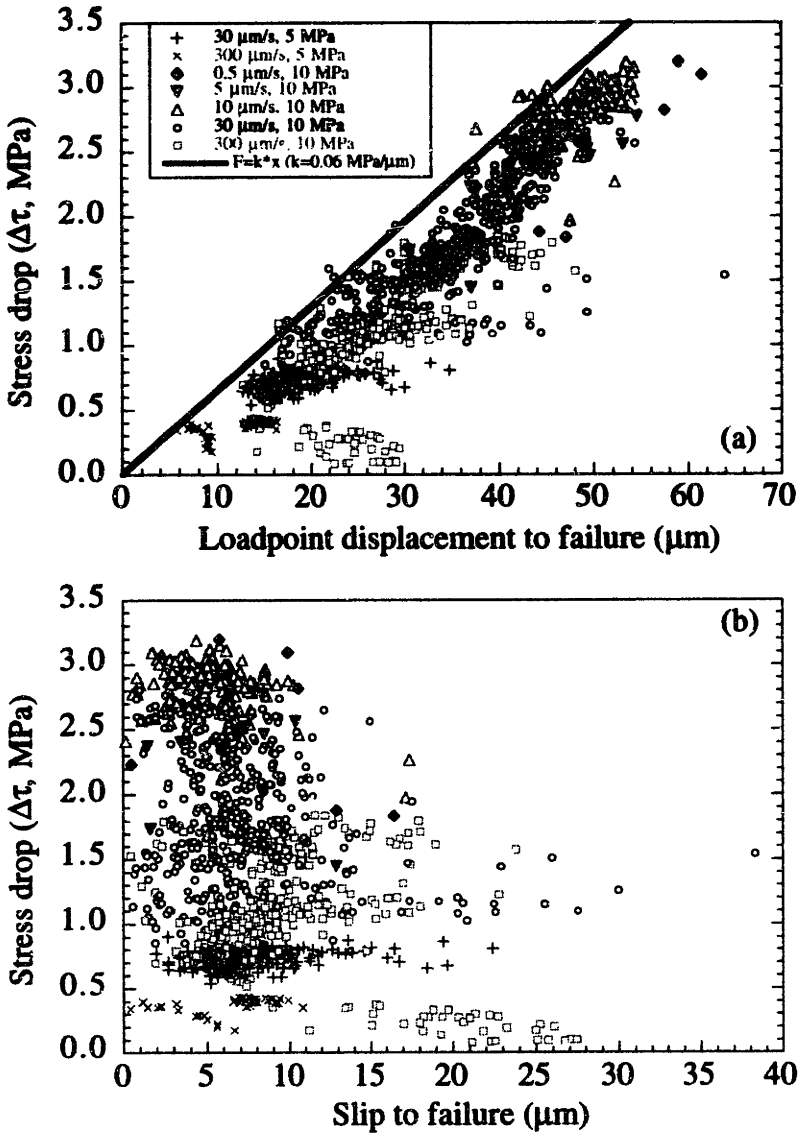

Figure 2.3. Stress drop data for the same events shown in Figure 2.2. **a).** Stress drop plotted as a function of loadpoint displacement prior to failure. The data from all events, including the different loading rates and normal loads, describe a single quasi-linear trend. For comparison to data, we show a line calculated for elastic loading of a material with stiffness of 0.065 MPa/µm. Our data hug the calculated loading curve, and show greater loadpoint displacements than for a perfectly elastic solid. **b).** Stress drop shown as a function of the calculated slip to failure. Data are for the same events shown in (a). Slip is calculated as the difference between observed loadpoint displacements, and the theoretical loading curve for a stiffness of 0.065 MPa/µm. There is no dependence of stress drop on pre-failure slip.

from observations of seismic data [*Kanamori and Allen* , 1986; *Marone et al.*, 1995]. By reanalyzing the data of *Kanamori and Allen* [1986] in terms of velocity, *Cao and Aki* [1986] found a systematic decrease of earthquake stress drop with increased tectonic loading rates. From this observation, they reasoned that the amount of stress drop may not depend completely on the effects of healing. Indeed, existing laboratory data do indicate that other factors effect stress drop levels, as observed from studies investigating the role of velocity (mentioned above), and the effects of stiffness [*Beeler et al.*, 1989; *Wong and Zhao*, 1990; *Baumberger et al.*, 1994; *Heslot et al.*, 1994; *Nasuno et al.*, 1998], among others. However, there have been many studies on geologic materials that indicate time of stationary contact, temperature, fluid-rock interactions, and variations in loadforce conditions can lead to significant restrengthening of faults [e.g. *Dieterich*, 1972, 1978; *Chester and Higgs*, 1992; *Linker and Dieterich*, 1992; *Fredrich and Evans*, 1992; *Marone and Kilgore*, 1993; *Beeler et al.*, 1994; *Karner et al.*, 1997; *Nakatani and Mochizuki*, 1996; *Marone*, 1998; *Nakatani*, 1998; *Karner and Marone*, 1998; *Richardson and Marone*, 1998]. Thus, it is important to separate the effects of healing from other parameters that may systematically effect the frictional behavior of faults. As such, we shall now investigate the velocity-dependence of our data further.

In a study of thin molecular films between mica surfaces for a wide range of loading rates, *Berman et al.* [1996] observed repetitive stick-slip motion that decreased in amplitude with increasing velocity. For increasing velocity, they observed that static friction levels decreased in conjunction with an increase in post-slip minimum friction. Their data define a critical velocity (V_c) above which stick-slip motion was replaced by continuous stable sliding (V_c ~ 7 to 8 μm/s for their tests). A similar critical velocity has been observed from dry friction experiments on bristol board and also on paper [*Baumberger et al.*, 1994; *Heslot et al.*, 1994]. These researchers observed a transition from stick-slip to stable sliding that depends on loading rate and stiffness. Their data showed that stable sliding is promoted by both increased stiffness and increased velocity. In the vicinity of the

bifurcation of slip behavior, they also found that frictional characteristics differed significantly for low and high loading rates. From these observations, they identified that the low velocity regime was creep dominated and could be defined by a characteristic length scale, while the high velocity regime was inertia dominated and has a characteristic time scale. Hence, the combined results of *Berman et al.* [1996], *Baumberger et al.* [1994], and *Heslot et al.* [1994] indicate that stiffness and loading rate can effect the behavior of stick-slip motion and the transition to stable sliding.

To remain consistent with the study of *Berman et al.* [1996], we show in Figure 2.4 the levels of peak stress (τ_{max}) and post-slip minimum stress (τ_{min}) as a function of loading rate, and for a constant normal stress of 10 MPa. For clarity, we have plotted the mean values and standard deviations of τ_{max} and τ_{min} for each velocity. The data show that τ_{max} is decreasing with loading rate, while τ_{min} is nearly constant (or may be increasing slightly) with velocity. Hence, τ_{max} and τ_{min} converge as loading rate increases, consistent with the observations of *Berman et al.* [1996]. For the conditions of our experiments, and in light of the results of *Berman et al.* [1996], *Baumberger et al.* [1994], and *Heslot et al.* [1994], our data suggest that a critical velocity exists above which stable sliding may be achieved. Hence, there may exist a Hopf bifurcation between unstable and stable sliding at a fast loading rate, similar to those reported previously [see *Scholz*, 1998, for a review]. Given that this critical velocity would be large (>1000 μm/s), we suggest that the transition from stick-slip to stable sliding would occur in an inertia-dominated regime. We are presently considering ways to investigate whether such a critical velocity exists for our samples. However, we first need to carefully calibrate inertial effects that may be introduced by the testing apparatus.

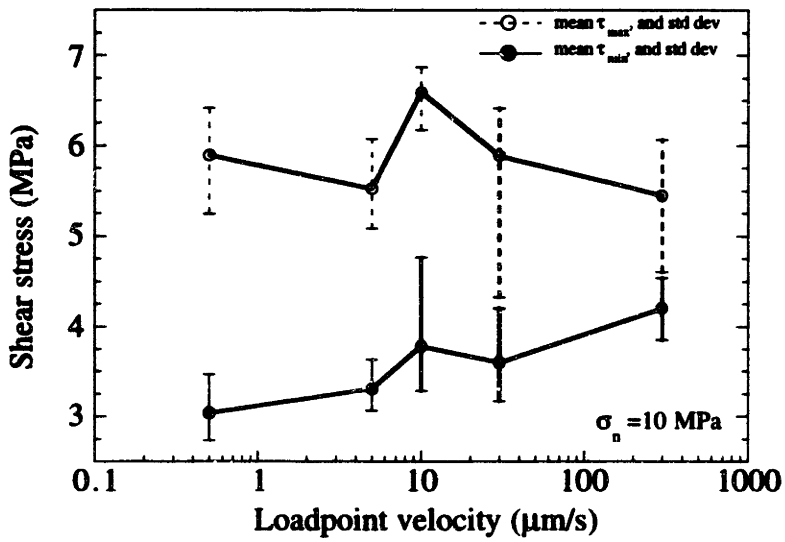

Figure 2.4. Peak and minimum stress levels shown as a function of loading rate. For clarity, we show the mean value of shear stress data for each velocity, plus/minus one standard deviation. For faster velocities, τ_{min} increases and τ_{max} is nearly constant (or may decrease). Thus, peak and minimum stress levels converge as velocity increases.

2.5. Summary

To study stick-slip behavior of bare rock surfaces, we have conducted experiments on Westerly granite in a biaxial apparatus at room-temperature and humidity. We have analyzed over 1500 instabilities, and the data show several interesting features. We observe that stress drop amplitude increases with greater normal stress, consistent with previous studies. We also observe two apparent rates of restrengthening. For a single loading rate, stress drop increases by ~4 MPa per decade time. The combined data from all velocities show stress drop increases by ~1 MPa per decade time. For the conditions of our tests, this discrepancy in restrengthening rates can be characterized in terms of stiffness of the loading column. After removing elastic effects, we do not observe any significant dependence of stress drop on premonitory slip. Measurements of pre-failure peak stress, and post-slip minimum stress, show convergence with faster loading rates. This is consistent with previous studies that identify a critical velocity marking a transition between stick-slip and stable sliding, and that this transition lies in an inertia-dominated regime.

[1]CHAPTER 3

Frictional restrengthening in simulated fault gouge for large shear load perturbations

Synopsis: Laboratory friction experiments are important for understanding fault restrengthening (healing) during the interseismic period. To date, attention has focused mainly on time and velocity dependence of friction observed for small perturbations about steady-state conditions. To investigate healing under a wider range of conditions, we vary shear load (τ_{hold}), hold time (t_h), loadpoint velocity (V), and initial gouge layer-thickness (T_0). We shear layers of granular quartz in a biaxial testing apparatus at room temperature and humidity. The experiments are similar to conventional slide-hold-slide (C-SHS) tests except that we rapidly reduce τ_{hold} prior to each hold. Healing ($\Delta\mu$) is defined as the difference between reload static friction and pre-hold sliding friction. For constant t_h (100s), T_0 (3 mm), and V (10 μm/s) we find a systematic increase in $\Delta\mu$ with decreasing τ_{hold} ($\Delta\mu$ ~0.007 for C-SHS tests, to ~0.05 for zero-load SHS tests, i.e. τ_{hold} =0). For zero-load SHS tests our data consistently show decreasing $\Delta\mu$ with increasing t_h (thus time-dependent weakening) and a slight decrease in $\Delta\mu$ with increasing V. We have also performed tests to study the effects of initial layer thickness (0.5-3 mm) on healing. For thicker layers, healing levels increase ($\Delta\mu$ ~0.03 to 0.05) and healing rates become more negative (-0.002 to -0.005 per decade t_h). Data from tests on thin layers (T_0 = 1 and 0.5 mm) show similar healing values and restrengthening rates. We compare our results to data from C-SHS tests on gouge, and zero-load SHS tests on initially bare rock surfaces. We have performed numerical simulations using existing rate and state friction laws. Healing predicted by the Dieterich law mimic the trend of our observed τ_{hold} dependence but

[1] A portion of this chapter was published in *Geophys. Res. Lett.*, 25, 4561-4564, 1998.

not the magnitude. The Ruina law does not match the τ_{hold} dependence shown by our data. Neither law predict our observed healing rates. As applied to earthquakes, our data indicate that coseismic stress drop has an effect on fault healing rates.

3.1. Background

Investigations of rupture processes that operate during instability, and the processes leading to restrengthening of shear zones, are key for understanding fault deformation during the earthquake cycle. To date, laboratory experiments on simulated faults have focused mainly on the velocity- and time-dependent behavior of rock friction [e.g. *Dieterich*, 1972, 1978; *Lockner et al.*, 1986; *Marone et al.*, 1990; *Blanpied et al.*, 1991; *Chester and Higgs*, 1992; *Fredrich and Evans*, 1992; *Beeler et al.*, 1994; *Karner et al.*, 1997; *Marone*, 1998a]. These experiments typically involve small deviations from the loading conditions required to maintain steady-state sliding (e.g. velocity-stepping and slide-hold-slide tests). However, in the spatio-temporal vicinity of earthquake rupture the loading variations on a fault may be large and complex. This may have significant bearing on the particular formulation of the friction laws used to model fault behavior and earthquake rupture dynamics.

Several empirically determined friction laws have emerged from the results of laboratory studies and their application to fault mechanics [e.g. *Dieterich*, 1979; *Ruina*, 1983; *Chester and Higgs*, 1992; *Perrin et al.*, 1995; *Segall and Rice*, 1995; *Sleep*, 1995; *Scholz*, 1998]. Of these laws, the slip-rate and state-variable formulations proposed by *Dieterich* [1979] and *Ruina* [1983] have received the most attention. The laws share certain features in that they describe second-order friction variations in terms of slip, loading rate, and the state of the frictional shear zone. However, these laws predict different scaling relations and dynamic behavior in earthquake rupture models [*Rice and Ben-Zion*, 1996]. Furthermore, the laws have been derived from laboratory experiments involving velocity-stepping and

slide-hold-slide tests, both of which impose only small perturbations in loading conditions. Thus, a key issue for laboratory studies of rock friction is that of validating the friction laws for a wider range of conditions.

Several researchers have conducted experiments designed to broaden the range of conditions for analyzing rock friction, and for developing a more fundamental understanding of shear along multi-contact interfaces and within granular material [e.g. *Heslot et al.*, 1994; *Nasuno et al.*, 1997, 1998; *Baumberger et al.*, 1999; *Berthoud et al.*, 1999; *Géminard et al.*, 1999]. In rock mechanics, these studies have concentrated on the frictional effects associated with variations in normal load [*Linker and Dieterich*, 1992; *Richardson and Marone*, 1998], shear load [*Nakatani and Mochizuki*, 1996; *Nakatani*, 1998; *Olsen et al.*, 1998; *Karner and Marone*, 1998], and fast loading velocities [*Mair and Marone*, 1998]. The results from these studies indicate that friction of geologic materials is more complicated than suggested by observations from velocity-stepping and slide-hold-slide tests. Furthermore, data from studies involving large perturbations in normal or shear load cannot be completely described by the existing friction laws [*Karner and Marone*, 1998].

To further distinguish between the friction laws, and to extend the range of conditions studied, we have performed experiments on simulated fault gouge involving large perturbations of shear load. We employed a modified form of the slide-hold-slide (SHS) technique useful for studies of frictional restrengthening (healing). For these tests, shear load was rapidly changed from the pre-hold sliding level (τ_{slide}) to a reduced level for holds (τ_{hold}). We study healing as a function of shear load (τ_{slide}/τ_{hold} was varied from 0-1), hold time (10-10000 s), loading rate (10-300 μm/s), and initial gouge layer thickness (0.5-3 mm). Our data show systematic variations in healing and healing rates as a function of these variables. We analyze our data using the time (Dieterich) and slip (Ruina) dependent friction laws. Our data are not well described by these laws, indicating that state evolution within fault gouge may depend on parameters other than loading rate and a critical slip

distance (e.g. porosity, extent of consolidation, particle size, particle size distribution). To explain the observations from our data, we adopt a model in which the mechanical behavior of fault gouge is effected by the generation and destruction of load-bearing particulate chains.

3.1.1. Previous investigations of time-dependent healing

To investigate fault restrengthening, *Dieterich* [1972, 1978] conducted experiments in which samples were sheared at a given loadpoint velocity followed by "holds" initiated by setting the loading velocity to zero (slide-hold-slide experiments). *Dieterich's* [1972] results, and those of subsequent researchers [e.g. *Chester and Higgs*, 1992; *Beeler et al.*, 1994; *Karner et al.*, 1997; *Marone*, 1998a] show that the frictional strength of simulated faults depends on the time of "quasi"-stationary contact. For initially bare sliding surfaces, *Dieterich* [1972] proposed that frictional restrengthening arises from a time-dependent increase in the real area of contact between the sliding surfaces. Studies of friction in simulated fault gouge show that time-dependent strengthening is accompanied by an increase in gouge compaction with time [e.g. *Marone*, 1998a]. This indicates that time-dependent consolidation of a granular material leads to an increase in frictional strength, in a manner similar to that observed for initially bare surfaces.

For convenience and to assist in this summary of results from previous studies, we show data from conventional slide-hold-slide tests (C-SHS) in Figures 3.1 and 3.2. All experiments were performed in a double-direct shear testing apparatus at room temperature and humidity. During each test the loading forces and loadpoint displacements were monitored. Measurements of layer thickness, slip across a gouge layer, and the calculated frictional response for a representative hold-cycle are shown in Figure 3.1. During a hold, friction decays due to creep and elastic interaction with the loading apparatus (Figure 3.1a). This decrease in friction and sample creep during holds is accompanied by continued thinning of the gouge layer (Figure 3.1b). When loading resumes after a hold, gouge

layers dilate and friction increases to a maximum value corresponding to the traditional definition of "static" friction. The difference between static friction and pre-hold sliding friction is taken as a measure of restrengthening ($\Delta\mu$, which we refer to as healing).

Healing and layer thickness data for a series of SHS tests are shown in Figure 3.2 [after *Marone*, 1998a]. For simulated fault gouge, $\Delta\mu$ is in the range 0.002-0.02 for hold times (t_h) of 10-100s (Figure 3.2a-b). The observed positive healing rates (defined as $\beta=\Delta\mu/\Delta\log_{10} t_h$) are typically between 0.005-0.02 (Figure 3.2b). Layer compaction for holds is also observed to increase with log t_h (Figure 3.2c). The observed gouge layer thinning, coupled with continued sample creep during holds, indicates that shear enhanced compaction may be the mechanism responsible for healing and time-dependent restrengthening of fault gouge. However, healing in these tests involves both time- and slip-dependent processes, making it difficult to separate their effects (see *Beeler et al.*, 1994, for a novel way to achieve this for C-SHS tests). Thus, it is important to conduct laboratory experiments designed to isolate the effects of time and slip on the evolution of friction.

3.1.2. Existing rate- and state- constitutive laws

An outgrowth of laboratory friction studies has been the development of several constitutive laws that describe friction evolution in terms of loading rate and the state of the sliding surface. Of the friction laws that have been proposed, the rate- and state-dependent friction laws of *Dieterich* [1979] and *Ruina* [1983] have been most frequently applied to analysis of rock friction data and to modeling of fault behavior, and are receiving the attention of researchers from other disciplines [e.g. *Géminard et al.*, 1998; *Baumberger et al.*, 1999; *Berthoud et al.*, 1999]. Hence, we shall concentrate here on the discussion of the above-mentioned formulations of the friction laws. The laws are similar in that they describe the time and velocity dependence of friction by the relation:

$$\mu = \mu_0 + a\ln\left(\frac{V}{V_0}\right) + b\ln\left(\frac{V_0\theta}{D_c}\right) \qquad (3.1)$$

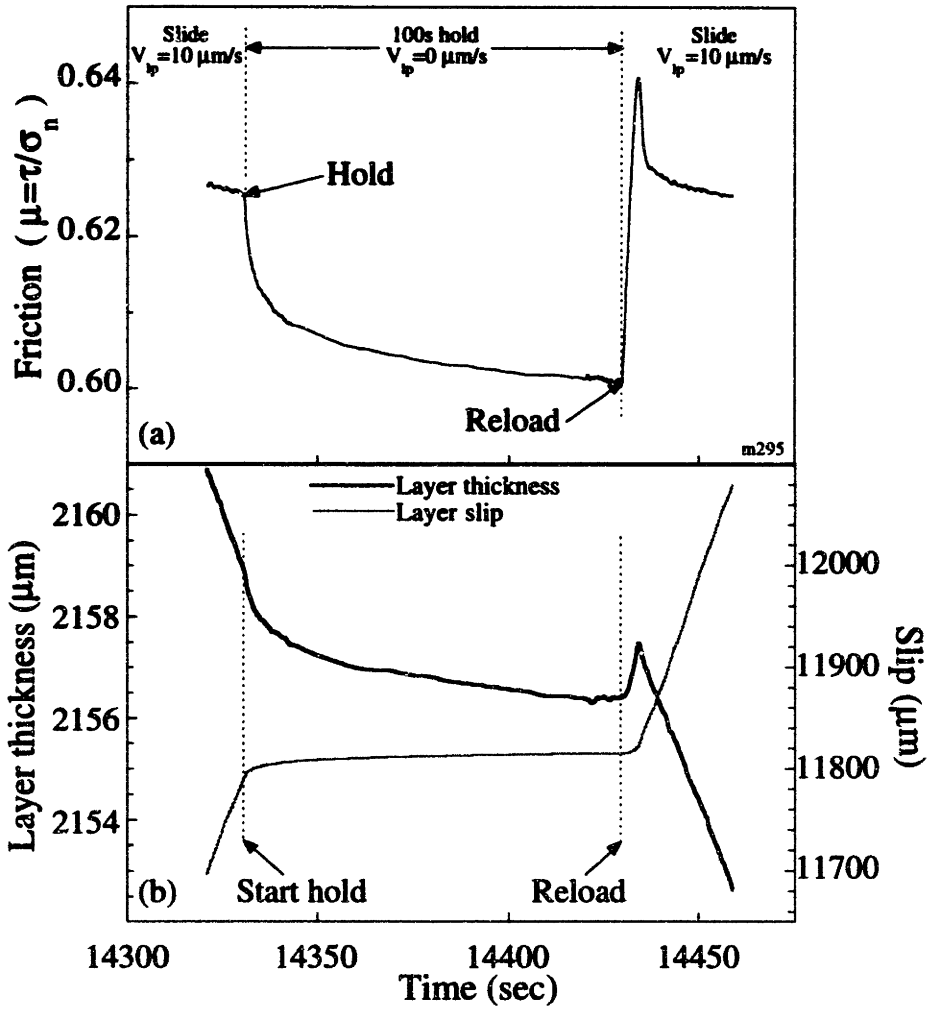

Figure 3.1. Data for a single hold cycle from a conventional slide-hold-slide test. **a).** Friction data for the hold. From the onset of holds, friction decays from steady-state sliding levels. On reload, friction increases to a maximum value (static friction) followed by return to stable sliding levels. Healing is defined as the difference between reload static friction and the pre-hold sliding friction. **b).** Layer thickness and slip measured directly across the gouge layer. Data are from the same hold shown in (a). For stable sliding, gouge layers thin with displacement, and sample slip equals the imposed loading velocity. During holds, layer slip continues and slip rate decays with time. Layers compact during holds. On reload, layers dilate, and slip-rate increases.

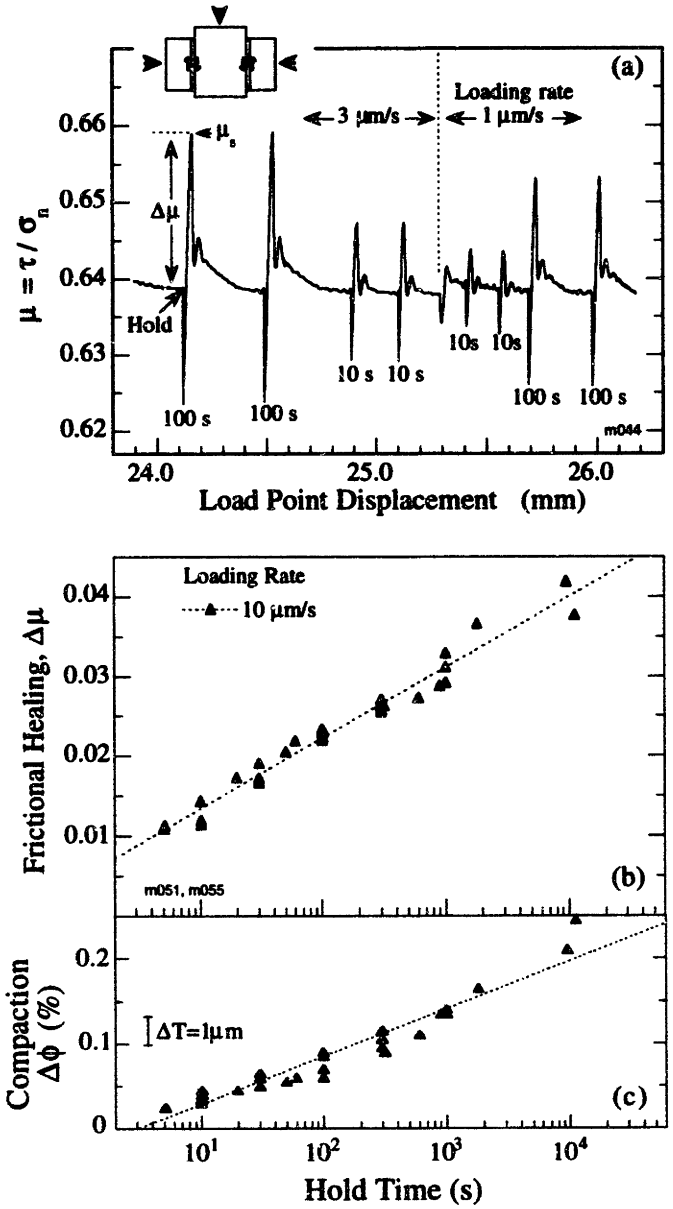

Figure 3.2. Data from fixed-load point slide-hold-slide experiments described by *Marone* [1998a]. **a).** Upper inset shows sample geometry for biaxial tests where two servo-controlled hydraulic pistons provide normal and shear load, and sample slip occurs in two layers. Friction data are plotted against load point displacement. During a hold, load point position is held constant. **b).** Healing data for loading velocity of 10 μm/s. Data indicate that $\Delta\mu$ is a function of hold time. **c).** The amount of compaction that occurs during a hold, for one layer of the double shear sample, is plotted versus hold time. Change in porosity during each hold is calculated from the measured change in layer thickness, ΔT, and nominal contact area, normalized by the initial volume of the gouge layer. Data are for the same experiments shown in (b), and show that compaction increases with hold time.

Here μ_0 represents steady-state friction for slip at a reference velocity V_0, V is sliding velocity, D_c is a critical slip distance, θ is a state variable, and a and b are scaling constants. However, the similarity between these laws does not extend to their description of evolution of the state variable. The evolution law of *Dieterich* [1979]:

$$\frac{d\theta}{dt} = 1 - \frac{V\theta}{D_c} \tag{3.2}$$

permits state evolution for frictional surfaces held in true stationary contact (i.e. V=0). However, the evolution law of *Ruina* [1983]:

$$\frac{d\theta}{dt} = -\frac{V\theta}{D_c} \ln\left(\frac{V\theta}{D_c}\right) \tag{3.3}$$

does not predict state evolution for true stationary contact, as this law requires some finite slip for state to evolve. The formulations shown in (3.2) and (3.3) are often referred to as the time (or slowness) and the slip evolution laws, respectively. However, we shall refer to them as the Dieterich and Ruina laws. In applying these laws to laboratory data, equations 3.1-3.3 must be coupled with a relation describing elastic interaction with the loading apparatus: $d\mu/dt = k\,(V_0\text{-}V)$, where V_0 is the loading velocity prior to a hold, and k is the apparatus stiffness divided by the normal stress (k=10^{-3} μm^{-1} for our apparatus, which shall be described further in the following section).

Both the Dieterich and Ruina laws are capable of describing a variety of friction observations from laboratory experiments, despite their different descriptions of state evolution. Considerable effort has been expended to distinguish between these friction laws, and to determine which state evolution law is more appropriate for modeling seismic and geologic observations of faults [see *Marone*, 1998b, for a review]. However, the

differences in frictional behavior predicted by these laws is often subtle and are not satisfactorily resolved by available data.

3.2. The experiments

3.2.1. Sample description and testing apparatus

Our tests were conducted on samples having a triple block geometry (Figure 3.3). Sample slip is accommodated within two zones for which shear and normal tractions are controlled directly. Gouge layers consisted of granular quartz obtained from the US Silica Company with an initial grain size of 50-150 μm (110 μm rms grain size). The layers were sandwiched between either steel or granite forcing blocks having a nominal contact dimensions of 10x10 cm^2. To ensure that slip was distributed throughout the layers, we machine evenly-spaced grooves on the shear surfaces of the steel forcing blocks, and the granite forcing blocks were roughened by sand-blasting with a 60-grit abrasive. To minimize gouge loss along the unconfined lateral edges of the layers, we attach lubricated plates to the stationary side blocks of each sample.

The testing apparatus consists of two hydraulically driven loading pistons that apply normal and shear loads directly to the sample. Loading tractions were electronically controlled using servo-controlled feedback loops. Gouge layers were sheared under loadpoint displacement control with 0.1 μm resolution. Throughout each test, normal force was maintained constant (25 MPa for steel forcing blocks, 15 MPa for granite) with a control resolution better than 0.1 kN. Shear and normal forces and displacements were monitored at the loadpoint position, and data were sampled at rates up to 1000 Hz. In a few experiments, we monitored gouge layer slip and thickness variations directly using displacement transducers mounted on the sides of the sample.

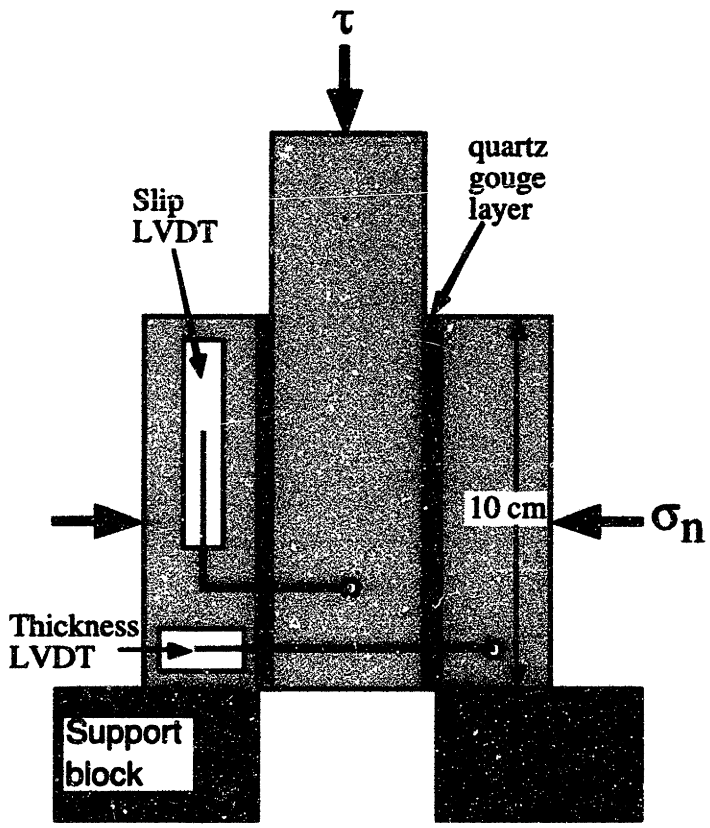

Figure 3.3. Schematic illustration of the sample assembly for the double-direct shear testing apparatus. Quartz gouge layers are situated between solid forcing blocks. The outer forcing blocks are supported from underneath, while the central block is permitted to slide freely between them. Normal force is applied perpendicular to the side blocks, and shear of the gouge layers is induced by loading the center block. In a few experiments we used displacement transducers mounted on the sample to directly measure sample slip and layer thickness.

3.2.3. Experiment procedure

For our experiments, we employed a technique similar to the slide-hold-slide tests described previously (section 3.1.1). Gouge layers were sheared at a reference loading rate that was interrupted for specified periods of time (holds). Our experiments differ from conventional slide-hold-slide (C-SHS) tests in that shear load was rapidly reduced prior to initiating holds [e.g. *Nakatani and Mochizuki*, 1996; *Karner and Marone*, 1998; *Nakatani*, 1998; *Olsen et al.*, 1998; see Figures 3.4 and 3.5]. The reduction in shear load was

achieved by retracting the loading piston at a rate of 300 μm/s. Complete removal of shear load occurred within 2.5-3 sec for the stiffness ($k=10^{-3}$), loading conditions, and sample dimensions of our tests. Holds were timed from the point when the reduced shear load (τ_{hold}) was reached, to the time that reloading began.

Data from numerous trial experiments indicated that the frictional response following hold cycles was strongly dependent on sample slip history. Thus, the data reported here were obtained from experiments with identical slip histories, including the initial load-up sequence to ~10 mm displacement (as seen in Figure 3.4). Samples were initially loaded at a rate of 300 μm/s, followed by a series of velocity-steps (30-300 μm/s) and a loading cycle at ~6 mm displacement (unload and reload rate of 300 μm/s). After the loading cycle, we imposed further changes in loading rate that gradually stepped towards the sliding velocity used for the remainder of the test. The latter set of velocity-steps allow for determination of the friction parameters (a, b, D_c) prior to holds, while the loading cycle conditions the gouge layers and sample assembly. Following the load-up sequence, hold cycles were implemented at regulated slip intervals. Holds were imposed as consecutive pairs, and three sets of hold pairs were implemented within the maximum displacement possible for our samples (30-35 mm). For zero-load SHS tests, identical hold times were used for the first and last hold pairs and we varied the hold time for the middle set. In this way, we can investigate the time-dependence of frictional restrengthening for the zero-load SHS cycles. The conditions for our experiments and the variables that were investigated are summarized in Table 3.1.

Experiment Number	Initial layer thickness (mm)	Loading rate (μm/s)	Normal stress (MPa)	Forcing block material	τ for hold (τ_{hold}/τ_{ss})	Nominal Hold time (sec)
m165	3	300	25	Steel	0	10, 100
m166	3	300	25	Steel	0	10, 100
m167	3	300	25	Steel	0	10, 1000
m168	3	300	25	Steel	0	10, 100
m169	3	300	25	Steel	0	100, 1000
m170	3	300	25	Steel	0	100, 1000
m175	3	300	25	Steel	0	1000, 10000
m204	3	10	25	Steel	0	100, 1000
m205	3	10	25	Steel	0	100, 1000
m206	3	10	25	Steel	0.346	100
m207	3	10	25	Steel	0	1000, 10000
m209	3	10	25	Steel	0.064	100
m210	3	10	25	Steel	0.195	100
m211	3	10	25	Steel	0.593	100
m213	3	10	25	Steel	1	100
m214	3	10	25	Steel	0.910	100
m231	3	10	15	Westerly	0	100, 1000
m232	2	10	15	Westerly	0	100, 1000
m233	1	10	15	Westerly	0	100, 1000
m235	2	10	15	Westerly	0	10, 100
m236	1	10	15	Westerly	0	10, 100
m244	0.5	10	15	Westerly	0	100, 1000
m246	0.5	10	15	Westerly	0	10, 100
m247	2	10	15	Westerly	0	1000, 10000
m248	1	10	15	Westerly	0	10, 100
m250	1	10	15	Westerly	0	1000, 10000
m251	0.5	10	15	Westerly	0	1000, 10000
m262	3	10	25	Steel	0 (and 1)	10, 100
m263	3	300	25	Steel	0	0, 10
m264	3	300	25	Steel	0	0, 10
m265	3	10	25	Steel	0	0, 10
m266	3	10	25	Steel	0.064	0, 10
m267	3	10	25	Steel	0.195	0, 10
m282	3	300	25	Steel	Constant V	
m283	3	30	25	Steel	Constant V	
m284	3	3	25	Steel	Constant V	
m295	3	10	25	Steel	Combination	10-10000

Table 3.1. Summary of loading conditions and sample data that were the tested variables for the experiments.

3.3. Results

3.3.1. Shear-load dependence of healing

For direct comparison to data from C-SHS tests (e.g. Figures 3.1 and 3.2), we conducted SHS tests on layers of quartz gouge and varied the shear load for holds (τ_{hold}). For comparison between experiments having different base-level sliding friction values, we normalize τ_{hold} by the measured pre-hold shear stress value, τ_{slide} (we define this dimensionless ratio as η). Thus, for C-SHS tests η equals unity, and for zero-load SHS the ratio is 0. The data from our tests show systematic variations in healing and layer thickness as η is varied between 0 and 1.

In Figure 3.4 we show friction and layer thickness data from SHS tests for different values of η. The general features of the reduced load SHS data are similar to those of C-SHS tests (compare Figure 3.4a with Figures 3.1-3.2). That is, on reload after a hold we observe a frictional maximum greater than the pre-hold value of sliding friction. Friction then decays to a "steady-state" sliding value. To remain consistent with previous studies, we quantify healing ($\Delta\mu$) as the difference between the reload peak friction level and the pre-hold sliding value. In the direct-shear geometry, gouge layers thin with progressive shear [e.g. *Scott et al.*, 1994]. We also observe compaction during holds and dilation upon reloading. However, our data show distinct and systematic differences as a function of η.

In Figure 3.5 we show data from two 100s holds, one in which shear load was partially reduced (Figures 3.5a-b), and for the other shear load was completely removed (Figures 3.5c-d). Peak friction and healing are larger for lower values of η (Figures 3.4, 3.5a, and 3.5c). Also, the data show that as τ_{hold} decreases more slip is required before friction returns to the pre-hold sliding level. We quantify measurements of layer thickness during hold cycles into three components corresponding to unloading, holding, and the reloading (Figure 3.5b). For unloads we observe significant layer thinning which continues through the holds, and layers dilate on reloading. Unload compaction (ΔT_u) and reload dilatancy (ΔT_r) are larger for lower values of η. Also, for a given hold cycle ΔT_u is greater than ΔT_r.

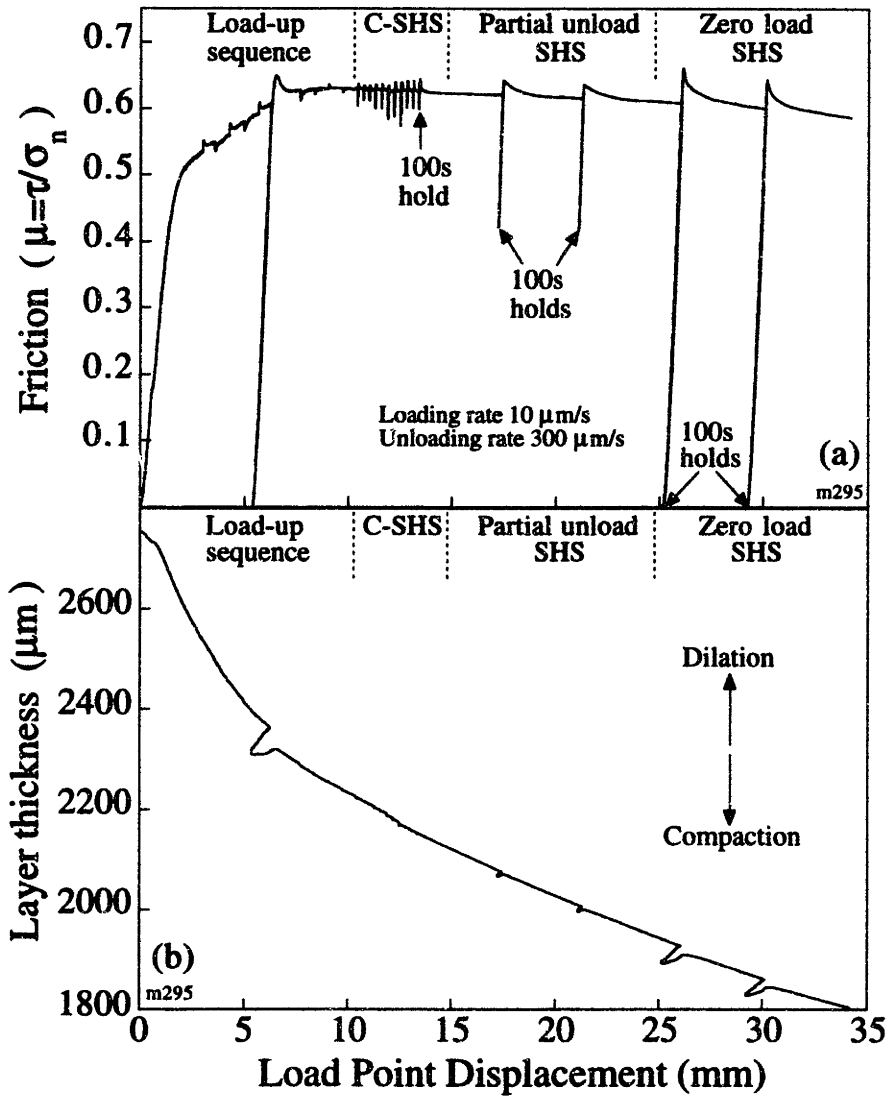

Figure 3.4. Data from a single experiment involving hold cycles conducted at different shear loads. **a).** Friction is calculated as the ratio of the measured shear and normal stresses, and the data is shown plotted against loadpoint displacement. Data show a set of conventional SHS tests with hold times of 10, 100, 1000, and 10000 seconds. The last three hold cycles of the series were of 100s duration. For comparison, the next two hold cycles (100s) were performed at a partially reduced shear load (μ_{hold}~0.4), and the last two hold cycles involved complete removal of shear load for the holds. For the 100s hold cycles, reload static friction levels increase as τ_{hold} decreases. **b).** Layer thickness data for the same test shown in (a). The data show that layers thin with increasing shear displacement. Also, we observe that the changes in layer thickness throughout a hold cycle are larger for holds involving lower levels of τ_{hold}.

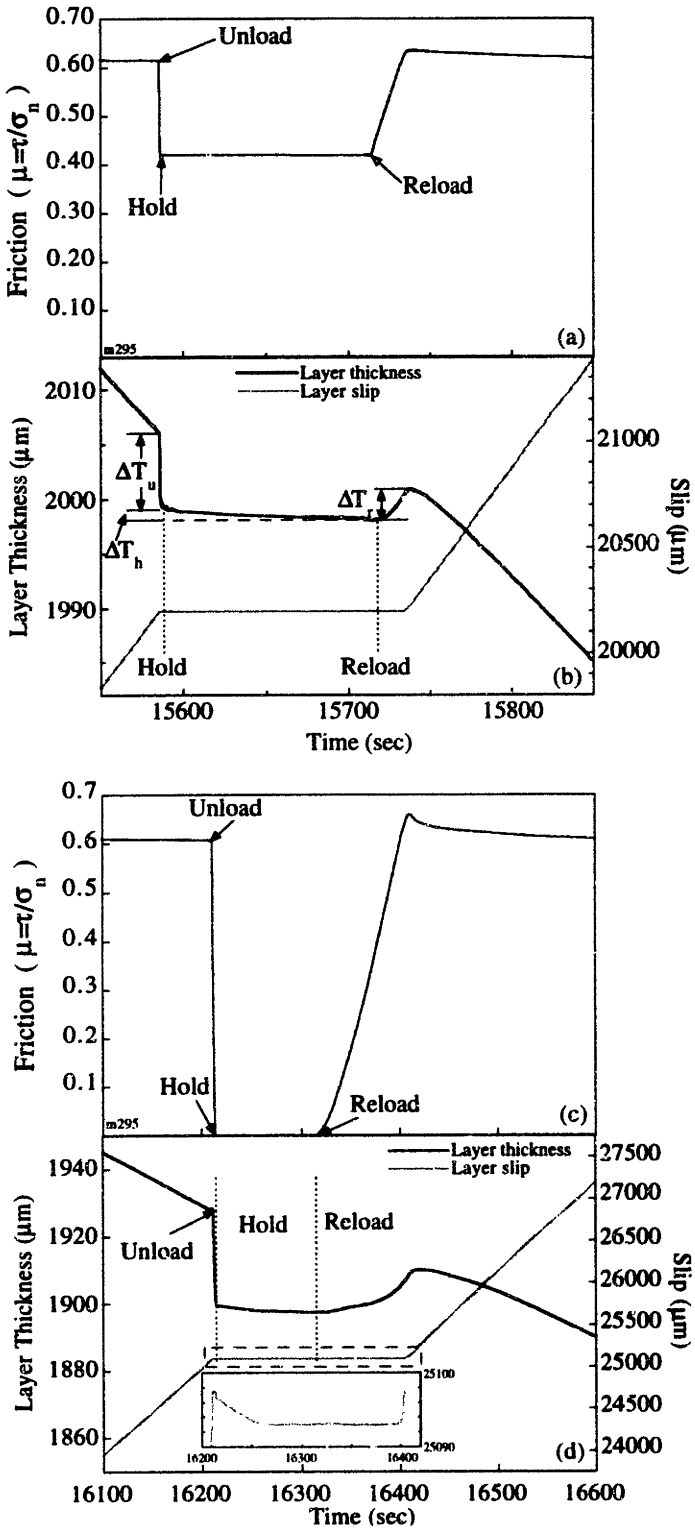

Figure 3.5. Data for a reduced-load SHS cycle. **a).** Friction data for the second 100s partial-load SHS cycle shown in Figure 3.4. Unloading from stable sliding occurs at 300 μm/s, and holds are timed from the point at which τ_{hold} is reached to the point of reloading. Friction is nearly constant during holds, and increases on reloading to a peak value. **b).** Layer thickness and slip measurements from the sample mounted LVDTs for the same hold shown in (a). Significant compaction occurs during unloading, and compaction continues into holds. On reload, gouge layers dilate but not enough to recover porosity loss during unloading. For partially stressed holds, sample slip stops soon after unloading is initiated. **c).** Friction data for the first zero-load SHS hold in Figure 3.4. The general features are similar to those of C-SHS and partial-load SHS tests. Reload static friction levels are greater than for stressed SHS tests. **d).** Layer thickness and slip for the hold shown in (c). Unload compaction and reload dilatancy are larger than for partial-load SHS holds. Layers compact during holds. During unloading and into holds slip reverses slightly.

Our direct measurements on the sample assembly (Figure 3.5d) show that gouge layers experience some reverse slip as η approaches zero (typically of order 1-10 μm). This is surprising because the loading piston is not rigidly connected to the center forcing block and, hence, cannot physically reverse the slip direction. Thus, we attribute the observed slip reversal to gouge compaction and time-dependent decay of elastic strain within the forcing blocks. However, our detailed measurements of apparatus and sample distortion show that such effects must be minor, as slip reversals are not observed for intermediate levels of η. Hence, we suspect that the slip reversals have a small effect on the resulting healing behavior.

During reduced-load SHS tests, the forcing blocks of our sample assembly experience a Poisson-like distortion owing to the large variations in applied shear load. To monitor thickness variations directly on the sample, displacement transducers must be fixed to the stationary side blocks. This limitation arises due to the motion of the center forcing block during shear. Thus, to remove the effects of the Poisson distortion we correct the layer thickness data from all our reduced-load tests using a plane-stress approximation:

$$\varepsilon_2 = \frac{1}{E}(\sigma_2 - \upsilon\sigma_1) \tag{3.4}$$

where σ and ε are the applied tractions and strains perpendicular to each loaded surface of the center block. The subscripts '1' and '2' refer to the loading axes of the shear and normal stresses (which are essentially σ_1 and σ_2 in equation 3.4, respectively), and ν and E are the Poisson ratio and Young's modulus for the forcing block material (ν=0.25 and E=293 GPa for steel; ν=0.26 and E=76 GPa for granite [from *Stacey*, 1992]). The data are then corrected by calculations incorporating the measured thickness and surface areas of the center forcing block. We have performed calibrations on the testing apparatus and forcing block materials and these indicate that the plane-stress approximation is sufficient

for correcting the layer thickness measurements (see Appendix B). For complete removal of shear load, this correction to the layer thickness data is ~1-5μm (depending on forcing block dimensions and material).

In Figure 3.6 we present data from experiments designed to investigate the effect of shear load. For these tests, hold time was fixed at 100 seconds. The data presented in Figure 3.6a show that healing levels decrease as η varies from 0 to 1 ($\Delta\mu$ varies from 0.047-0.06 for η=0, to 0.003-0.01 for η=1). Preliminary data for different hold times show similar results. Our data also show a local minimum of $\Delta\mu$ when η is approximately 0.9. The occurrence of the minimum is consistent with previous observations that sample creep is significantly reduced when shear load falls below 90% of the sliding friction level [*Olsen et al.*, 1998].

Layer thickness variations for the unload, hold, and reload portions for each of the 100s holds are shown in Figures 3.6b-d. Unload compaction decreases systematically as η increases (Figure 3.6b). We observe little (or no) η-dependence on compaction during holds, and a systematic decrease in reload dilatancy greater levels of η. For a given level of η, data scatter correlates with the slip-dependent layer thinning (e.g. Figures 3.4, 3.5) with larger ΔT values corresponding to smaller shear displacements (thus, layers are thicker).

3.3.2. Time-dependence for τ_{hold}=0

In Figures 3.7-3.8 we show data from experiments designed to investigate the effects of hold time (t_h). For reference, we show in Figure 3.7a the loading curve for a representative experiment where t_h for the middle hold pair differs from those of the other holds. We show the healing data from this experiment in Figure 3.7b, together with healing data from another test involving the same hold times but in reverse order. For a given experiment $\Delta\mu$ and sliding friction decrease with increased slip. Healing for the third and fourth holds depart systematically from the nearly linear displacement dependent trend of the other holds. Data for the two 100s holds from 'm165' show lower $\Delta\mu$ compared to the trend

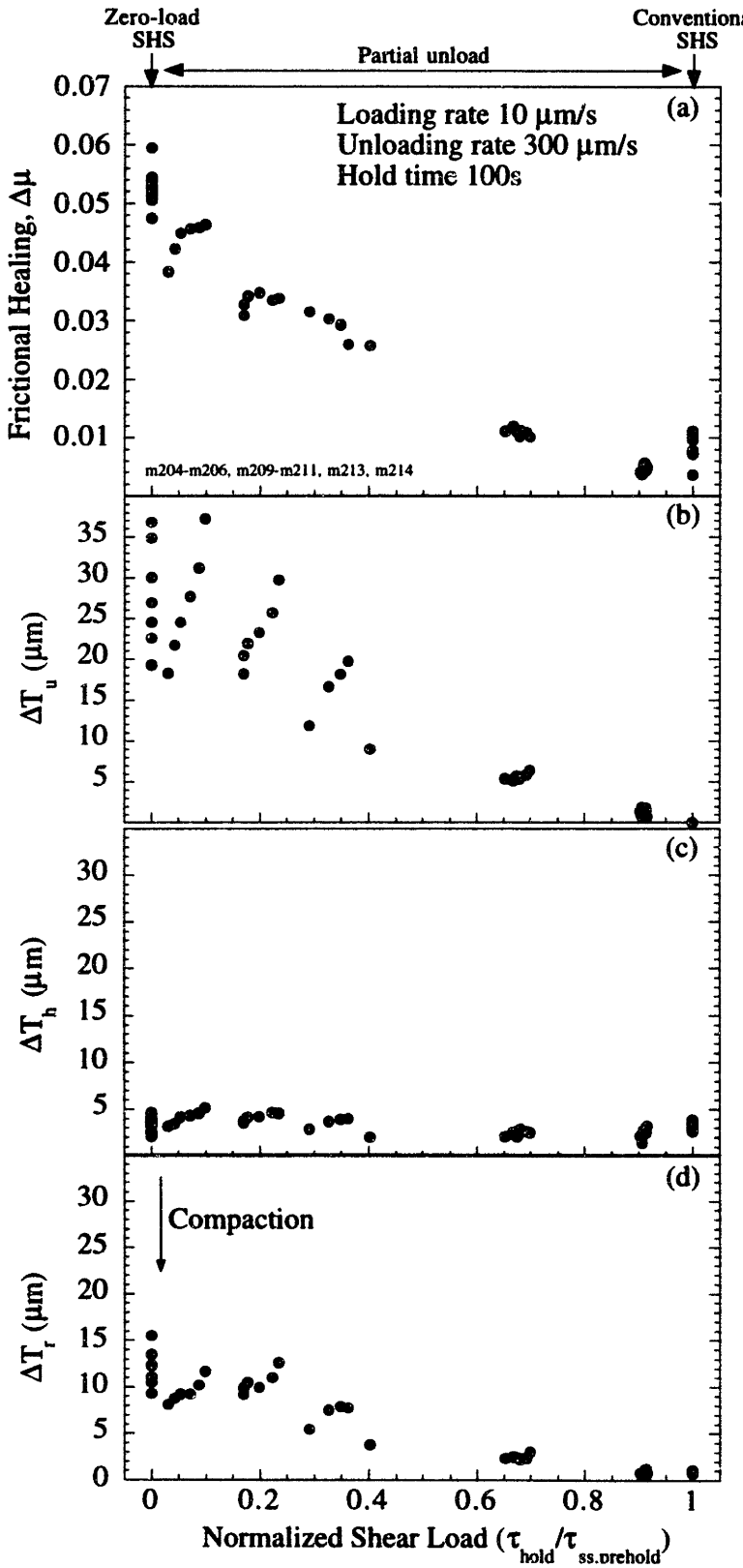

Figure 3.6. Friction and layer thickness data as a function of η. Layer thickness data have been corrected for elastic interaction with the testing apparatus, and for distortion of the forcing blocks. **a).** Healing increases as η decreases. Data scatter for a given experiment (e.g. 'm209' for η~0.064) is due to the displacement-dependent decrease in sliding friction. **b).** Changes in layer thickness measured during unloading for the same hold cycles shown in (a). Layers compact more for lower levels of τ_{hold}. Data scatter for a given η is due to displacement-dependent thinning (and hence, porosity reduction) of the gouge layer. **c).** Compaction measured during 100s holds. The data show little, or no, dependence of hold compaction on η. **d).** Reload dilatancy is larger for lower levels of η, but dilatancy is less than the total compaction that occurs during the hold cycle prior to reloading.

defined by the 10s holds. Conversely, for 'm166' the two 10s holds yield larger $\Delta\mu$ compared to the trend of the other holds. This observation is reproducible, in that our zero-load SHS data consistently show lower $\Delta\mu$ for longer hold times. Furthermore, this observation is independent of hold sequence order. In Figures 3.7c-e we show the layer thickness data corresponding to the hold cycles of Figures 3.7a-b. The first order observation is that the layer thickness variations are smaller as total displacement increases. However, the data also show that longer hold times result in more gouge compaction (Figure 3.7d). For both tests, compaction during the 10s holds is less than the compaction that occurs for 100s holds.

To compare between experiments, we remove the displacement effect using a linear approximation to the data from the first and last hold pairs and then reference the values to a displacement of 20 mm. In Figure 3.8a we show the detrended healing data for tests involving loading rates of 10 and 300 μm/s. The detrended values are large compared to C-SHS tests, consistent with the inverse η-dependence of healing (e.g. Figure 3.6a). Furthermore, we observe negative healing rates (thus, time-dependent weakening) consistent with observations from individual experiments (e.g. Figure 3.7b) yet in contrast to the positive healing rates from C-SHS tests (Figure 3.2b).

In Figure 3.8b-d we present compaction data for the same tests shown in Figure 3.8a. The compaction data are corrected for the observed displacement dependence in the manner outlined above. We do not observe any significant hold time dependence of ΔT_u or ΔT_r (Figure 3.8b). That there is no hold time dependence on ΔT_u is not surprising, given that the holds were imposed after unloading had occurred. Hold compaction (ΔT_h) increases with hold time (Figure 3.8c), comparable to the compaction rates observed from C-SHS tests (Figure 3.2c). We do not observe any significant time-dependent trend for ΔT_h (Figure 3.8d).

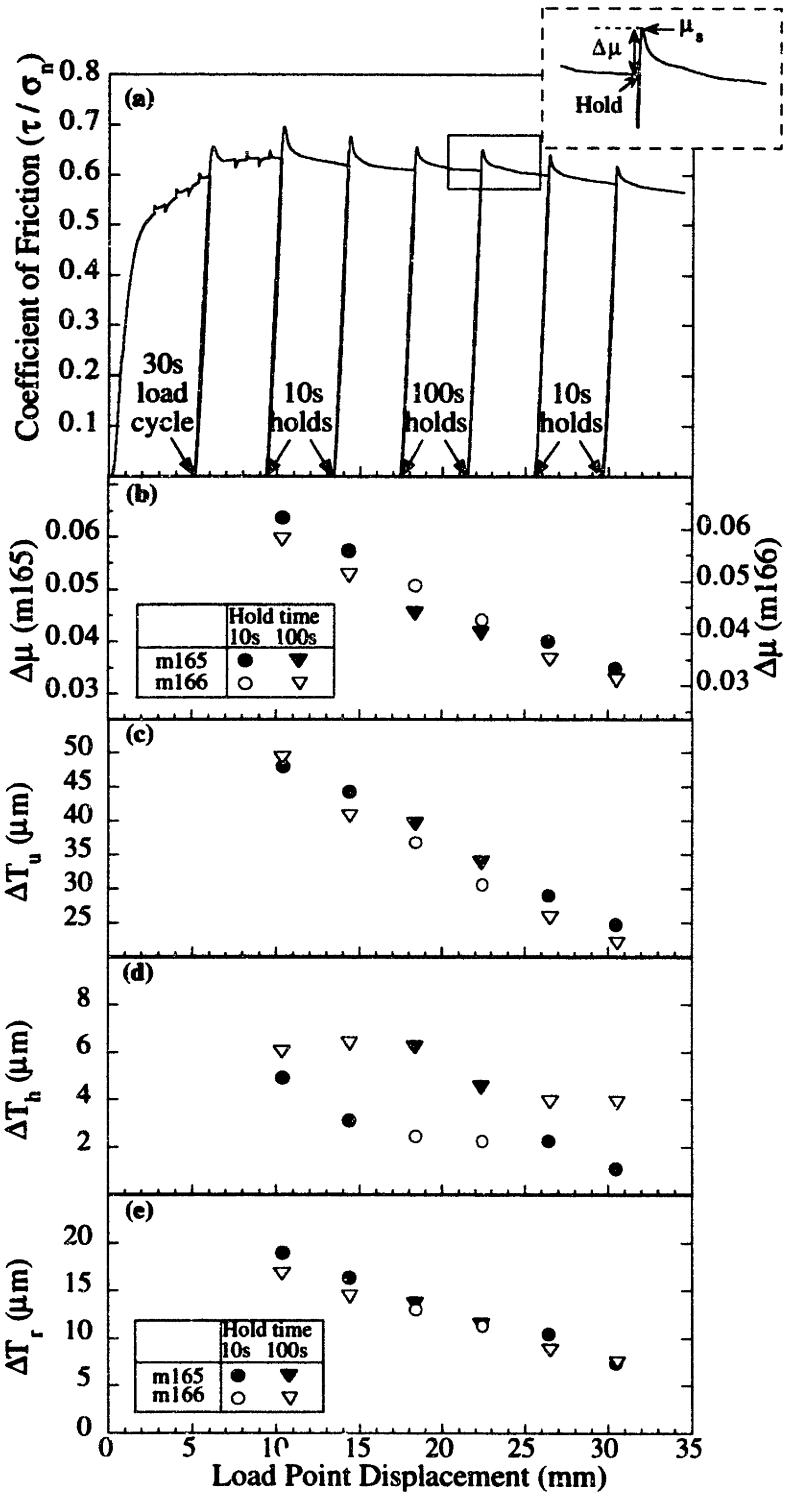

Figure 3.7. Data from zero-load SHS tests. Layer thickness data are corrected for elastic effects and gouge loss. **a).** Loading curve for a typical test. All samples were subjected to the same load-up sequence prior to holds. Inset shows values used to determine healing ($\Delta\mu$). **b).** Healing data from two tests. Y-axes are offset to account for differences in base-level friction, and to allow direct comparison. Data show a strong dependence of healing on displacement, and a systematic effect of t_h. **c).** Compaction during unloading for the same holds in (b). Data show that displacement-dependence of unload compaction is similar for the two tests. **d).** Compaction during holds is greater for longer hold times. **e).** Layer dilatancy data show displacement-dependent decrease, and little dependence on hold time.

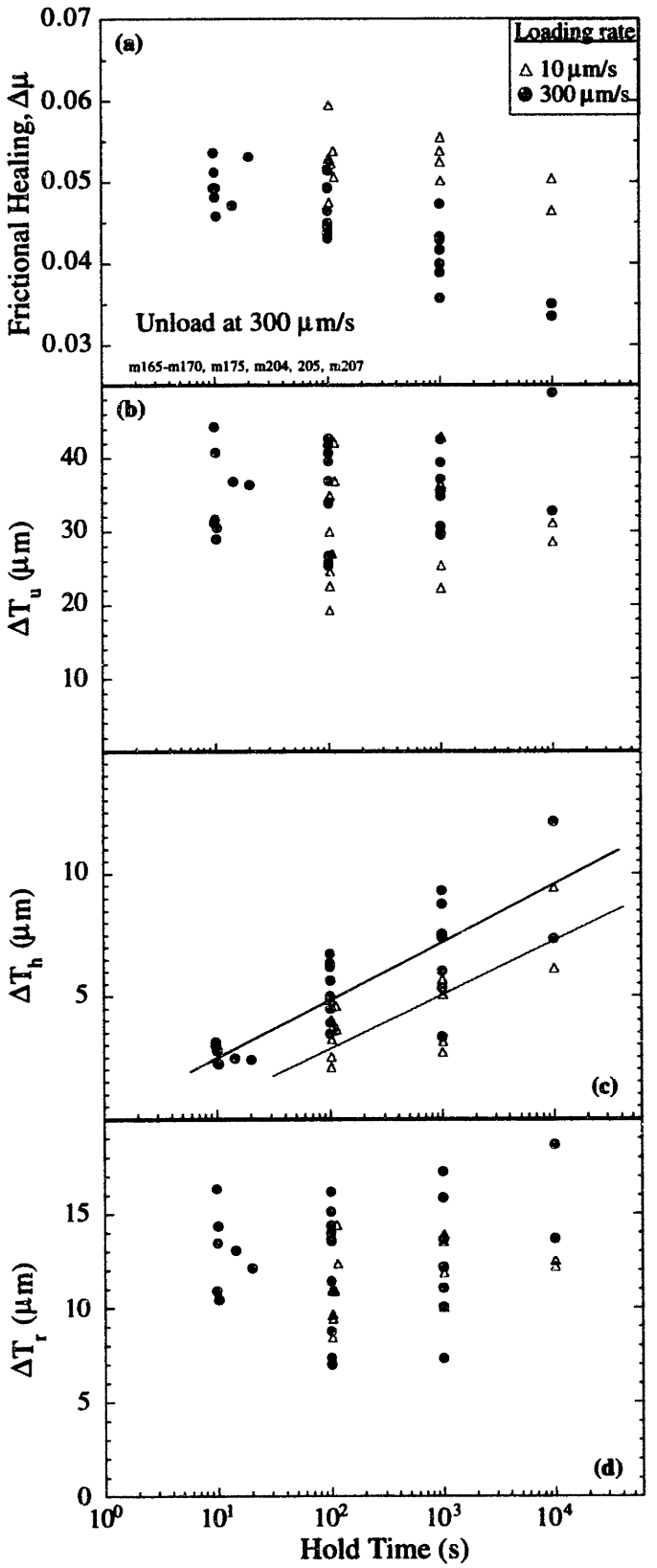

Figure 3.8. Data from all zero-load SHS tests performed on layers of gouge initially 3mm thick. Two different loading rates are shown (10 and 300 μm/s). Healing and thickness data have been corrected for the observed displacement-dependence in the manner outlined in the text. Layer thickness data have also been corrected for elastic distortions of the testing apparatus and forcing blocks. **a).** Δμ values from all experiments plotted as a function of hold time. Data scatter indicates experiment reproducibility. Static friction and Δμ decrease with increasing hold time. **b).** Compaction during unloading plotted for the same hold cycles shown in (a). Data does not show any significant dependence of unload compaction on hold time. **c).** Layer compaction during zero-load holds is plotted as a function of time. Compaction during holds increases with hold time. **d).** Reload dilatancy for the same hold cycles shown above. For any given hold cycle, the amount of dilatancy is less than the net compaction that occurs during unloading and through holds. The data do not show any significant dependence on hold time.

3.3.3. Loading-rate dependence of healing

In Figure 3.8 we show data from zero-load SHS tests for two different loading rates (note that the unloading rate was 300 μm/s for all tests). Both loading rates indicate time-dependent weakening as described in the previous section (Figure 3.8a). However, static friction levels and $\Delta\mu$ are slightly smaller for the loading rate of 300 μm/s. As expected, gouge compaction during unloading is about the same for all hold cycles (Figure 3.8b). Layers compact during holds, with greater compaction for longer hold times. However, samples loaded at 10 μm/s undergo less compaction during holds than samples loaded at 300 μm/s. Thus, faster loading rates result in greater hold compaction and lower healing levels. This correlation is consistent with our observations that time-dependent weakening is associated with greater compaction during holds. We also note, within the scatter of the data, that the levels of ΔT_r are similar for each loading rate. This indicates that the different reload times for each loading rate do not significantly influence reload dilatancy.

3.3.4. Layer thickness dependence of healing

To investigate the effect of gouge layer thinning on healing and sliding friction (Figures 3.4 and 3.7), we performed zero-load SHS tests on layers with differing starting thickness (T_0 between 0.5-3 mm). For these tests we used Westerly Granite forcing blocks with surfaces roughened by sand-blasting with a 60-grit abrasive. The gouge material used was identical to that for our other tests. Data for a given hold time show lower healing values as T_0 decreases (Figure 3.9a), a trend that is consistent with the observed displacement-dependence on healing (e.g. Figure 3.7b). Healing data from tests with T_0 of 2 and 3 mm show time-dependent weakening, consistent with our previous observations (e.g. Figures 3.7-3.8). Healing values from tests with T_0 of 0.5 and 1 mm are almost coincident, and the data show little or no time-dependent weakening.

To illustrate the relationship between healing and layer compaction for different T_0, we present the measured layer thickness changes for unloads, holds, and reloads of 100s hold

cycles in Figures 3.9b-d. As described previously, our layer thickness data have been corrected for Poisson distortion of the forcing blocks and for the observed displacement-dependent layer thinning. For a given T_0, the data are consistent with our previous observations in that unload compaction is significantly larger than compaction during the holds and also larger than the reload dilatancy. For 100s holds, thicker samples experience larger changes in layer thickness which are associated with greater levels of healing. We observe similar trends from our data for other hold times.

3.3.5. A note on experiment reproducibility

In comparing data from holds that occur within a single experiment, we note systematic variations in healing and layer thickness values as a function of displacement (e.g. Figure 3.7). As the error for a given measurement is smaller than the symbol used to plot the data, we can attribute measurement differences to the observed displacement dependence. As samples are sheared, some gouge is lost from the layers owing to the geometry of the sample assembly. For some tests, we have measured the mass of gouge loss at discrete intervals of displacement (see Appendix D). The volume of gouge loss from a single layer is responsible for some of the observed layer thinning. Assuming 10 g of gouge is lost by the end of a test, and that the final porosity is 15%, then gouge loss would account for ~450 μm of total layer thinning. However, we observe minimal gouge loss during hold cycles. Thus, the observed compaction during hold cycles is due to porosity loss. Data from tests with different initial layer thickness (Figure 3.9) indicate that displacement-dependent layer thinning is associated with lower healing values and smaller changes in layer thickness during hold cycles. This is consistent with observations from individual experiments (Figure 3.7). However, there is another factor that may effect our healing and layer thickness measurements for holds. Granular comminution with increased shear acts to consolidate gouge layers. Such a systematic change in consolidation would effect healing levels, and also result in smaller layer thickness variations during hold cycles.

We also observe scatter when comparing data from one experiment to another. It has long been recognized that base friction levels between experiments are difficult to reproduce [e.g. *Scholz*, 1992]. For our experiments, this may arise due to several reasons despite our efforts to maintain consistency in sample preparation and experiment procedure. Differences in grain packing may occur during sample preparation, and this would result in variations of the population of grain contacts. Deformation of gouge layers may evolve differently between experiments and result in changes of thickness, geometry, and number of shear bands. As our experiments are performed at room-humidity conditions, daily variations of humidity may influence the mechanical behavior of the gouge [e.g. *Dieterich and Conrad*, 1984]. During a reduced-load hold cycle, the gouge would undergo considerable microstructural rearrangement and deformation. If the deformation pathway depends on the pre-hold state of the gouge layers, then any variation in gouge state would lead to different microstructural evolution during holds. These are but a few possible causes that address experiment reproducibility.

3.4. Discussion

3.4.1. Comparison with previous work

It is instructive to compare our results to data from similar experiments on bare rock surfaces and granitic fault gouge. *Nakatani and Mochizuki*, [1996] conducted reduced-load SHS tests on bare granite surfaces in a double-direct shear testing apparatus and at a normal stress of 5 MPa. Their data show large healing values ($\Delta\mu$ between 0.03-0.13), positive healing rates (thus, time-dependent strengthening), and increased healing for higher levels of η (Figure 3.10a). Their results contrast with the inverse η-dependence and time-dependent weakening we observe from our experiments. This disparity may be due, in part, to the presence of gouge. To this end we can compare our results to those of *Nakatani* [1998] who performed reduced-load SHS tests on layers of granitic gouge. His data show lower healing levels as η increases (consistent with our observations) yet exhibit

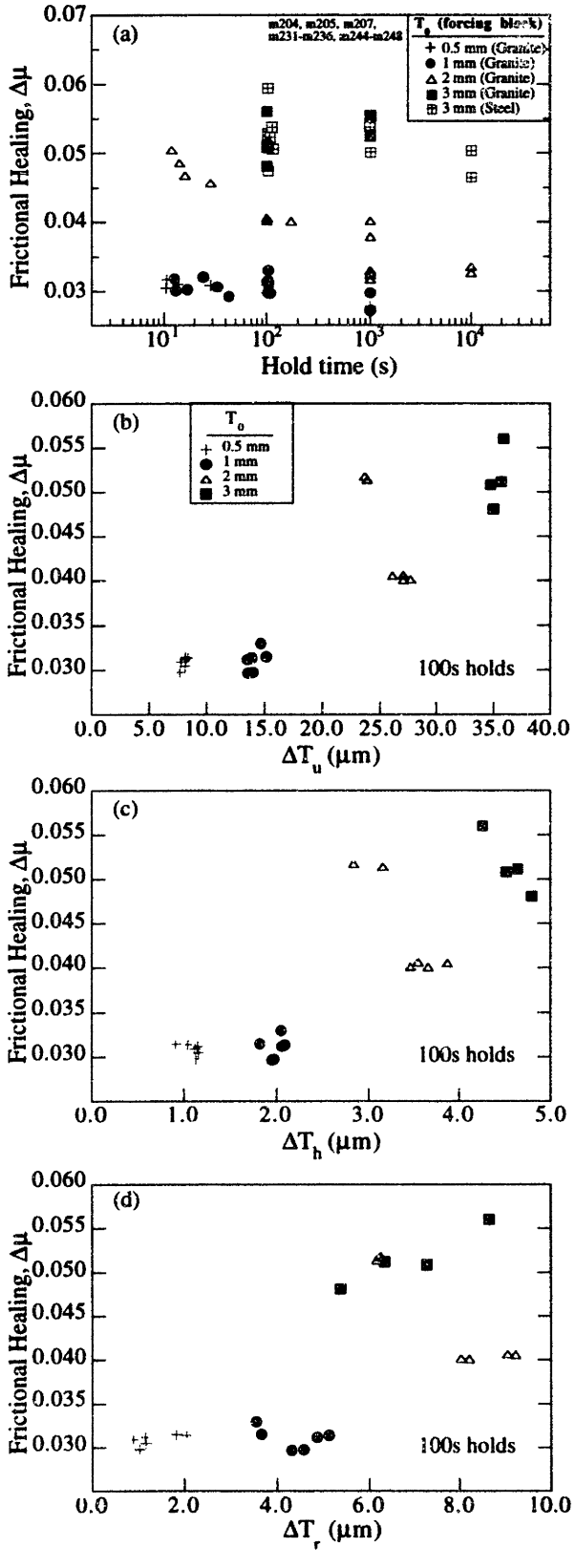

Figure 3.9. Data from tests designed to investigate the effects of the starting gouge layer thickness. Data have been corrected for the observed displacement-dependence, and layer thickness data have been corrected for elastic and volumetric distortions of the loading frame and forcing blocks, respectively. **a).** Healing data as a function of initial layer thickness, and hold time. Data from tests on 2mm and 3mm layers display time-dependent weakening. Data from tests on 0.5mm and 1mm layers show similar healing levels, and little time-dependent behavior. For a given hold time, healing levels are lower for decreasing T_0. **b).** Healing plotted as a function of compaction during unloading for all 100s holds. Data show that healing and unload compaction both increase with increasing T_0. **c).** Data for compaction during holds is plotted for the same 100s hold cycles shown in (b). Data show that healing levels and amount of hold compaction are larger for thicker gouge layers. **d).** Dilatancy data for the same hold cycles shown in (b) and (c). Data show that healing values and dilatancy are larger for increasing T_0. Data also show that for a given hold cycle, dilatancy is less than the net compaction that occurs prior to reloading.

time-dependent strengthening, similar to the healing rates reported by *Nakatani and Mochizuki* [1996].

At present, it is difficult to reconcile the discrepancies between our results and those of *Nakatani and Mochizuki* [1996] and *Nakatani* [1998]. Their tests were similar to ours, yet differed in three ways. First, the tests of *Nakatani and Mochizuki* [1996] were conducted on initially bare granite surfaces, whereas our tests involved shear within quartz gouge. This is significant because the micro-mechanical processes associated with sliding on bare surfaces are inherently different to shear within gouge [e.g. *Byerlee*, 1967; *Scholz*, 1987; *Logan et al.*, 1992; *Beeler et al.*, 1996; *Marone*, 1998b]. Second, in their tests it was shear load that was directly controlled, and not loadpoint velocity as for our experiments. Controlling the shear stress may influence levels and rates of healing should the maximum reload velocity differ between hold cycles. However, our results for different loading rates indicate that this effect may only be minor (e.g. Figure 3.8). Third, our experiments were conducted at normal stresses of 15 and 25 MPa, while those of *Nakatani and Mochizuki* [1996] were performed at 5 MPa. Our data suggest that the effect of normal load on healing is small (see Figure 3.9). This is corroborated by the tests of *Nakatani* [1998] conducted at normal loads of 5 and 10 MPa which show only a minor influence of normal stress on healing. We also note that *Nakatani and Mochizuki* [1996] and *Nakatani* [1998] define "healing" as the difference between the reload peak friction and the sliding friction level reached after reload (different to the definition adopted for this study). In their studies it was also reported that the reload sliding friction levels varied considerably which makes direct comparison of our data to theirs somewhat tricky. However, as they consistently used the alternate definition of healing it is still useful to make the comparisons.

Similar experiments have also been performed on multi-contact interfaces between polymer glasses [*Berthoud et al.*, 1999], and on layers of wet granular material [*Géminard et al.*, 1999]. *Berthoud et al.* [1999] used a spring slider track to investigate the effects of shear stress and temperature (25-125°C) on static friction levels. They performed both

conventional- and zero-load SHS tests (their "stressed-aging" and "free-aging" tests, respectively). Their data from stressed-aging tests show large healing levels ($\Delta\mu$~0.075 to 0.85), and positive healing rates (their β_s^{τ}, expressed per decade time) that range from ~0.015 at room temperature to 0.13 for the higher temperatures. They also observe that healing rates for stressed-aging tests are approximately two times greater that the rates observed for free-aging, which is in qualitative agreement with observations from bare rock surface experiments [*Nakatani and Mochizuki*, 1996].

Géminard et al. [1999] also used a spring slider apparatus to shear layers of fluid-saturated glass beads at room-temperature and a low normal stress (M_{slider} = 14.5 g). While the effects of time were not investigated, they do present data from two experiments similar to conventional and zero-load SHS tests. Upon loading, their data show a peak in friction and subsequent decay to stable sliding levels. The difference between static and sliding friction levels can be up to twice as large for samples loaded from zero shear stress compared to loading from a pre-stressed state [*W. Losert and J. Gollub*, personal communication]. Thus, their data indicate lower healing levels as η increases, which agrees with our observations for tests on simulated fault gouge.

Olsen et al. [1998] reported on reduced-load SHS experiments performed in a triaxial pressure vessel under hydrothermal conditions (P_c = 60 MPa, P_f = 10 MPa, temperatures 25°C to 250°C). Their gouge layers (T_0 = 3.5 mm) consisted of feldspar/quartz granular aggregates with particle sizes between 210-500 μm. While it may not be appropriate to directly compare results from their hydrothermal tests to the data from our room-temperature experiments, there are features of their data that warrant comparison. *Olsen et al.* [1998] imposed hold times that extended to 2 days, and axial load for holds was 40 MPa lower than the steady-state sliding level (η = 0.7). They observed healing levels (in terms of shear stress) from ~0.75-5.35 MPa, in qualitative agreement with the healing levels from our tests. Their data show no significant dependence of hold time on healing levels, consistent with observations from our zero-load SHS tests. However, the physico-

chemical conditions of their study may involve different mechanisms than for our tests. As hydrothermal conditions favor feldspar diagenesis [e.g. *Karner and Schreiber*, 1993; *Scholz et al.*, 1995; *Tenthorey et al.*, 1998; *Aharonov et al.*, 1998], they suggested that the formation of authigenic clays had a significant influence on healing and frictional behavior of their gouge layers.

3.4.2. Modeling using rate and state friction laws

For comparison to our data, and to data from *Nakatani and Mochizuki* [1996], we have performed numerical simulations using existing rate- and state-dependent friction laws [*Dieterich*, 1979; *Ruina*, 1983; equations 3.1-3.3]. The simulations were performed using the boundary conditions of our experiments, and results from the calculations are shown in Figures 3.10-3.11. The rate and state friction parameters used in the simulations (a=0.0066, b=0.0066, D_c=45 μm) were obtained from inversion of velocity steps that occur within the load-up sequence of our experiments (e.g. Figures 3.4, 3.7).

Forward modeling of our reduced load tests (Figures 3.10-3.11) indicate that the Dieterich and Ruina laws predict dramatically different healing levels as a function of η, and different healing rates as a function of hold time. For short hold times (10-100s) the Dieterich law predicts less healing as η increases and that this dependence is greatly diminished for large hold times (Figure 3.11a). While the inverse η-dependence for short hold times is in qualitative agreement with our observations, the slope of the predicted η-dependence does not match the trend of our data (Figure 3.10a). Furthermore, the simulations do not match the large positive η-dependence observed by *Nakatani and Mochizuki* [1996]. As a function of hold time, the Dieterich law predicts positive healing rates which have little dependence on η for hold times larger than 100s (Figure 3.11b). The simulations match the time-dependent strengthening observed by *Nakatani and Mochizuki* [1996], but do not predict the time-dependent weakening we observe (Figure 3.10b).

Simulations using the Ruina law show that healing initially decreases with decreasing η (to η~0.9), and that there is no influence on healing for lower values of η. Also, the Ruina law predicts time-dependent strengthening when η>0.9 and no time-dependence below this level of η. We find that the Ruina law simulations do not agree with the healing trends observed by *Nakatani and Mochizuki* [1996], except for the predicted time-dependent strengthening when η is large. The Ruina law does not match our data very well either. That is, for η larger than 0.9 the simulations do predict an increase in healing. However, below this level the Ruina law does not match the trend of our data. Finally, the simulations predict much lower healing levels compared to our observations from zero-load SHS tests.

It is apparent that neither friction law can predict the healing trends we observe for gouge, nor the trends for the bare surface tests of *Nakatani and Mochizuki* [1996]. Thus, the present friction laws cannot adequately characterize friction evolution when loading perturbations are far from steady-state sliding conditions. By incorporating terms that describe the nature of the material being sheared, the laws may be able to predict the observations from our data. For gouge, these factors may include particle size, grain packing, degree of consolidation, porosity, and permeability (for fluid saturated gouge) as well as thickness, number, and geometry of shear bands. In the next section we shall explore the role that porosity may have when associated with the rate- and state-dependent friction laws.

3.4.3. The role of porosity in frictional healing of fault gouge

The correlation between changes in fault gouge porosity and frictional strength has been documented previously by several researchers [e.g. *Marone and Scholz*, 1988, 1989; *Morrow and Byerlee*, 1989; *Marone et al.*, 1990; *Beeler et al.*, 1996; *Marone*, 1998a, 1998b ; *Richardson and Marone*, 1998]. From velocity-stepping experiments, *Morrow and Byerlee* [1989] showed that frictional velocity-dependence varied as a function of

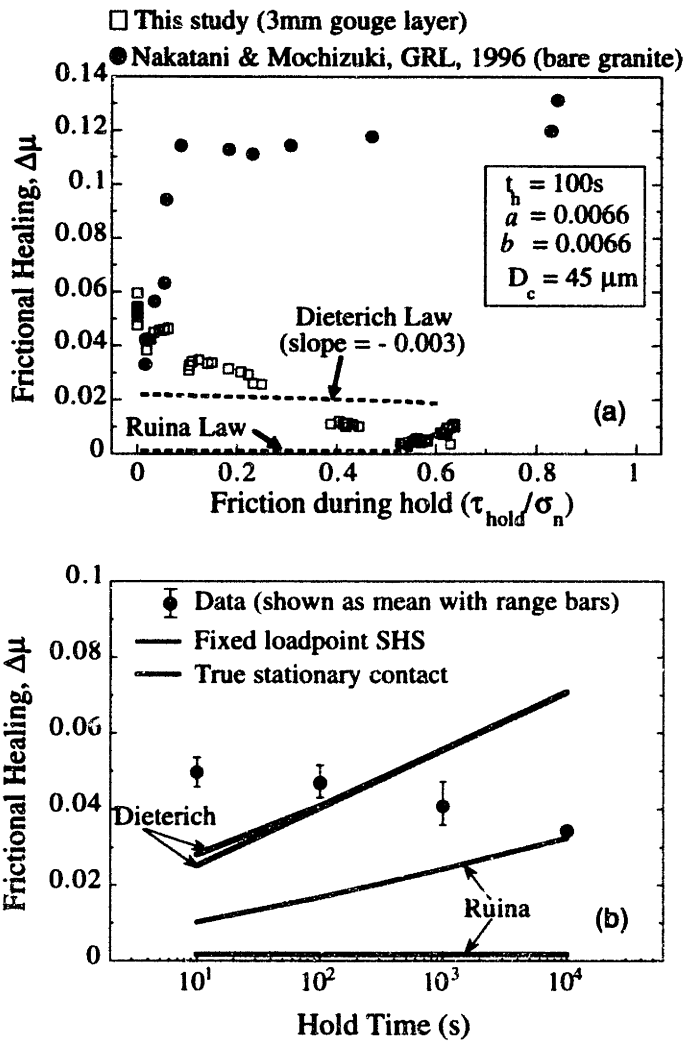

Figure 3.10. Healing predicted by the Dieterich and Ruina laws compared to our data, and the bare surface friction data of *Nakatani and Mochizuki* [1996] (we interpolate their data to 100s hold time). For simulations, friction parameters were determined from velocity steps within our tests. **a).** Comparison between data and simulations, as a function of τ_{hold}. All holds were 100s. Our data show lower healing levels and an inverse load-dependence, compared to data from bare granite surfaces. Dieterich law predicts similar healing levels to our data, and show a slight inverse load-dependence (for short t_h). Ruina law predicts the initial reduction in healing, as η decreases from 1 to ~0.9. Below this level, the Ruina law does not predict a healing dependence on τ_{hold}, and healing levels are much lower than data. **b).** Healing predictions are shown for SHS tests where η=0 and η=1. We show the mean values of our zero-load data (bars indicate data range). Dieterich law predicts large positive healing rates, even for holds with true stationary contact. Ruina law predicts distinctly different healing rates depending on shear load. Neither the absolute value of $\Delta\mu$ nor the time-dependence from our data are well matched by the model predictions.

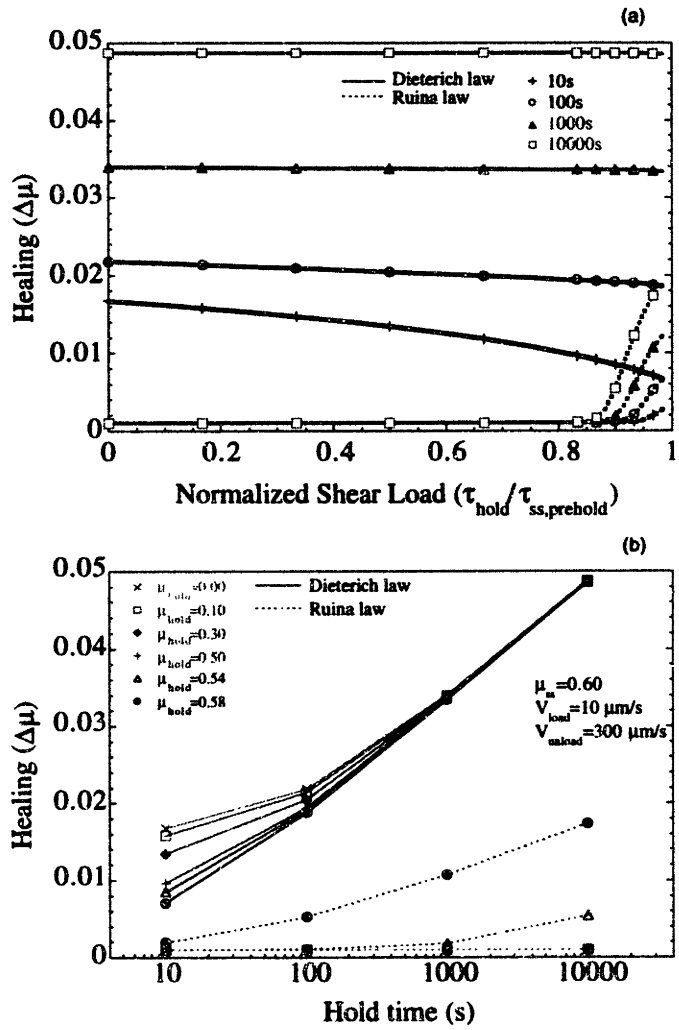

Figure 3.11. Numerical simulations for the boundary conditions of our experiments. Friction parameters used are the same as for Figure 3.10. **a).** Modeling using Dieterich and Ruina laws predict very different healing behavior as functions of η and t_h. For t_h of 10-10000 s, Ruina law predicts a decrease in healing to a η level of ~0.9. For all t_h and for $\eta < 0.9$, Ruina law predicts no η-dependence. Dieterich law predictions of healing show an inverse dependence on η for short t_h only (< 1000s). For larger t_h, the Dieterich law predicts little, or no, η-dependence. For a given η, Dieterich law always predicts larger healing values as t_h is increased. **b).** Simulations showing healing as a function of t_h. The results are as for (a). The Dieterich law always predicts time-dependent strengthening, independent of τ_{hold}. However, the levels of healing predicted by the Dieterich law for hold times shorter than 1000s show a minor dependence on τ_{hold}. Simulations using the Ruina law show no time-dependence for τ_{hold} less than ~0.5. For τ_{hold} greater than ~0.5, the Ruina law predicts time-dependent strengthening.

porosity, and that porosity evolution varied with strain rate. This work was extended by the velocity-stepping experiments of other researchers [*Marone et al.*, 1990; *Beeler et al.*,1996] who showed that frictional strength depends on the rate of porosity change instead of absolute porosity. Detailed measurements of gouge layer thickness during conventional SHS tests [e.g. *Marone*, 1998a; *Richardson and Marone*, 1998] show a clear relationship between frictional healing and compaction during holds. For longer hold times, the data show increased healing and greater compaction [e.g. *Marone*, 1998b; see Figure 3.2]. *Richardson and Marone* [1998] reported on data from conventional SHS tests where normal stress was vibrated during holds. As a function of increasing vibration amplitude, they observed larger healing values coupled with greater porosity reduction.

Data from our experiments also demonstrate connections between frictional healing and porosity changes. As a function of η, we observe that larger healing values are associated with increased compaction (Figure 3.12a), which is in qualitative agreement with data from conventional SHS tests. However, the data shown in Figure 3.12a indicate that the porosity-dependence of healing is different for C-SHS tests and the reduced shear-load hold tests of this study. Despite the different trends, it appears that healing levels are, for the most part, directly dependent on the amount of gouge compaction that occurs during a given hold cycle.

The time-dependent weakening shown by our zero-load SHS data (Figures 3.6 and 3.7) that is accompanied by time-dependent gouge compaction is an observation that seemingly contradicts the data from C-SHS tests, and our τ_{hold}-dependent data (Figure 3.12a). This may imply that the processes associated with healing in granular materials differ for the zero-load SHS cycles, and those of C-SHS and reduced-load SHS tests. From our zero-load experiments, we note that the largest healing values occur for the shorter hold times. This suggests that the initial restrengthening of gouge is due to the large amount of compaction that occurs during the unloading to zero shear stress. The time-dependent compaction that occurs during the holds appears to be a second phase of gouge

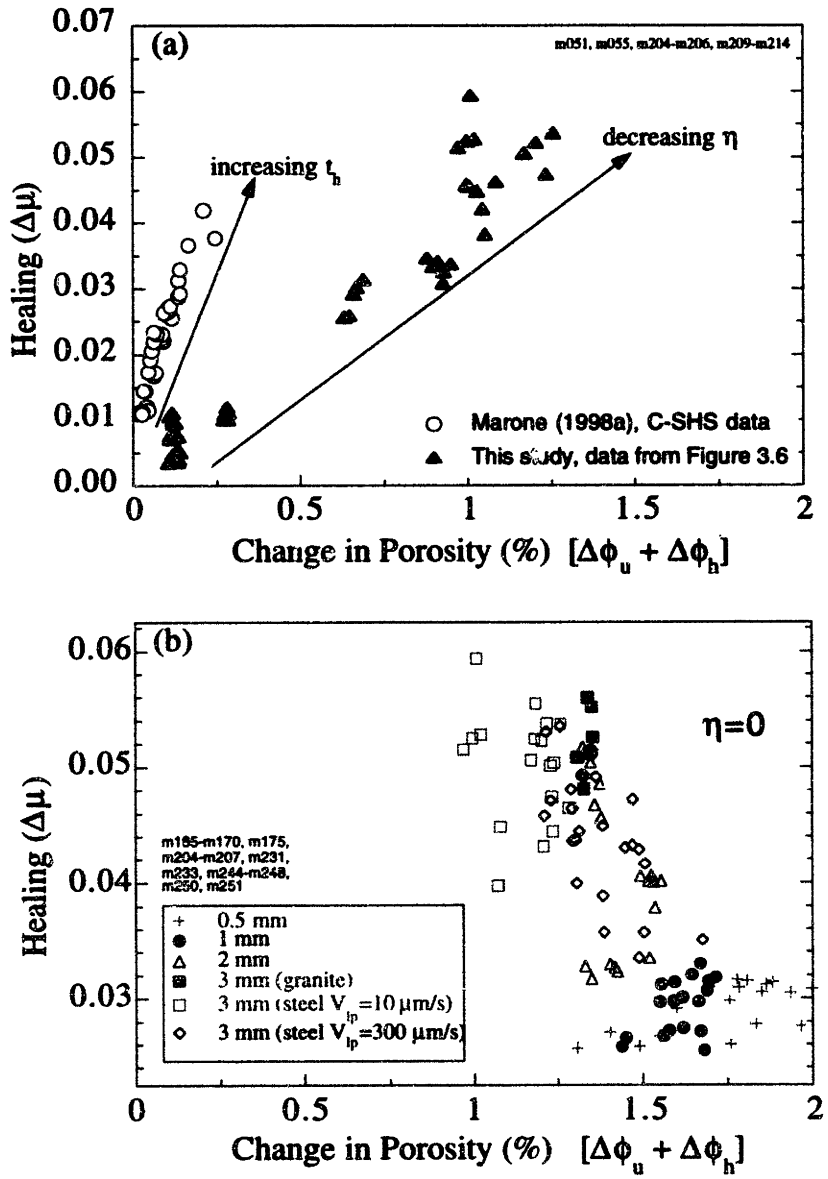

Figure 3.12. Layer thickness data from our experiments are shown here cast in terms of changes in porosity. **a).** Data from our reduced-load SHS tests show a qualitatively similar dependence of healing on porosity compared to data from C-SHS tests. That is, healing levels increase with greater amounts of porosity reduction. However, the data show that the slope of the porosity-dependence on healing differs between the C-SHS tests and our reduced-load SHS data. **b).** Data from all zero-load SHS tests, including experiments where hold time, loading rate, and initial layer thickness were the variable tested. Data show that healing for these zero-load SHS tests is larger for hold cycles involving greater reduction in porosity.

deformation. In this stage, the micro-mechanisms that operate within the gouge must differ from those mechanisms operative during unloading. During the holds, the layers continue to compact and this may be accompanied by internal rearrangement of the gouge. The rearrangement within the gouge may take the form of time-dependent backslip at the granular level, or fracturing of grains. Such rearrangement may act to remove the barriers encountered when slip is reinitiated upon reloading of the sample after the hold. We are presently investigating procedures to isolate the effects of the rapid unloading from the processes that operate during holds.

In order to investigate further the role of porosity in frictional healing of fault gouge, we can reanalyze our data obtained from experiments involving different initial layer thicknesses (i.e. Figure 3.9). We show in Figure 3.12b the healing data from all zero-load SHS cycles plotted against the net change in porosity that occurs during unloading and holds. Our data indicate a systematic relationship between healing and compaction that occurs through the hold cycle prior to reloading. We observe that lower healing levels are associated with greater amounts of compaction prior to reloading. This observation is consistent with our data that show time-dependent weakening is associated with increased compaction (Figures 3. 6 and 3.7).

3.4.4. Modified rate and state friction laws

The notion of incorporating gouge porosity into the rate- and state- dependent friction laws has been discussed by *Sleep* [1995] and *Segall and Rice* [1995]. In applying the rate and state friction laws to ductile fault zone rheology, *Sleep* [1995] described the friction state variable (θ) and critical slip distance (D_c) in terms of porosity (ϕ). *Segall and Rice* [1995] derived an alternative relation where porosity evolution depended solely on loading rate and D_c (their equations 14-15). However, they recognized that these coupled equations could not predict the time-dependent compaction observed from conventional SHS

experiments. Thus, by following *Sleep's* [1995] assumption that porosity depended on state evolution, they proposed an expression of the form:

$$\phi = \phi_0 - c \ln\left(\frac{V_0 \theta}{D_c}\right) \tag{3.5}$$

where ϕ_0 is a reference porosity, c is a variable (their dilatancy parameter), and V_0, θ, and D_c are as described previously. In this formulation, the state variable may evolve in the same manner as described by *Dieterich* [1979] or *Ruina* [1983] (equations 3.2 and 3.3, described previously). *Segall and Rice* [1995] compared results from their simulations to data from velocity-stepping experiments [*Marone et al.*, 1990], and found reasonable fits to the data (for c=1.7x10^{-4}, a=0.010, b=0.006, D_c=20μm).

We have also performed numerical simulations to test the state-dependent porosity relation (equation 3.5) for the boundary conditions of velocity-stepping and conventional SHS tests. We begin by using equations 3.1-3.3, coupled with an expression describing the elastic interaction with the testing apparatus, for inversion of our friction data. From the inversions, we obtain the friction parameters (a, b, and D_c) and the state evolution variable, θ. These parameters are then used to forward model the evolution of porosity using equation 3.5 coupled with the evolution laws (equations 3.2-3.3). We then compare the predicted porosity to data from our experiments.

In Figure 3.13 we show data from velocity step tests together with results from models. Owing to the symmetry of the friction data during these tests, we use the Ruina law for models. In this section of the experiment, friction exhibited slight strain hardening. Thus, a linear term was added to friction calculated from modeling. We show results for inversion using a single state variable. We also ran inversions using the two state variable form of the Ruina law. However, in each case the inversions degenerated to a single state variable case. We then used the rate and state parameters determined from inversion

(Figure 3.13a) to forward model porosity evolution (Figure 3.13b). Porosity data are also shown, and have been corrected slip-dependent gouge loss and for geometric layer thinning (described previously). We find that the predicted changes in porosity capture the basic elements shown by the data including the initial rapid change in porosity and the difference between steady state levels.

We have also performed simulations on conventional SHS tests. In Figure 3.14 we show data from a single C-SHS test. From inversions of the friction data we found that a two state variable version of the Dieterich law modeled the entire hold cycle better (Figure 3.14a). The parameters determined by the inversions were then used to predict porosity evolution (Figure 3.14b). Porosity data for the hold have been corrected in the manner described above. The modeled porosity matches the compaction during the hold very well. However, on reloading we find that the predicted amount of porosity recovery is greater than the observed amount. We attribute this to a net loss of porosity during the hold. The modeling predicts the general reloading character of the porosity data. That is, layers initially dilate rapidly on reloading followed by a sharp transition to a slower dilatancy rate. The results from the simulations for the velocity-step and C-SHS tests are encouraging. In both cases, the predictions closely resemble the observed data. We are presently exploring the applicability of the state-dependent porosity relations to our reduced load SHS tests. In order to describe data from those hold cycles, the friction laws may need to include terms accounting for variations in shear stress [similar to the normal stress dependent law of *Linker and Dieterich*, 1992]. Furthermore, in order to incorporate data from tests involving perturbations in normal stress [*Linker and Dieterich*, 1992; *Richardson and Marone*, 1998] it might be necessary to include mean stress in a modified friction law (rather than only normal stress or shear stress).

3.4.5. Micro-mechanical model of gouge deformation

Studies of deformation within a granular media indicate that the state of the system cannot be adequately described by the macroscopically measured stress and strain [*Williams and Rege*, 1997]. Researchers from different disciplines are investigating other factors to help understand the deformation of granular assemblages. These factors include porosity, amount of overconsolidation, particle shape, grain packing, grain size, particle size distribution, and geometry of the fabric that develops (e.g. shear bands) [*Chester and Logan*, 1989; *Biegel et al.*, 1989; *Marone and Kilgore*, 1993; *Beeler et al.*, 1996; *Oda*, 1997; *Williams and Rege*, 1997; *Morgan*, 1998; *Morgan and Boettcher*, 1998].

Oda [1997] presented a model to describe dilatancy of shear bands that occur in deforming sands. The model was based on his observations that porosity within the shear bands was greater than the porosity outside the shear bands, although such a correlation may not be universally observed in natural fault gouge [*Antonellini et al.*, 1994]. *Oda* [1997] suggested that chains of particles oriented parallel to the shear stress direction act to support a sizable portion of the applied load. Near the point of failure of the granular media (e.g. the peak friction we observe in our tests) these chains begin to buckle and rotate due to interparticle sliding and grain rotation. As the chains deform, voids begin to develop between the chains giving rise to the observed dilatancy.

It is interesting to note that *Oda's* [1997] model has basic elements in common with another concept that may have application to the deformation of granular media: jamming. In studies of colloidal materials deforming by simple shear, it has been observed that a constant rate of shear cannot be achieved [e.g. *Ball and Melrose*, 1995; *Farr et al.*, 1997]. This observation has been ascribed to the development of load-bearing particulate chains that form along the axis of the maximum compressive stress. As the chains grow they lock up the colloidal material thereby creating a logjam within the system. If the system is slightly perturbed (e.g. an incompatible load, fluctuation in temperature) the logjam collapses (unjams) and the system is forced to rearrange itself and may later produce a new

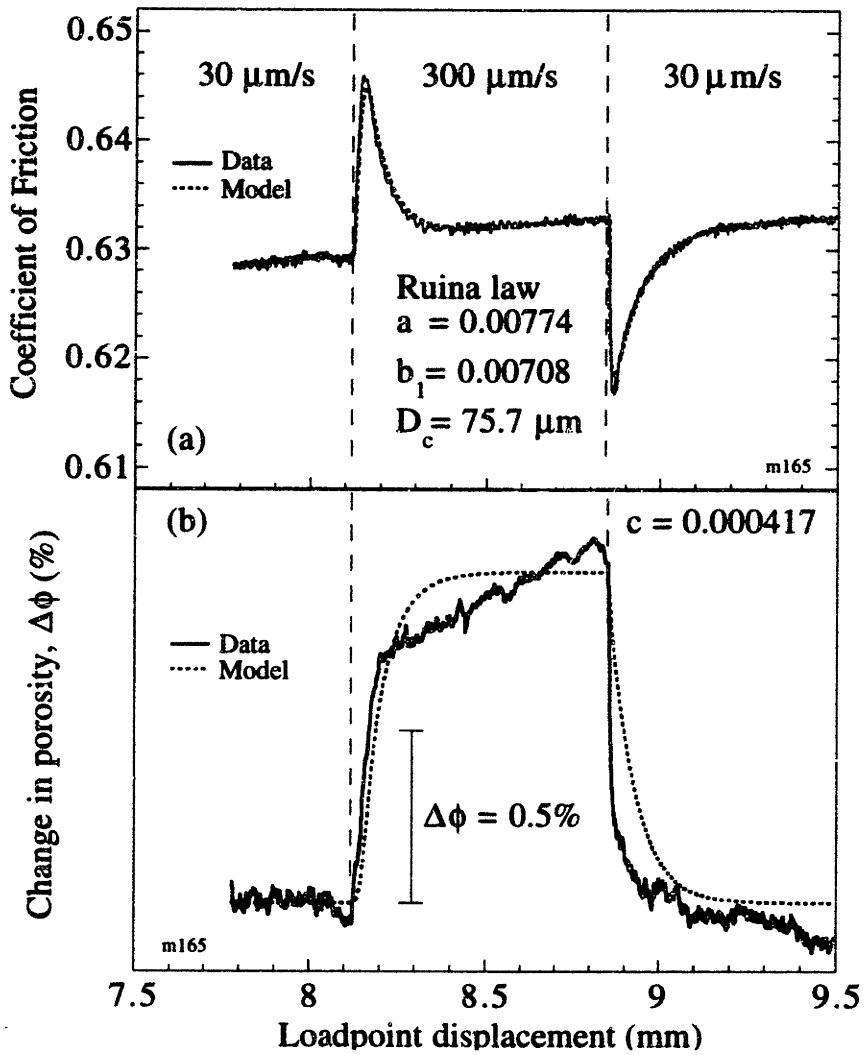

Figure 3.13. Data from velocity-step tests compared to numerical simulations. **a).** Friction data was inverted using the Ruina law to determine the friction rate and state parameters. **b).** Detrended porosity data for velocity-step tests in (a) are compared to predictions. The friction parameters and state evolution determined from inversion of the friction data were used in equation 3.5. The predicted changes in porosity closely match the data.

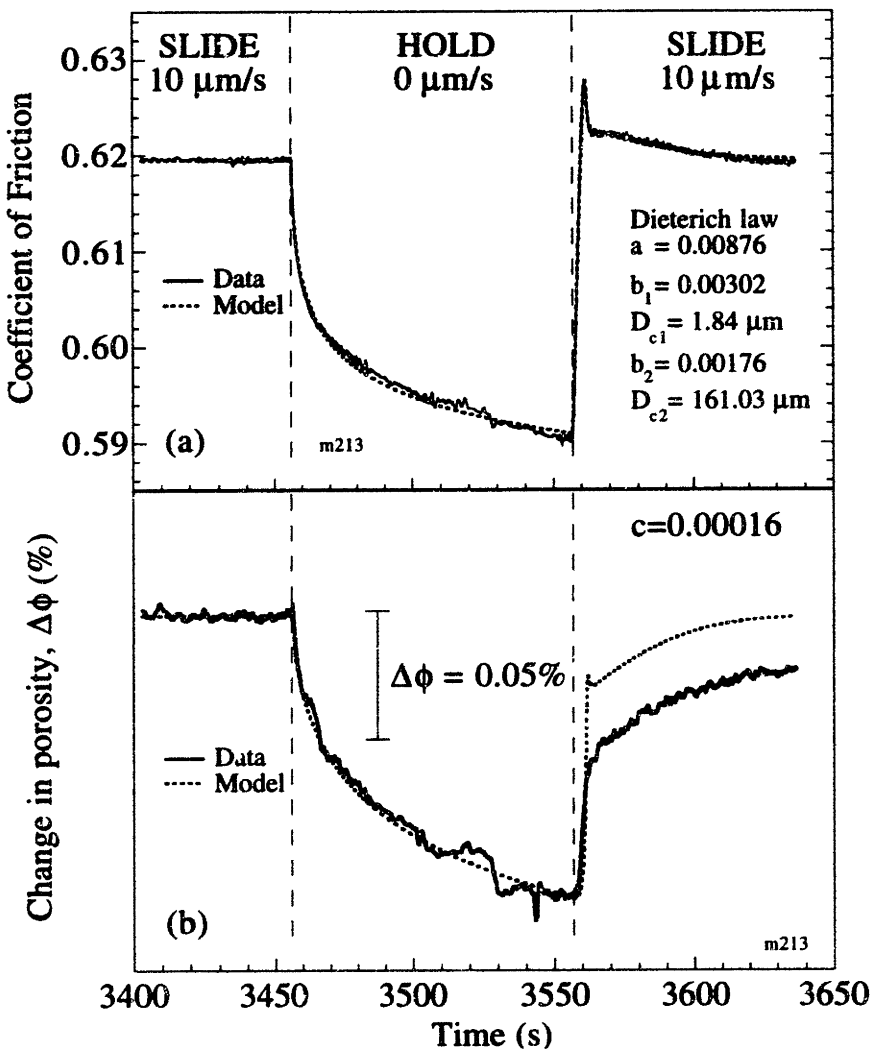

Figure 3.14. Data from conventional slide-hold-slide test compared to numerical simulations. **a).** Friction data was inverted using a two state-variable Dieterich law to obtain the friction rate and state parameters. **b).** Detrended porosity data for slide-hold-slide test in (a) are compared to predictions. The friction parameters and state evolution determined from inversion of the friction data were used in equation 3.5. The predicted changes in porosity closely match the data.

jammed state [*Cates et al.*, 1998]. Recently, it has been suggested that the concept of jamming may find application to problems involving flow of granular media, such as stoppage of flow through grain hoppers, and clogging of powder-carrying conduits in factories [*Liu and Nagel*, 1998]. When these problems occur, the typical course of action is to vibrate the jammed system in order to reinitiate granular flow (i.e. unjam the stoppage). The vibration acts at perturb the stress field and, hence, the load-bearing particulate chains collapse (either by grain rotation or frictional sliding at grain contacts).

We propose that similar jamming and unjamming may occur in experiments on layers of simulated fault gouge. The macroscopic frictional response of the deforming layers would depend on the number of particulate chains, the load-bearing capacity of these chains, and the stress field experienced by the layer. The number of chains participating in jamming would be controlled by the physical characteristics of the gouge layer (e.g. layer thickness, particle size, particle shape, size distribution etc.) while the load-bearing capacity of the chains would be determined by the physical properties of the grains and their contacts (e.g. yield and ultimate strengths of grains, intergranular strength due to cohesion or cementation). The porosity of the gouge layer may also determine how easily the chains can deform and unjam the system. For low porosity the chains may not be able to buckle owing to the proximity of neighboring grains, and the chains may only be able to collapse via a net rotation or by perturbing the stress field.

We envision that steady-state shear of granular layers represents an equilibrium between the number of particulate chains generated to induce jamming, and the number of chains that are destroyed (unjamming). Optimally oriented particulate chains that form within the deforming gouge would act to support considerable applied load (Figure 3.15). As shearing continues, the loading force on the chains would increase resulting in deformation of the chains by frictional sliding at grain contacts, or by grain rotation (Figure 3.15b). With further shear, the chains would be deformed to the point where they are no longer optimally oriented to support the applied load, resulting in collapse of the force chains

(Figures 3.15c-d). While existing force chains are collapsing, neighboring grains that are permitted to move somewhat freely may encounter clusters of other particles. For sufficiently high grain density, these moving particles may participate in the logjam and new force chains would develop.

During holds for either conventional SHS tests or reduced-load SHS tests (not zero-load SHS), gouge is subjected to a non-zero shear force that could act to sustain existing chains. The layer compaction observed during these holds is an indication of particle rearrangement within the gouge that may promote the formation of new chains. For conventional SHS tests, hold compaction increases with time, and thus the creation of new chains should increase with hold time. Similarly, we observe from our reduced-load SHS tests that gouge compaction increases with decreasing τ_{hold}, which would result in an increase in the number of new chains produced. The level of peak friction achieved on reloading after a hold (either conventional or reduced-load SHS test) depends on the force required to overcome the total load-bearing capacity of all the participating chains within the gouge. If the number of chains increases with hold time (conventional SHS test) or with decreasing τ_{hold} (reduced-load SHS test) then the force required to overcome the load-bearing capacity of the chains will also increase. Hence, the macroscopic peak friction level increases with hold time and with decreasing τ_{hold}, consistent with observations from our data.

The data from our zero-load SHS tests show that healing decreases and gouge compaction increases with longer hold times. While our data are surprising in the context of present models relating real area of contact to time-dependent healing, our data may be consistent with a jamming/unjamming model. The positive dependence of gouge compaction on hold time observed from our zero-load SHS tests suggests an internal rearrangement of gouge occurs during holds. Under zero macroscopic shear-load, particles that form load-bearing chains would also be permitted to reposition themselves. The rearrangement of gouge particles may result in some chains collapsing, and thus a time-dependent reduction in the total number of optimally oriented force chains. Upon reloading

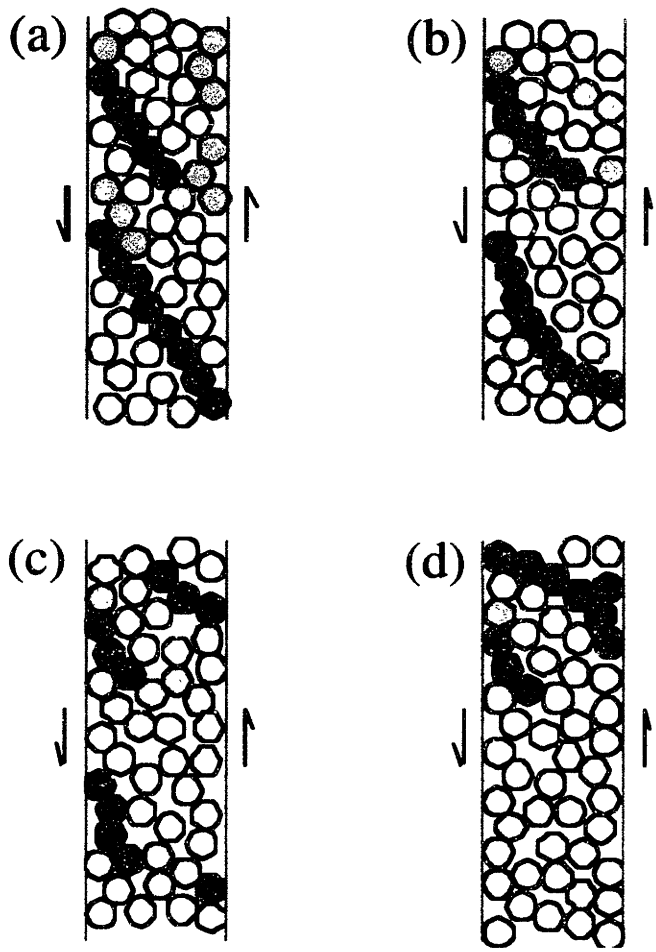

Figure 3.15. Schematic illustration of a micro-mechanical model involving chains of gouge particles that support shear load, and are involved in creating logjams within the deforming gouge layer. Grains responsible for significant resistance to layer deformation (i.e. jamming) are shaded dark. Grains that have a small role in jamming are shaded light gray, while grains that do not participate in jamming have no shading. (**a**) through (**d**) are schematic illustrations of particulate rearrangement for consecutive intervals of shear, and for shear at a constant rate. The two active force chains shown in (a) act to resist shear as the participating grains are tightly locked together by the imposed load. With progressive shear of the layer, the force on these active chains increases and the chains will begin to deform (as they are only ably to bear a finite load). As illustrated in (b) and (c), the deformation of the chains may occur by buckling as the grains slide, or rotate, past each other. With continued shear, the force chains will eventually collapse permitting granular flow to occur more easily (unjamming). However, under steady-state sliding conditions the number of chains that are being destroyed may be in equilibrium with the number of newly created force chains, such as the creation of the uppermost chain shown schematically in (c) and (d).

after zero-load holds, peak friction would be lower for gouge that has experienced more internal rearrangement and unjamming. Hence, zero-load SHS tests would result in lower healing levels with increasing hold time, consistent with the time-dependent weakening shown by our data.

Insight into the deformation of granular media may be obtained from experiments designed to directly view the deformation features, or from numerical simulations that investigate shear within simulated fault gouge [e.g. *Morgan*, 1998; *Morgan and Boettcher*, 1998]. The numerical simulations of shear in simulated fault gouge [e.g. *Morgan and Boettcher* , 1998] suggest that regions within the layers can episodically lock-up and become more resistant to continued deformation. Chains of load-bearing particles develop in front of the locked regions and are approximately collinear with the orientation of the maximum compressive stress. With continued macroscopic shear, these chains rotate with the sense of shear and eventually collapse. The collapse of the chains correlates with increased granular flow, consistent with unjamming of the system, and can be subsequently followed by jamming in other regions of the layer. Whether a micro-mechanical model involving jamming and unjamming can be universally applied to deformation within granular fault gouge remains to be seen. However, the data from our zero-load SHS tests cannot be described in the context of models involving changes in real area of contact. This suggests that different micro-mechanical processes occur during the holds for our zero-load SHS tests, and we propose that a jamming model could explain the observations from our data.

3.5. Summary

In order to broaden the range of physical conditions studied for the mechanical behavior of faults, and to test the existing rate- and state-dependent friction laws, we have performed a series of slide-hold-slide (SHS) experiments on simulated fault gouge in a double-direct shear testing apparatus. We have investigated the effects of shear load, hold time, loading

rate, and initial layer thickness on frictional restrengthening (healing). Our data show systematic trends as a function of the variables we tested. We observe that healing and layer compaction both increase with decreasing shear load for holds (τ_{hold}). From tests where τ_{hold}=0, our data consistently show that longer hold times result in less healing (time-dependent weakening), despite showing that layer compaction increases with hold time. We observe from the data that loading rate has a small effect on healing in that slower velocities are associated with slightly larger healing values. Our data also show that healing decreases as a function of decreasing initial layer thickness. However, when cast in terms of porosity, our zero-load SHS data show that healing decreases with greater porosity reduction prior to reloading.

The results from our experiments are surprising when compared to studies of frictional healing in gouge from conventional SHS tests where shear load is not decreased prior to holding. In order to investigate the observed differences, we have conducted numerical simulations using the existing rate- and state-dependent friction laws. We find that neither the Dieterich law, nor the Ruina law, are capable of describing the trends shown by our data. This suggests that the friction laws require modification if they are to describe friction evolution for large changes in loading conditions.

We have presented a micro-mechanical model where load-bearing particulate chains developed within the gouge may act to resist shear (jamming). The existence of a given force chain may be short-lived, but we propose that these chains are both destroyed and created during macroscopic deformation of the gouge. Thus, steady-state sliding would represent an equilibrium between the generation of, and collapse of, the force chains. While the applicability of this model to gouge deformation remains to be tested, the model may be capable of explaining the frictional behavior we observe from our experiments.

[2]Chapter 4

Laboratory Study of Fault Healing and Lithification in Simulated Fault Gouge Under Hydrothermal Conditions

Synopsis: We report on experiments to investigate the influence of healing duration and temperature on the strength and healing rate of simulated faults. Layers of μm-sized quartz powder were used to simulate granular fault gouge. Gouge layers were sheared within Sioux quartzite in a triaxial pressure vessel at elevated pressures (P_c=250 MPa), elevated temperatures (230-636 °C), and in the presence of water (P_{H20}=75 MPa). We performed "hold-slide" experiments in which samples were subjected to a period of healing under hydrostatic load, followed by shear deformation. Healing times ranged from a few hundred s to 10^5 s. To isolate the effects of lithification and temperature on friction, we ran two types of hold-slide experiments: 1) samples were subjected to healing and shear deformation at elevated temperature, and 2) following healing at elevated temperature, temperature was reduced prior to shear. We also ran slide-hold-slide experiments in which samples were healed under shear load at elevated temperature (636 °C). Experiments in which deformation was carried out at a lower temperature than healing show that both the static and sliding coefficient of friction increase with heal time. Samples healed and deformed at higher temperature showed lower peak strengths, and within the scatter of our data, did not exhibit time dependent strengthening. These data are interpreted to result from enhanced lithification rates at elevated temperature. Samples healed under shear load exhibited a log-linear decrease in friction with hold time. Modeling using rate- and state-dependent friction laws indicates velocity strengthening behavior, with friction a-b values of 0.05 to 0.08. The data indicate that at high temperature, the effective state-evolution

[2] This chapter has been published in *Tectonophysics*, 277, 41-55, 1997.

term b is negative. Moreover, the rate of frictional strengthening varies significantly for hydrostatic and non-hydrostatic load conditions. The measurements of healing are consistent with seismic estimates of fault healing rates, if stress drop is a fraction of the total shear stress and effective fault normal stress is 60 to 100 MPa.

4.1. Background

In the stick-slip model for earthquakes [*Bridgeman*, 1936, 1951; *Brace and Byerlee*, 1966] instabilities occur on a pseudo-regular basis, with sudden stress drops separated by periods of stationary (or quasi-stationary) contact. The behavior of stick-slip motion is governed by various factors including the loading velocity, system stiffness and friction of the sliding surface [*Ohnaka*, 1973]. During the period of relative quiescence (stick), friction may evolve as a function of the real area of contact between opposing fault walls [*Dieterich*, 1972; *Scholz et al.*, 1972; *Scholz and Engelder*, 1976; *Dieterich*, 1978] or, if fault gouge is present, as a function of gouge consolidation [*Byerlee et al.*, 1978; *Shimamoto and Logan*, 1981; *Marone et al.*, 1990; *Angevine et al.*, 1982; *Fredrich and Evans*, 1992). Understanding the evolution of frictional strength is thus of central importance to understanding fault strength and the seismic cycle.

This chapter describes a suite of experiments to determine the effects of temperature and contact time on the frictional strength and healing rate of simulated fault gouge. We also investigated the effect of load conditions (hydrostatic versus non-hydrostatic load). To avoid complex mineralogic alteration and to focus attention on the effects of temperature and lithification, we performed experiments on water-saturated quartzitic samples.

4.1.1. The time-dependence of friction based on room temperature laboratory data

Laboratory experiments have provided considerable insight into the frictional behavior of geologic materials. These experiments involve frictional sliding on rock surfaces in

direct contact or surfaces separated by fault gouge. Existing friction constitutive laws are derived from experiments designed to measure variations in static friction and from velocity-stepping experiments, in which the imposed slip rate is stepped from an initial value, V_0, to a new value, V_1. When subjected to such a velocity step, the coefficient of friction is immediately altered (the direct effect), followed by a gradual change toward a new, steady value (the evolution effect) [*Dieterich*, 1979, 1981; *Ruina*, 1983; *Rice and Ruina*, 1983].

Dieterich [1978, 1979] proposed that the dependence of steady-state friction on slip rate is due to time-dependent processes that affect the real area of contact for the sliding surface. Studies of these processes usually involve experiments where the initial loading velocity, V_L, is changed to zero for some period of time before being reset to V_L (slide-hold-slide experiments). The peak friction value observed upon reloading is taken as a measure of the "static" coefficient of friction and is generally observed to increase with hold time. Such experiments yield friction strengthening rates, which we refer to as healing rates.

Data from room temperature experiments on geologic materials show that static friction obeys an empirical relation that is logarithmic with respect to time of contact [*Dieterich*, 1972, 1978; *Scholz and Engelder*, 1976; *Beeler et al.*, 1994]. In these studies, healing rates (expressed as the increase of friction) are 0.009-0.05 per decade increase in hold time. These values may be consistent with seismic estimates of fault healing rates, if effective normal stress is high and stress drop is a fraction of the total shear stress [*Marone et al.*, 1995]. On the other hand, fault healing rates may be much greater than laboratory estimates, inasmuch as seismic stress drop increases by a factor of 2-5 per decade increase in earthquake recurrence interval, whereas laboratory friction studies show only 5-10% change in friction per decade change in hold time [e.g., *Scholz et al.*, 1986; *Cao and Aki*, 1986; *Wong and Zhao*, 1990]. Resolution of this apparent discrepancy is important for two reasons: 1) time-dependent frictional strengthening is a cornerstone of rate- and state-dependent friction laws, which have been widely used to model earthquakes and faulting

(for recent reviews see *Scholz*, 1992; *Scholz*, 1998; *Marone*, 1998], and 2) comparison of laboratory- and seismically-derived healing rates is important for addressing the problem of scaling laboratory friction results to natural faults.

4.1.2. Laboratory experiments under hydrothermal, seismogenic conditions

Experiments performed under elevated temperature and pressure demonstrate some of the complexities involved in understanding rock friction. Relevant factors include the choice of material used for the experiments, the presence and type of fluids, and the physical conditions of the experiment (pressure, temperature, sliding velocity).

The introduction of pore-fluids dramatically changes the frictional behavior of granite with increasing temperature. Nominally-dry Westerly granite gouge exhibits stable-sliding and increasing friction with temperature [*Lockner et al.*, 1986]. Similar tests under hydrothermal conditions [*Blanpied et al.*, 1995] show a more complex frictional behavior with velocity-weakening occurring at temperatures between 100-350° C and velocity-strengthening outside this range (up to 600° C).

Loading history also appears to affect the frictional characteristics of laboratory samples. The slide-hold-slide, fluid-saturated experiments of *Chester and Higgs* [1992] on Tennessee Sandstone (with quartz gouge) exhibit increasing frictional strengths and velocity-weakening in the temperature range 23-300° C, and slightly decreasing frictional strengths from 300-600° C. During the hold stage, samples relax and friction decreases with increasing hold time. *Chester and Higgs* [1992] suggested pressure solution-assisted deformation as a mechanism to explain the observed frictional behavior of their samples. In their hold-slide experiments, *Fredrich and Evans* [1992] observed frictional strengthening with both increasing hold time and temperature. In their experiments, gouge healing occurred under hydrostatic pressure and strengthening was attributed to enhancement of fluid-rock reactions (pressure solution) under the hydrothermal conditions of their experiments.

4.2. Experiment Procedure

4.2.1. Testing apparatus and sample

We conducted experiments in an argon confining medium, internally heated, servo-controlled deformation apparatus [e.g. *Kohlstedt and Goetze*, 1974; *Schwenn and Goetze*, 1978; and *Caristan*, 1982]. The apparatus consists of a main pressure vessel, a hydraulic ram for axial loading, and a custom built two-zone wire-wound furnace. Confining and pore-fluid pressures were established by independently-controlled pressure generators located external to the main vessel. Confining pressure is generated in a Haskell intensifier and maintained to within ±3 MPa by air-driven Haskell boosters. Pore-fluid pressure was generated and maintained to within ±2 MPa by an HIP-brand pressure generator (which has been converted to operate under hydraulic servo-control). All fluid pressures are monitored and controlled using the signal output from pressure transducers.

Shear deformation was achieved by a servo-controlled hydraulic piston. Axial displacement of the hydraulic piston is measured by a direct-current displacement transducer (maximum non-linearity of 0.5%) and this signal is used in a servo-control feedback loop with a resolvable control step-size of 0.1 μm. The axial displacement rate for the experiments reported here was 1.75 and 2 μm/sec. Axial force was measured by a loadcell external to the main vessel. Load variations due to piston-seal friction is assumed to be negligible owing to the constant piston displacement rate used during sample deformation. All pressures, the control point temperature, and the load piston displacement were electrically monitored and digitally acquired.

The loading assembly located within the main vessel consists of the jacketed sample and column spacers encased by the heating furnace. The furnace was controlled to within ±2° C by a thermocouple located near the top of the sample, and temperature within the sample was constant to ±5° C (Figure 4.1). Two thermocouples are used to measure thermal profiles of replica sample columns so that the furnace controller settings are optimized for the sample column and conditions of interest.

Simulated faults were saturated with distilled/deionized water and sheared within Sioux quartzite. Sioux quartzite is a pure (99% equigranular quartz) sedimentary orthoquartzite with a mean grain size of 160 μm [*Mardon et al.*, 1990]. Fault gouge consisted of a pure, fine-grained quartz powder (mean diameter = 2-3 μm) obtained from the U.S. Silica Company. The chemical system was thus relatively simple (quartz and water). Quartzite forcing blocks consisted of cylindrical samples (length = 33 mm, diameter = 16 mm) cut at 30° to the axis and ground with a #100 wheel to provide a uniform surface roughness. Gouge layers were prepared in a copper-foil form using a pre-weighed quantity of quartz powder. Initial layer thickness was 0.6 mm and layers were pre-saturated with water. Fluid access to the gouge layer was provided by a blind hole (diameter = 2.5 mm) drilled into one half of the quartzite cylinder to within 1 mm of the fault surface (Figure 4.1). The loading assembly consisted of the sample and alumina, zirconia and steel spacers, all of which were enclosed in thin-walled (0.3 mm) copper tubing.

4.2.2. Operational Technique for the Experiments

Experimental conditions are given in Table 4.1. During deformation the velocity of the axial ram was held constant at 1.75 μm/sec resulting in slip rates along the fault zone of 2.0 μm/sec. We varied the temperature at which deformation took place (T_d = 230° C, 250° C or 636° C), the time the sample was held at the healing temperature (up to 10^5 sec), and the load conditions under which samples were healed (Table 4.1). Deformation conditions are representative of hypocentral conditions for large earthquakes (8-14 km).

Hold-slide experiments: We performed two types of hold-slide experiments, as illustrated in Figure 4.2. Both began with healing at elevated temperature for a predetermined time. In one set, temperature was reduced prior to shear deformation, and in the other set shear deformation took place at elevated temperature (Figure 4.2). It is important to note that the loading conditions in these experiments differ from the slide-hold-

slide experiments of other studies [e.g. *Chester and Higgs*, 1992; *Beeler et al.*, 1994]. In our hold-slide experiments, gouge healing occurs under hydrostatic load.

After an initial air-evacuation of the pore fluid system and loading assembly, confining and pore pressures were increased by tracking them at the ratio P_c:P_f = 10:3 to the final values (P_c=250 MPa, P_p=75 MPa). Temperature was then raised manually over a period of up to 40-70 minutes. In later experiments (#S09 on), temperature was raised by a ramp

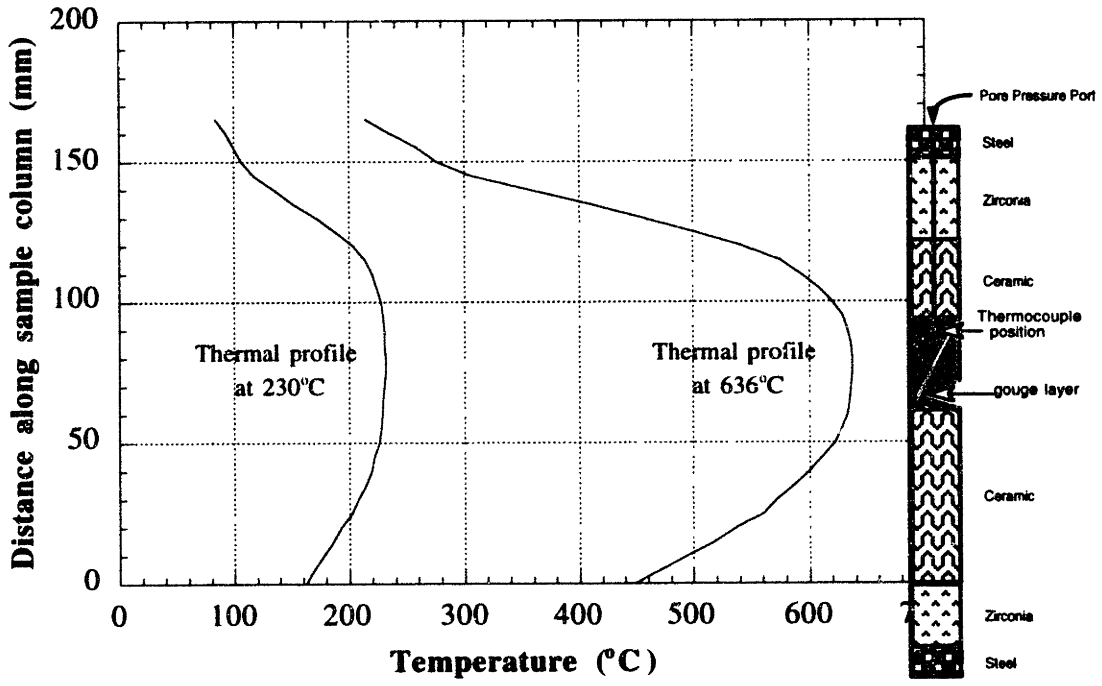

Figure 4.1. Sample column assembly and thermal profiles for fault healing experiments. Typical thermal profiles are shown for 230° C and 636° C. Temperature variations along the sample are < ±5°C. Gouge layers consist of micron-sized quartz powder, are 0.6mm-thick and are oriented 30° to the axis of Sioux quartzite forcing blocks. Ceramic and zirconia spacers minimize axial heat dissipation from the sample.

controller at a rate of ≈10° C per minute (Figure 4.2). Once the heal temperature was reached, the sample remained at that temperature for a predetermined period of time. Temperature was then either decreased (at 10° C per minute) or kept at the healing value, and finally the sample was sheared. At the conclusion of the experiment the system was quenched to room temperature (~ 25° C /min) and unloaded.

Slide-hold-slide experiments: We also performed a limited number of slide-hold-slide experiments. The initial pressurization and heating sequence for these experiments are the same as the hold-slide experiments. However, slide-hold-slide experiments differ from the experiments described above in that samples are sheared immediately upon reaching temperature and healing is initiated later, after the sample has undergone shear. Holds consist of setting the load-point velocity to zero while monitoring load.

4.2.3. Healing time

Reaction rates of a quartz-water system increase considerably with increasing temperature [*Rimstedt and Barnes*, 1980] and this relationship must be considered in high temperature laboratory studies involving time-dependent phenomenon. Available geochemical data are not sufficient to quantitatively address this issue for the pressure-temperature conditions of this study. However, we can approximate the effect of increased reactivity during the time required to reach a given temperature by calculating an equivalent time at temperature using linear weighting and include both heating and cooling (T_{up} and T_{dn}, respectively):

$$t_{equiv} = t_h + \frac{1}{636^\circ C} \int_{t(400^\circ C)}^{t(636^\circ C)} T_{up}(t)\ dt + \frac{1}{636^\circ C} \int_{t(636^\circ C)}^{t(400^\circ C)} T_{dn}(t)\ dt \qquad (4.1)$$

where T is temperature and t is time. The ramp-equivalent times were added to the actual hold-times at 636° C (t_h) and the resulting times are used below. This approximation can be improved by incorporating quantitative results from detailed kinetic studies at elevated temperatures and pressures.

Experiment	Healing temperature (°C)	Deformation temperature (°C)	Time of healing at T_h (sec)	Experiment type
S01	636	230	3600	hold-slide
S02	636	636	3600	hold-slide
S03	636	636	10000	hold-slide
S04	636	636	300	hold-slide
S05	636	230	10000	hold-slide
S06	636	230	300	hold-slide
S07	636	636	0	hold-slide
S07L	636	636	60 and 600	slide-hold-slide
S08	230	230	0	hold-slide
S09L	636	636	600	slide-hold-slide
S10	450	250	3600	hold-slide
S11L	636	636	60	slide-hold-slide
S12	636	230	100000	hold-slide
S15	636	230	100000	hold-slide
S16	636	230	100000	hold-slide
S17	636	636	100000	hold-slide
S18	636	230	3600	hold-slide
S19L	636	636	600 and 6000	slide-hold-slide
S20	636	636	3600	hold-slide
S23	600	600	3600	hold-slide
S24	600	600	3600	hold-slide
S25	600	600	3600	hold-slide
S26	636	636	100000	hold-slide
S27	636	636	100000	hold-slide
S28	600	600	36000	hold-slide
S29	600	600	0	hold-slide
S30	600	600	0	hold-slide
S31	600	600	0	hold-slide
S32	600	600	3600	hold-slide
S33	636	230	36000	hold-slide
S34L	600	600	60000	slide-hold-slide
S35L	600	600	60 and 600	slide-hold-slide
S36L	450	450	6000	slide-hold-slide
S37L	450	450	60 and 600	slide-hold-slide
S38	600	600	100000	hold-slide
S39L	250	250	60, 600, 6000	slide-hold-slide
S42L	250	250	60, 600, 3000	slide-hold-slide
S43	350	350	3600	hold-slide
S43L	350	350	60 and 600	slide-hold-slide

Table 4.1. Summary information from the experiments performed for this study. The primary variables include the temperature at which samples were deformed and the time that the samples were healed at the healing temperature.

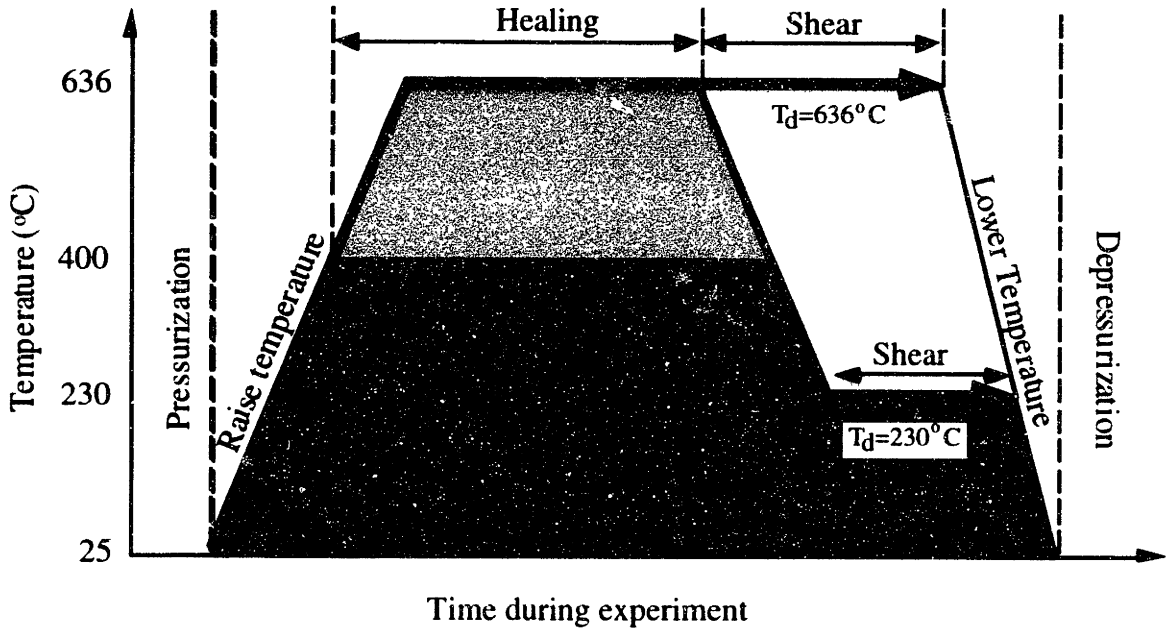

Figure 4.2. Experimental procedure of this study showing pressurization, heating, and "healing", followed by deformation. Heavy lines show paths for two types of "hold-slide" experiments: one in which healing and deformation temperatures are $T_h = T_d = 636°C$ and one in which temperature is reduced prior to deformation ($T_h = 636°C$, $T_d = 230°C$). These two types of experiments were done to assess the individual effects of temperature and lithification. We also report on "slide-hold-slide" experiments in which elevated temperature was maintained during healing under non-hydrostatic stress.

4.3. Results

From the recorded displacement and pressure signals, we calculate shear displacements, shear and normal stresses, and the coefficient of friction resolved onto the fault plane. Displacements reported here were corrected for apparatus stiffness, which is 0.206 MPa/μm when expressed as shear stress per shear displacement. It is important to note that the maximum slip is limited to less than 3 mm owing to jacket perforation and that stable-sliding of some samples was achieved at displacements in excess of 1.5 mm.

Our preliminary analyses of microstructure indicate that gouge layers become well indurated during healing, with significantly increased layer competence relative to the starting material. Layers indicate shear along distinct localized surfaces, including oblique, R_1 Riedel shears and boundary parallel shears.

4.3.1. Hold-Slide Experiments

Figure 4.3 shows data from samples healed at 636° C and deformed at 230° C. Friction data from a representative experiment are shown in Figure 4.3a along with data from a control experiment. The unhealed sample shows displacement hardening prior to shear at a coefficient of friction of roughly 0.6, consistent with results from room temperature experiments under similar conditions [*Marone et al.*, 1990]. Healed samples exhibited a longer period of elastic behavior, followed by yielding and instability (Figure 4.3a). These experiments exhibited a distinct peak stress prior to instability and then a second, lower, yield point followed by stable sliding. Samples did not exhibit repeated stick-slip behavior and the initial peak friction value was always the ultimate strength. We define μ_{ss} as the stable sliding friction measured at 2.0 mm shear displacement.

Both peak frictional strength and μ_{ss} increased with heal time (Figure 4.3). Peak friction increased at a rate of 0.103 ±0.025 per decade increase in hold time and stable-sliding friction increased 0.080 ±0.023 per decade increase in hold time. Experimental reproducibility was assessed for two sets of conditions (Figures 4.3b and 4.3c). These data indicate that reproducibility of the absolute value of friction is ± 0.05, consistent with previous observations (e.g. Figure 2.18 in *Scholz*, 1992).

Figure 4.4 shows data from samples healed and sheared at 636° C. For reference, we show friction displacement data for an "unhealed" layer (Figure 4.4a). In the "unhealed" test, shear began as soon as temperature reached 636° C, and thus the healing time is only that given by the ramp-up time from equation 4.1. Comparison of the data indicates that healing causes increased effective shear modulus and frictional strength (Figure 4.4a).

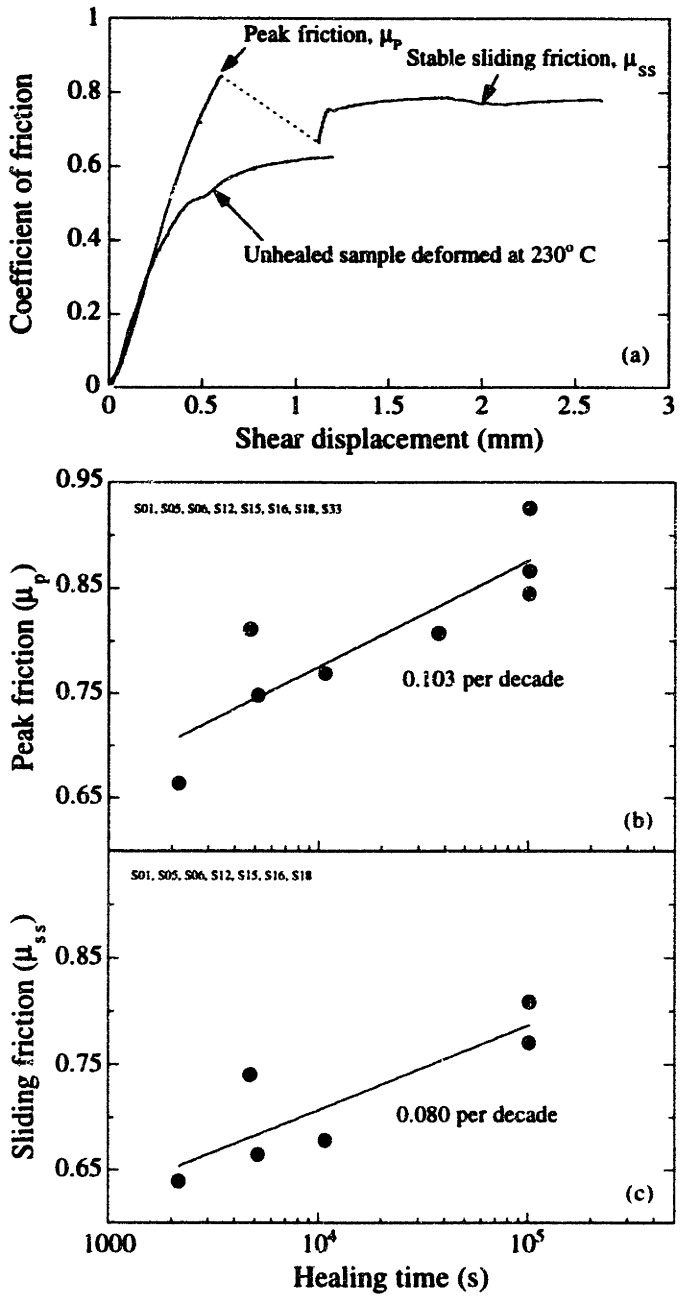

Figure 4.3. Friction data from the hold-slide experiments with T_h=636° C and T_d=230° C. **a)** Data from a representative experiment are shown along with data from a control experiment. **b)** Peak friction values are plotted against heal time for 7 experiments. The best fit log-linear slope is 0.103 ±0.025 per decade increase in time. **c)** Stable sliding friction at 2.0 mm shear displacement, showing increasing frictional strength with heal time. The healing rate is 0.080 ±0.023 per decade increase in time, indicating that the effects of healing and lithification in our experiments are not limited to the peak friction.

In these experiments neither peak friction nor stable sliding friction exhibit a simple relationship with heal time (Figures 4.4b and 4.4c). Peak friction increases at a rate of 0.001 per decade if the full range of heal times are considered (Figure 4.4b). Data for heal times less than 10^5 s indicate possible strengthening (note that the dashed line in Figure 4.4b is shown for reference only). For stable sliding friction, the best-fit line indicates weakening with increasing heal time (Figure 4.4c). However, as we discuss more fully below, the data for $t_h = 10^5$ s may be anomalously low due to sealing and pore pressure buildup within the layer.

4.3.2. Temperature effect on healing rate and peak friction

In Figure 4.5a we show the effect of heal temperature on peak friction. Data are for t_h=3600 s and shear at 230° C, with the exception of one experiment in which deformation occurred at 250° C (see Table 4.1). We also include two data points from *Fredrich and Evans* [1992] who performed experiments under the same conditions (P_c=250 MPa, P_p=75 MPa). The data indicate increasing peak strength with heal temperature, consistent with accelerated lithification and, possibly, enhanced precipitation during cooling prior to shear. For comparison, our data showing the effect of heal time are plotted in Figure 4.5b together with those of *Fredrich and Evans* [1992]. These data clearly demonstrate a temperature effect on healing rate. For experiments with constant heal-time but with heal temperature varying from 450-817° C, peak friction values increase from ~0.59 to 0.88, i.e. peak friction increases ~0.08 per 100° C. When healing time is the only variable, peak friction increases about 0.1 per decade increase in heal-time, indicating the expected trade-off between time and temperature for healing. From these data, a change in T_h of order 120 -140° C would correspond to a decade change in healing time.

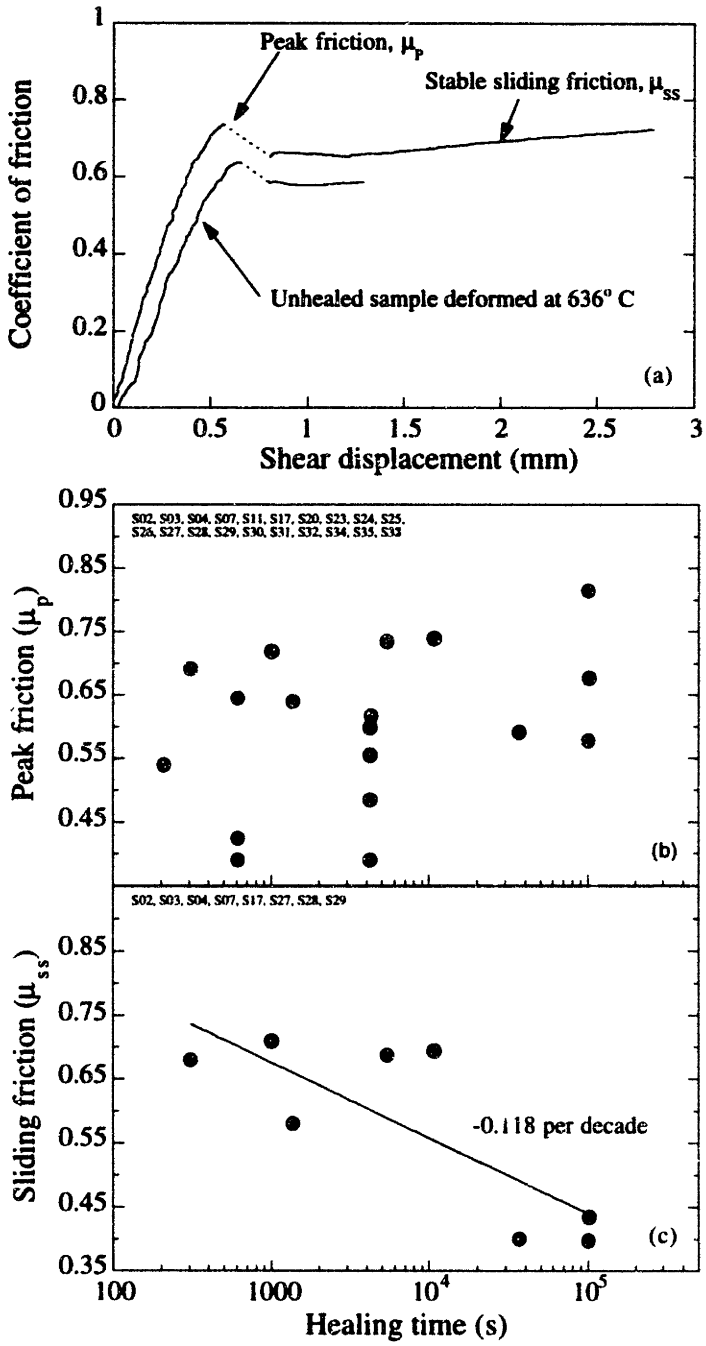

Figure 4.4. Friction data from the hold-slide experiments with $T_h = T_d = 636°$ C. **a)** Data from a representative experiment are shown along with data from a control experiment. **b)** Peak friction values are plotted against heal time for 5 experiments. **c)** Stable sliding friction at 2.0 mm displacement versus hold time. Solid line shows the best fit log linear relation. The experiments with healing time of 10^5 s indicate anomalously low strength, which may be due to pore pressure build-up within the gouge layer.

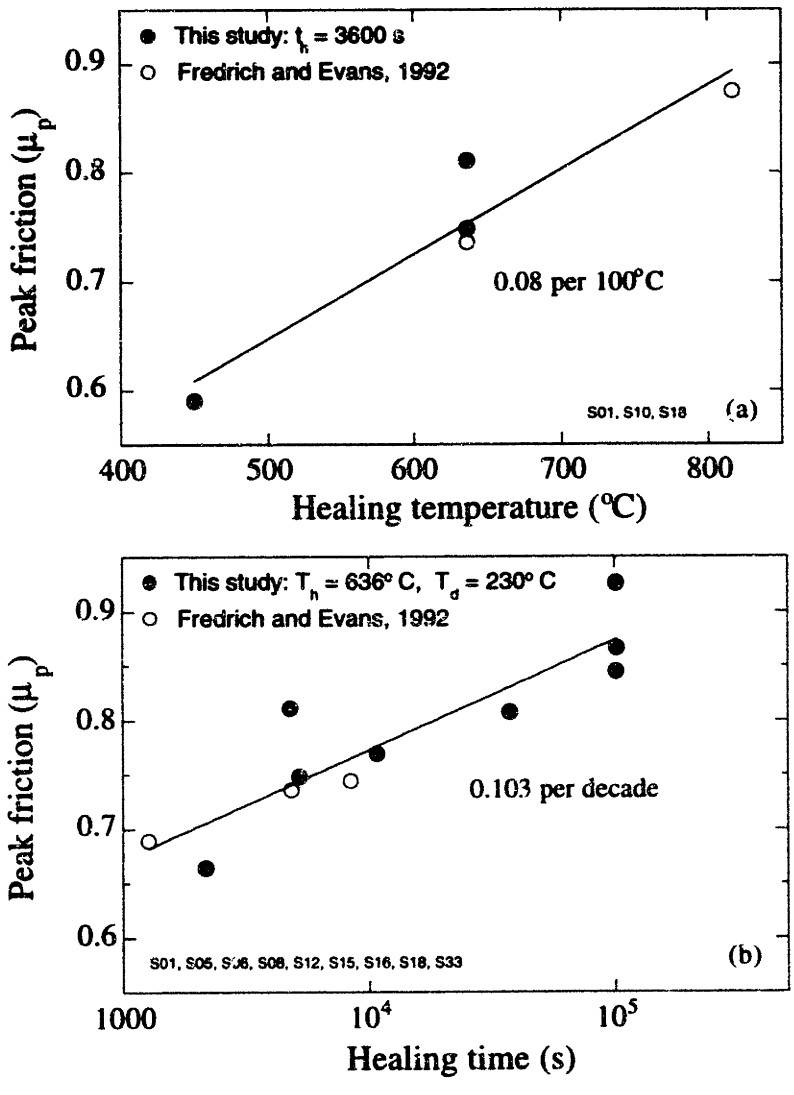

Figure 4.5. Effect of temperature on peak friction for hold-slide experiments. Solid circles are data from this study; open circles are from Fredrich and Evans, 1992. a) Peak friction is plotted versus temperature for heal time of 3600 s. b) Peak friction data for T_d=230° C experiments are plotted. Note that peak friction values of this study are consistent with those of Fredrich and Evans, 1992. Comparison of (a) and (b) indicates a link between temperature and heal time which may result from enhanced reaction rates at elevated temperature.

4.3.3. Slide-hold-slide experiments

In slide-hold-slide tests at high temperature, friction decreased during holds and upon reloading increased to a stable value without exhibiting a peak stress (Figure 4.6a). Thus, these experiments show no time-dependent increase in "static" friction , in contrast with our hold-slide experiments and previous studies at room temperature.

We quantify friction changes in these experiments in two ways: as the difference in steady-state friction before and after the hold (Figure 4.6b), and as the differential reduction in friction during the hold (Figure 4.6c). The data indicate frictional weakening of order -0.01 to -0.02 (corresponding to ~3% decrease in frictional strength), per decade change in hold time.

4.4. Discussion

4.4.1. Hold-slide experiments

The role of temperature in laboratory experiments: The observed positive relation between peak friction and heal temperature (Figure 4.5a) indicates that shear strength is a function of healing rate in our experiments. Increased frictional strength is likely the result of greater consolidation and lithification of the gouge due to enhanced dissolution-precipitation kinetics at higher temperature.

We used a relatively high healing temperature so that experiments could be run in a realistic laboratory time frame (hours to days). Elevated temperatures may be traded for time as long as there are no changes in deformation mechanism or other complexities such as phase changes [*Rutter*, 1983; *Hirth and Tullis*, 1994]. The high healing temperature is justified by the fact that the chemical system used was binary (quartz-water) thereby restricting fluid-rock interaction to a single chemical reaction.

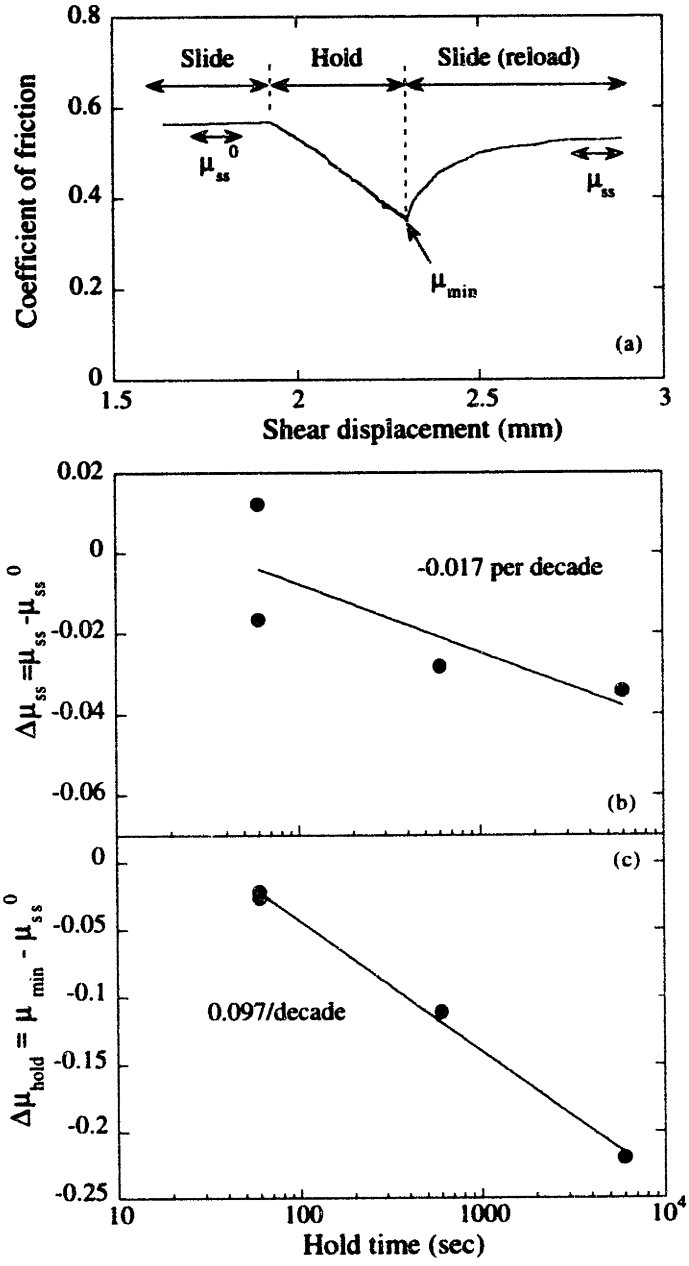

Figure 4.6. Friction data from the slide-hold-slide experiments with $T_h = T_d = 636°$ C. a) Representative data showing stable sliding friction level, μ_{ss}^0, stress relaxation during the hold, and frictional response to reloading. We denote the stable sliding friction level following the hold as μ_{ss}. Note that shear displacement is corrected for elastic unloading and thus indicates slip during the hold. b) The difference between μ_{ss}^0 and μ_{ss} decreases with heal time. c) The difference between the minimum coefficient of friction during the hold (μ_{min}) and μ_{ss}^0 is plotted versus hold time.

Our observation of unstable sliding in the control experiment deformed at high temperature (Figure 4.4) raises an important technical issue for experiments in which temperature is not reached instantaneously. With the nominal heal-time of 0 s in this experiment, it was expected that the sample would slide stably (as for the control experiment at 230° C). However, healing was apparently well underway by the time temperature reached 636° C and thus the sample was already sufficiently lithified to deform unstably.

The effects of temperature on reaction rates: The time necessary to reach chemical equilibrium is important in our experiments. Significant crack-healing of quartz has been observed with increasing temperature (>400° C) for samples saturated with distilled water [*Smith and Evans*, 1984; *Brantley et al.*, 1990]. The increased rates of crack-healing have been attributed to enhanced reactivity with increased temperature. *Rimstedt and Barnes* [1980] determined the degree of saturation, S, for a quartz-water system at time, t, to be:

$$S = 1 - e^{-k_r^* t} \quad where \quad k_r^* = \left(\frac{A}{M}\frac{M_0}{A_0}\right)\gamma_{H_4SiO_4}\, k_r \tag{4.2}$$

Here k_r^* is the apparent precipitation rate constant (sec^{-1}), A is the interfacial area (m^2), M is the mass of water in the system (kg), (M_0/A_0) describes the extent of a standard system (kg/m^2), γ is the activity coefficient and k_r is the precipitation rate coefficient (sec^{-1}). The time constant for the saturation equation is the inverse of the apparent precipitation rate $\left(t_c = 1/k_r^*\right)$, and thus the fluid would reach 99.3% of the equilibrium saturation at time $t=5t_C$. The combination of equation (4.2) with the equilibrium constant and Arrhenius relations gives an expression that describes the temperature dependence of the time taken to reach equilibrium:

$$t = 5t_c = 5e^{\left(E_a/RT\right)}\left[\alpha\, a_{H_4SiO_4}\right]^{-1}\left(M/A\right) \tag{4.3}$$

where E_a is the activation energy, R is the gas constant, T is temperature (°K) and α is a pre-exponential constant.

Using *Rimstedt and Barnes* [1980] kinetic data for fused silica powder less than 140 μm (E_a=49.8 kJ/mol, α=0.1963 and A/M=135) the time taken to reach equilibrium rapidly decreases from 20.5 days to 3.5 days to 1.8 hours as temperature increases from 100 to 200 to 300° C, respectively. Forward extrapolation of their data to 636° C may not be reasonable but an acceptable extrapolation to 400° C gives a time to equilibrium of 20-25 minutes. Thus, in our experiments, the heating time from 400 °C to 636° C (~23.6 min) is of similar order as the time to equilibrium, which explains the need to correct for healing during this time (Equation 4.1).

Hold-slide experiments: A significant goal of these experiments was to isolate the effects of temperature and lithification on healing. Static friction of the samples deformed at 230° C (Figure 4.3b) increases with heal-time as do sliding friction values. For these experiments, time-dependent strengthening may arise from physical compaction of the grains and/or thermally induced solution transfer processes. The healing temperature is sufficiently high for solution-precipitation to play a major role in gouge lithification (e.g. by increasing the "welded" contact area). On the other hand, experiments healed and deformed at high temperature do not indicate increased static friction with heal time.

It may be argued that the relative strengthening observed from the 230° C experiments results from increased precipitation induced by the temperature drop from 636° C to 230° C [*Rimstedt and Barnes*, 1980]. The temperature decrease from 636° C to 230° C would favor precipitation and the rather fast cooling rate (10° C/min) may promote supersaturation of the solution. The net precipitation during the temperature drop would result in an increased cementation of the gouge relative to the samples that remain at 636 ° C. However, as argued in the previous section, our samples likely reach chemical steady-state rapidly at the elevated healing temperature, implying that the amount of silica in solution should plateau with increasing healing time. Thus, increased cementation by silica

precipitation accompanying the temperature drop does not appear to explain the time-dependence of peak friction for samples healed for times longer than ~20-30 minutes.

It may also be argued that the strengthening of the 230° C data could arise from a decrease in pore-pressure locally within the gouge layer that accompanies the decrease in temperature prior to shearing of the samples. This argument would invoke a sealing mechanism that disconnects the gouge pore volume from the pressure generator. If this were to occur, and if we assume a constant initial pore-pressure for each experiment at the end of healing, then the magnitude of the pore-pressure decrease during the temperature drop would remain constant with varying heal time (the magnitude of the temperature decrease being invariant with heal time). Furthermore, sealing of the sample during healing would likely promote increased pore-pressures with increased heal times which should result in decreasing peak friction with heal time.

The difference between the healing rates for 230° C and 636° C experiments hinges on the one long experiment at 636° C. The sliding friction value for this sample (~0.39) is considerably lower than the values for other experiments (~0.6-0.7) and if we consider only the shorter heal time experiments, the trend is in relative agreement with the strengthening rate observed for the experiments at 230° C. While we cannot resolve the issue with the available data, it is plausible that increased pore-pressure due to sealing caused anomalously low friction in this experiment [e.g. *Blanpied et al.*, 1992]. Alternatively, the inclusion of this data point suggests that the peak coefficient of friction does not strengthen significantly with increased heal times. Assuming that the real area of contact increases with increased healing time, then the 636° C data implies that the deformation mechanism does not depend on the contact area in the same way that low temperature data suggests. At this time, this issue has not been resolved and it will be addressed by pore-pressure pulsing experiments in future experiments.

In the lower temperature experiments, sliding friction also increased with heal time (Figure 4.3c). This is a somewhat unexpected result if one takes the view that the initial

peak stress represents failure of the layer and development of a through-going shear plane that accommodates all subsequent slip. However, in a gouge layer of finite thickness, shear deformation is accommodated by slip on a combination of oblique and boundary parallel shears [*Marone et al.*, 1990; *Scott et al.*, 1994; *Beeler et al.*, 1996]. Since geometric constraints limit the net slip that can be accommodated on a given oblique shear surface these must form quasi-continuously during shear. Thus, our observation of increased stable sliding friction with heal time is consistent with increased layer strength and higher friction needed to initiate oblique shear. Although this effect is a function of the boundary conditions for shear, it is a reproducible, systematic effect in the experiments and one that can be exploited to investigate gouge microstructure. Since this effect involves lithification and longer term friction memory it may be particularly important for fault models that invoke deep-seated crustal fluid flow as the mechanism for determining fault frictional behavior [e.g. *Rice*, 1992].

4.4.2. Slide-hold-slide experiments

In slide-hold-slide experiments, friction relaxes during holds and "static" friction (as measured by the differential increase in friction with hold time) decreases with increasing hold time (Figure 4.6). The experiments differ significantly from "hold-slide" tests, which shows a distinct peak stress and unstable sliding. These friction characteristics are likely the result of differences in load conditions during healing. In slide-hold-slide experiments, samples are subjected to a relaxing shear load. Hence, the gouge layer creeps during healing, possibly by solution transfer, thereby inhibiting lithification and cementation. This indicates that the porosity and frictional state of the gouge layer is continuously altered during the hold stage. The state of the gouge (and hence, friction) may change in at least two ways. First, shear-enhanced compaction of the gouge may reduce gouge permeability and, in turn, increase pore pressure. This would be a time-dependent process resulting in

decreased friction with time. Second, the real contact area of the gouge may not increase with hold time as the gouge is shearing during the hold.

4.4.3. Constitutive Modeling of slide-hold-slide experiments

For comparison with previous studies and to assess the internal consistency of our slide-hold-slide data, we modeled friction data using rate- and state-dependent friction constitutive laws coupled to an equation describing elastic interactions with the experimental apparatus. We used the "slip" [*Ruina*, 1983] and "slowness" [*Dieterich*, 1979] versions of the laws [see *Beeler et al.*, 1994 for a recent summary] and the hybrid law suggested by *Perrin, Rice and Zheng* [1995]. Two approaches were used (Figure 4.7). In the first, we modeled friction data from slide-hold-slide tests (Figure 4.7a). Then, using these values of the constitutive parameters, we computed minimum friction values as a function of hold time for comparison with our measurements (Figure 4.7b).

In Figure 4.7a we show results of inverting the friction-time data for individual slide-hold-slide tests. These were done using an iterative, least-squares method similar to that described by *Reinen and Weeks* [1993]. The model calculates frictional relaxation during the hold and the effect of reloading. For relatively short duration holds (the upper data set of Figure 4.7a) each of the laws produces a reasonable fit. For longer hold times, the Ruina law fits least well, with relaxation decaying too quickly near the end of the hold and restrengthening occurring too quickly upon reloading. Table 4.2 gives the best fit parameters and error estimates for the data of Figure 4.7a. For each of the laws, a reasonable fit could only be obtained if the state evolution parameter b was negative. Models with $b>0$ result in significant strengthening and a distinct peak stress upon reloading, and these features are not observed in the data.

Models using two state variables were also used to determine if a shorter displacement positive b effect could be present. These models converge to degenerate one state-variable models with $D_{c1} \approx D_{c2}$. Since slip is negligible during the holds, the critical slip distance

is poorly resolved. However, our modeling indicates that a short evolution-distance, positive b term can only be present if a large negative b_2 term exists with similar evolution distance. Otherwise we would see the b_1 effect during reloading.

We also compared data (Figure 4.6c) with predictions based on model inversions of individual tests (Figure 4.7b). For these comparisons, numerical simulations of slide-hold-slide tests were carried out using two approaches. 1) Constitutive parameters were obtained by averaging the values for model fits to individual tests (Figure 4.7a). 2) Constitutive parameters from inversion of the longest hold increment were used. The predicted fits (Figure 4.7b) show that minimum friction decreases at -0.105 (for the averaged friction parameters) and -0.092 (parameters from inversion of the long hold) per decade change in hold time. These are consistent with the data (Figure 4.6c).

This modeling exercise indicates that measurements of minimum friction, rather than peak or static friction, may also be used to determine friction constitutive parameters. At temperatures in the range of 600°C our data indicate that friction exhibits velocity strengthening (a-b=0.05-0.1) with negative state evolution parameter b (Table 4.2) and thus measurements of minimum friction reached during a hold are more reliable than peak friction.

4.4.4. Comparison with other hydrothermal experimental data

Our slide-hold-slide tests show similar relaxation rates to those obtained by *Chester and Higgs* [1992] at 600° C. *Chester and Higgs* [1992] interpreted their data using a constitutive model that added temperature to the existing friction constitutive laws. The model fit their observation of velocity weakening up to 300° C and velocity strengthening at 600° C. Our modeling indicates negative state evolution values based on the absence of a peak friction value upon reloading. This is consistent with *Chester and Higg's* [1992] data at 600°C (their Figure 8), who also found velocity strengthening at this temperature,

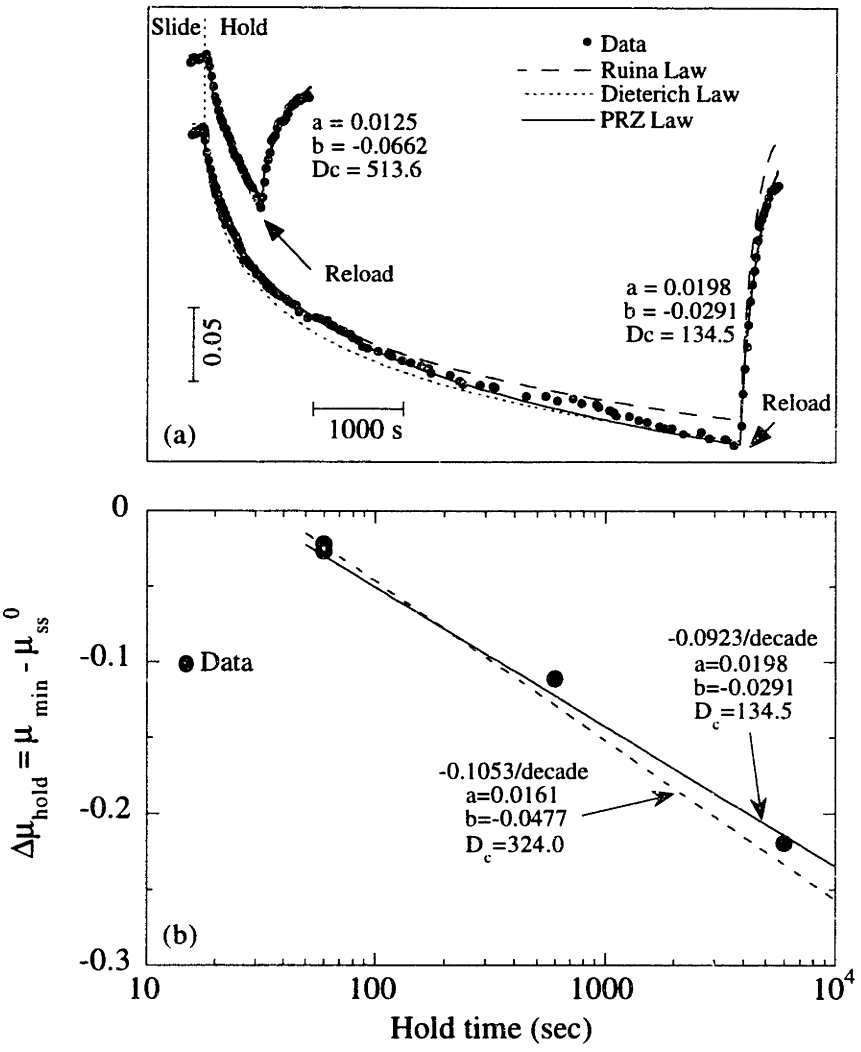

Figure 4.7. Friction data from the slide-hold-slide experiments are shown together with modeled fits. a) Friction-time data for two tests are shown with model inversions determined from a least-squares inversion. Note that the inversion using the Ruina law underpredicts the minimum value of friction at the end of the 6000 s hold while the Dieterich and Perrin-Rice-Zheng laws give reasonable fits to the data. b) Constitutive parameters determined in (a) for the Dieterich law were used to predict the minimum friction value as a function of hold time and are compared with experimental data (from Figure 4.6c). Two sets of values were used in the modeling. The dashed line shows the model fit using the average values of a, b, and D_c determined from the inversions. The solid line shows the model fit for the a, b, D_c values from the inversion of the long hold. The slopes of these model fits are within the standard deviation of the best-fit slope to the data.

Hold time (s)	Law	μ_{ss}^0	μ_{ss}^0 std ($x10^{-4}$)	a ($x10^{-2}$)	a std ($x10^{-4}$)	b ($x10^{-2}$)	b std ($x10^{-4}$)	D_c μm	D_c std μm	a-b ($x10^{-2}$)
600	r	0.5972	1.8	1.19	1.5	-13.44	11.1	510.6	6.5	14.63
	d	0.5978	1.8	1.25	1.7	-6.63	4.2	513.6	7.2	7.87
	p-r-z	0.5970	1.6	1.26	1.5	-10.10	6.4	587.7	7.1	11.36
6000	r	0.5672	3.2	1.75	5.1	-4.81	5.5	226.6	8.6	6.56
	d	0.5712	5.6	1.98	9.0	-2.91	8.8	134.5	8.6	4.89
	p-r-z	0.5664	2.9	1.54	6.1	-4.58	5.2	286.9		6.12

Table 4.2. Friction constitutive parameters and standard deviations (std) determined from least squares inversions of the Ruina (r), Dieterich (d), and Perrin-Rice-Zheng (p-r-z) constitutive laws. μ_{ss}, μ_{min} and μ_{ss} relate to the pre-hold, end of hold, and reload friction values (e.g. as in Figure 4.7) and a, b, and D_c are the determined rate-state friction parameters.

although they report a positive *b* value. They report only one experiment at 600°C and they did not carry out detailed numerical inversions of the data, thus it is difficult to assess the discrepancy. It may be due to differences in the friction law or to large uncertainties in their values of *b*. Velocity stepping experiments done under similar conditions on crushed granite show two-state variable behavior with large negative b2 values [*Blanpied et al.*, 1996] and thus we favor the interpretation that the effective friction state evolution parameter is negative at temperatures of about 600°C.

Our hold-slide experiments at 230°C show time-dependent strengthening, which implies positive *b* values and velocity weakening of similar magnitude to that reported by others [*Rutter and Maddock*, 1992; *Fredrich and Evans*, 1992; *Blanpied et al.*, 1995]. *Rutter and Maddock* [1992] sheared quartz-kaolinite and Tennessee sandstone gouges at temperatures of 400° -600° C and obtained relative magnitudes and rates of strengthening that are in good agreement with the data from this study. At higher temperature, our hold-slide experiments indicate a lack of time-dependent strengthening. Taken together with the

data from slide-hold-slide experiments, our data indicate a significant difference between frictional healing under hydrostatic load and healing under shear load, as has been noted recently in room temperature experiments [*Nakatani and Mochizuki*, 1996].

4.4.5. Comparison of laboratory analyses to seismic observations

Seismic data from large interplate and intraplate earthquakes and detailed studies of small plate boundary events indicate that earthquake stress drop increases with waiting time between events [*Kanamori and Anderson*, 1975; *Scholz et al.*, 1986; *Vidale et al.*, 1994; *Marone et al.*, 1995]. Furthermore, interplate faults exhibit a distinct upper stability transition, marked by a lack of seismicity above 3-5 km, whereas intraplate faults exhibit shallow seismicity and no upper stability transition [*Marone and Scholz*, 1988]. These observations are consistent with our laboratory data, which indicate healing and time-dependent frictional strengthening. In nature, the upper stability transition is likely the result of a balance between production of fault gouge via wear and healing via lithification and cementation. The latter involve thermally activated processes (chemical alteration of minerals, porosity-permeability variations, fracture sealing) and thus should prevail at temperatures above a critical value. Since the rate of gouge production is proportional to slip rate, the upper stability transition depth is expected to vary inversely with fault slip rate, as indicated by the seismic observations [*Marone and Scholz*, 1988]. These inferences are also consistent with field observations, in the sense that intraplate faults typically have negligible active gouge zones and little surface expression.

The seismic data also indicate that earthquake stress drop increases by 1-4 MPa per decade change of earthquake recurrence interval [*Kanamori and Allen*, 1986; *Marone et al.*, 1995]. These values represent changes of a factor of 2-5 per decade change in time, and thus previous investigators have argued that the rate of fault healing is significantly greater than laboratory measurements of the rate of frictional strengthening [*Kanamori and Allen*, 1986; *Scholz et al.*, 1986; *Wong and Zhao*, 1990]. However, these arguments are based

on comparing the rate of stress drop change with the absolute rate of friction change, ≈0.02 per decade or 2-3% of its absolute value. Since stress drop represents a differential change, the frictional healing values should be cast as a fraction of the expected friction drop. Taking a nominal stress drop of 10% of the absolute shear stress, the laboratory healing rates would indicate a 30-50% increase in stress drop per decade increase in heal time. Moreover, one may compare the expected strength changes directly. Assuming a nominal effective lithostatic gradient of 15 MPa/km, a fault at 8km would have an effective normal stress of 120 MPa. From the seismic estimates of stress drop change, this implies friction change of order 0.01-0.04 per decade change in earthquake recurrence time, in reasonable agreement with the laboratory values from our experiments and from those at room temperature.

4.5. Summary

Our data from the hold-slide experiments show that the frictional strength of quartz gouge increases with both temperature and heal-time. Data from experiments in which deformation was carried out at a lower temperature than healing show frictional strengthening rates of approximately 0.1 per decade change in hold time. We interpret this high rate of strengthening as the result of enhanced rates of lithification at elevated temperature and pressure, possibly due to solution-transfer mechanisms. Data from higher-temperature experiments, in which healing and deformation were carried out at 636°C show lower values of absolute strength compared to those deformed at lower temperature. Furthermore, the former do not display a significant time-dependent healing. The data presented show that when deformation is carried out at a lower temperature than healing, frictional strength increases with heal temperature. This indicates that temperature may be traded for time in laboratory studies of fault healing. The data indicate that time-dependent frictional strengthening is not limited to peak strength, since sliding friction also increases with heal time. Our data show that frictional strengthening varies significantly

between the hold-slide and slide-hold-slide experiments. Lower peak strengths and rates of healing for the latter tests may indicate that simultaneous deformation and growth of intergranular cements, via solution transfer mechanisms, inhibits lithification and frictional strengthening.

LIST OF REFERENCES

Chapter 2

Baumberger, T., Heslot, F., and Perrin, B., Crossover from creep to inertial motion in friction dynamics, *Nature*, 367, 544-546, 1994.

Beeler, N.M., Tullis, T.E., and Weeks, J.D, The roles of time and displacement in the evolution effect in rock friction, *Geophys. Res. Lett.*, 21, 1987-1990, 1994.

Beeler, N.M., Tullis, T.E., and Weeks, J.D, Frictional behavior of large displacement experimental faults, *J. Geophys. Res.*, 101, 8697-8715, 1996.

Berman, A.D., Ducker, W.A., and Israelachvili, J.N., Experimental and theoretical investigations of stick-slip friction mechanisms, **IN**: PHYSICS OF SLIDING FRICTION, Eds. B.N.J. Perrson and E. Tossatti, Kluwer Academic Publ., Netherlands, 1996.

Brace, W.F., and Byerlee, J.D., Stick-slip as a mechanism for earthquakes, *Science*, 153, 990-992, 1966.

Brace, W.F., Laboratory studies of stick-slip and their application to earthquakes, *Tectonophys.*, 14, 189-200, 1972.

Brace, W.F., Experimental studies of seismic behavior of rocks under crustal conditions, *Engin. Geology*, 8, 109-127, 1974.

Byerlee, J.D., Frictional characteristics of granite under high confining pressure, *J. Geophys. Res.*, 72, 3639-3648, 1967.

Byerlee, J.D., and Brace, W.F., Stick-slip, stable sliding, and earthquakes - Effect of rock type, pressure, strain rate, and stiffness, *J. Geophys. Res.*, 73, 6031-6037, 1968.

Cao, T., and Aki, K., Effect of slip rate on stress drop, *Pageoph.*, 515-529, 1986.

Chester, F.M., and Higgs, N.G., Multimechanism friction constitutive model for ultrafine quartz gouge at hypocentral conditions, *J. Geophys. Res.*, 97, 1857-1870, 1992.

Dieterich, J.H., Time-dependent friction in rocks, *J. Geophys. Res.*, 77, 3690-3697, 1972.

Dieterich, J.H., Time-dependent friction and the mechanics of stick-slip, *Pure Appl. Geophys.*, 116, 790-805, 1978.

Engelder, J.T., Logan, J.M., and Handin, The sliding characteristics of sandstone on quartz fault-gouge, *Pageoph.*, 113, 69-86, 1975.

Engelder, J.T., and Scholz, C.H., The role of asperity indentation and ploughing in rock friction II, *Int. J. Rock Mech. Mining Sci. Geomech. Abstr., 13, 155-163, 1976.*, 113, 69-86, 1976.

Fredrich, J.T., and Evans, B., Strength recovery along simulated faults by solution transfer processes, *Proc. 33rd Nat.l. Rock Mech. Symp.*, ed. W. Wawersik, 121-130, Rotterdam: Balkema, 1992.

Heslot, F., Baumberger, T., Perrin, B., Caroli, B., and Caroli, C., Creep, stick-slip, and dry-friction dynamics: Experiments and a heuristic model, *Pys. Rev. E*, 49, 4973-4988, 1994.

Johnson, T., Time dependent friction in granite: implication for precursory slip on faults, *J. Geophys. Res.*, 86, 6017-6028, 1981.

Johnson, T.L., and Scholz, C.H., Dynamic properties of stick-slip friction of rocks, *J. Geophys. Res.*, 81, 881-889, 1976.

Kanamori, H., and Allen, C.R., Earthquake repeat time and average stress drop, IN: *AGU Geophys. Mono. Vol. 37*, Eds. S. Das, J. Boatwright and C.H. Scholz, 227-236, 1986.

Karner, S.L., and Marone, C., The effect of shear load on frictional healing in simulated fault gouge, *Geophys. Res. Lett.*, 25, 4561-4564, 1998.

Karner, S.L., Marone, C., and Evans, B., Laboratory study of fault healing and lithification in simulated fault gouge under hydrothermal conditions, *Tectonophysics*, 277, 41-55, 1997.

Li, Y-g, Vidale, J.G, Aki, K., Xu, F., and Burdette, T., Evidence of shallow fault zone strengthening after the 1992 M7.5 Landers, California, earthquake, *Science*, 279, 217-220, 1998.

Linker, M.F., and Dieterich, J.H., Effects of variable normal stress on rock friction: observations and constitutive equations, *J. Geophys. Res.*, 97, 4923-4940, 1992.

Mair, K., and Marone, C., Friction and shear heating of simulated fault gouge at high velocity and variable normal stress, submitted to *J. Geophys. Res.*, 1998.

Marone, C., The effect of loading rate on static friction and the rate of fault healing during the earthquake cycle, *Nature*, 391, 69-72, 1998.

Marone, C., and Kilgore, B., Scaling of the critical slip distance for seismic faulting with shear strain in fault zones, *Nature*, 362, 618-621, 1993.

Marone, C., Vidale, J.E., and Ellsworth, W., Fault healing inferred from time dependent variations in source properties of repeating earthquakes, *Geophys. Res. Lett.*, 22, 3095-3098, 1995.

Nakatani, M., A new mechanism of slip-weakening and strength recovery of friction associated with the mechanical consolidation of gouge, *J. Geophys. Res.*, 103, 27239-27256, 1998.

Nakatani, M., and Mochizuki, H., Effects of shear stress applied to surface in stationary contact on rock friction, *Geophys. Res. Lett.*, 23, 869-872, 1996.

Nasuno, S., Kudrolli, A., Bak, A., and Gollub, J.P., Time-resolved studies of stick-slip friction in sheared granular layers, *Pys. Rev. E*, 58, 2161-2171, 1998.

Ohnaka, M., Experimental studies of stick-slip and their application to the earthquake source mechanism, *J. Phys. Earth*, 21, 285-303, 1973.

Rabinowicz, E., The intrinsic variables affecting the stick-slip process, *Proc. Phys. Soc. London*, 71, 668-675, 1958.

Richardson, E., and Marone, C., Effects of normal force vibrations on frictional healing, submitted to *J. Geophys. Res.*, 1998.

Roy, M., and Marone, C., Earthquake nucleation on model faults with rate and state dependent friction: the effects of inertia, *J. Geophys. Res.*, 101, 13919-13932, 1996.

Scholz, C.H., Earthquakes and friction laws, *Nature*, 391, 37-42, 1998.

Scholz, C., Molnar, P., and Johnson, T., Detailed studies of frictional sliding and implications for the earthquake mechanism, *J. Geophys. Res.*, 77, 6392-6406, 1972.

Shimamoto, T., and Logan, J.M., Effects of simulated fault gouge on the sliding behavior of Tennessee sandstone: nonclay gouges, *J. Geophys. Res.*, 86, 2902-2914, 1981.

Teufel, L.W., and Logan, J.M., Effect of displacement rate on the real area of contact and temperature generated during frictional sliding of Tennessee sandstone, *Pageoph.*, 116, 840-872, 1978.

Wong, T-f., and Zhao, Y., Effects of loadpoint velocity on frictional instability behavior, *Tectonophys.*, 175, 177-195, 1990.

Chapter 3

Aharonov, E., Tenthorey, E., and Scholz, C.H., Precipitation sealing and diagenesis 2. Theoretical analysis, *J. Geophys. Res.*, 103, 23969-23981, 1998.

Antonellini, M.A., Aydin, A., and Pollard, D.D., Microstructure of deformation bands in porous sandstones at Arches National Park, Utah, *J. Struct. Geol.*, 16, 941-959, 1994.

Ball, R.C., and Melrose, J.R., Lubrication breakdown in hydrodynamic simulations of concentrated colloids, *Adv. Colloid Interface Sci.*, 59, 19, 1995.

Baumberger, T., Berthoud, P., and Caroli, C., Physical analysis of the rate- and state-dependent friction law: II. Dynamic friction, submitted to Phys. Rev B., 1999.

Beeler, N.M., Tullis, T.E., and Weeks, J.D., The roles of time and displacement in the evolution effect in rock friction, *Geophys. Res. Lett.*, 21, 1987-1990, 1994.

Beeler, N.M., Tullis, T.E., and Weeks, J.D, Frictional behavior of large displacement experimental faults, *J. Geophys. Res.*, 101, 8697-8715, 1996.

Berthoud, P., Baumberger, T., G'Sell, C., and Hiver, J.-M., State- and rate- dependent friction at multicontact surfaces: I. Static friction, submitted to Phys. Rev B., 1999.

Biegel, R.L., Sammis, C.S, and Dieterich, J.H., The frictional properties of a simulated gouge having a fractal particle distribution, *J. Struct. Geol.*, 11, 827-846, 1989.

Blanpied, M.L., Lockner, D.A., and Byerlee, J.D., Fault stability inferred from granite sliding experiments at hydrothermal conditions, *Geophys. Res. Lett.*, 18, 609-612, 1991.

Byerlee, J.D., Frictional characteristics of granite under high confining pressure, *J. Geophys. Res.*, 72, 3639-3648, 1967.

Cates, M.E., Wittmer, J.P., Bouchaud, J-P, and Claudin, P., Jamming, force chains, and fragile matter, *Phys. Rev. Lett.*, 81, 1841-1844, 1998.

Chester, F.M., and Higgs, N.G., Multimechanism friction constitutive model for ultrafine quartz gouge at hypocentral conditions, *J. Geophys. Res.*, 97, 1857-1870, 1992.

Chester, F.M., and Logan, J.M., Composite planar fabric of gouge from the Punchbowl Fault, California, *J. Struct. Geol.*, 9, 621-634, 1989.

Dieterich, J.H., Time-dependent friction in rocks, *J. Geophys. Res.*, 77, 3690-3697, 1972.

Dieterich, J.H., Time-dependent friction and the mechanics of stick-slip, *Pure Appl. Geophys.*, 116, 790-805, 1978.

Dieterich, J.H., Modeling of rock friction 1: Experimental results and constitutive equations, *J. Geophys. Res.*, 84, 2161-2168, 1979.

Dieterich, J. and Conrad, G., Effect of humidity on time- and velocity-dependent friction in rocks, *J. Geophys. Res.*, 89, 4196-4202, 1984.

Farr, R.S., Melrose, J.R., and Ball, R.C, Kinetic theory in hard-sphere startup flows, *Phys. Rev. E*, 55, 7203-7211, 1997.

Fredrich, J.T., Evans, B., Strength recovery along simulated faults by solution transfer processes, *Proc. 33rd Natl. Rock Mech. Symp.*, ed. W. Wawersik, 121-130, Rotterdam: Balkema, 1992.

Géminard, J.-C., Losert, W., and Gollub, J.P., Frictional mechanics of wet granular material, submitted to Phys. Rev. E, 1998.

Heslot, F., Baumberger, T., Perrin, B., Caroli, B., and Caroli, C., Creep, stick-slip, and dry-friction dynamics: Experiments and a heuristic model, *Pys. Rev. E*, 49, 4973-4988, 1994.

Karner, S.L., and Marone, C., The effect of shear load on frictional healing in simulated fault gouge, *Geophys. Res. Lett.*, 25, 4561-4564, 1998.

Karner, S.L., Marone, C., and Evans, B., Laboratory study of fault healing and lithification in simulated fault gouge under hydrothermal conditions, *Tectonophysics*, 277, 41-55, 1997.

Karner, S.L. and Schreiber, B.C., Experimental simulation of plagioclase diagenesis at P-T conditions of 3.5 km burial depth, *Pure Appl. Geophys.*, 141, 221-247, 1993.

Linker, M.F., and Dieterich, J.H., Effects of variable normal stress on rock friction: observations and constitutive equations, *J. Geophys. Res.*, 97, 4923-4940, 1992.

Liu, A.J., and Nagel, S.R., Jamming is not just cool any more, *Nature*, 396, 21-22, 1998.

Lockner, D.A., Summers, R., and Byerlee, J.D., Effects of sliding rate and temperature on frictional strength of granite, *Pure Appl. Geophys.*, 124, 445-469, 1986.

Logan, J.M., Dengo, C.A., Higgs, N.G., and Wang, Z.Z., Fabrics of experimental fault zones: their development and relationship to mechanical behavior, IN: Fault Mechanics and Transport Properties of Rocks, Eds. B. Evans and T-f Wong, Academic Press: London, 33-67, 1992.

Mair, K., and Marone, C., Friction and shear heating of simulated fault gouge at high velocity and variable normal stress, submitted to *J. Geophys. Res.*, 1998.

Marone, C., The effect of loading rate on static friction and the rate of fault healing during the earthquake cycle, *Nature*, 391, 69-72, 1998a.

Marone, C., Laboratory derived friction laws and their application to seismic faulting, *Annu. Rev. Earth Planet. Sci.*, 26, 643-696, 1998b.

Marone, C., and Kilgore, B., Scaling of the critical slip distance for seismic faulting with shear strain in fault zones, *Nature*, 362, 618-621, 1993.

Marone, C., and Scholz, C.H., The depth of seismic faulting and the upper transition from stable to unstable slip regimes, *Geophys. Res. Lett.*, 15, 621-624, 1988.

Marone, C., and Scholz, C.H., Particle-size distribution and microstructures within simulated fault gouge, *J. Struct. Geol.*, 11, 799-714, 1989.

Marone, C., Raleigh, C.B., and Scholz, C.H., Frictional behavior and constitutive modeling of simulated fault gouge, *J. Geophys. Res.*, 95, 7007-7025, 1990.

Morgan, J.K., Numerical simulations of granular shear zones using the distinct element method, 2: Effects of particle size distribution and interparticle friction on mechanical behavior, *J. Geophys. Res.*, 104, 2721-2732, 1998.

Morgan, J.K., and Boettcher, M.S., Numerical simulations of granular shear zones using the distinct element method, 1: Shear zone kinematics and the micromechanics of localization, *J. Geophys. Res.*, 104, 2703-2719, 1998.

Morrow, C.A., and Byerlee, J.D., Experimental studies of compaction and dilatancy during frictional sliding on faults containing gouge, *J. Struct. Geol.*, 11, 815-825, 1989.

Nakatani, M., A new mechanism of slip-weakening and strength recovery of friction associated with the mechanical consolidation of gouge, *J. Geophys. Res.*, 103, 27239-27257, 1998.

Nakatani, M., and Mochizuki, H., Effects of shear stress applied to surface in stationary contact on rock friction, *Geophys. Res. Lett.*, 23, 869-872, 1996.

Nasuno, S., Kudrolli, A., and Gollub, J.P., Friction in granular layers: Hysteresis and Precursors, *Pys. Rev. Lett.*, 79, 949-952, 1997.

Nasuno, S., Kudrolli, A., Bak, A., and Gollub, J.P., Time-resolved studies of stick-slip friction in sheared granular layers, *Pys. Rev. E*, 58, 2161-2171, 1998.

Oda, M., A micro-deformation model for dilatancy of granular materials, IN: *Mechanics of Deformation and Flow of Particulate Materials*, eds. C.S. Chang, A. Misra, R.Y. Liang, and M. Babic, 24-37, Am. Soc. of Civil Engineers: New York, 1997.

Olsen, M.P., Scholz, C.H., and Léger, A., Healing and sealing of a simulated fault gouge under hydrothermal conditions: Implications for fault healing, *J. Geophys. Res.*, 103,7421-7430, 1998.

Perrin, G., Rice, J.R., and Zheng, G., Self-healing slip pulse on a frictional surface, *J. Mech. Phys. Solids*, 43, 1461-1495, 1995.

Rice, J.R. and Ben-Zion, Y., Slip complexity in earthquake fault models, Proc. Natl. Acad. Sci. USA, 93, 3811, 1996.

Richardson, E., and Marone, C., Effects of normal force vibrations on frictional healing, submitted to *J. Geophys. Res.*, 1998.

Ruina, A., Slip instability and state variable friction laws, *J. Geophys. Res.*, 88, 10359-10370, 1983.

Scholz, C.H., War and gouge formation in brittle faulting, *Geology*, 15, 493-495, 1987.

Scholz, C.H., The Mechanics of Earthquakes and Faulting, Cambridge University Press, New York, 1992.

Scholz, C.H., Earthquakes and friction laws, *Nature*, 391, 37-42, 1998.

Scholz, C.H., Léger, and Karner, S.L., Experimental diagenesis: Exploratory results, *Geophys. Res. Lett.*, 22, 719-722, 1995.

Scott, D.R., Marone, C., and Sammis, C.G., The apparent friction of granular fault gouge in sheared layers, *J. Geophys. Res.*, 99, 7231-7246, 1994.

Segall, P., and Rice, J.R., Dilatancy, compaction, and slip instability of a fluid infiltrated fault, *J. Geophys. Res.*, 100, 22155-22171, 1995.

Sleep, N.H., Ductile creep, compaction, and rate and state dependent friction within major fault zones, *J. Geophys. Res.*, 100, 13065-13080, 1995.

Stacey, F.D., PHYSICS OF THE EARTH, 3rd ed., Brookfield Press: Brisbane, 1992.

Tenthorey, E., Scholz, C.H., and Aharonov, E., Precipitation sealing and diagenesis 1. Experimental results, *J. Geophys. Res.*, 103, 23951-23967, 1998.

Williams, J., and Rege, N., Granular vortices and shear band formation, IN: *Mechanics of Deformation and Flow of Particulate Materials*, eds. C.S. Chang, A. Misra, R.Y. Liang, and M. Babic, 62-76, Am. Soc. of Civil Engineers: New York, 1997.

Chapter 4

Angevine, C.L., Turcotte, D.L. and Furnish, M.D., Pressure solution lithification as a mechanism for the stick-slip behavior of faults, *Tectonics*, 1 (2): 151-160, 1982.

Beeler, N.M., Tullis, T.E. and Weeks, J.D., The roles of time and displacement in the evolution effect in rock friction. *Geophys. Res. Lett.*, 21 (18): 1987-1990, 1994.

Beeler, N.M., Tullis, T.E., Blanpied, M.L., and Weeks, J.D., Frictional behavior of large displacement experimental faults. *J. Geophys. Res.*, 101 (B4): 8697-8715, 1996.

Blanpied, M. L., Lockner, D. A., and J. D. Byerlee, An earthquake mechanism based on rapid sealing of faults, *Nature*, 358: 574-576, 1992.

Blanpied, M.L., Lockner, D.A., and Byerlee, J.D., Frictional slip of granite at hydrothermal conditions. *J. Geophys. Res.*, 100 (B7): 13045-13064, 1995.

Blanpied, M.L., Marone, C.J., Lockner, D.A., and Byerlee, J.D., and King, D.P., Quantitative measure of the variation in fault rheology. *Manuscript in preparation.*, 1996

Brace, W.F. and Byerlee, J.D., Stick-slip as a mechanism for earthquakes. *Science*, 153: 990-992, 1966.

Brantley, S.L., Evans, B., Hickman, S.H. and Crerar, D.A., Healing of microcracks in quartz: Implications for fluid flow. *Geology*, 18: 136-139, 1990.

Bridgeman, P.W., Shearing phenomena at high pressure of possible importance to geology. *J. Geol.*, 44: 653-669, 1936.

Bridgeman, P.W., Some implications for geophysics of high-pressure phenomena. *Geol. Soc. Am. Bull.*, 62: 533-536, 1951.

Byerlee, J., Mjachkin, V., Summers, R. and Voevoda, O., Structures developed in fault gouge during stable sliding and stick-slip. *Tectonophysics*, 44: 161-171, 1978.

Cao, T. and K. Aki, Effect of slip rate on stress drop. *Pure Appl. Geophys.*, 124: 515-529, 1986.

Caristan, Y., The transition from high temperature creep to fracture in Maryland Diabase. *J. Geophys. Res.*, 87 (B8): 6781-6790, 1982.

Chester, F.M. and Higgs, N.G., Multimechanism friction constitutive model for ultrafine quartz gouge at hypocentral conditions. *J. Geophys. Res.*, 97 (B2): 1859-1870, 1992.

Dieterich, J.H., Time-dependent friction in rocks. *J. Geophys. Res.*, 77 (20): 3691-3697, 1972.

Dieterich, J.H., Time-dependent friction and the mechanics of stick-slip. *Pure Appl. Geophys.*, 116: 790-805, 1978.

Dieterich, J.H., Modeling of rock friction I: Experimental results and constitutive equations. *J. Geophys. Res.*, 84: 2161-2168, 1979.

Dieterich, J.H., Constitutive properties of faults with simulated gouge, In: N.L. Carter, M. Friedman, J.M. Logan, and D.W. Stearns (Editors), Mechanical Behavior of Crustal Rocks, *Geophys. Mono. Ser. 24*, AGU Washington DC, pp. 103-120, 1981.

Fredrich, J.T. and Evans, B., Strength recovery along simulated faults by solution transfer processes, In: W. Wawersik (Editor), *Proc. 33rd Nat. Rock Mech. Symp.*, pp. 121-130, 1992.

Hirth, G. and Tullis, J., The brittle-plastic transition in experimentally deformed quartz aggregates. *J. Geophys. Res.*, v 99 (B6): 11731-11747, 1994.

Kanamori, H. and Anderson, D.L., Theoretical basis of some empirical relations in seismology. *Bull. Seismol. Soc. Am.*, 65: 1073-1095, 1975.

Kanamori, H. and Allen, C.R., Earthquake repeat time and average stress drop, In: Das et al. (Editors), Earthquake Source Mechanics, A*m. Geophys. Union Mono. 37*, pp. 227-235, 1986.

Kohlstedt, D.L. and Goetze, C., Low-stress high-temperature creep in olivine single crystals. *J. Geophys. Res.*, 79 (14): 2045-2051, 1974.

Lockner, D.A., Summers, R. and Byerlee, J.D., Effects of temperature and sliding rate on frictional strength of granite. *Pure Appl. Geophys.*, 124 (3): 445-469, 1986.

Mardon, D., Kronenberg, A.K., Handin, J., Friedman, M. and Russell, J.E, Mechanisms of fracture propagation in experimentally extended Sioux quartzite. *Tectonophysics*, 182: 259-278, 1990.

Marone, C., Laboratory derived friction laws and their application to seismic faulting, *Annu. Rev. Earth Planet. Sci.*, 26, 643-696, 1998.

Marone, C., Raleigh, C.B. and Scholz, C.H., Frictional behavior and constitutive modeling of simulated fault gouge. *J. Geophys. Res.*, 95: 7007-7025, 1990.

Marone, C. and Scholz, C.H., The depth of seismic faulting and the upper transition from stable to unstable slip regimes. *Geophys. Res. Lett.*, 15 (6): 621-624, 1988.

Marone, C., Vidale, J.E. and Ellsworth, W.L., Fault healing and time dependent variations in source properties of repeating earthquakes. *Geophys. Res. Lett.*, 22: 3095-3098, 1995.

Nakatani, M., and Mochizuki, H., Effects of shear stress applied to surface in stationary contact on rock friction, *Geophys. Res. Lett.*, 23: 869-872, 1996.

Ohnaka, M., Experimental studies of stick-slip and their application to the earthquake source mechanism. *J. Phys. Earth*, 21: 285-303, 1973.

Perrin, G., Rice, J.R., and Zheng, G., Self-healing slip pulse on a frictional surface, *J. Mech. Phys. Solids*, 43: 1461-1495, 1995.

Reinen, L. A., and Weeks, J. D., Determination of rock friction constitutive parameters using an iterative least-squares inversion method, *J. Geophys. Res.* 98: 15,937-15,950, 1993.

Rice, J.R., Fault stress states, pore pressure distributions, and the weakness of the San Andreas Fault, In: B. Evans and T-f. Wong (Editors), Fault Mechanics and Transport Properties of Rocks, Academic Press, San Diego, pp. 475-504, 1992.

Rice, J.R., and Ruina, A.L., Stability of steady frictional slipping. *J. App. Mech.*, 50: 343-349, 1983.

Rimstedt, J.D. and Barnes, H.L, The kinetics of silica-water reactions. *Geochim. Cosmochim. Acta*, 44: 1683-1699, 1980.

Ruina, A., Slip instability and state variable friction laws. *J. Geophys. Res.*, 88 (B12): 10359-10370, 1983.

Rutter, E.H., Pressure solution in nature, theory and experiment. *Geol. Soc. London J.*, 140: 725-740, 1983.

Rutter, E.H. and Maddock, R.H., On the mechanical properties of synthetic kaolinite/quartz fault gouge. *Terra Nova*, 4: 489-500, 1992.

Scholz, C.H., The Mechanics of Earthquakes and Faulting, Cambridge University Press, New York, 1992.

Scholz, C.H., Earthquakes and friction laws, *Nature*, 391, 37-42, 1998.

Scholz, C.H., Aviles, C.A., and Wesnousky, S.G., Scaling differences between large interplate and intraplate earthquakes. *Bull. Seismol. Soc. Am.*, 76 (1): 65-70, 1986.

Scholz, C.H. and Engelder, J.T., The role of asperity indentation and ploughing in rock friction - I: Asperity creep and stick-slip. *Int. J. Rock Mech. Min. Sci. Geomech.*, 13: 149-154, 1976.

Scholz, C.H., Molnar, P. and Johnson, T.,. Detailed studies of frictional sliding of granite and implications for the earthquake mechanism. *J. Geophys. Res.*, 77 (32): 6392-6406, 1972.

Schwenn, M.B. and Goetze, C.,. Creep of olivine during hot-pressing. *Tectonophysics*, 48: 41-60, 1978.

Scott, D., Marone, C., and Sammis, C., The apparent friction of granular fault gouge in sheared layers. *J. Geophys. Res.*, 99 (B4): 7231-7247, 1994.

Shimamoto, T. and Logan, J.M., Effects of simulated fault gouge on the sliding behavior of Tennessee Sandstone: Nonclay gouges. *J. Geophys. Res.*, 86 (B4): 2902-2914, 1981.

Smith, D.L. and Evans, B., Diffusional crack healing in quartz. *J. Geophys. Res.*, 89 (B6): 4125-4135, 1984.

Vidale, J.E., Ellsworth, W.L., Cole, A., and Marone, C., Variations in rupture process with recurrence interval in a repeated small earthquake. Nature, 368: 624-626, 1994.

Wong, T.-f., and Y. Zhao, Effects of load point velocity on frictional instability behavior. Tectonophysics, 175: 177-195, 1990.

APPENDIX A

Apparatus details

This section contains a brief description of the testing systems that were used to conduct the research presented in this thesis. Both the biaxial and triaxial deformation machines received constant maintenance and were periodically modified. Several of the key elements of each apparatus were furnished by outside contractors, and modifications to each system were performed by the author. Specific information about each apparatus are held at the Rock Mechanics laboratory in the Department of Earth, Atmospheric and Planetary Sciences (MIT 54-715).

In essence, each apparatus consists of three components: a hydraulic servo-control system, an electronic control system, and a pressure generating system. The main difference between the machines lies with the pressure generating component. This is due to the inherent nature of experiments that can be performed in each apparatus. The biaxial testing machine has two perpendicular loading frames that are used for deformation tests. The triaxial apparatus consists of three separate pressure generating systems that provide confining pressure, pore-fluid pressure, and loading for sample deformation. For both testing machines the pressures are generated by the hydraulic systems, which are controlled electronically.

A.1. Pressure generation

A.1.1. The biaxial apparatus

This testing machine consists of two loading frames that can deform samples from perpendicular directions (Figure A1). To date, this apparatus has been chiefly used for experiments that investigate the behavior of sliding friction (such as those discussed in Chapters 2 - 3 of this thesis). However, tests involving uniaxial compression of rock

cylinders have also been performed. This apparatus is well suited for friction tests, as the sample geometry permits direct control of loading in the normal and shear directions. Loadforces and displacements are monitored

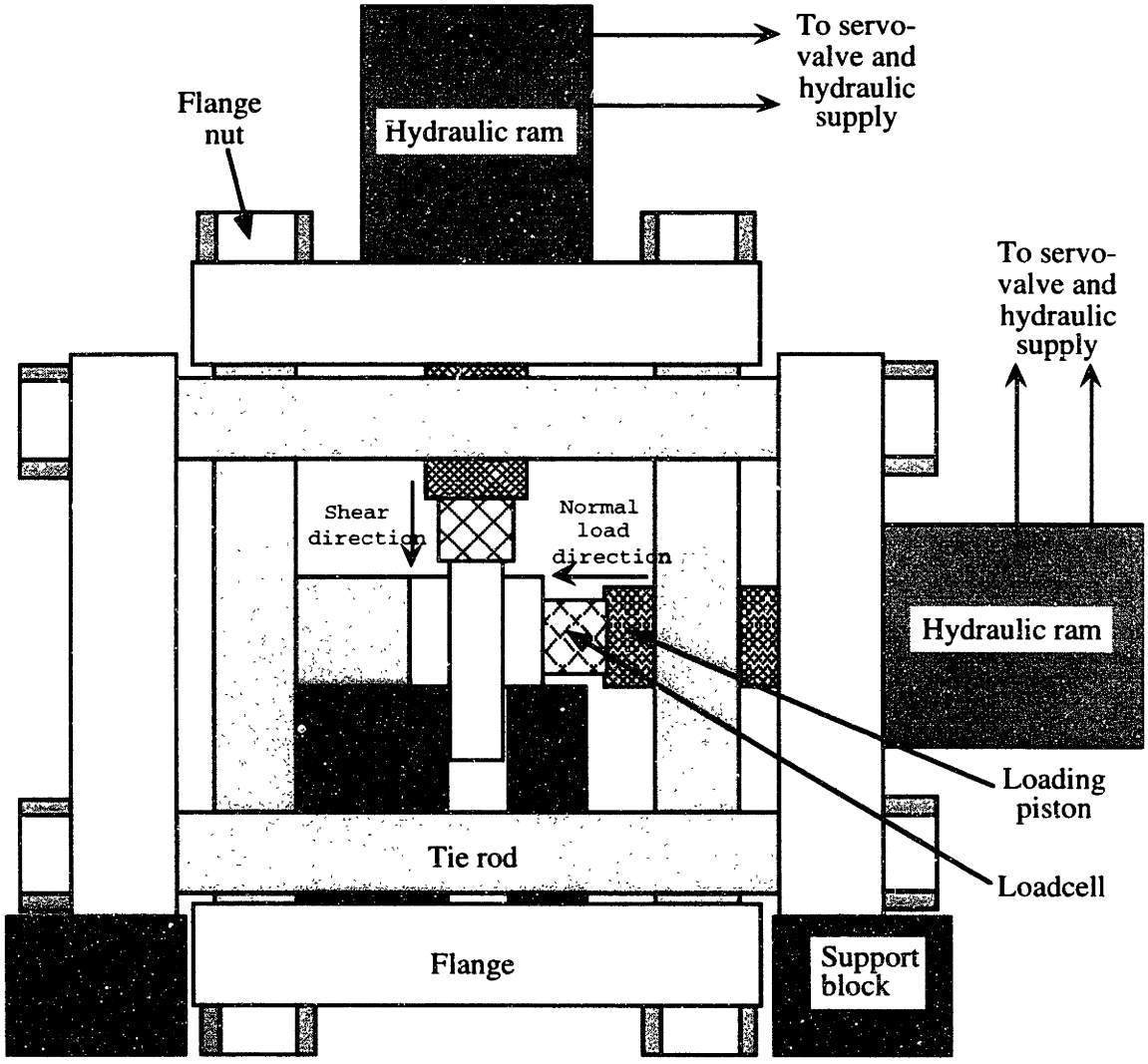

Figure A1. Schematic representation of the biaxial testing apparatus showing the two loading frames that provide normal and shear loads for sample deformation. Displacements and forces are monitored at the loadpoint position. Loading pistons are driven by independently servo-controlled hydraulic fluid actuators.

at the loading piston. The applied forces are measured by hollow, beryllium-copper loadcells with strain gages fixed onto them in a wheatstone bridge configuration. Displacements are monitored using LVDTs mounted between the loading piston and the loadframe. Our apparatus has been configured to control loadpoint displacements to within 0.1 μm, and resolve loadforce to better than 0.1 kN.

Another benefit of this apparatus is that relatively large sample dimensions can be accommodated. Samples consist of a triple block geometry where a central forcing block is allowed to slide past two fixed outer blocks. With this configuration, shear occurs along two zones and a considerable amount of sample slip can be achieved (as much as 5 cm). These are important features for studies of the effects of shear displacement on frictional sliding, and for controlled studies of friction at fast loading rates (to 1 cm/s for our apparatus). The accessibility of the sample assembly also permits monitoring the characteristics of the shearing surfaces directly. For example, to monitor slip and thickness variations the user can mount displacement transducers on the rigid forcing blocks. To monitor heat production during shear, thermocouples may be embedded in the forcing blocks, or recessed on the sliding surfaces.

At present, the biaxial apparatus in the Rock Mechanics laboratory is not equipped to control the chemical environment for tests, to control a confining or pore-fluid pressure, nor to impose temperature. These are not limitations of the testing apparatus, rather these are items that have not yet been addressed. For example, a research program is in progress whereby samples may be deformed in a controlled humidity environment.

A.3.2. The triaxial pressure vessel

This apparatus contains more components than the biaxial machine, owing to the experiments that are performed on it. The triaxial pressure vessel is capable of producing the physico-chemical conditions likely to exist at depth within the Earth. The apparatus is composed of three pressure generating systems, and an electrical furnace that subjects

samples to high temperatures (Figure A2). Samples that are jacketed by an impermeable material can be subjected to confining pressure

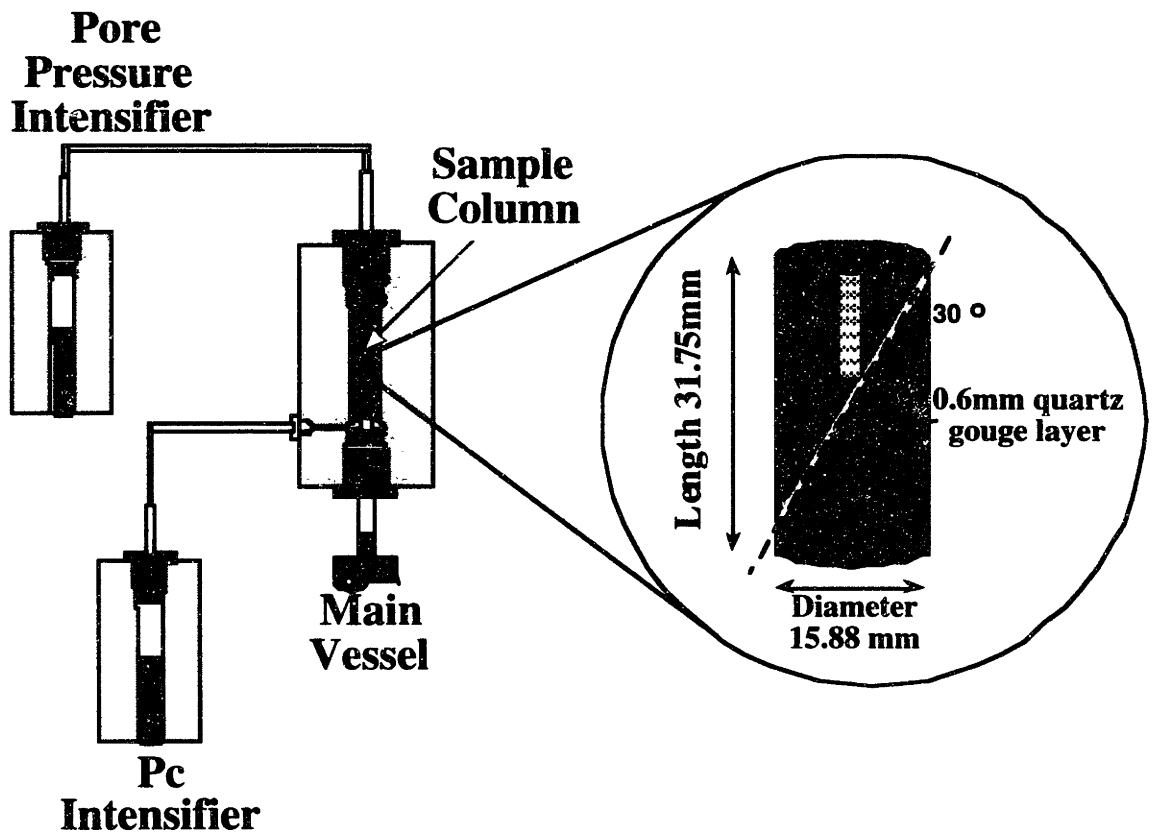

Figure A2. Schematic representation of the triaxial deformation apparatus, and the samples used for this study. Shown here are the two components that generate confining and pore-fluid pressures. Also shown is the main vessel in which the sample assembly is located during experiments. Sample deformation is achieved by a hydraulically servo-controlled actuator that drives a piston into the main vessel. For the experiments described in Chapter 4, samples consisted of thin gouge layers sandwiched between quartzitic forcing blocks (dimensions as shown).

(as high as 700 MPa for our apparatus). Argon gas is used as the confining medium as it is chemically inert and poses no threat for using electrical devices within the main pressure vessel (e.g. furnaces). Confining pressures are established by a "quasi" servo-control system that is described in the following sections. The argon pressure is monitored by transducers located at the pressure intensifier and on the line to the main vessel. The transducer monitoring the main vessel pressure is used in the servo-control feedback loop, and the system controls to within ±0.5 MPa.

Fluids may also be introduced to the sample and are pressurized by a hydraulically driven servo-controlled pressure generator. Fluid pressures are monitored by a transducer at the pressure generator, and the displacement of the generator piston is monitored to determine pore volume changes. The signal from the pressure transducer is used in the servo-control feedback loop to control pore pressure to within ±0.2 MPa. Thus, the piston displacement transducer is merely a passive monitoring device.

Samples are deformed by a hydraulically driven loading piston in the main pressure vessel. The motion of this piston is monitored at the loadpoint by a displacement transducer, with a resolution of 0.1 μm. The imposed loading force is monitored by a loadcell located outside of the pressure vessel, and between the hydraulic piston and sample assembly. The loadcell consists of a solid steel cylinder with strain gages fixed onto it in a wheatstone bridge configuration. Loadforce resolution is better than 0.02 kN. The electronic control system is configured so that either the piston displacement, or the imposed loadforce, can be used as the feedback signal for sample deformation. For the experiments described in Chapter 4 of this thesis it was loadpoint position that was servo-controlled, whereas loading force was passively monitored.

Samples are subjected to temperature by using an electrical furnace. The furnace surrounds the sample assembly and is inserted into the main pressure vessel with the sample. The furnace consists of molybdenum wire wrapped around a ceramic casing. The

wire windings span the length of the ceramic cylinder and a grounding wire is connected at the center. Thus, the windings delineate two zones for which voltage and current may be controlled independently. Temperature is regulated using the signal from a thermocouple located inside the sample column. The resolution of temperature control depends on several factors including the desired temperature level, the length of the sample, and the position of the thermocouple, among others. Thus, the control parameters for the furnace are obtained from along-axis temperature profiles of dummy sample assemblies. At 600 °C, temperature can be maintained to better than 2 °C and the along-axis variation for the sample is typically not more than 5 °C. For lower temperatures, temperature regulation becomes even better. Thermal convection currents surrounding the sample assembly (i.e. between the jacketing material and the furnace ceramic wall) are minimized by using a densely packed, fine-grained boron nitride powder.

A.2. The hydraulic component

Two separate hydraulic systems shall be discussed here. The first is shared by both testing machines and drives a majority of the pressure generating units, while the second is used specifically by the triaxial apparatus to provide confining pressure. We use hydraulic servo-control in the biaxial apparatus to impose shear and normal stresses on samples, and in the triaxial machine to deform samples and provide a pore fluid pressure. To achieve this, a large pump circulates hydraulic oil to the loading pistons at a maximum flow rate of 10 gallons per minute, and fluid pressure of 3000 psi. The pump regulates the output pressure and flow rate of the hydraulic oil. The fluid is then ported to each apparatus via a series of air-actuated solenoid valves. For each machine, movement of the loading pistons occurs with the aid of servo-valves. The servo-valves control the flow of oil to the loading pistons by reacting to signals from the electronic control system. Efficient response of the

hydraulic servo-control system is achieved with large flow rates, high fluid pressure, and careful adjustment of the electronic feedback loop (which is discussed below).

Confining pressure for the triaxial apparatus is generated using a separate, self-contained hydraulic system (Figure A3). Here, hydraulic oil is also used to drive a piston in the confining pressure generator. However, this system differs from the one described above in that a series of air-actuated valves and boosters control the hydraulic oil pressure and fluid flow. It is the variation of oil pressure that ultimately regulates the pressure of the confining medium. An air-operated booster is used to increase the pressure of the hydraulic oil. An increase in oil pressure moves the generator piston and, thus, intensifies confining pressure. Air-actuated valves port the fluid to, and from, the pressure generator piston thereby increasing, or decreasing, confining pressure. An electronic control system regulates the pressure of the confining medium within a user-defined range. Thus, the system behaves in a manner similar to the servo-controlled system described above.

A.3. Electronic control system

The electronic systems for each apparatus involve both analog and digital circuitry. The biaxial and triaxial testing machines are equipped with essentially the same instrumentation. For both, the digital circuitry serves the same purpose (to generate a command signal). The analog components are also quite similar, except their application and interaction with the testing apparatus differ. For the biaxial system, there are two sets of analog instrumentation that each control one loading frame. For the triaxial apparatus, there are separate analog systems that interact with the loading piston that deforms samples, the pore pressure generator, the confining pressure generator, and the temperature controller. The triaxial confining pressure system also utilizes an AC circuit for control of the air-actuated hydraulic valves (e.g. Figure A4).

The instrumentation is used to output control signals, and also to deal with the input signals from the various monitoring devices. Signals from these devices (such as

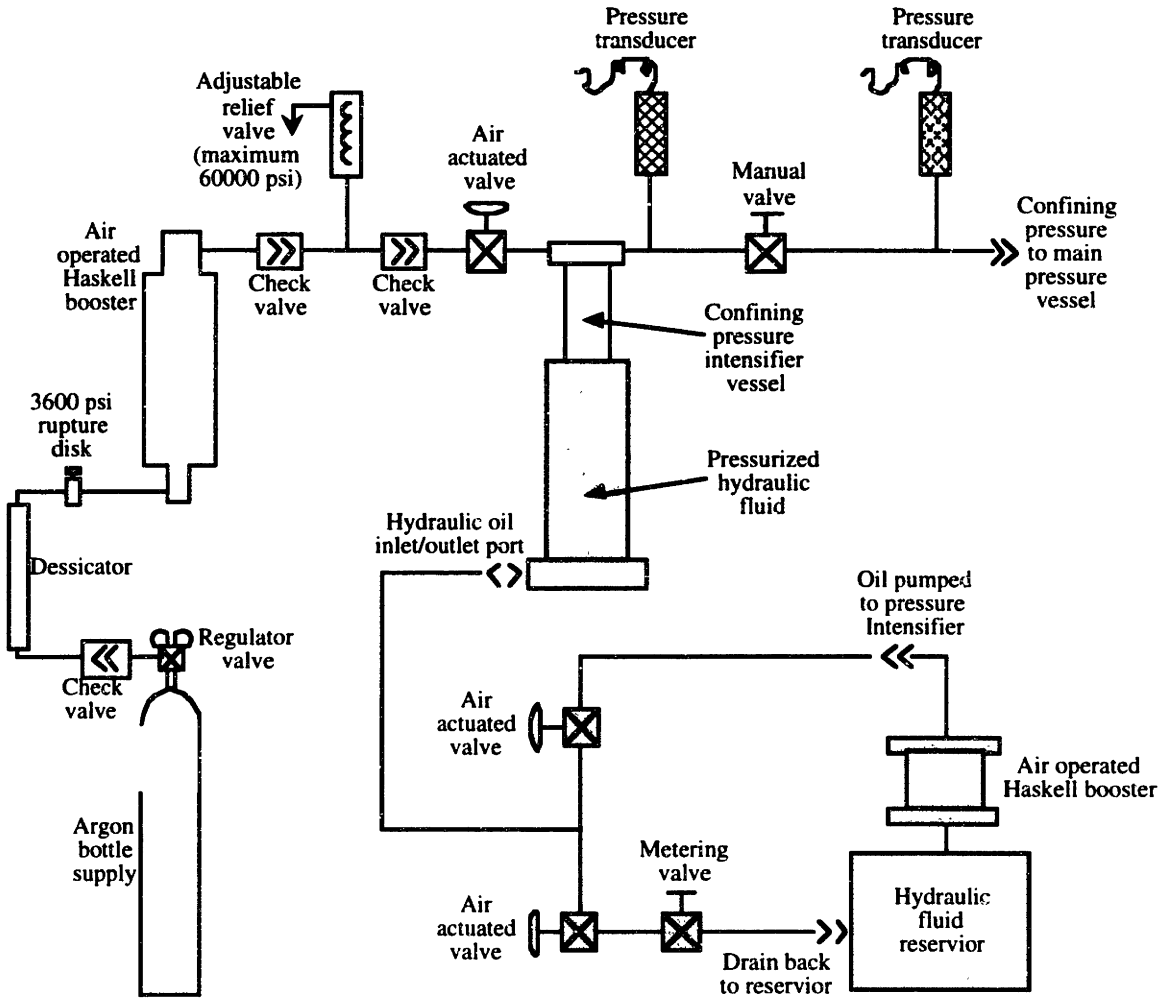

Figure A3. Schematic representation of the confining pressure system of the triaxial deformation apparatus. The confining medium is argon gas, and the components that pressurize the argon are shown unshaded. Pressures are generated using a "quasi" servo-controlled hydraulic system (shown shaded). Pressures may be maintained to within ±0.25 MPa.

loadcells, displacement transducers, pressure transducers, and thermocouples) are used by the electronic system in two ways. First, the signals are conditioned and sent to computer for data recording. Signal conditioning typically involves adjustment of levels (e.g. offsetting and gain) and in some cases filtering to minimize electrical noise. All input signals are converted to a range of ±5 volts for data acquisition. Second, the signals are used in closed-loop feedback circuits for control of the testing apparatus (e.g. Figure A5). To achieve this, the input levels are electronically compared to user-defined command values. Command signals can be generated from the analog circuitry, from the digital instrumentation, or by an external device (such as a computer). The difference is then output to the apparatus as an error signal. For example, the hydraulic servo-valves strive to satisfy a zero error condition. They will respond to a non-zero error signal by porting hydraulic fluid to the loading piston. The piston then moves and changes the signal from the monitoring device in a way that more closely matches the user-defined command signal.

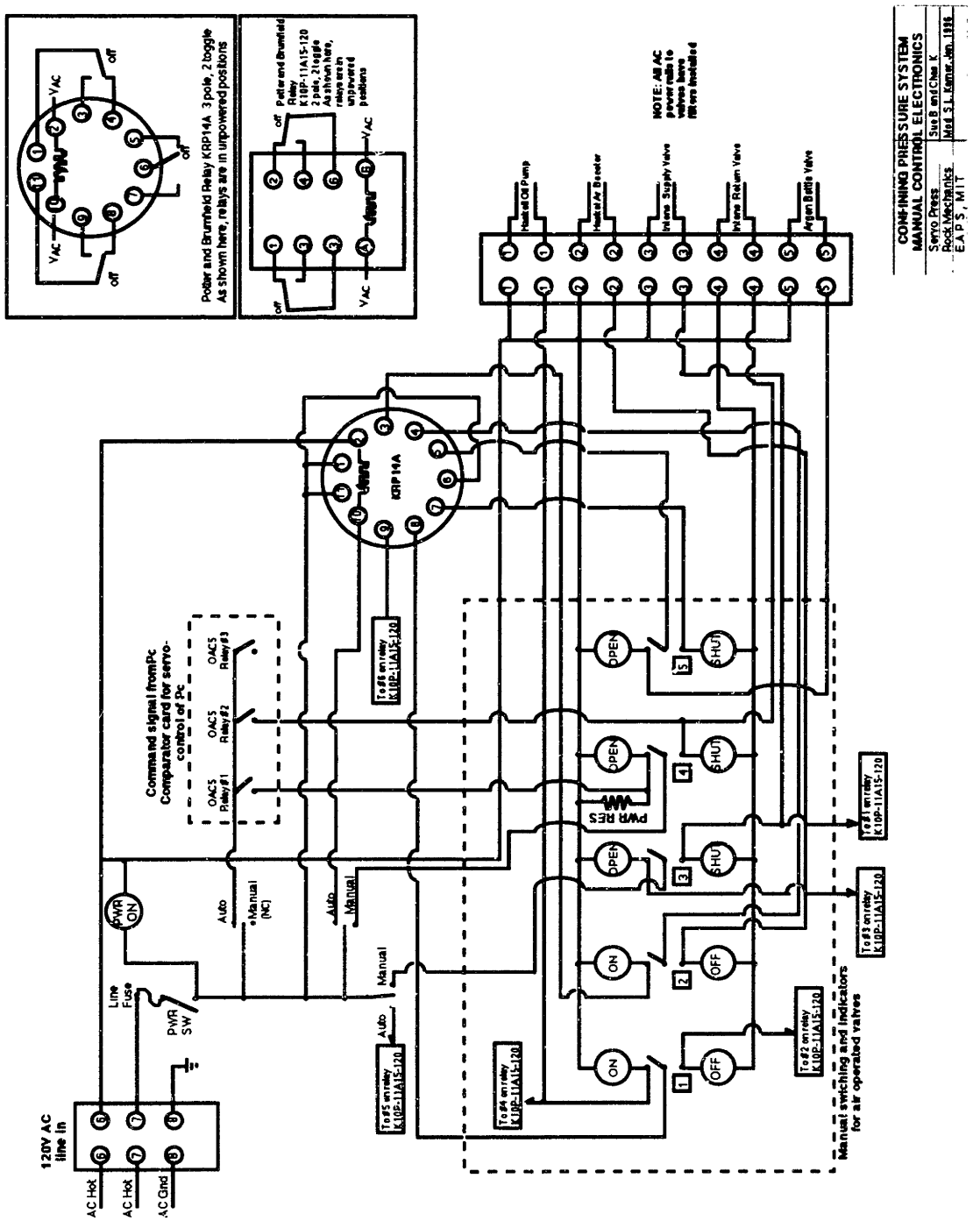

Figure A4. Electronic schematic diagram showing the AC circuitry for the triaxial confining pressure system. Analog DC signals trigger relays that provide AC power to the air-actuated hydraulic valves.

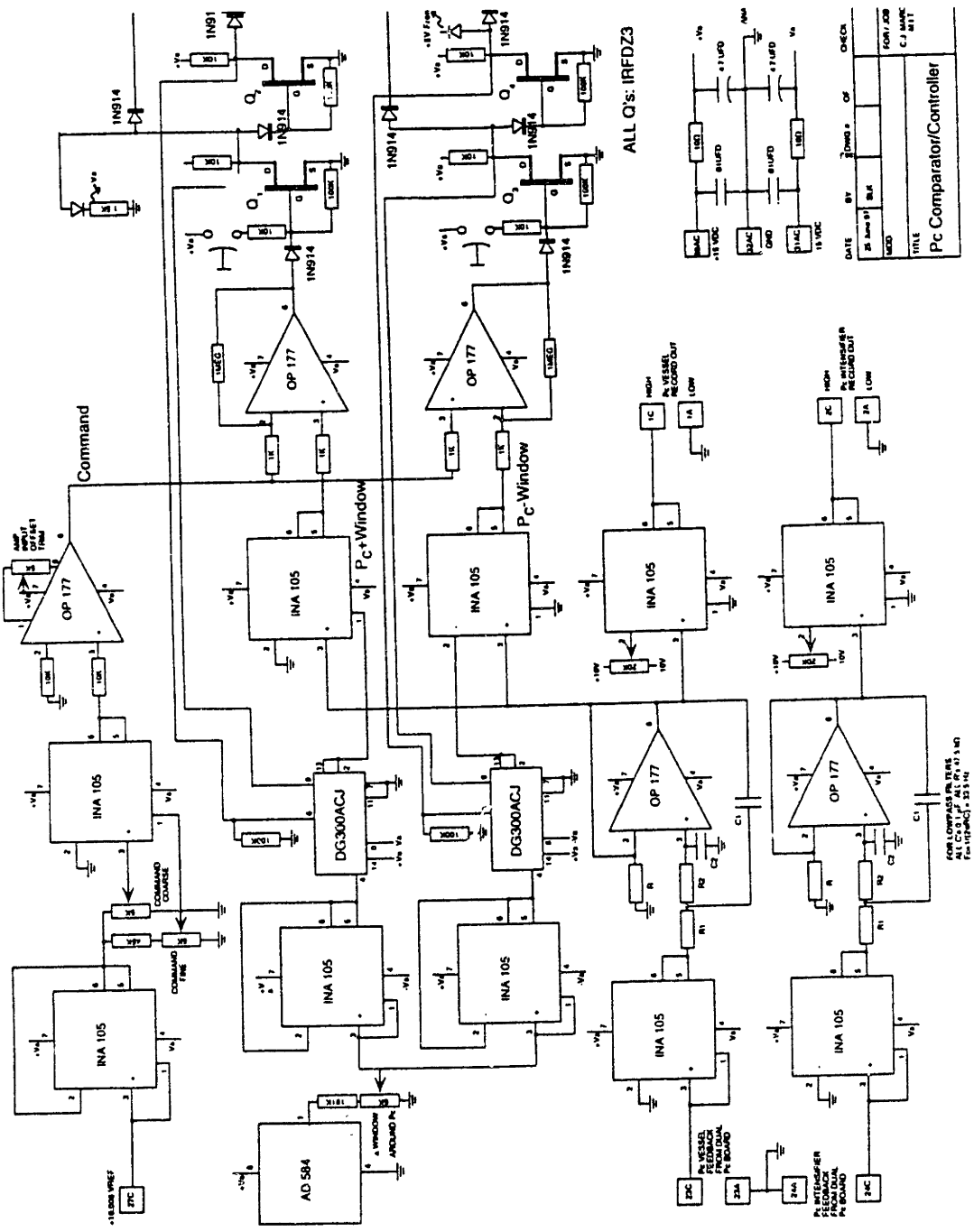

Figure A5. Electronic schematic diagram showing the analog circuitry for "quasi" servo control of the triaxial confining pressure system. The input signal from a pressure transducer is compared to a window about a reference level. When confining pressure is outside of the desired range, a DC signal is sent to trigger AC relays that control the hydraulic system (as shown in Figure A4).

APPENDIX B

Data analysis

B.1. Tests performed in the biaxial apparatus

The experiments described in Chapters 2 and 3 of this thesis were performed in a biaxial testing apparatus, using samples having a triple block geometry (e.g. Figure 3.3). The applied forces and displacements were monitored at the loading pistons. As the loading forces in the normal and shear directions are controlled directly, the calculation of shear and normal stresses is straightforward. Normal stress is determined from the applied loading force divided by the nominal contact area of the sample. Shear stress is determined in a similar manner. However, the applied shearing force must also be divided by two in order to obtain shear stress. This is because there are two contacting surfaces that participate in deformation. Thus, each surface contributes one-half of the total amount of frictional resistance to shear.

B.1.1. Determination of layer thickness

Variations in gouge layer thickness are determined from the measured displacement of the loading piston. The data must first be corrected for elastic distortion of the testing apparatus. From calibration tests, the stiffness of the loading frame is ~0.4kN/μm (expressed as normal force per unit loadpoint displacement). For data correction, the measured normal force is used to determine how much of the loadpoint displacement contributes to load frame distortion. This contribution is subtracted from the measured loadpoint displacement. As the result indicates thickness variations for both shear zones together, the data must be divided by two in order to obtain values for a single layer.

Owing to the large changes in applied shear load for the tests described in Chapter 3, a second correction must also be performed on the layer thickness data. This correction accounts for Poisson distortion of the central forcing block during a reduced-load hold cycle. The configuration of the biaxial testing apparatus lends itself to interpreting sample assembly deformation in terms of plane stress or strain. Thus, to correct the layer thickness data we have employed the plane stress assumption (as discussed in section 3.3.1 of this thesis). The values of Young's modulus and Poisson ratio are selected based on the forcing block material (e.g. granite, steel, and so forth). The applied loading forces are also used in conjunction with the dimensions of the stressed faces of the forcing block. The resulting normal strain induced by the shear force variations are then subtracted from the layer thickness measurements.

To determine whether the plane stress assumption is appropriate for our experiments, we performed calibration tests on solid steel samples. In these tests, we maintained a constant normal force on the sample and varied the shear force (to represent a reduced shear load cycle). The results from a single loading cycle are shown in Figure B1. The data show that for steel forcing blocks, and for the conditions of our experiments, the Poisson distortion amounts to only a few microns.

B.1.2. For shear

In describing results from the biaxial testing apparatus, the only mention of sample slip made in this thesis were derived from displacement transducers mounted on the sides of the sample assembly. It is common for investigators studying rock friction in the laboratory to describe shear in terms of the measured loadpoint displacement. Thus, no corrections to the data are required to account for elastic distortion of the loading frame. Having said this, we do need to account for these elastic effects when modeling the data with the friction constitutive laws. From apparatus calibrations, the loading frame has a stiffness of ~0.5 kN/μm (expressed as shear force per unit loadpoint displacement). For a $10 \times 10\ cm^2$

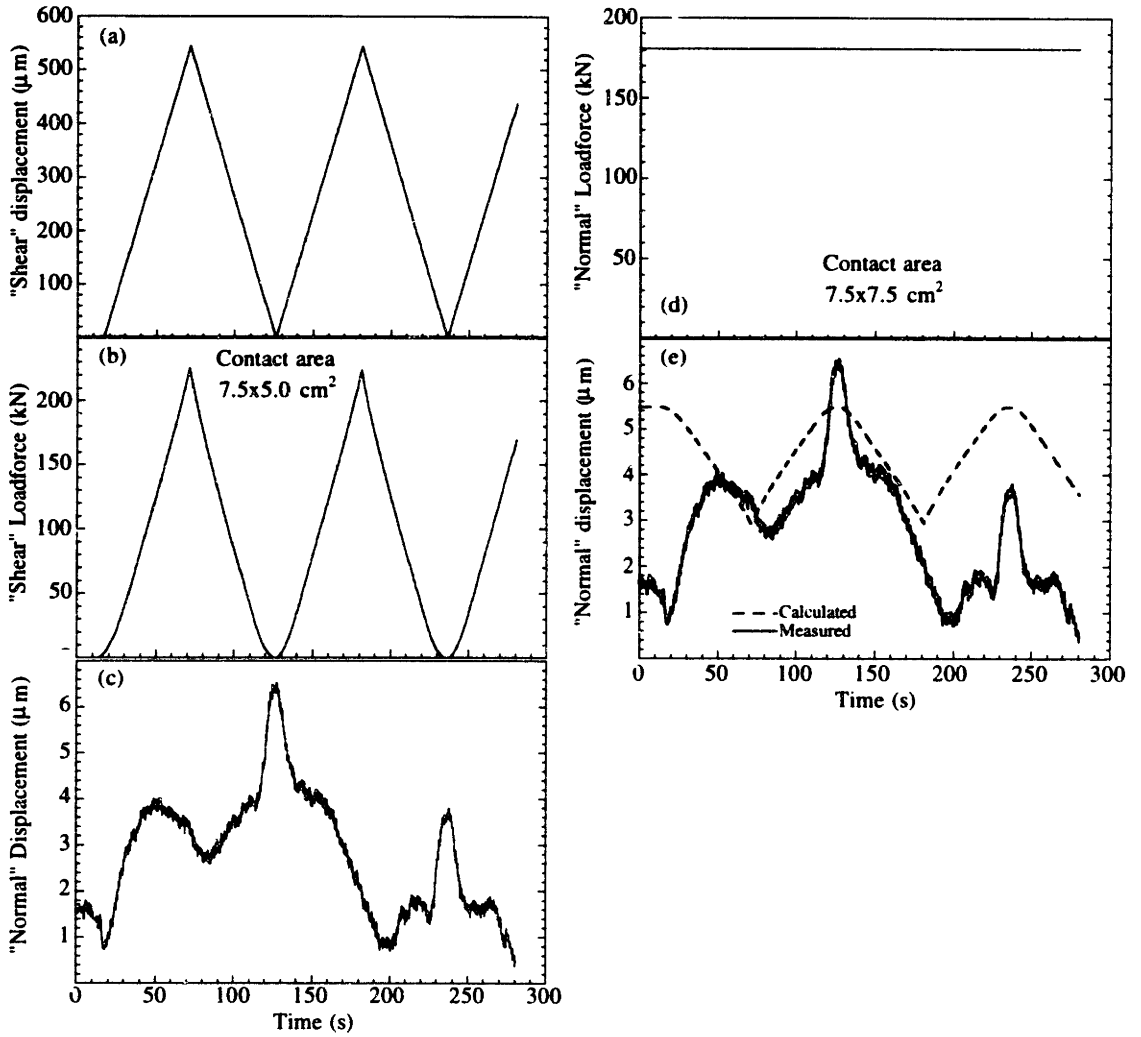

Figure B1. Calibration test to determine effects of Poisson distortion. All measurements were at the loadpoint. a). For the test, loadpoint displacement in the "shear" direction was controlled at a rate of 10 μm/s. b). As the loading piston extends, the loadforce in the "shear" direction increases. c). Displacement in the "normal" direction. The data show some wander due to electrical noise issues. However, we observe a systematic response to the imposed variations in shear load. d). Loading force in the "normal" direction. For the test, "normal" loadforce was maintained constant. e). Comparison of observed changes in "normal" displacement to that calculated from a plane-stress approximation (equation 3.4). The amplitudes and phase of the observed variations is close to the calculated changes.

sample and for the conditions of our tests, the apparatus stiffness is ~0.001 per micron (expressed as friction per unit displacement). However, a more refined stiffness estimate can be obtained from sample loading data.

B.2. Tests performed in the triaxial apparatus

The material used for the experiments described in Chapter 4 of this thesis were cylindrical samples of Sioux Quartzite machined to the dimensions shown in Figure B2. To simulate the failure plane, samples were cut at an angle of 30° to the cylinder axis. Fine-grained quartz powder (5 μm rms grain diameter) was used to simulate fault gouge, and was sandwiched between the two sawcut forcing blocks. The experiments were conducted at constant confining pressure, pore-fluid pressure, and at a axial loading rate. Signals from the loadcell, displacement transducers, pressure transducers, and the thermocouple were digitally recorded.

B.2.1. Determination of normal and shear stress

Normal and shear stresses in the plane of the sawcut are calculated from the recorded axial loadforce. In the following, compression is taken to be positive. As confining pressure on a sample is radially uniform, we can consider a two-dimensional problem (Figure B3). The x-axis shall be chosen to correspond to the σ_1 axis (loading direction), the y-axis as the σ_3 direction and f is. The traction vector, **T**, acting on the face of the sawcut is given by:

$$\mathbf{T} = \sigma\,\hat{\mathbf{n}} = \begin{bmatrix} \sigma_1 & 0 \\ 0 & \sigma_3 \end{bmatrix} \begin{bmatrix} \sin\theta \\ \cos\theta \end{bmatrix} = \begin{bmatrix} \sigma_1 \sin\theta \\ \sigma_3 \cos\theta \end{bmatrix} \tag{B1}$$

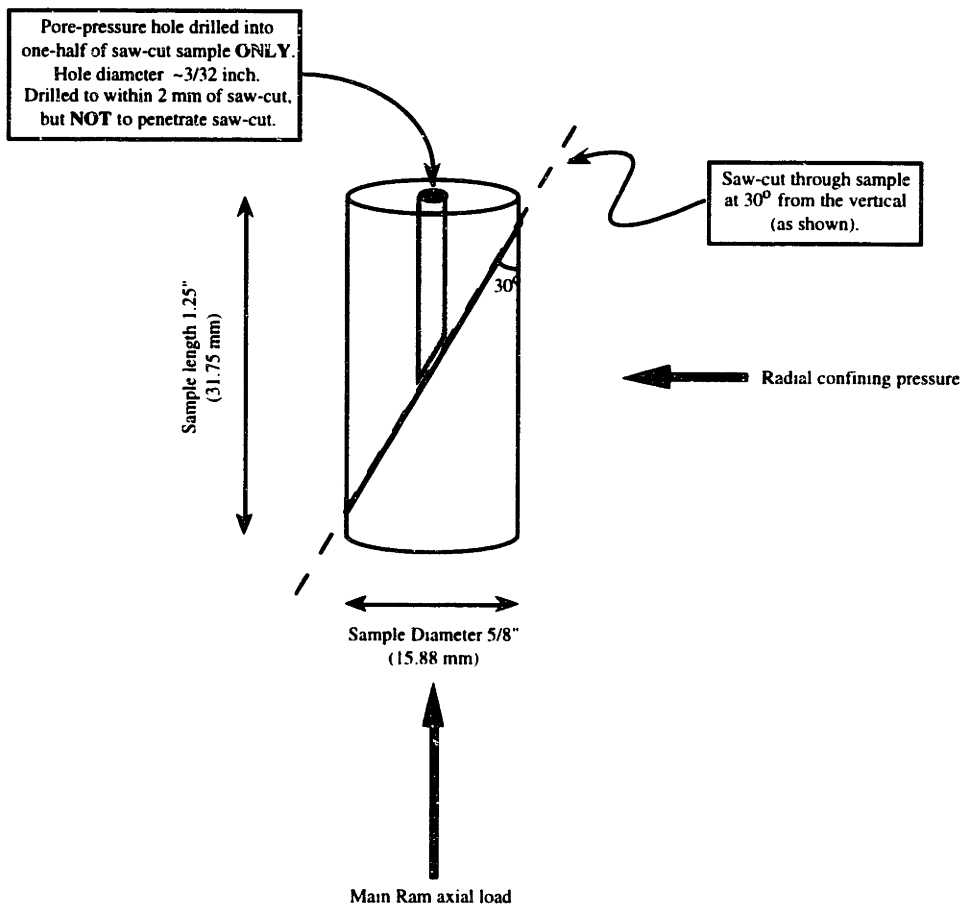

Figure B2. Sample geometry of the Sioux Quartzite forcing blocks of the triaxial friction experiments.

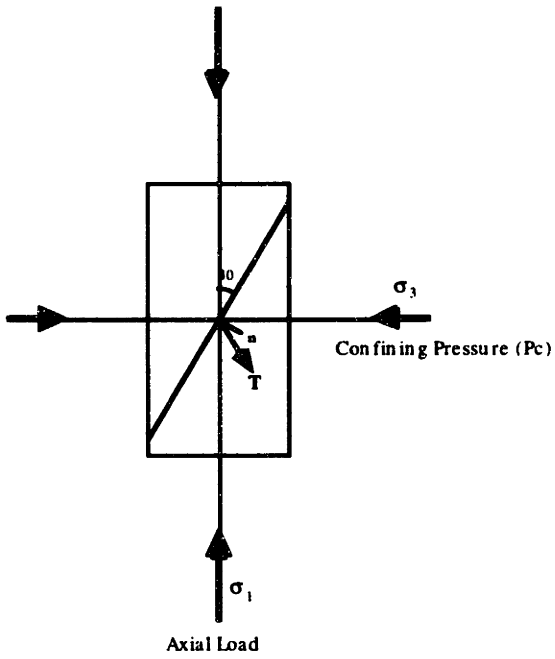

Figure B3. Two dimensional treatment of the stressed sample. The confining pressure is the least compressive principal stress and the axial load is the greatest compressive stress. The traction vector, T, on the sawcut can be calculated from a continuum mechanics approach using the geometry of the problem.

For the case of triaxial compression, confining pressure may be expressed as $\sigma_3=P_c$ and axial load may be expressed as $\sigma_1=P_c + \Delta\sigma$, where $\Delta\sigma= \sigma_1 - \sigma_3$. Hence, the system of equations describing the traction vector are:

$$\mathbf{T} = \begin{bmatrix} (\Delta\sigma + P_c)\sin\theta \\ P_c \cos\theta \end{bmatrix} \tag{B2}$$

From this traction vector, **T**, the normal and tangential (shear) components (σ_n and τ, respectively) can be determined from the relations:

$$\sigma_n = \mathbf{T} \bullet \hat{\mathbf{n}} = \begin{bmatrix} (\Delta\sigma + P_c)\sin\theta \\ P_c \cos\theta \end{bmatrix} \bullet \begin{bmatrix} \sin\theta \\ \cos\theta \end{bmatrix}$$
$$= \Delta\sigma \sin^2\theta + P_c \sin^2\theta + P_c \cos^2\theta \qquad \text{(B3)}$$
$$= \Delta\sigma \sin^2\theta + P_c$$

$$\tau = \sqrt{|\mathbf{T}|^2 - {\sigma_n}^2}$$
$$= \sqrt{\Delta\sigma^2 \sin^2\theta + {P_c}^2 \sin^2\theta + 2P_c\Delta\sigma\sin^2\theta + {P_c}^2\cos^2\theta - \left(\Delta\sigma^2\sin^4\theta + 2P_c\Delta\sigma\sin^2\theta + {P_c}^2\right)}$$
$$= \sqrt{\Delta\sigma^2\sin^2\theta - \Delta\sigma^2\sin^4\theta}$$
$$= \Delta\sigma\sin\theta\sqrt{1-\sin^2\theta}$$
$$= \Delta\sigma\sin\theta\cos\theta$$
$$= \frac{\Delta\sigma\sin 2\theta}{2}$$

(B4)

For the experiments described in this thesis, the initial axial load (σ_0) translated to the sample assembly is equal to confining pressure. The stress difference, $\Delta\sigma$, will be the change in the applied load at a given time (σ_t) relative to σ_0 (thus, $\Delta\sigma=\sigma_t-P_c$). The coefficient of friction can be determined from the calculated shear and normal stresses, and the pore fluid pressure (P_f), by the relation:

$$\mu = \frac{\tau}{(\sigma_n - P_f)} \qquad \text{(B5)}$$

B.2.2. Determination of shear displacement

Shear displacement is determined from the measured position of the loading piston. For an infinitely stiff testing system and sample column assembly, and for steady sliding

on the sawcut surface, the shear displacement (x) can be calculated directly from the geometry of the sample (Figures B2-B3). That is, for an imposed loadpoint displacement, D, the amount of shear on the sawcut is:

$$x = \frac{D}{\cos(30°)} \tag{B6}$$

However, in our tests we must account for the finite stiffness of the testing apparatus. This is achieved in the same manner described previously for the Biaxial apparatus (section B.1). For the sample dimensions and conditions for this study, the apparatus stiffness is 0.206 MPa/μm (expressed as shear stress per unit shear displacement). This stiffness was used to calculate sample slip for the experiments presented in Chapter 4.

APPENDIX C

Data from repetitive stick-slip tests (Chapter 2)

The following figures show data from experiments performed on bare granite surfaces, as described in Chapter 2 of this thesis. All experiments were conducted in a biaxial deformation apparatus at room-temperature and humidity. For all tests, shear was imposed by controlling the velocity of the loading piston. Normal stress was maintained constant throughout each test.

The following figures show data from each experiment. For all tests, loadforces and displacements were measured at the loadpoint and friction is determined from the measured shear and normal stresses. Figures (a) to (e) show data for the entire test. Figures (f) onwards show the same data in (a) and (b), but at a different timescale for clarity.

a). Loadpoint displacement in the shear direction is plotted as a function of experiment time. Thus, the slope of the data indicates the imposed loading rate.

b). Shear stress on a sliding surface.

c). Normal stress during the test.

d). Normal displacement across a surface.

e). Coefficient of friction.

f). An enlarged view of loadpoint displacement data for the first section.

g). An enlarged view of the same section plotted in (f) showing shear stress.

g) - q). These plots show consecutive sections of data for each test. The plots are paired in the same way as (f) and (g) to show loadpoint displacement and shear stress more clearly.

For reference, the following table summarizes the conditions of the experiments.

Experiment Number	Loading rate (μm/s)	Normal stress (MPa)	Forcing block material
m154	30 and 300	5 and 10	Westerly granite
m155	10, 30, 300	10	Westerly granite
m156	0.5, 5, 10, 30, 100	10	Westerly granite

Table C.1. Summary of loading conditions and sample data that were the tested variables for the experiments.

Experiment m254

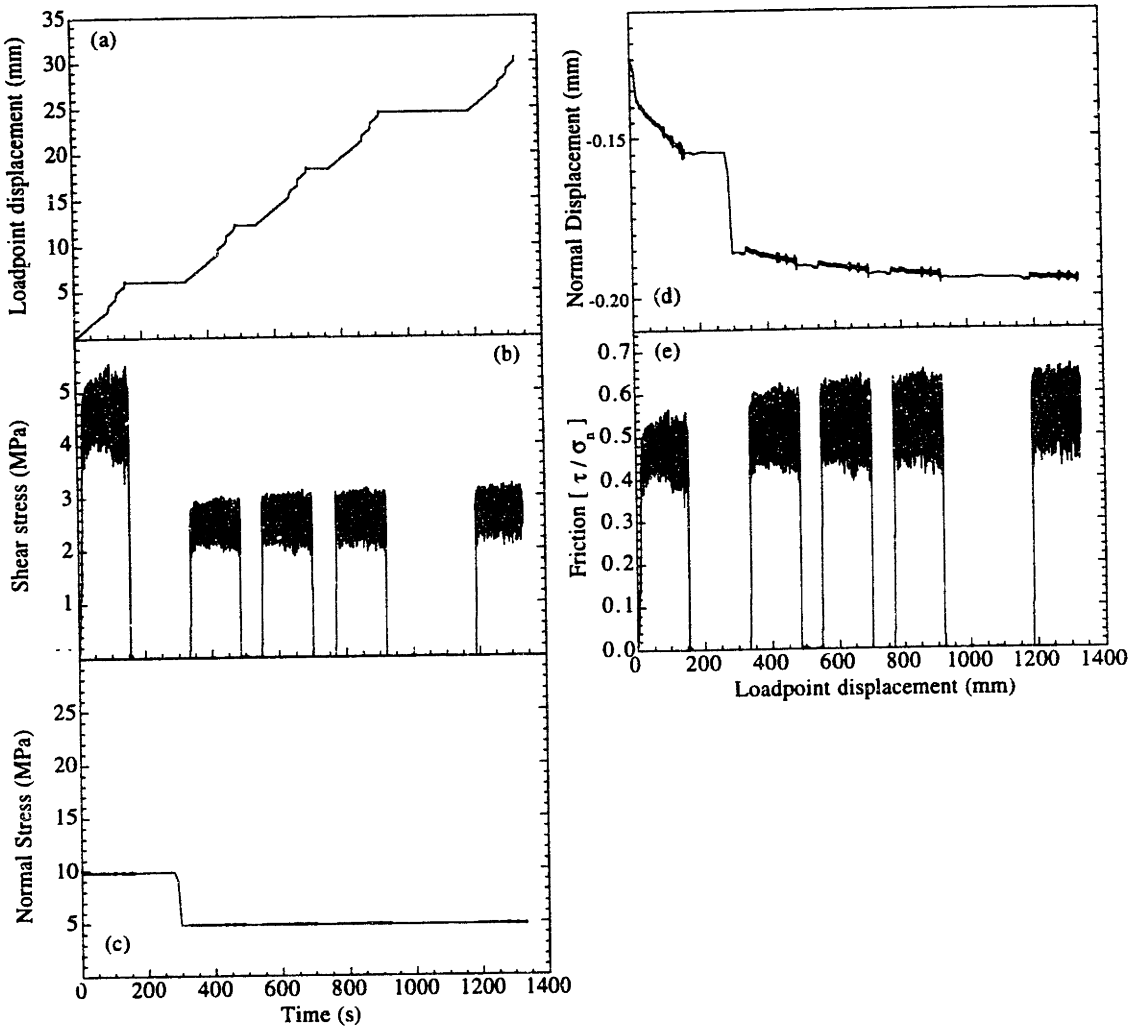

Experiment m254 (continued)

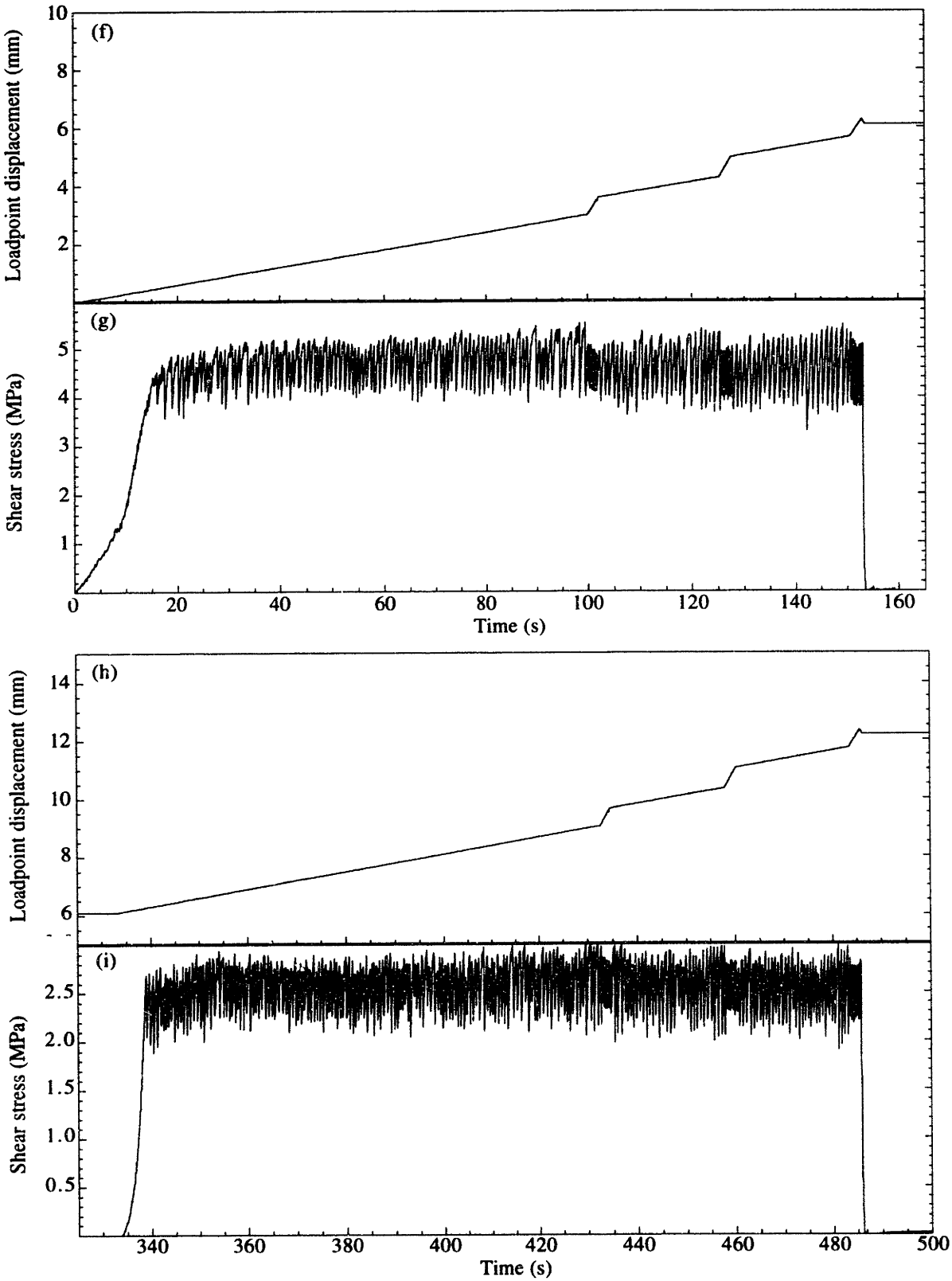

Experiment m254 (continued)

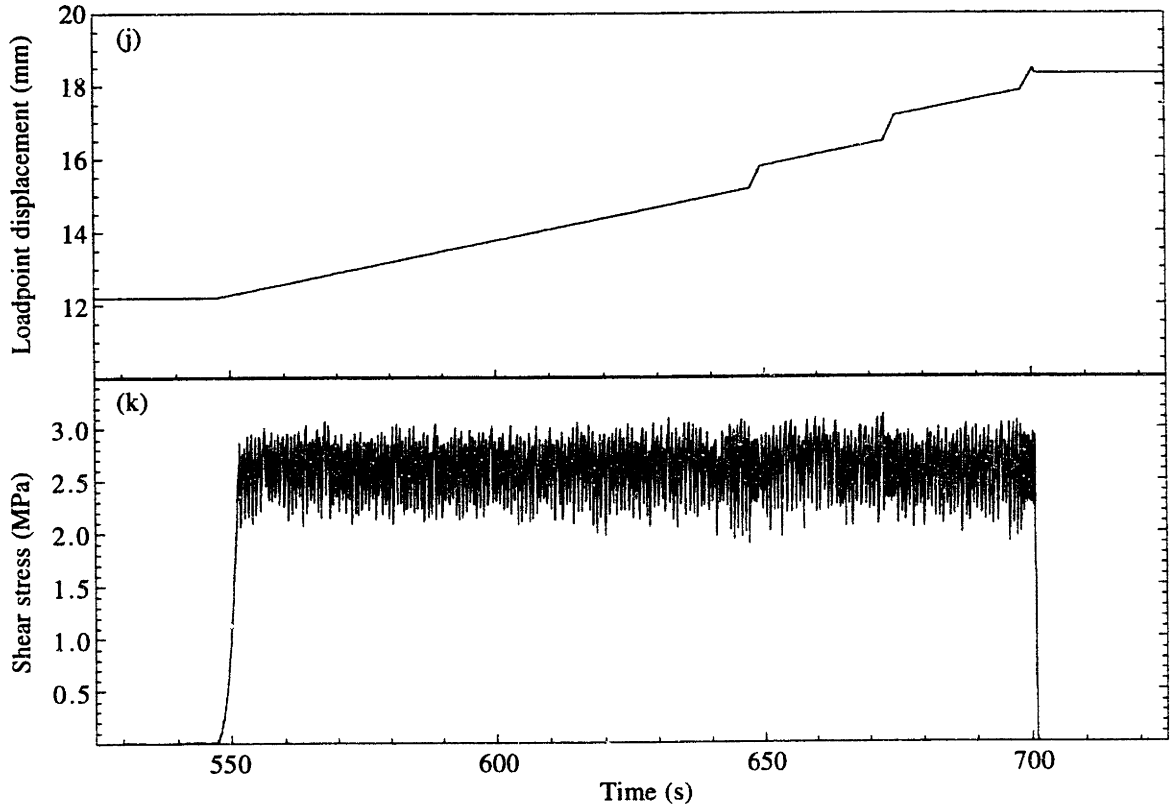

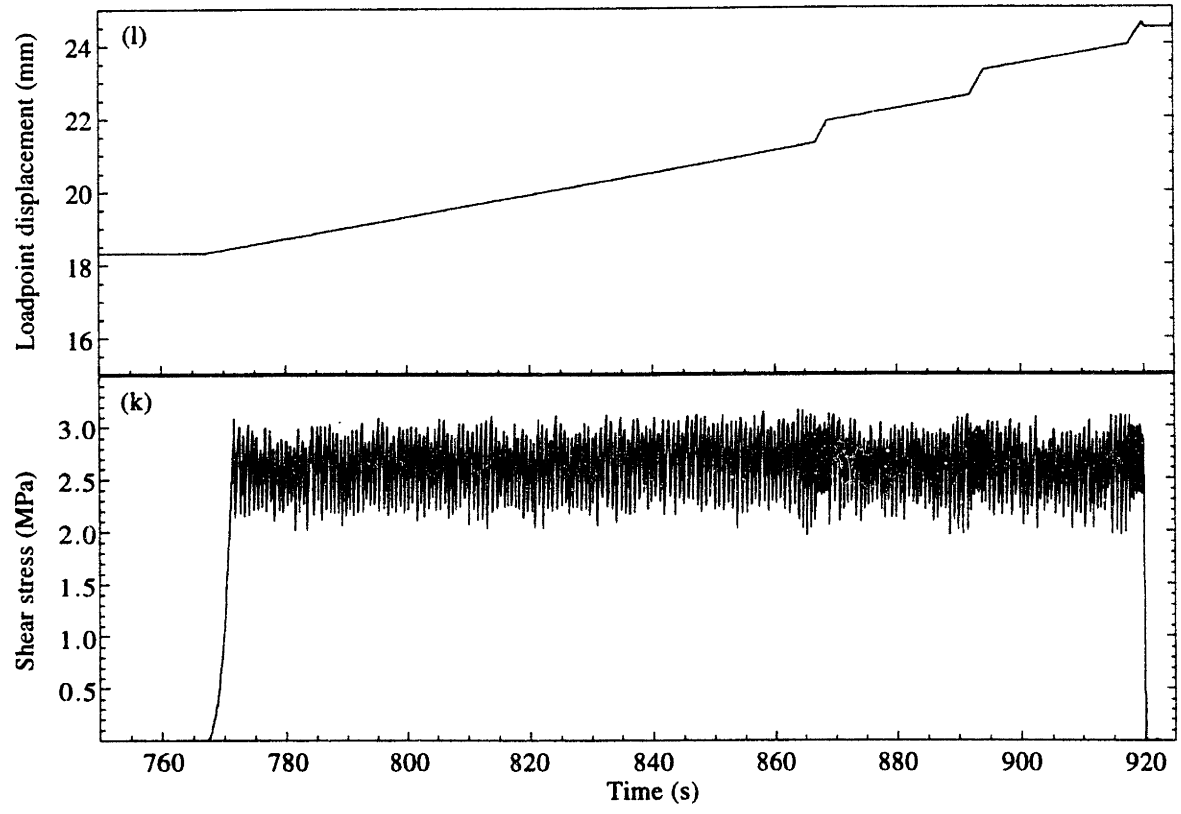

Experiment m254 (continued)

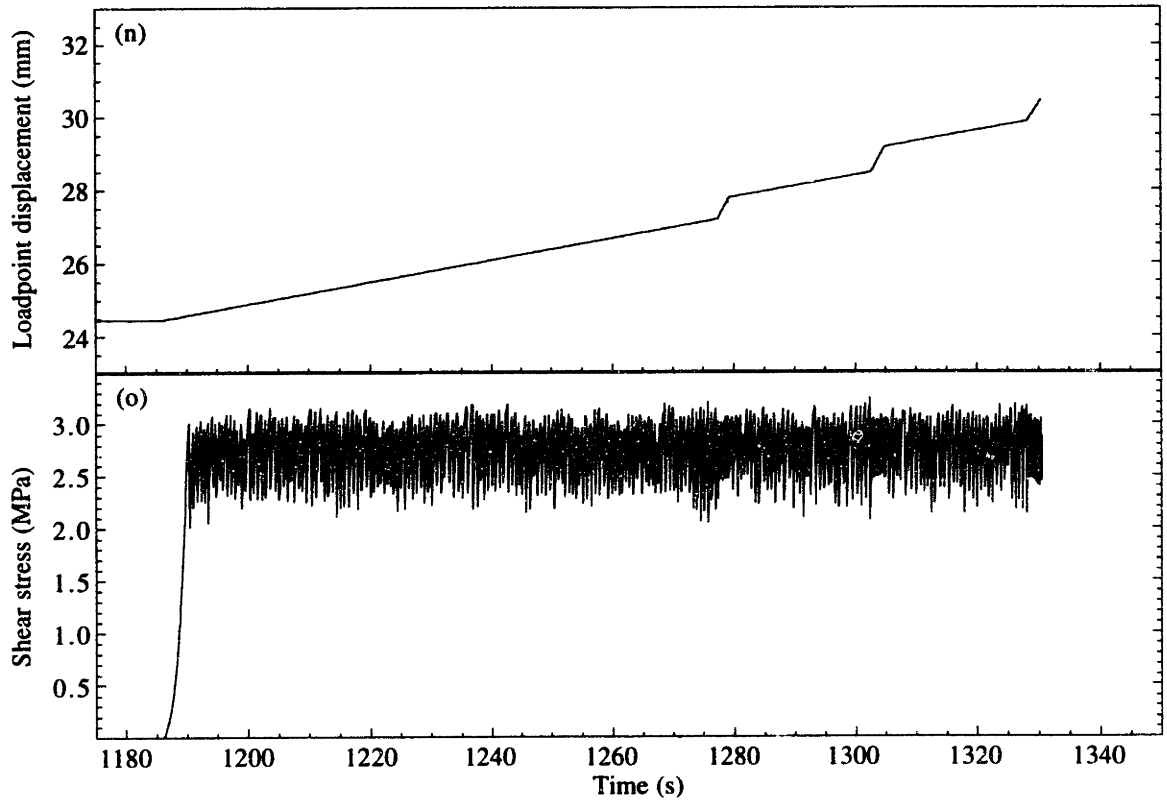

Experiment m255

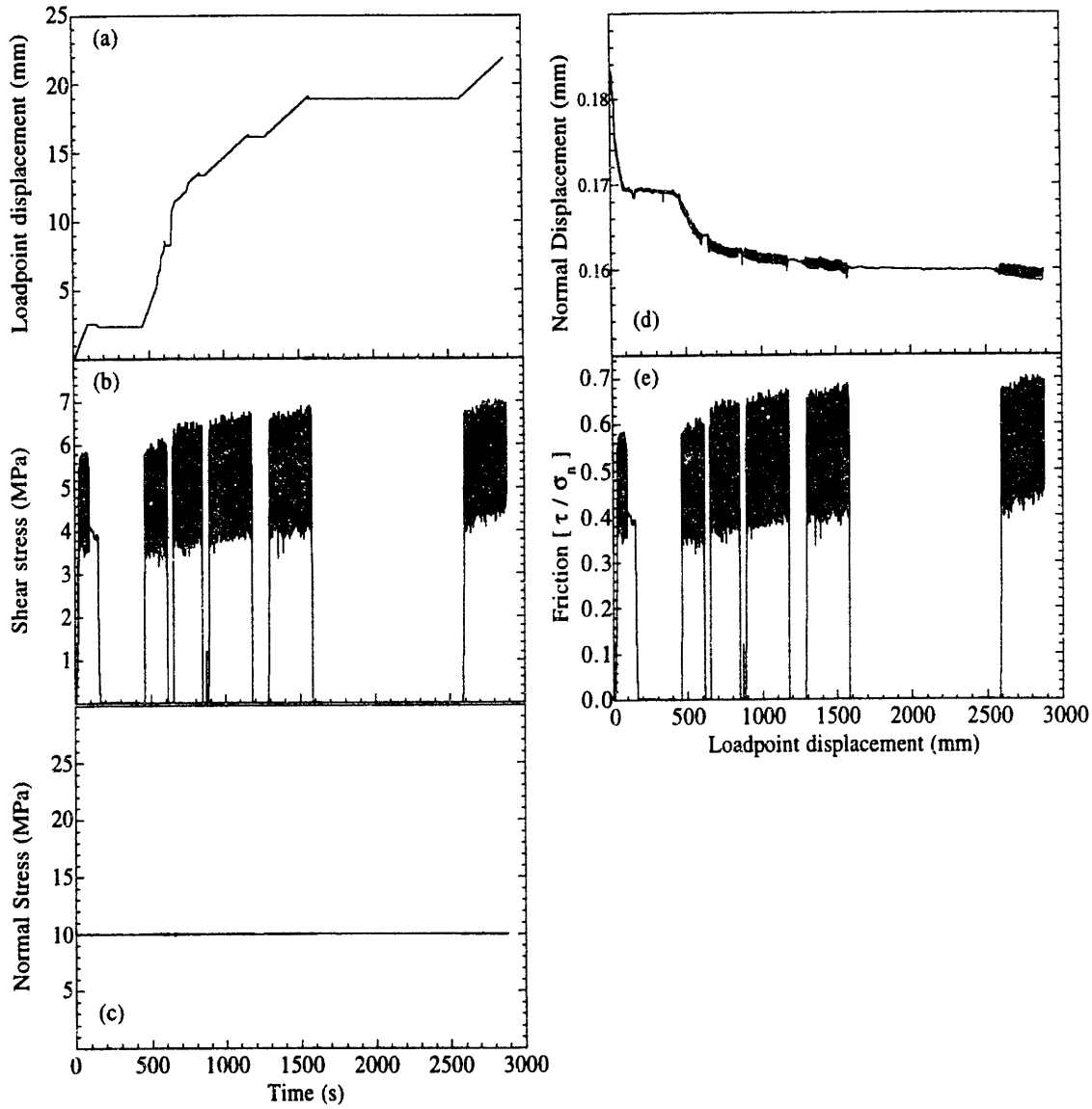

Experiment m255 (continued)

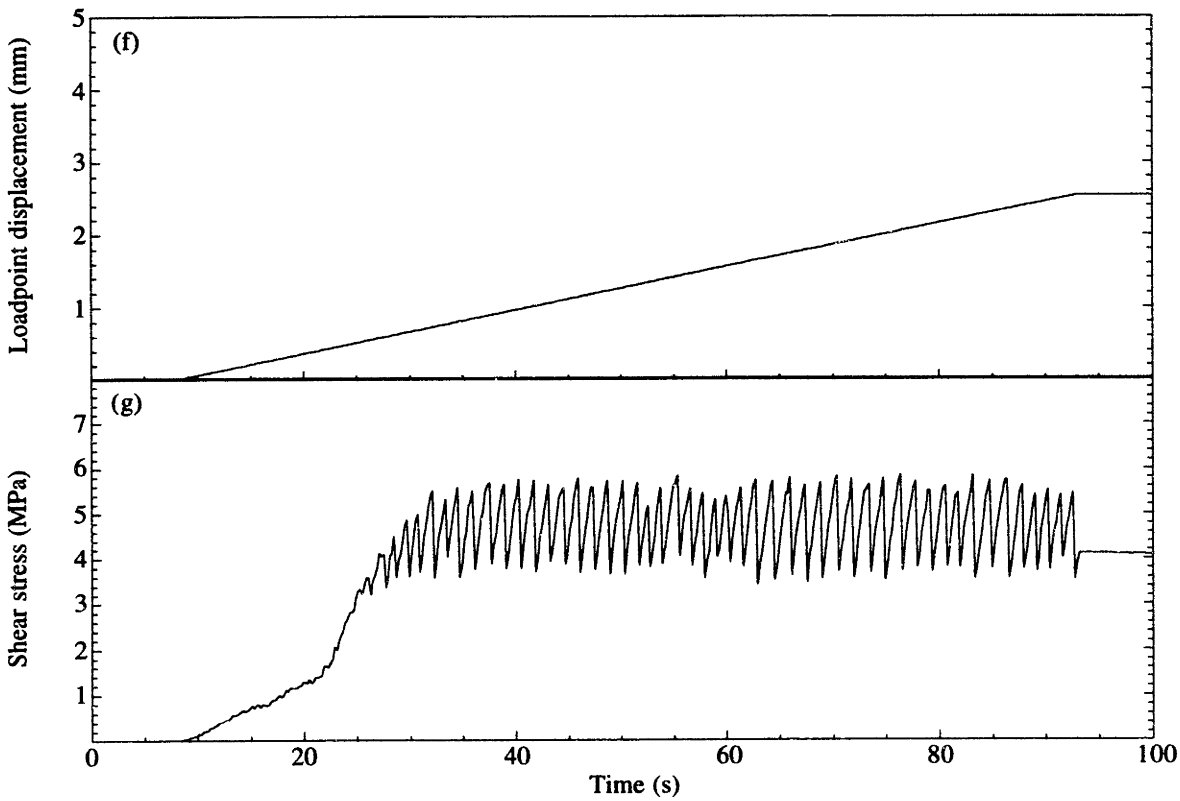

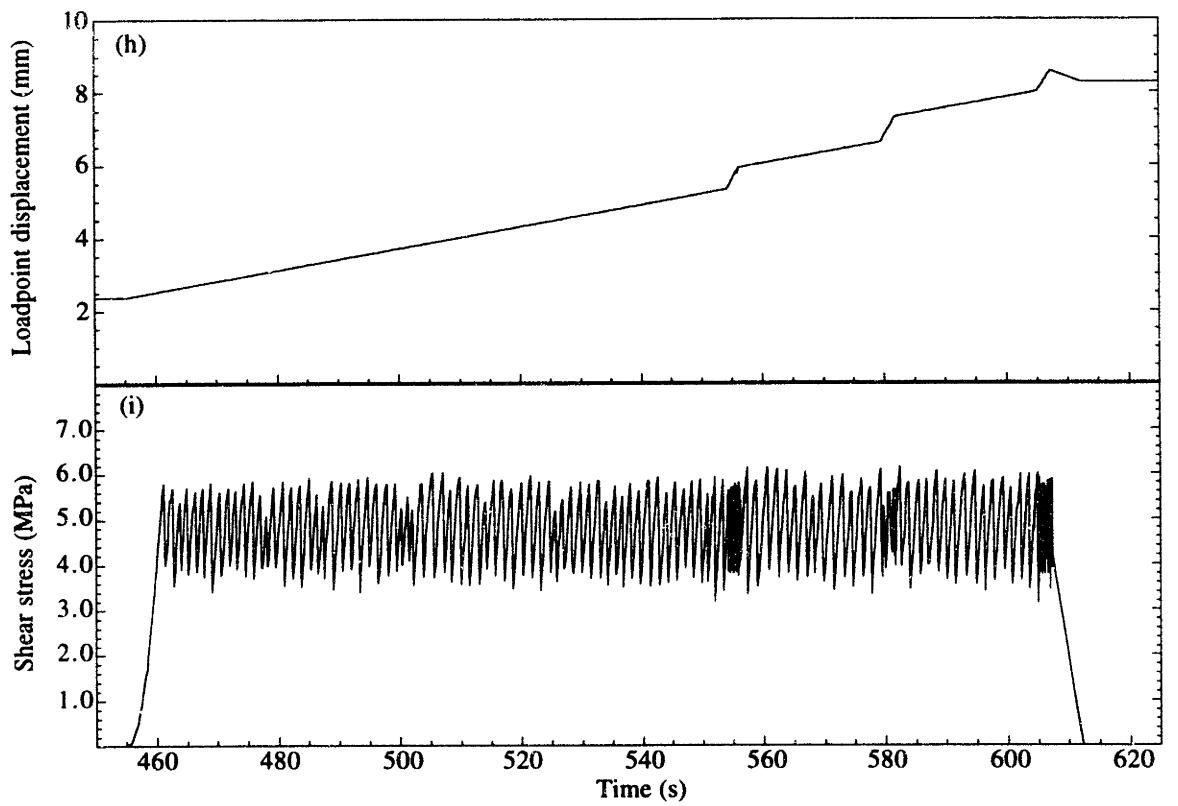

Experiment m255 (continued)

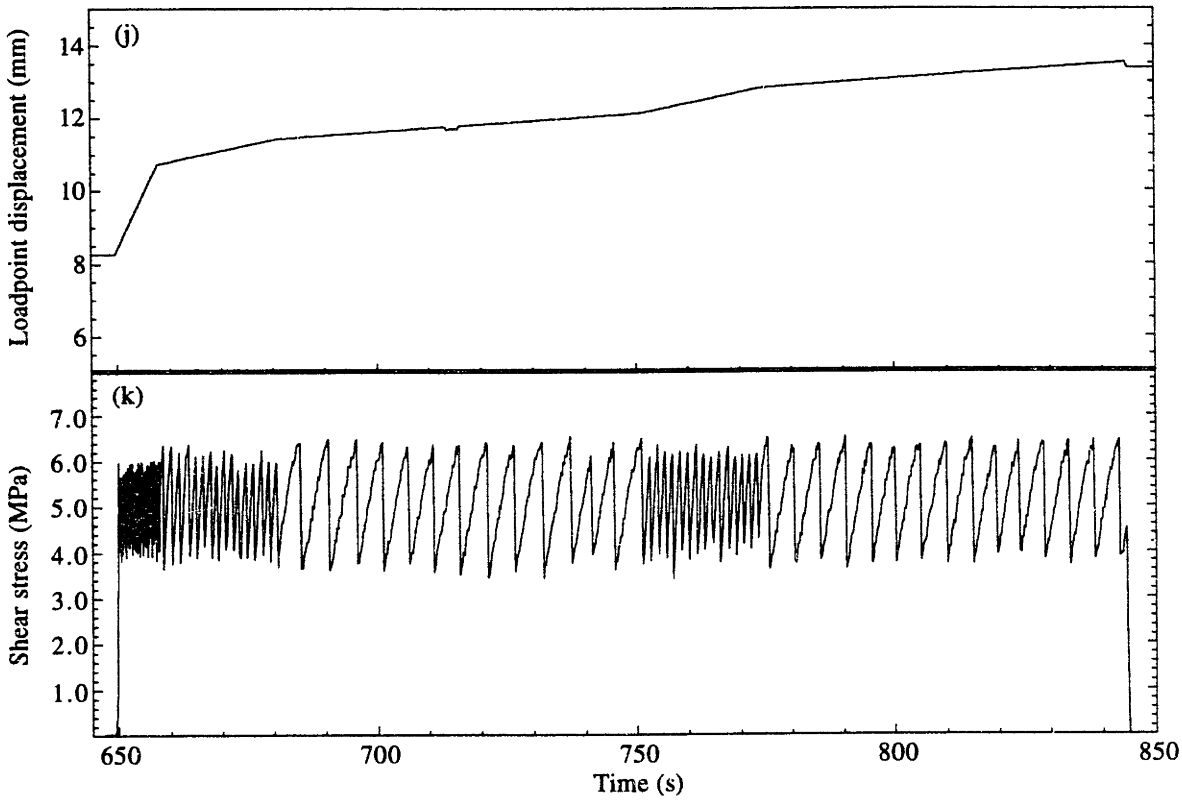

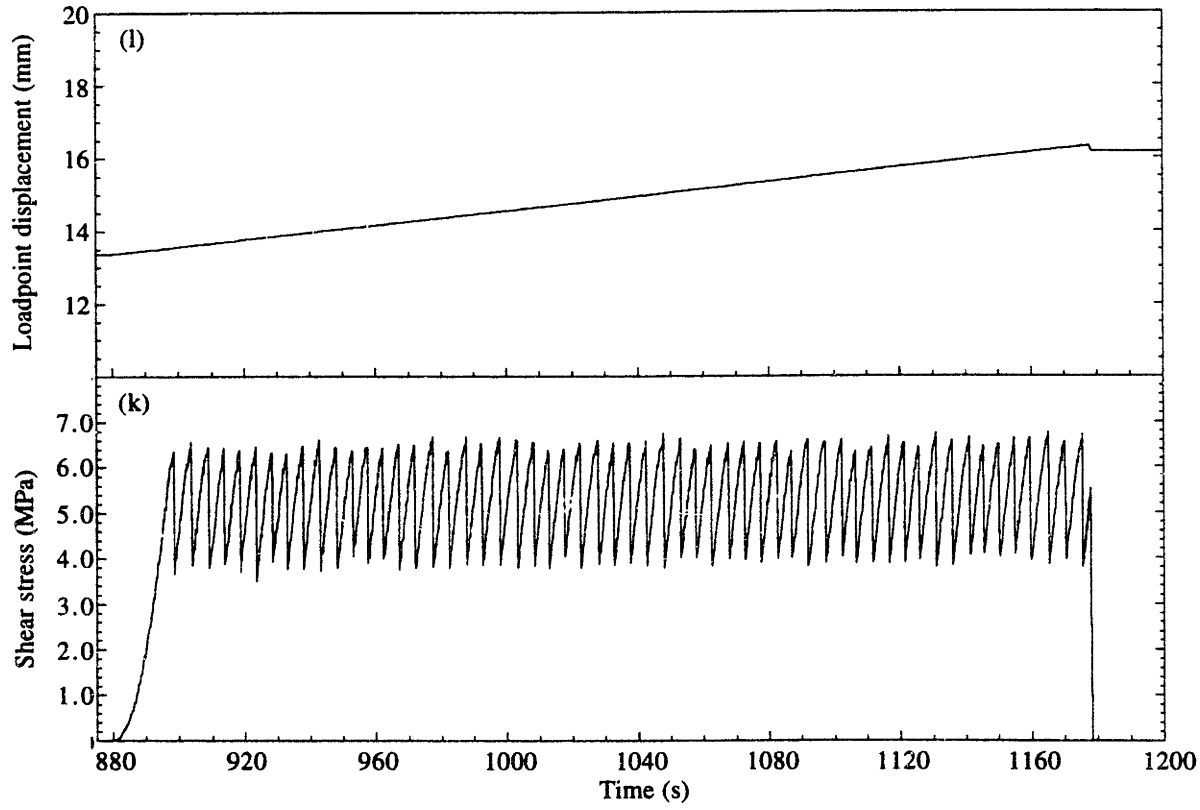

Experiment m255 (continued)

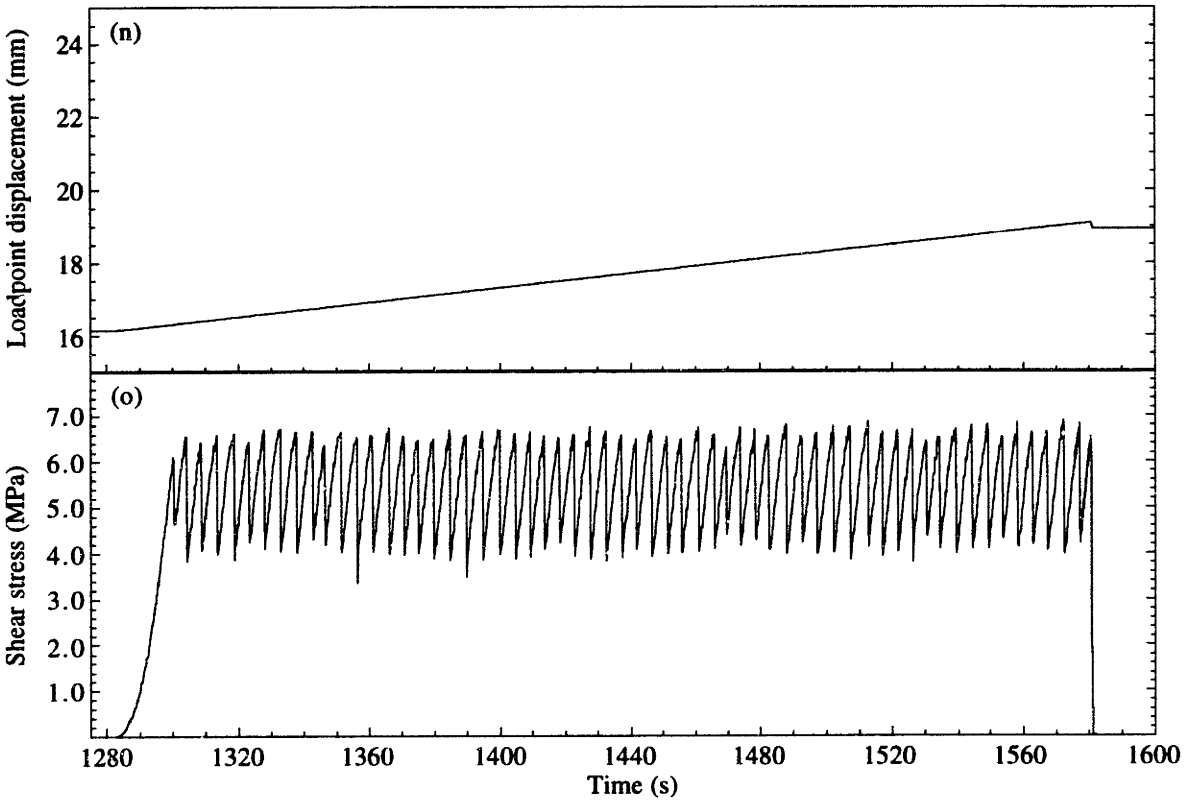

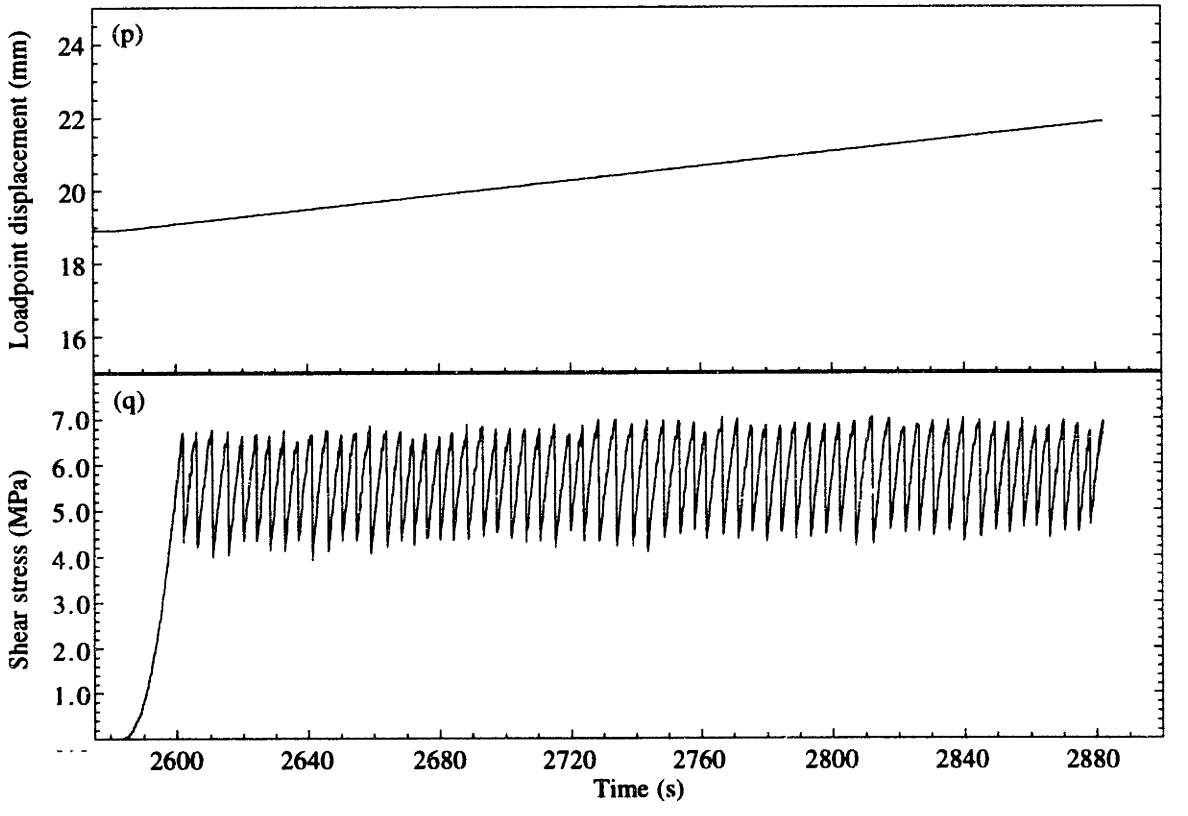

Experiment m256

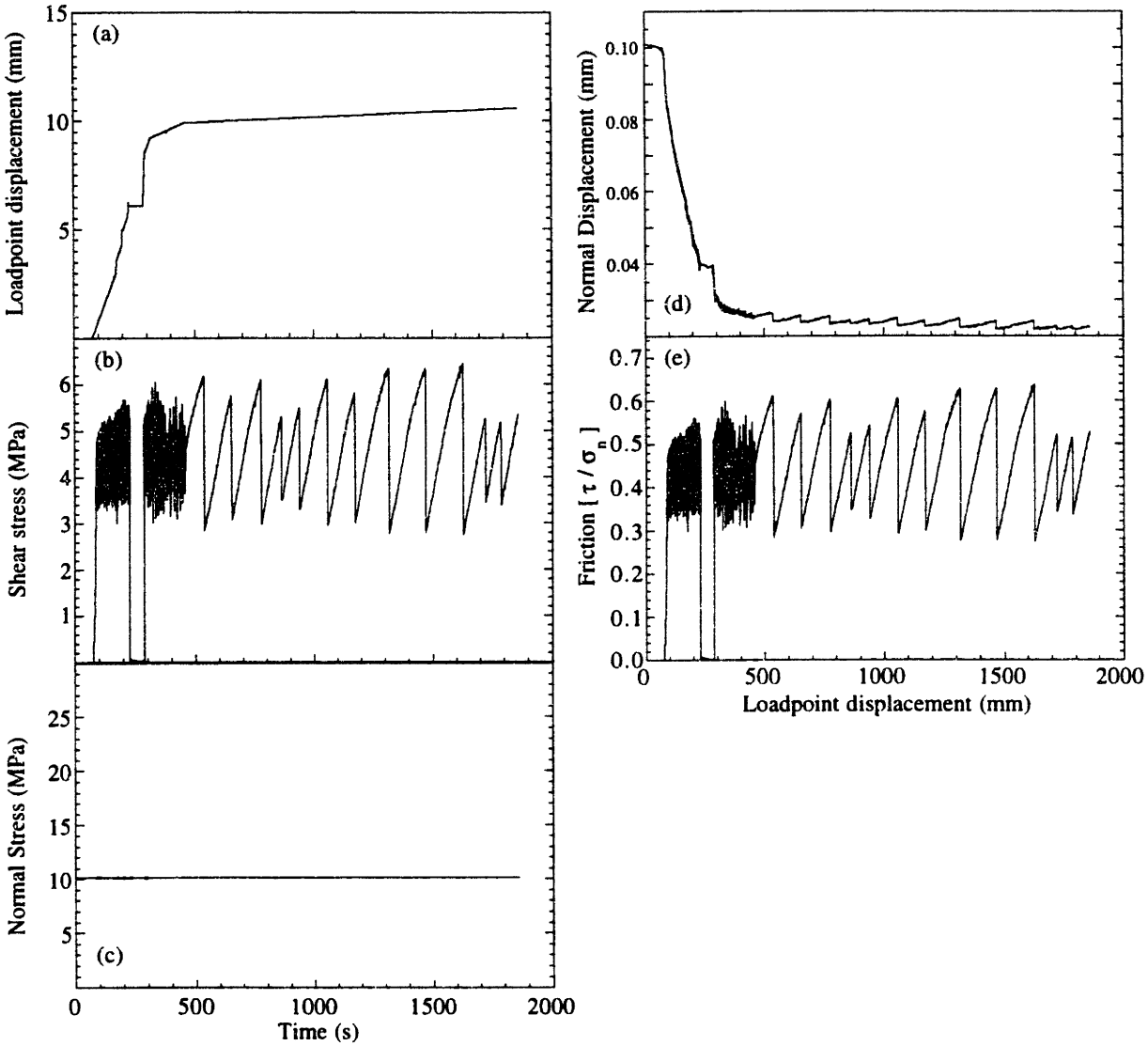

Experiment m256 (continued)

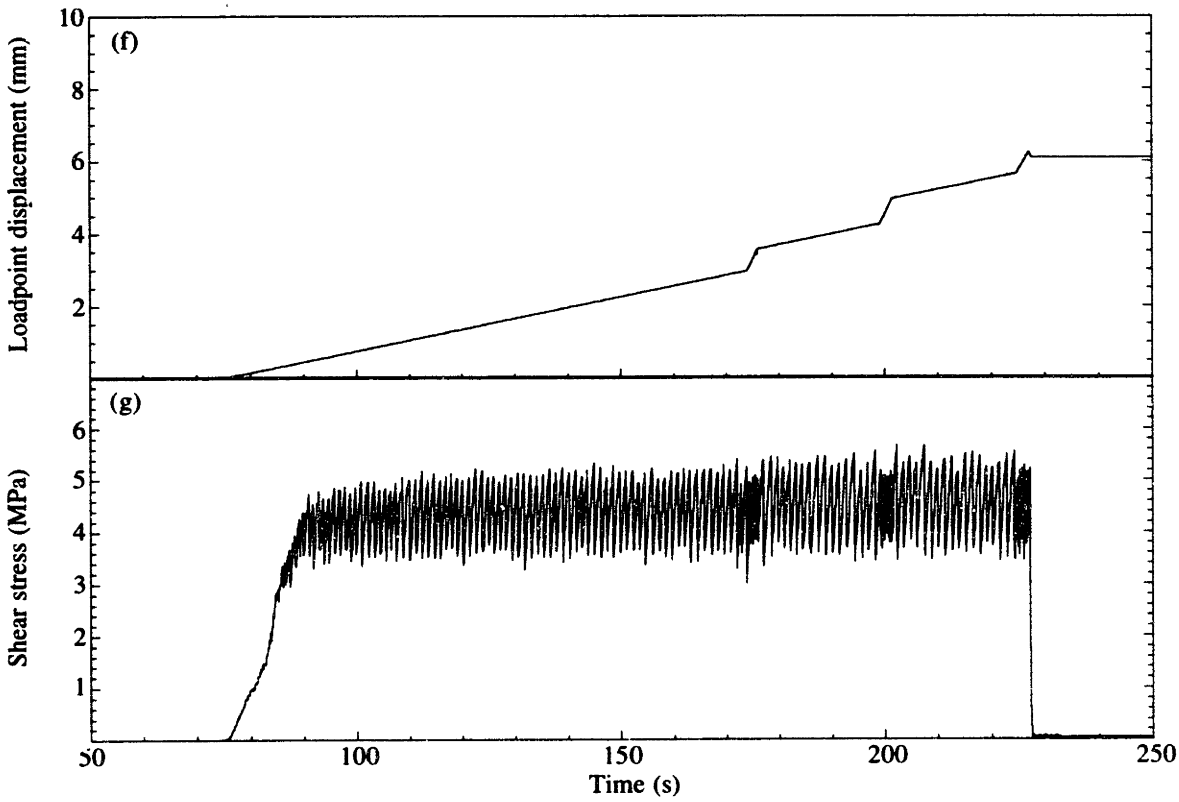

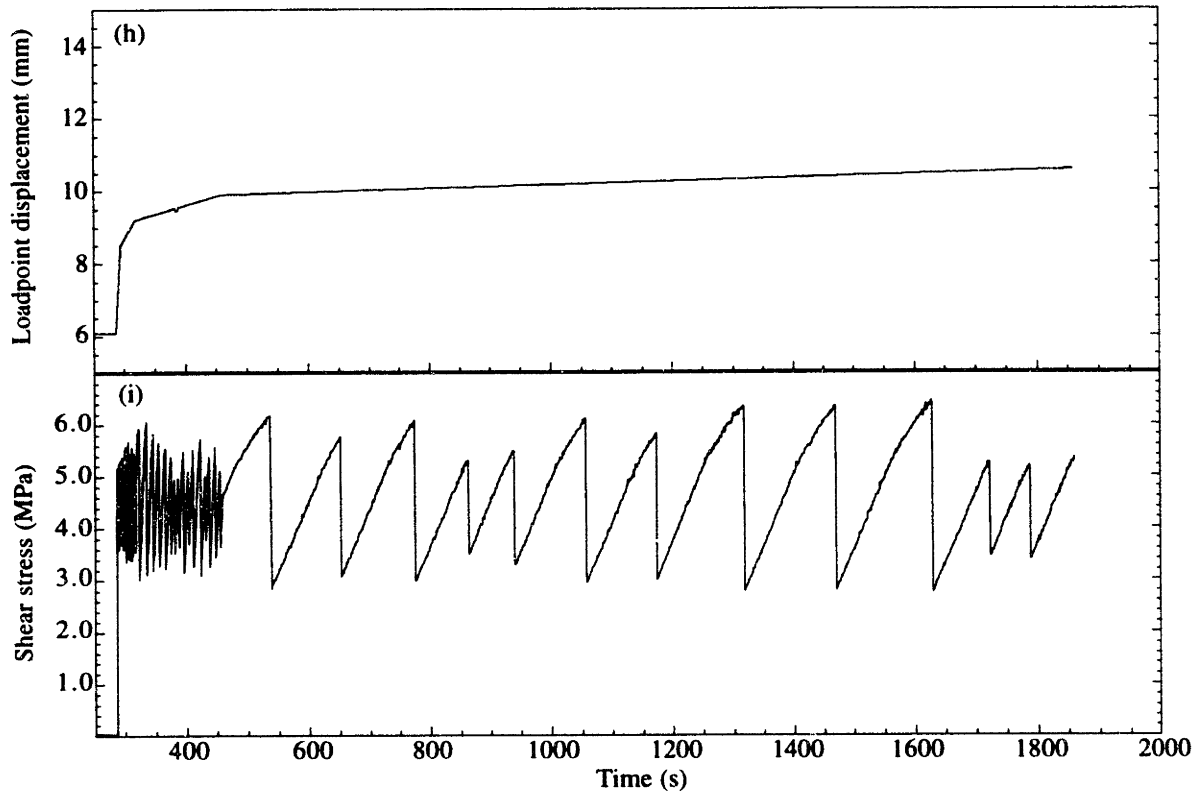

APPENDIX D

Data from biaxial tests on quartz gouge (Chapter 3)

The following figures show data from experiments performed on layers of quartz gouge, as described in Chapter 3 of this thesis. All experiments were conducted in a biaxial deformation apparatus at room-temperature and humidity. For all tests, shear was imposed by controlling the velocity of the loading piston. Normal stress was maintained constant throughout each test. For a summary of experiment conditions refer to Table 3.1.

The following figures show data from each experiment. For all tests, loadforces and displacements were measured at the loadpoint and friction is determined from the measured shear and normal stresses (Figures a-e). During shear, some gouge is lost from the layers owing to geometric spreading of the layers. For some tests, this material was collected throughout the experiment to determine the volume of gouge loss (Figure f). In a few experiments, we monitored layer slip and thickness changes using transducers mounted on the sample. Two transducers monitored layer slip, and another two monitored sample thickness. These data are shown in Figures g-j.

a). Loadpoint displacement in the shear direction is plotted as a function of experiment time. Thus, the slope of the data indicates the imposed loading rate.

b). Shear stress for a single gouge layer.

c). Normal stress during the test.

d). Thickness of a single gouge layer plotted against loadpoint displacement. Layer thickness is determined from the measured displacement of the loading piston. Data have been corrected for elastic effects (as described in Chapter 3, and Appendix B).

e). Coefficient of friction shown as a function of loadpoint displacement.

f). Cumulative mass of gouge lost during experiment.

g). Sample slip as measured at the top of the sample (towards the loading piston).

h). Sample slip as measured at the bottom of the sample (away from the loading piston).

i). Thickness of a single gouge layer measured at the top of the sample. Data have been corrected for Poisson distortion of the center block (as described in Chapter 3, and Appendix B).

j). Thickness of a single gouge layer measured at the bottom of the sample. Data have been corrected for Poisson distortion of the center block.

For reference, the Table 3.1 containing the summary information for the experiments shown in this Appendix is reproduced on the following page.

Experiment Number	Initial layer thickness (mm)	Loading rate (μm/s)	Normal stress (MPa)	Forcing block material	τ for hold (τ_{hold}/τ_{ss})	Nominal Hold time (sec)
m165	3	300	25	Steel	0	10, 100
m166	3	300	25	Steel	0	10, 100
m167	3	300	25	Steel	0	10, 1000
m168	3	300	25	Steel	0	10, 100
m169	3	300	25	Steel	0	100, 1000
m170	3	300	25	Steel	0	100, 1000
m175	3	300	25	Steel	0	1000, 10000
m204	3	10	25	Steel	0	100, 1000
m205	3	10	25	Steel	0	100, 1000
m206	3	10	25	Steel	0.346	100
m207	3	10	25	Steel	0	1000, 10000
m209	3	10	25	Steel	0.064	100
m210	3	10	25	Steel	0.195	100
m211	3	10	25	Steel	0.593	100
m213	3	10	25	Steel	1	100
m214	3	10	25	Steel	0.910	100
m231	3	10	15	Westerly	0	100, 1000
m232	2	10	15	Westerly	0	100, 1000
m233	1	10	15	Westerly	0	100, 1000
m235	2	10	15	Westerly	0	10, 100
m236	1	10	15	Westerly	0	10, 100
m244	0.5	10	15	Westerly	0	100, 1000
m246	0.5	10	15	Westerly	0	10, 100
m247	2	10	15	Westerly	0	1000, 10000
m248	1	10	15	Westerly	0	10, 100
m250	1	10	15	Westerly	0	1000, 10000
m251	0.5	10	15	Westerly	0	1000, 10000
m262	3	10	25	Steel	0 (and 1)	10, 100
m263	3	300	25	Steel	0	0, 10
m264	3	300	25	Steel	0	0, 10
m265	3	10	25	Steel	0	0, 10
m266	3	10	25	Steel	0.064	0, 10
m267	3	10	25	Steel	0.195	0, 10
m282	3	300	25	Steel	Constant V	
m283	3	30	25	Steel	Constant V	
m284	3	3	25	Steel	Constant V	
m295	3	10	25	Steel	Combination	10-10000

Table D.1. Summary of loading conditions and sample data that were the tested variables for the experiments.

Experiment m165

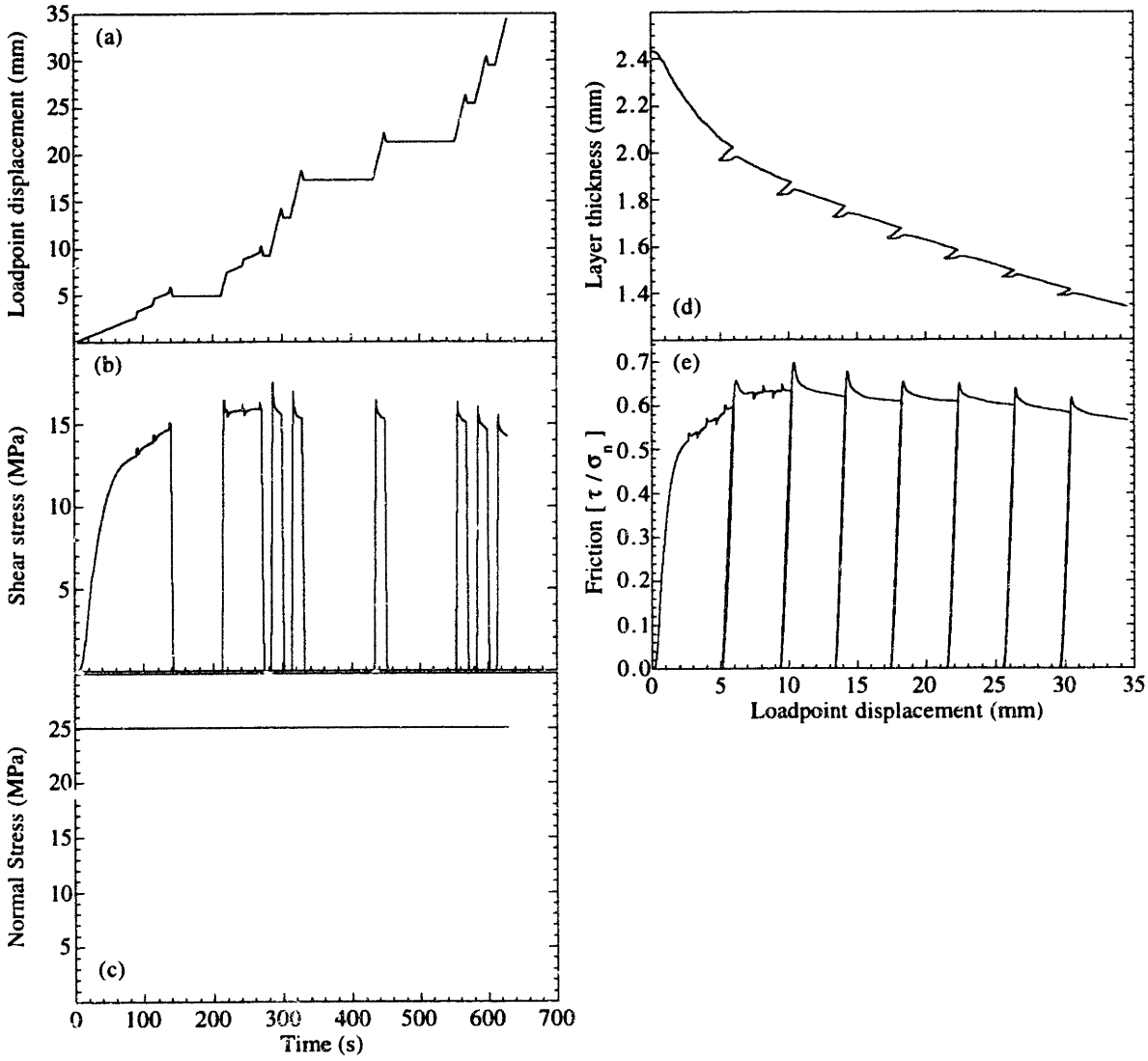

Experiment m166

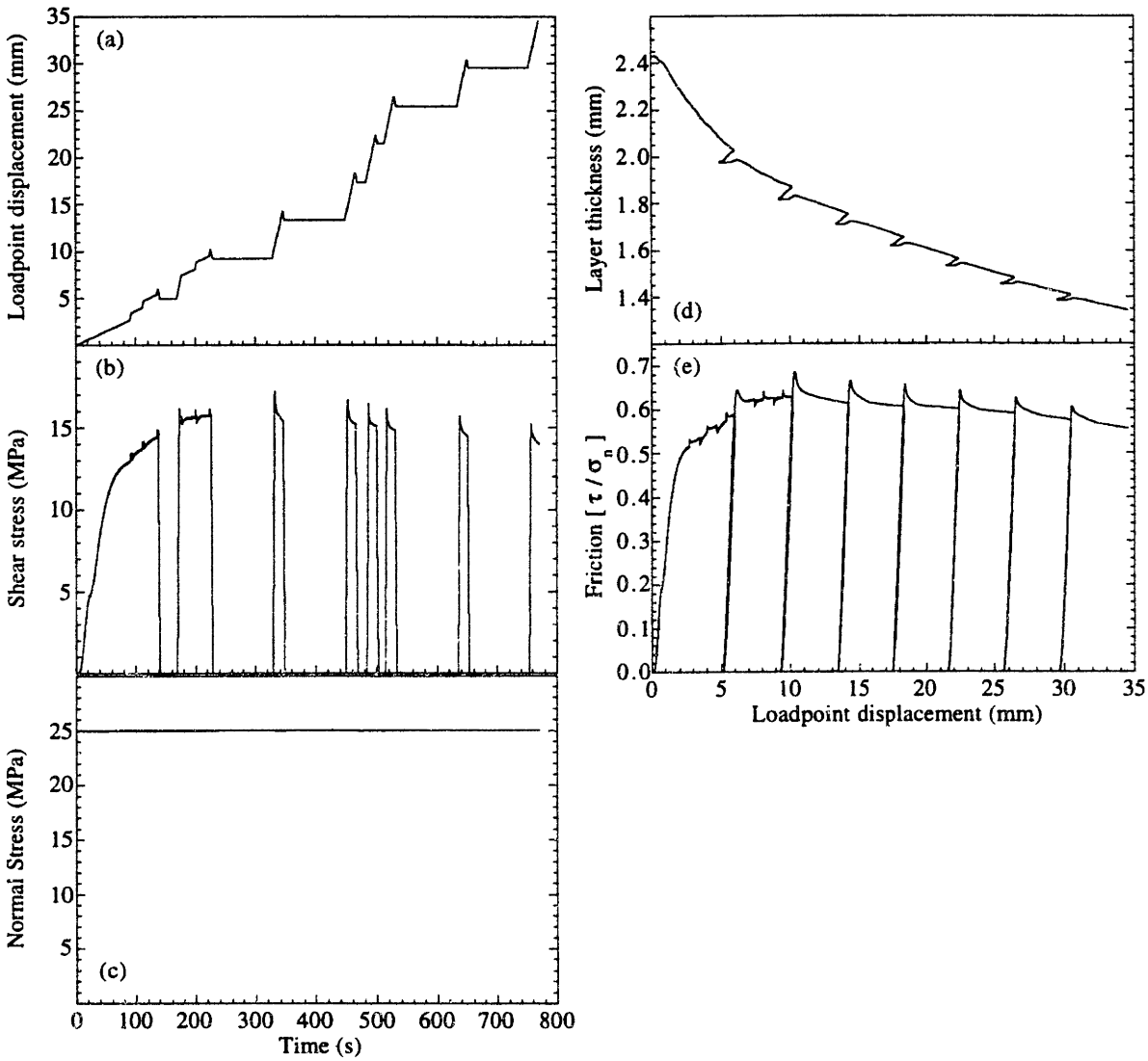

Experiment m167

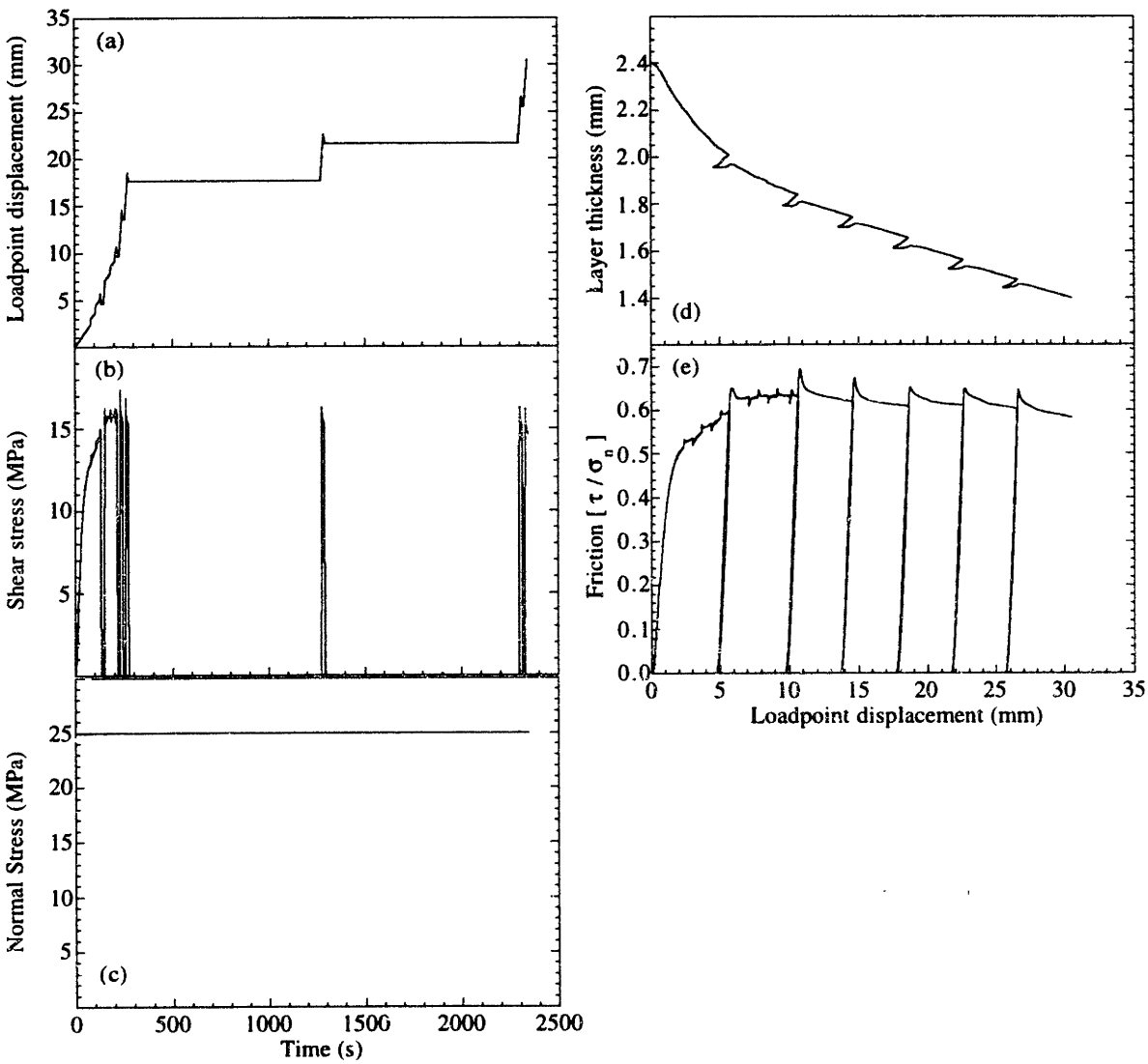

Experiment m168

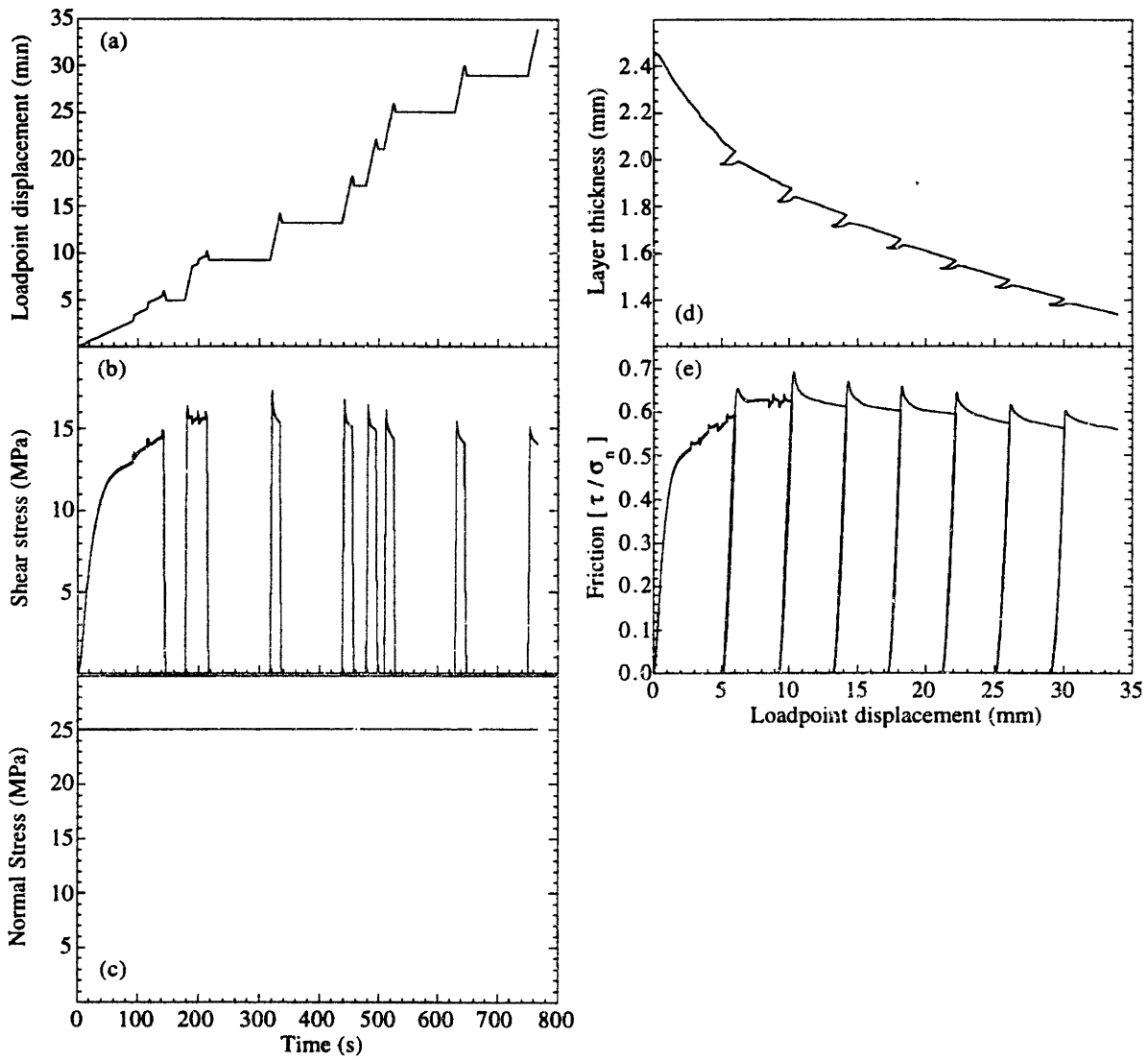

Experiment m169

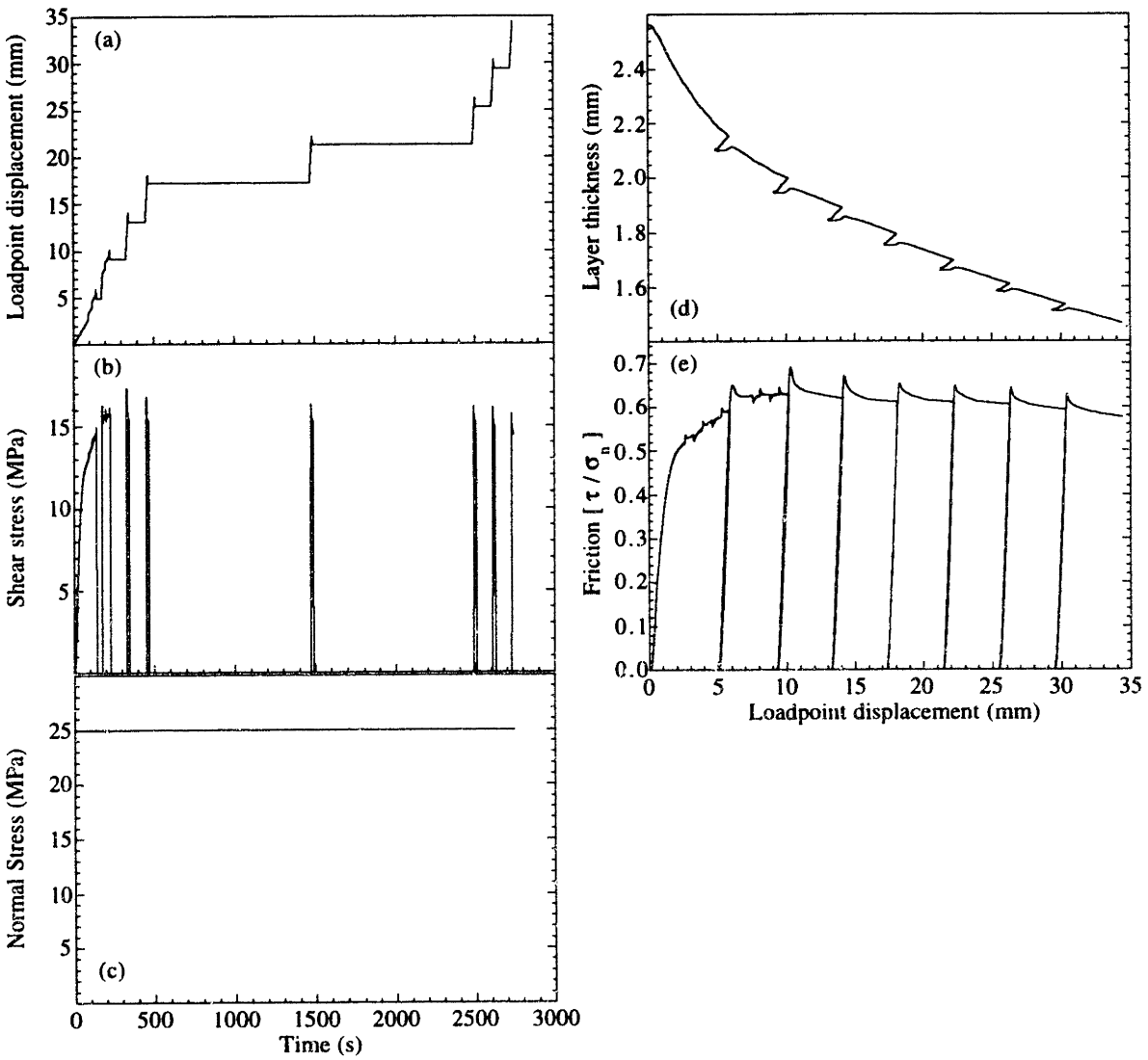

Experiment m170

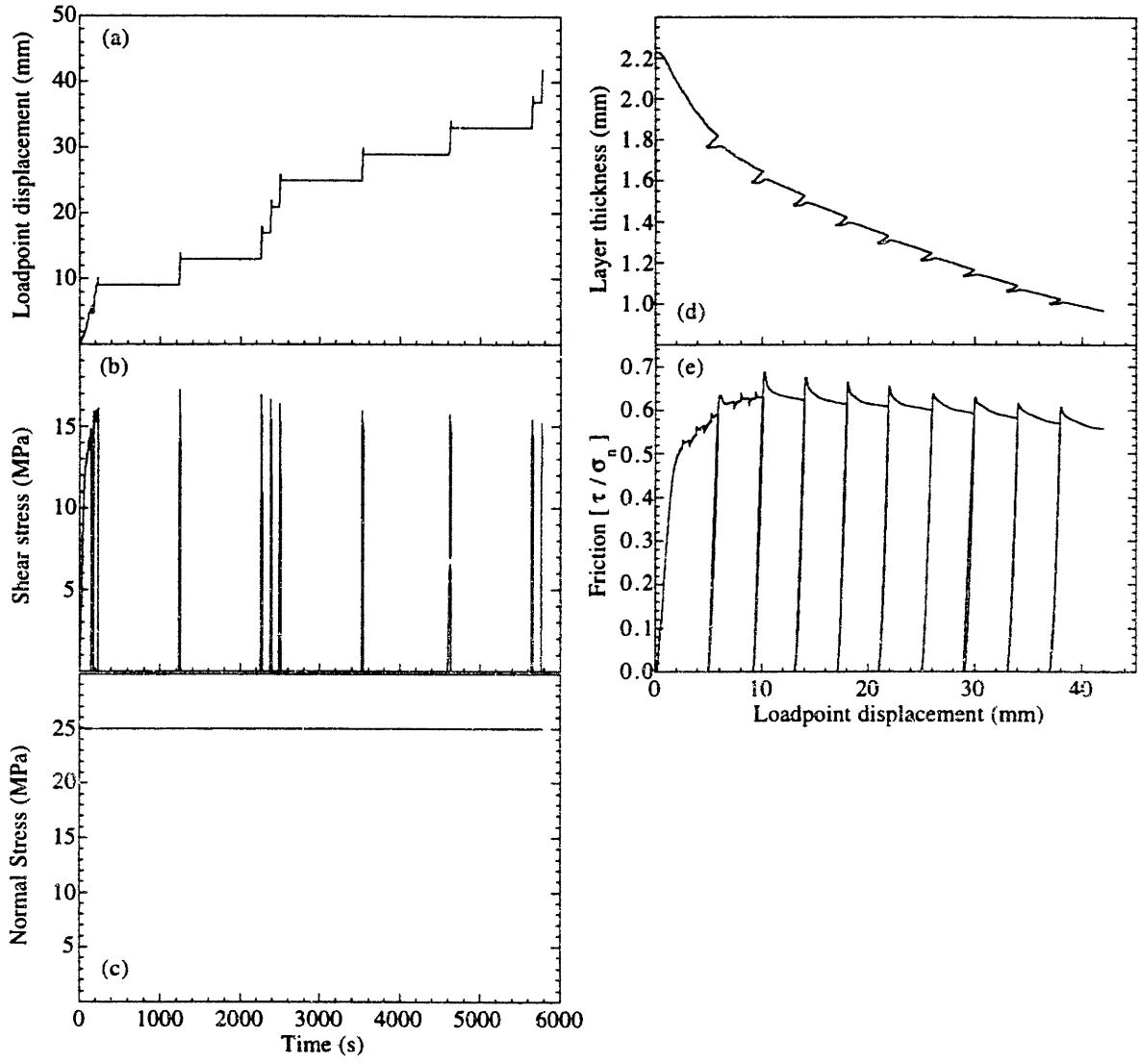

Experiment m171

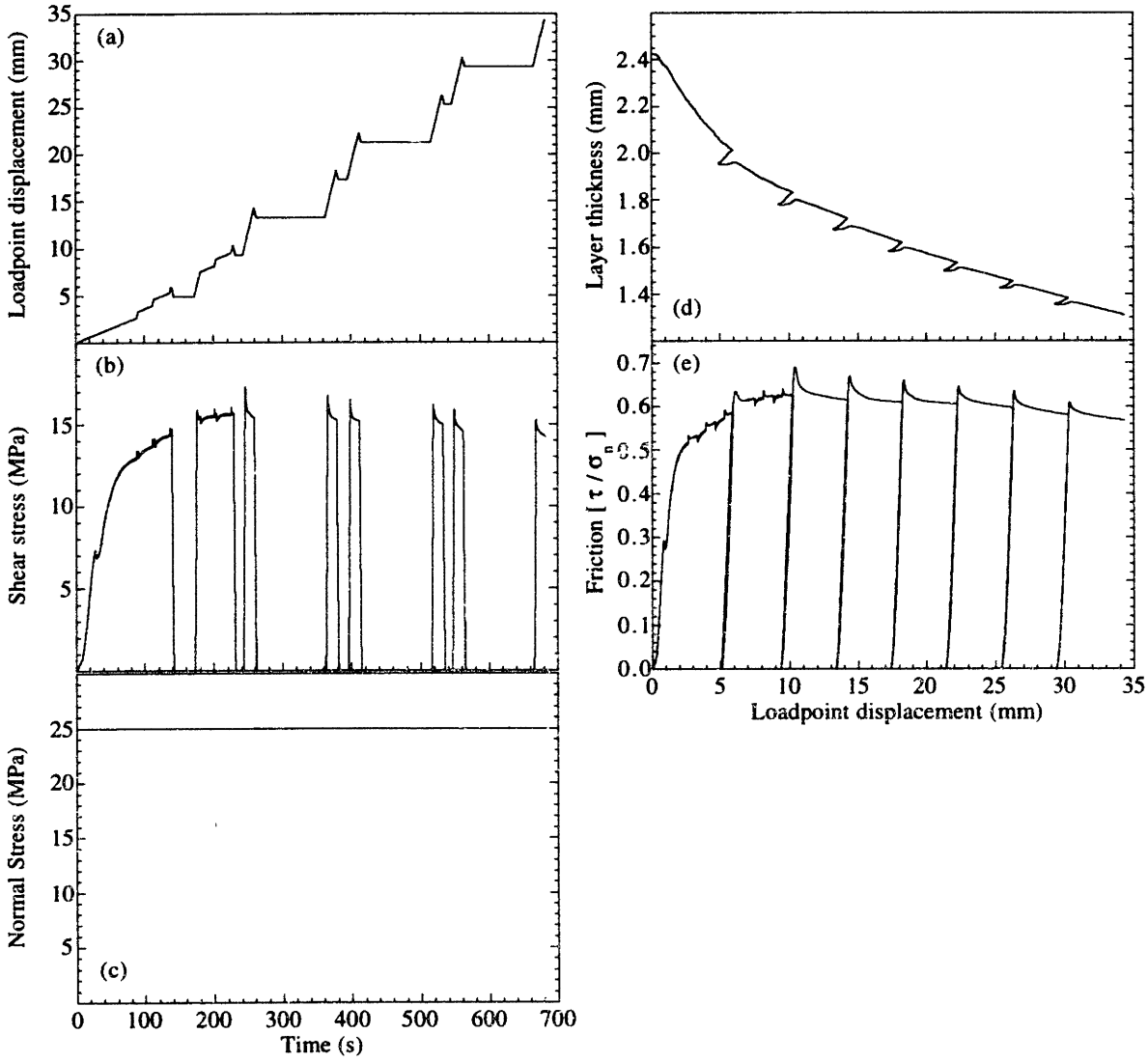

Experiment m172

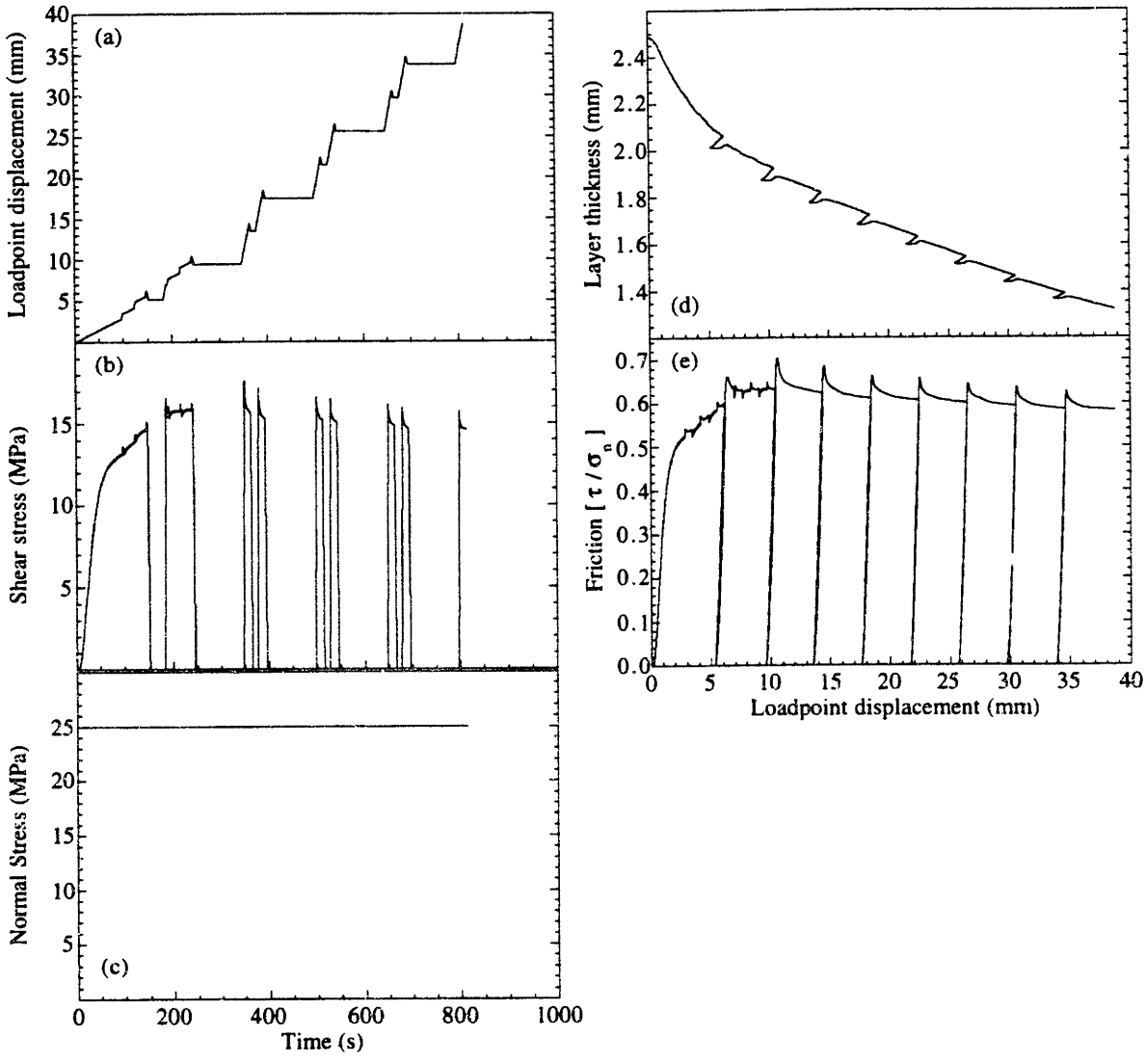

Experiment m173

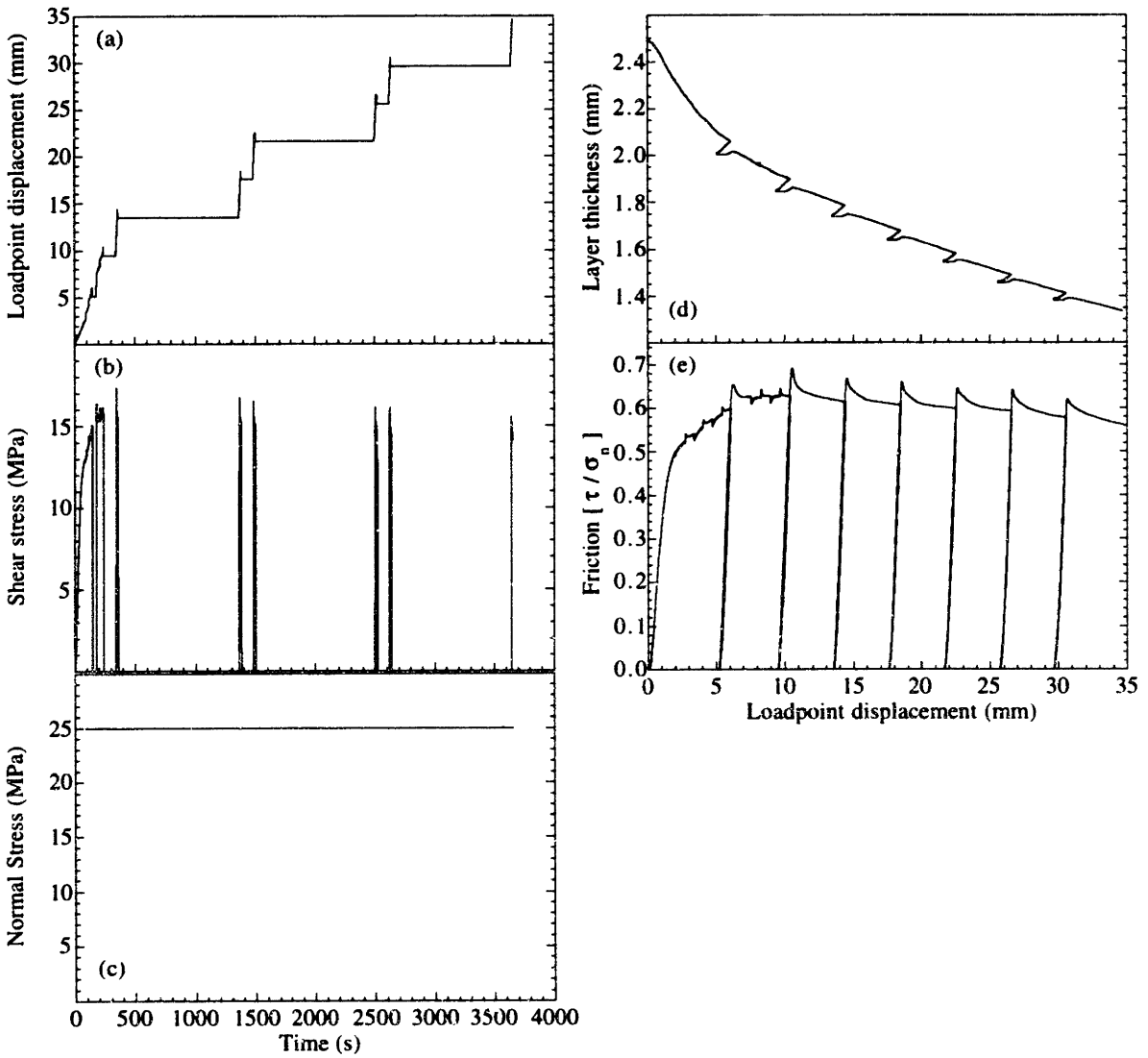

Experiment m174

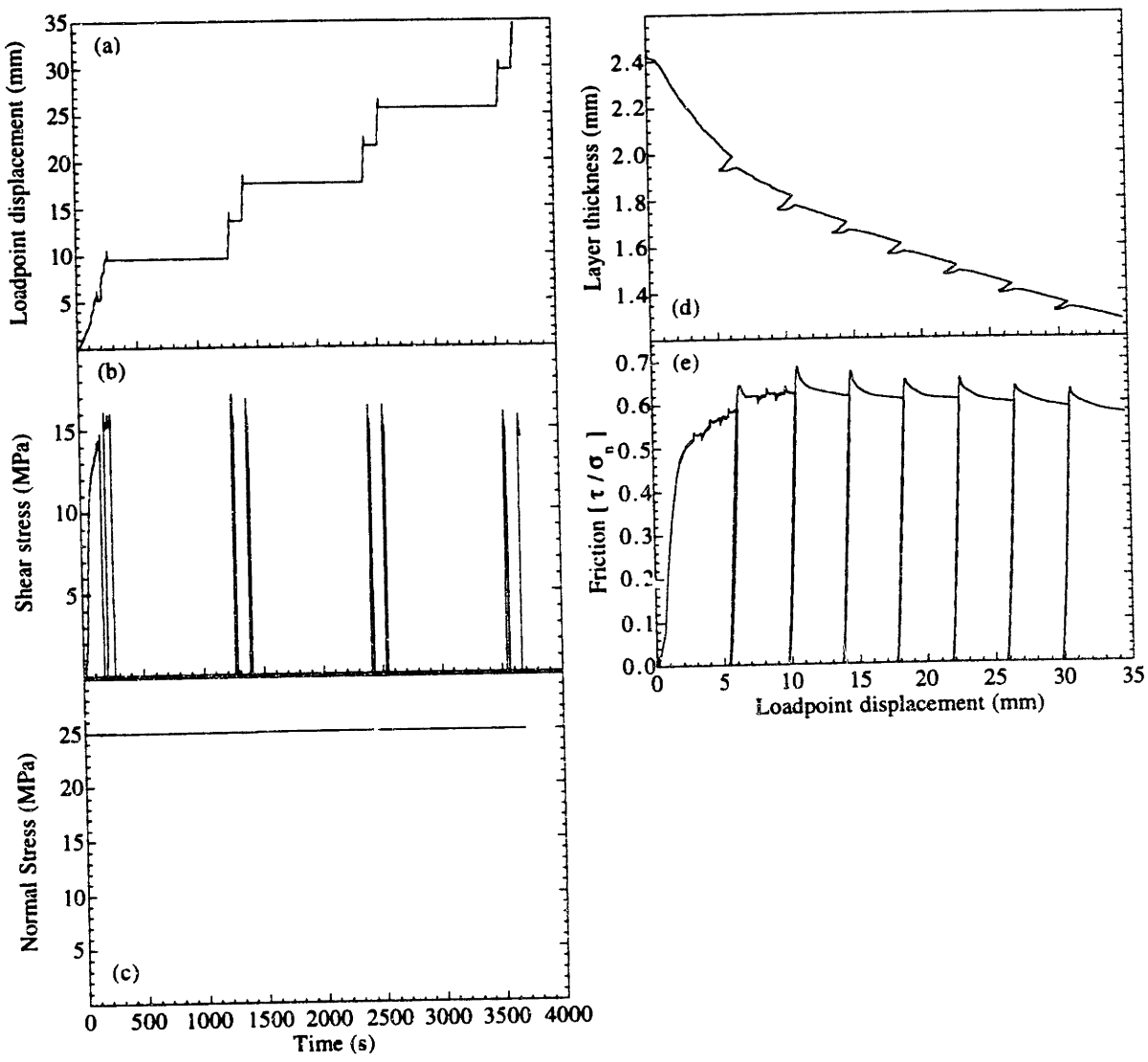

Experiment m175

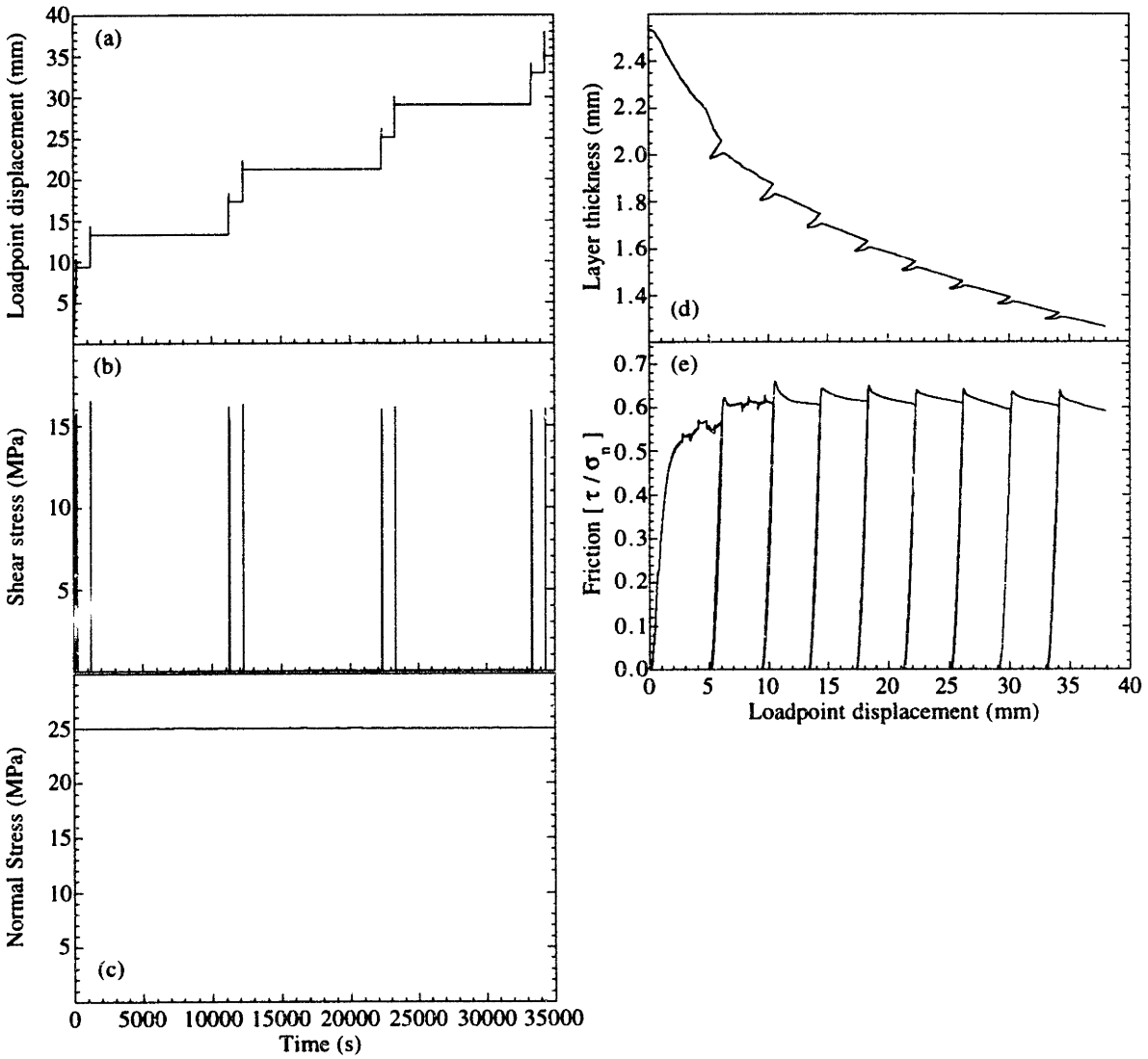

Experiment m176

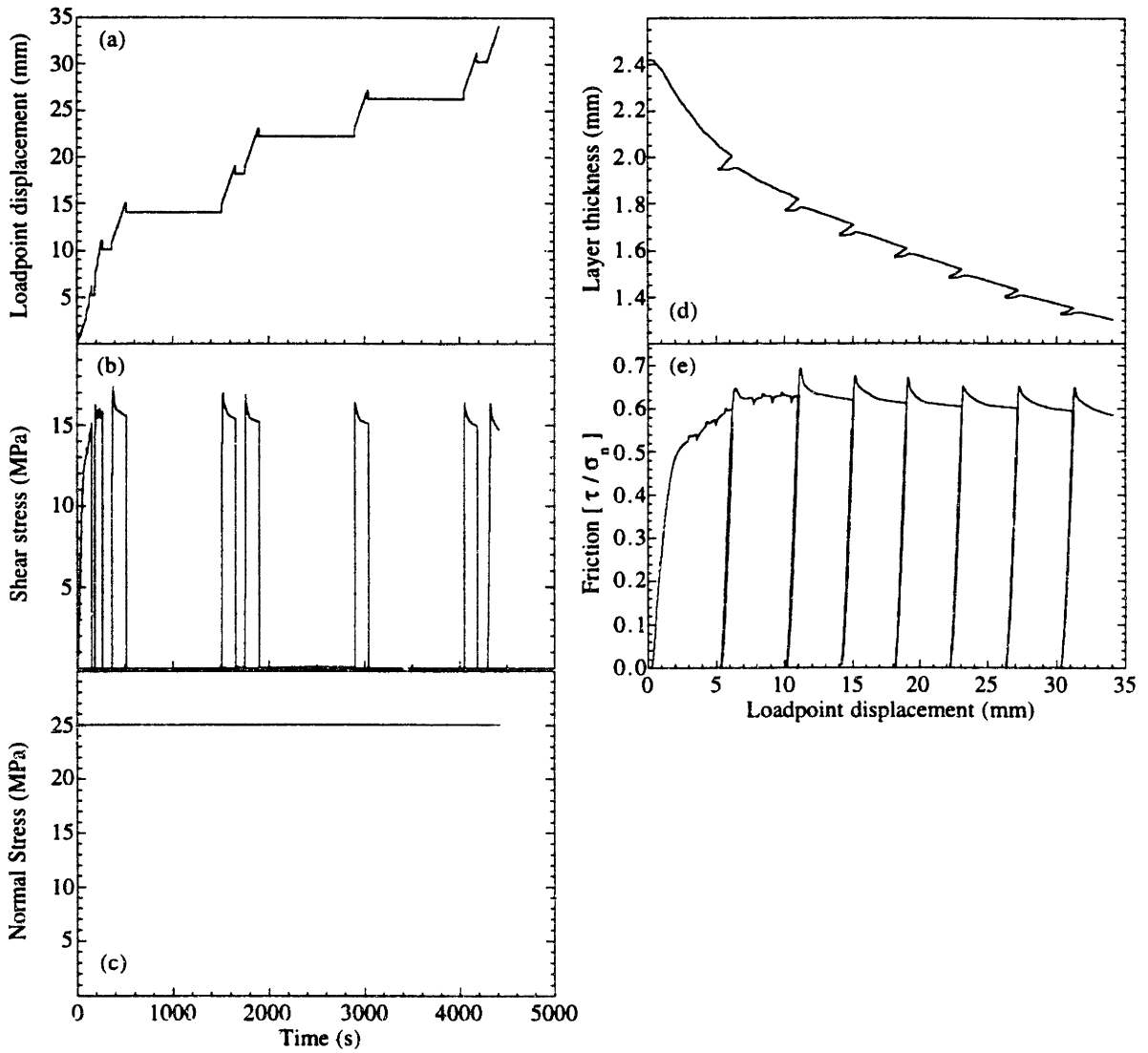

Experiment m187

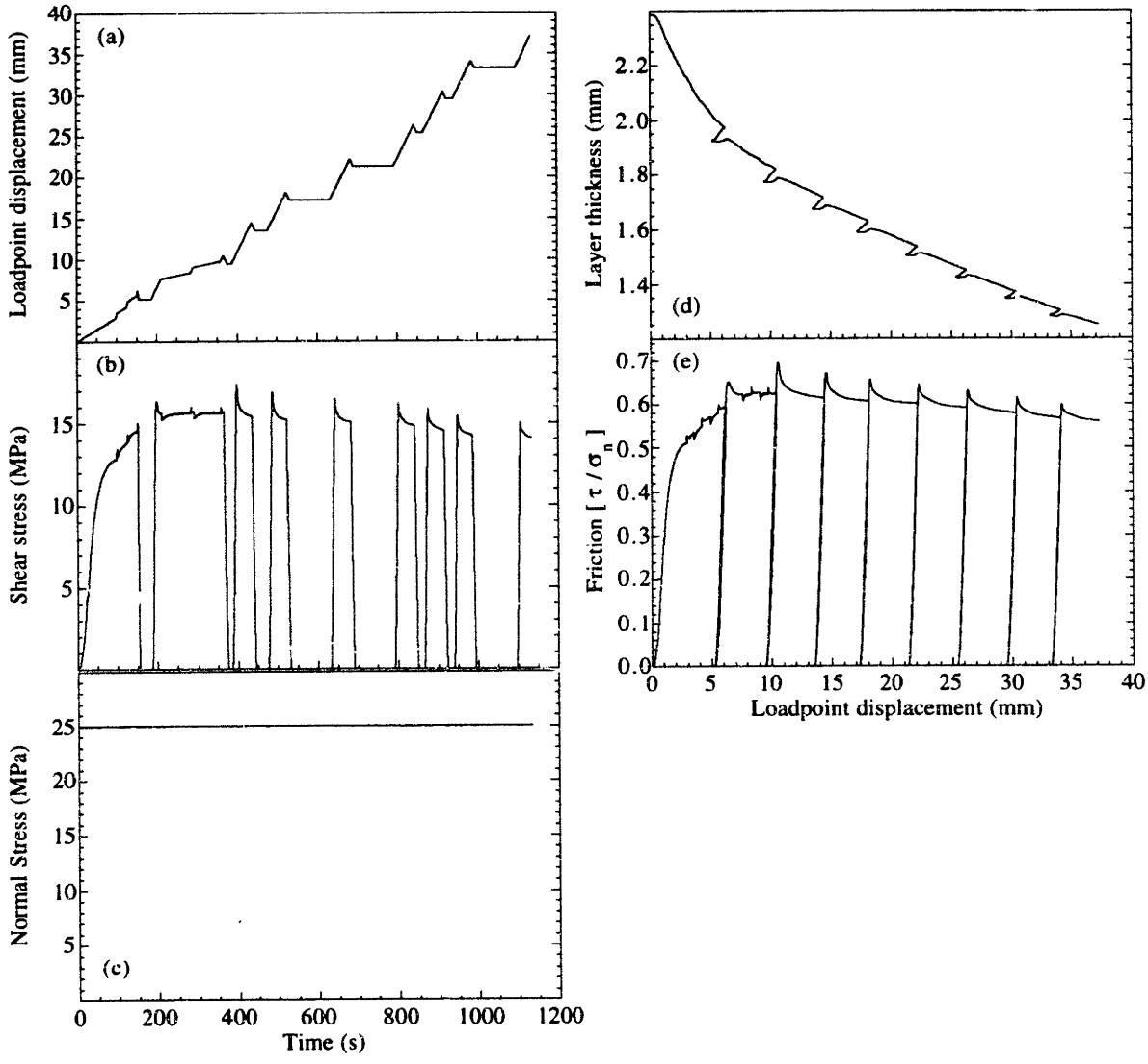

Experiment m203

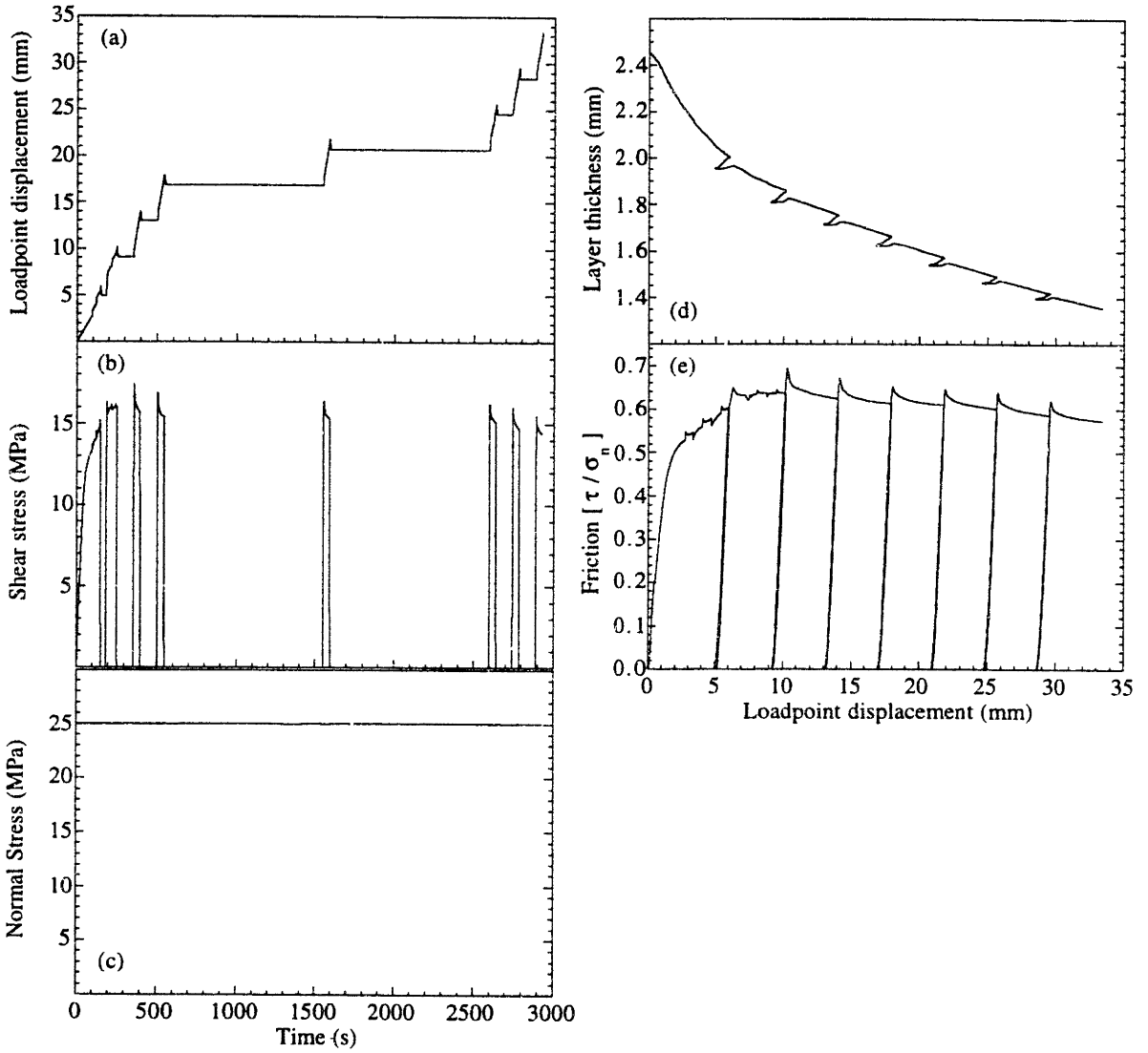

Experiment m204

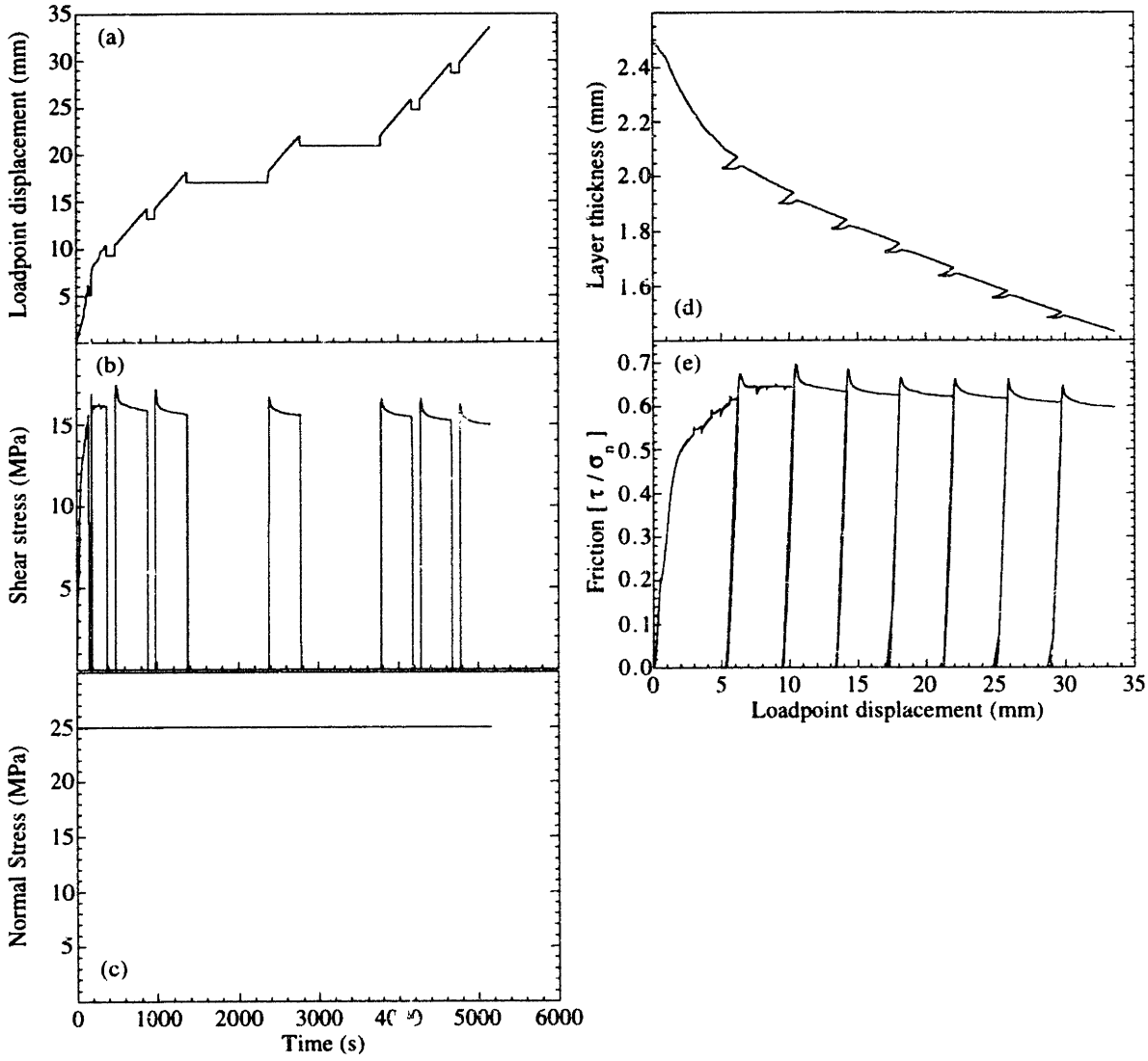

Experiment m205

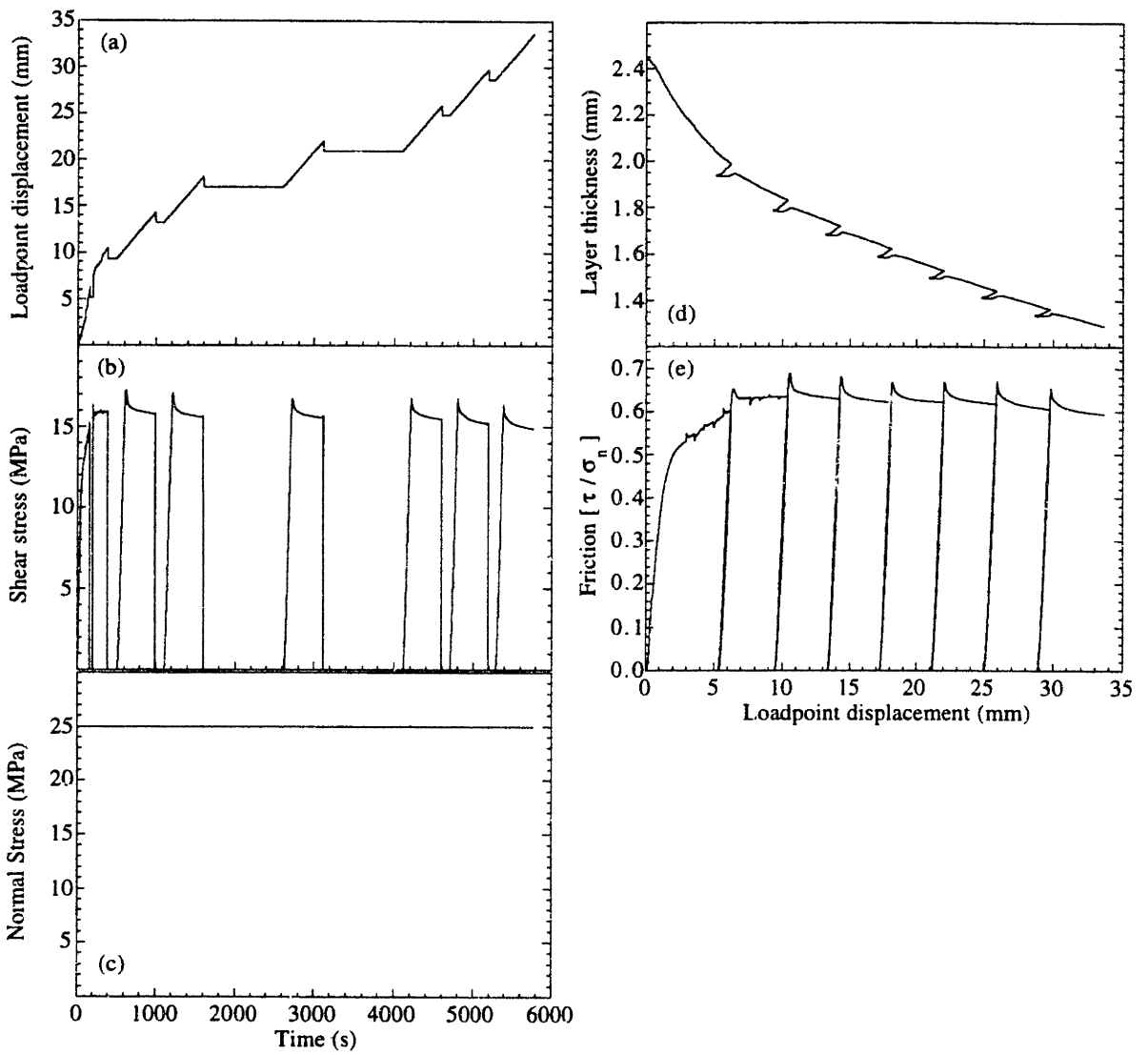

Experiment m206

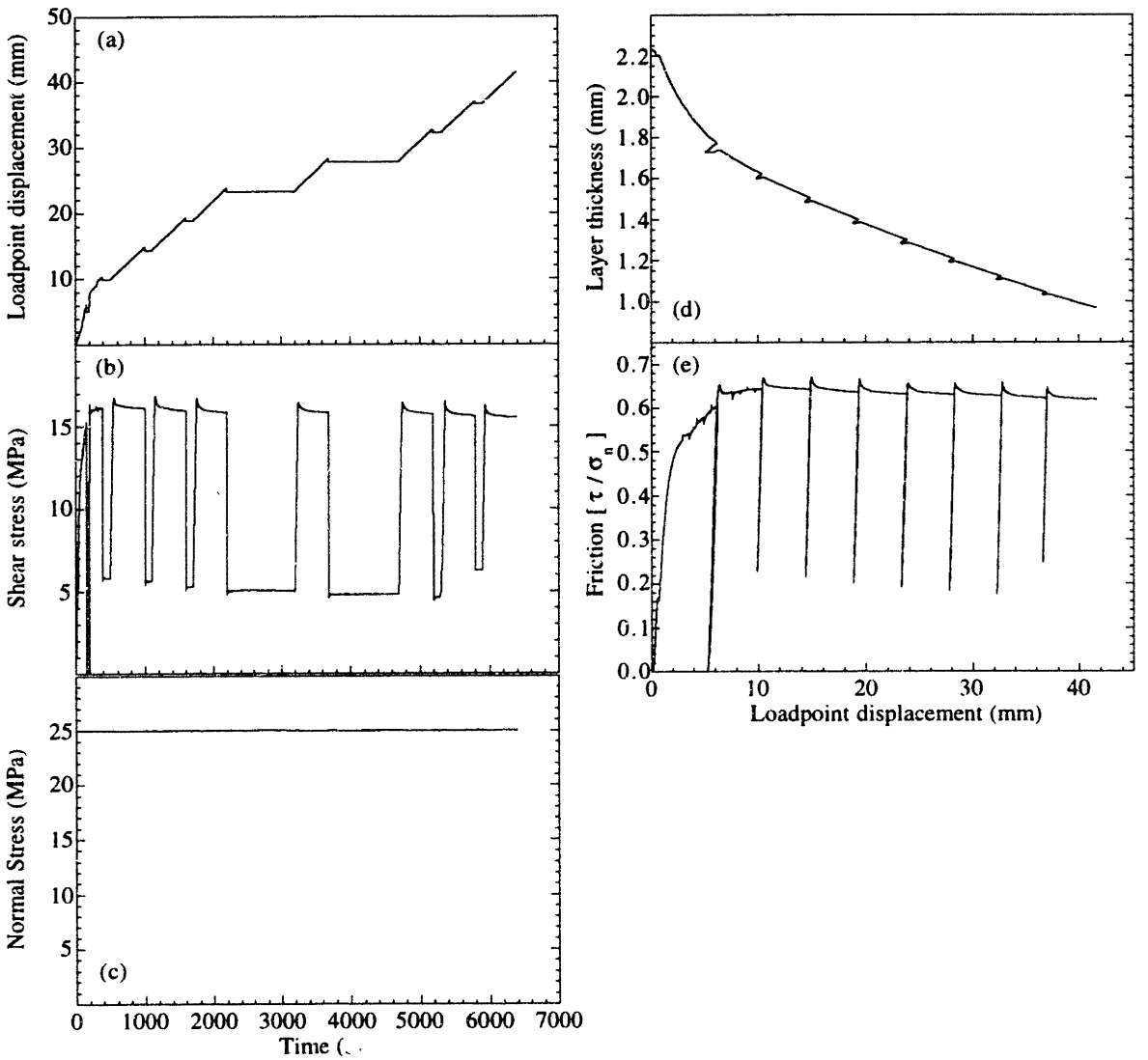

Experiment m207

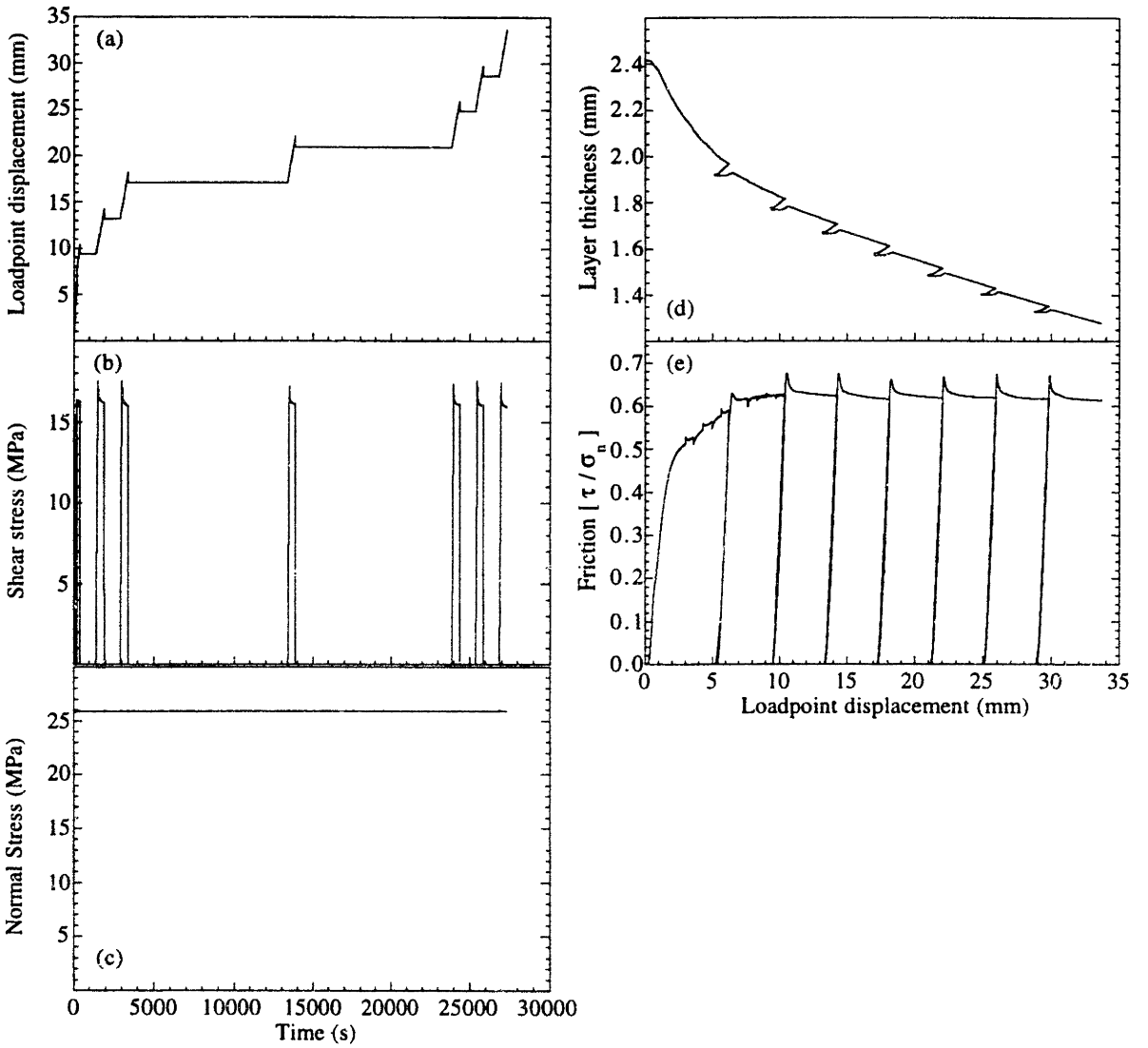

Experiment m208

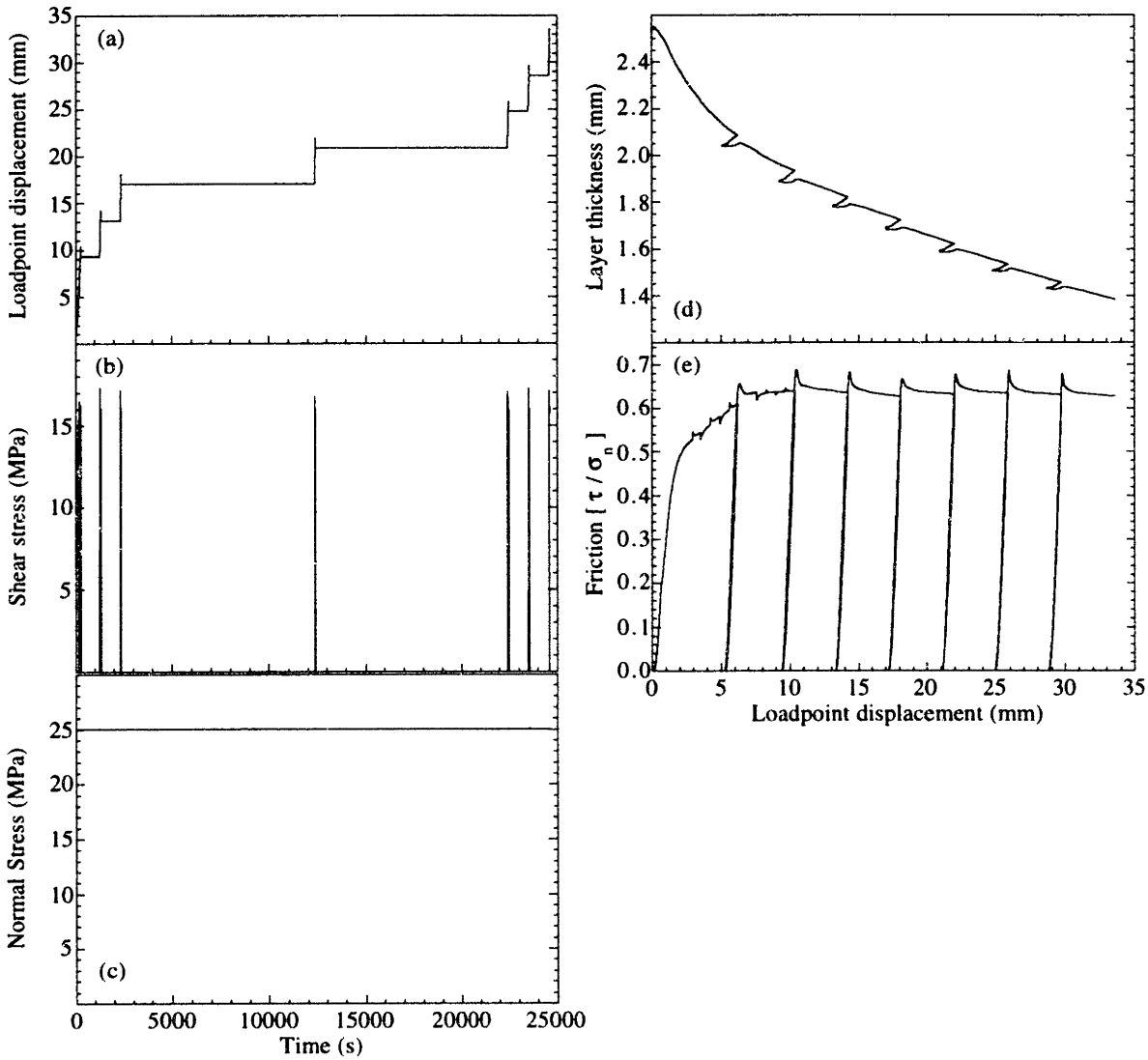

Experiment m209

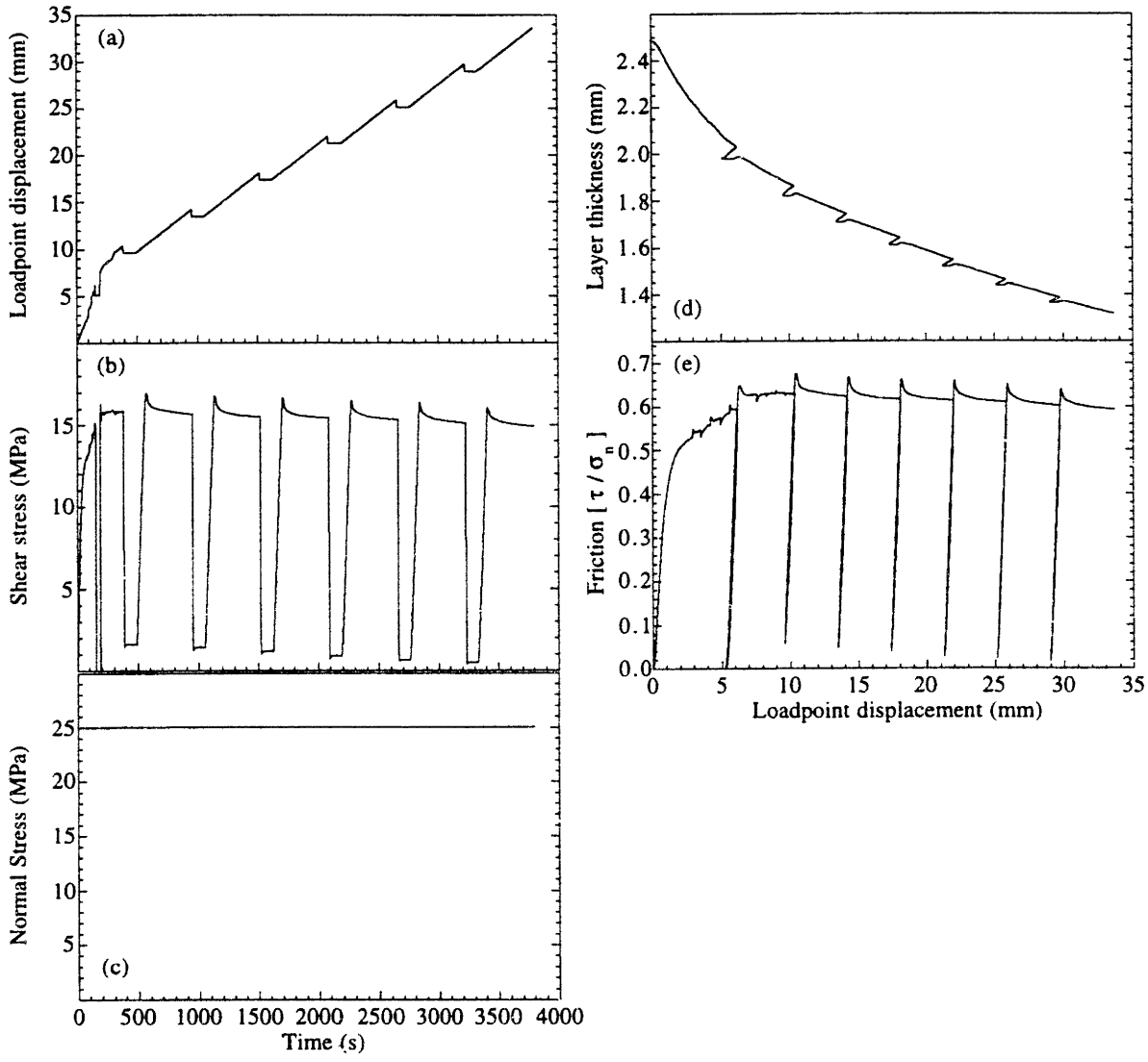

Experiment m210

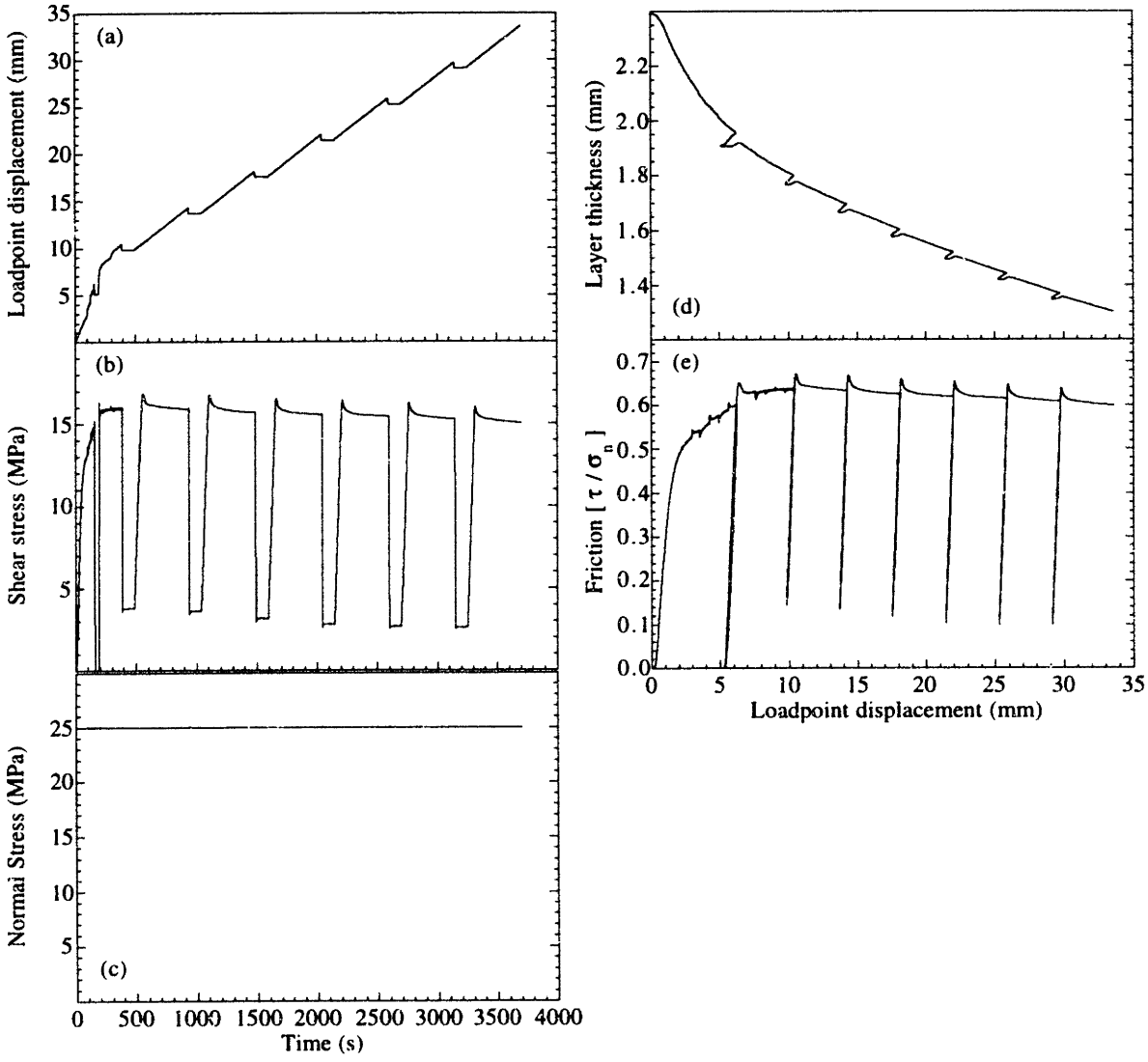

Experiment m211

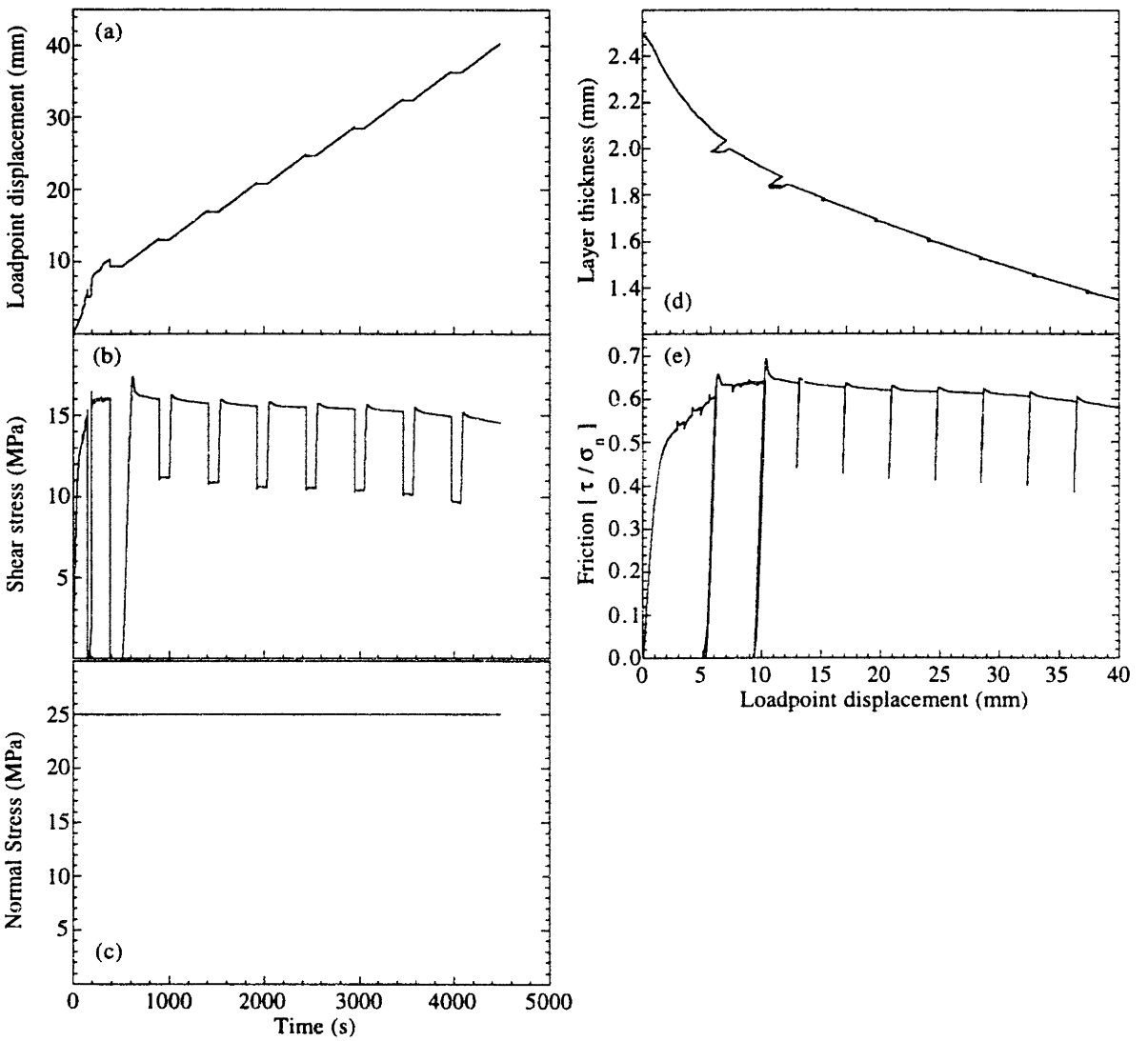

Experiment m213

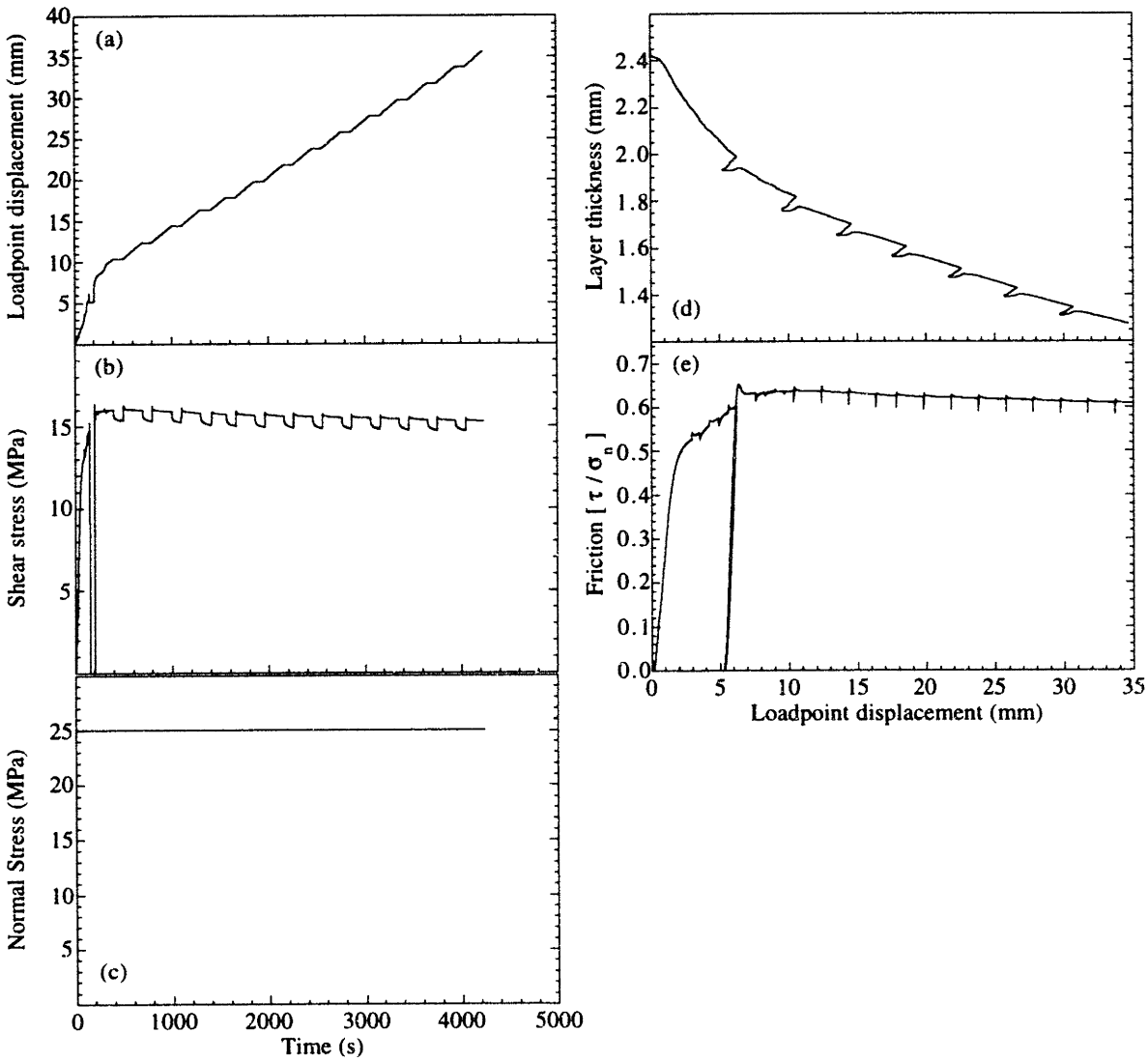

Experiment m214

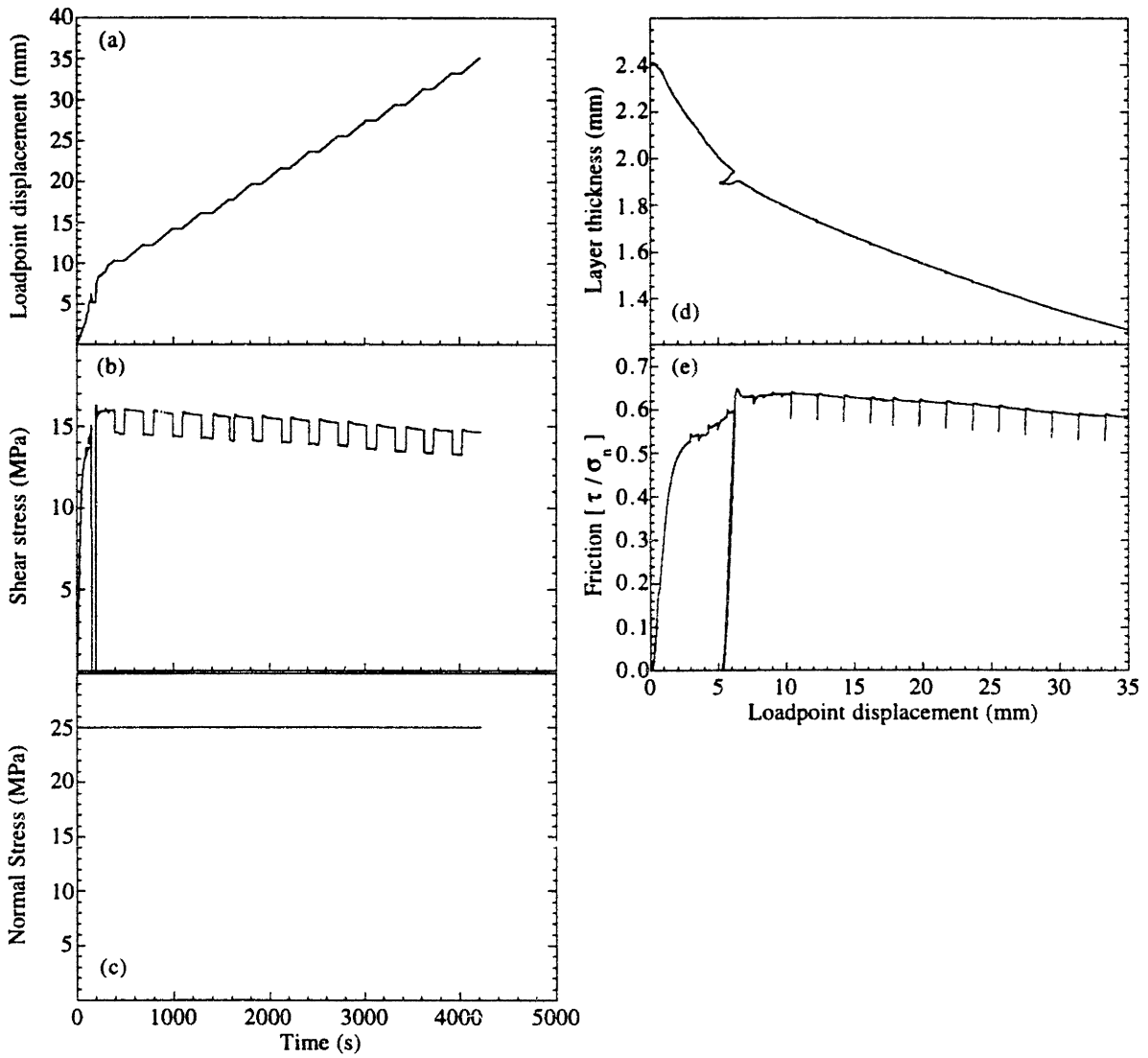

Experiment m231

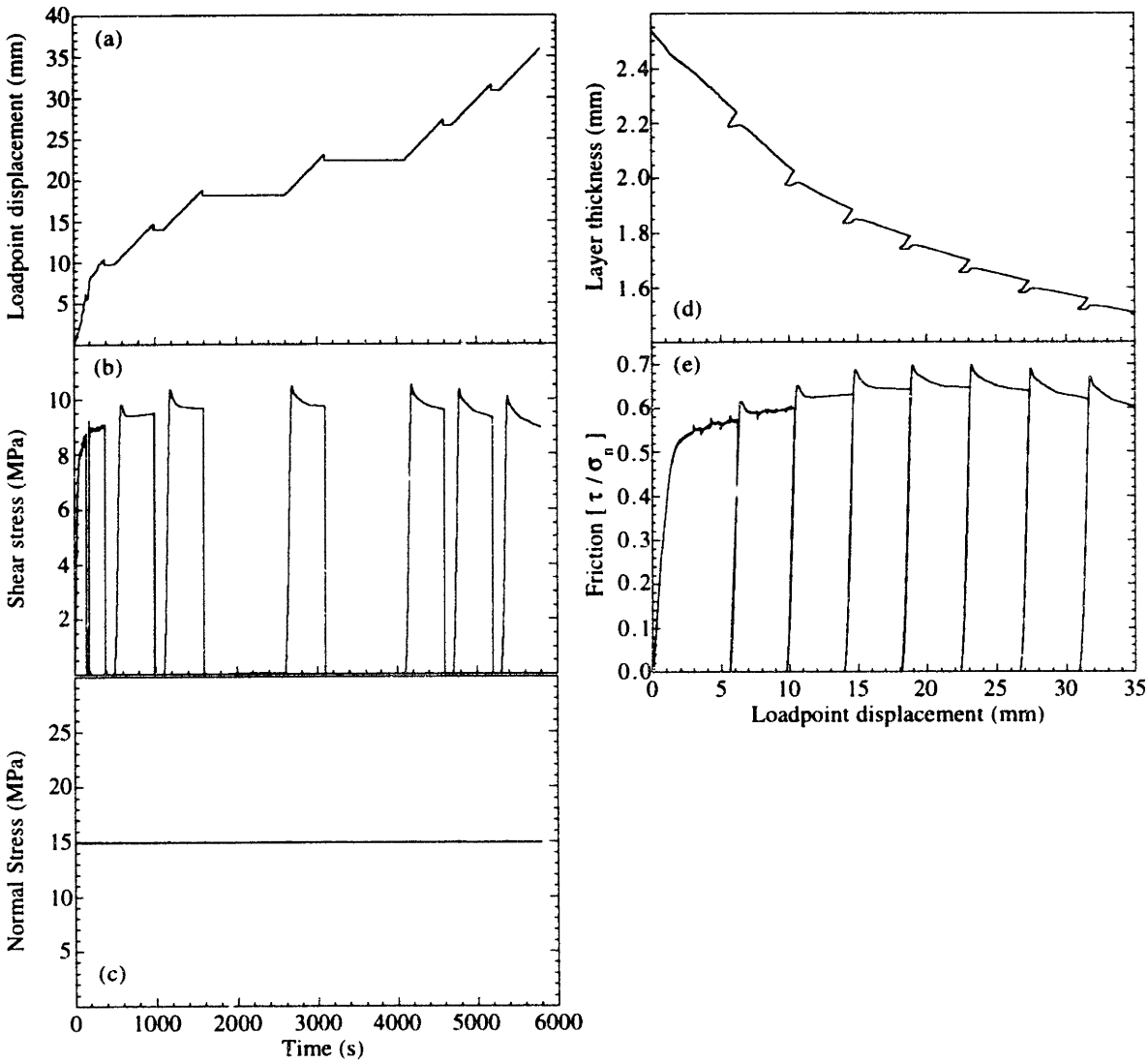

Experiment m232

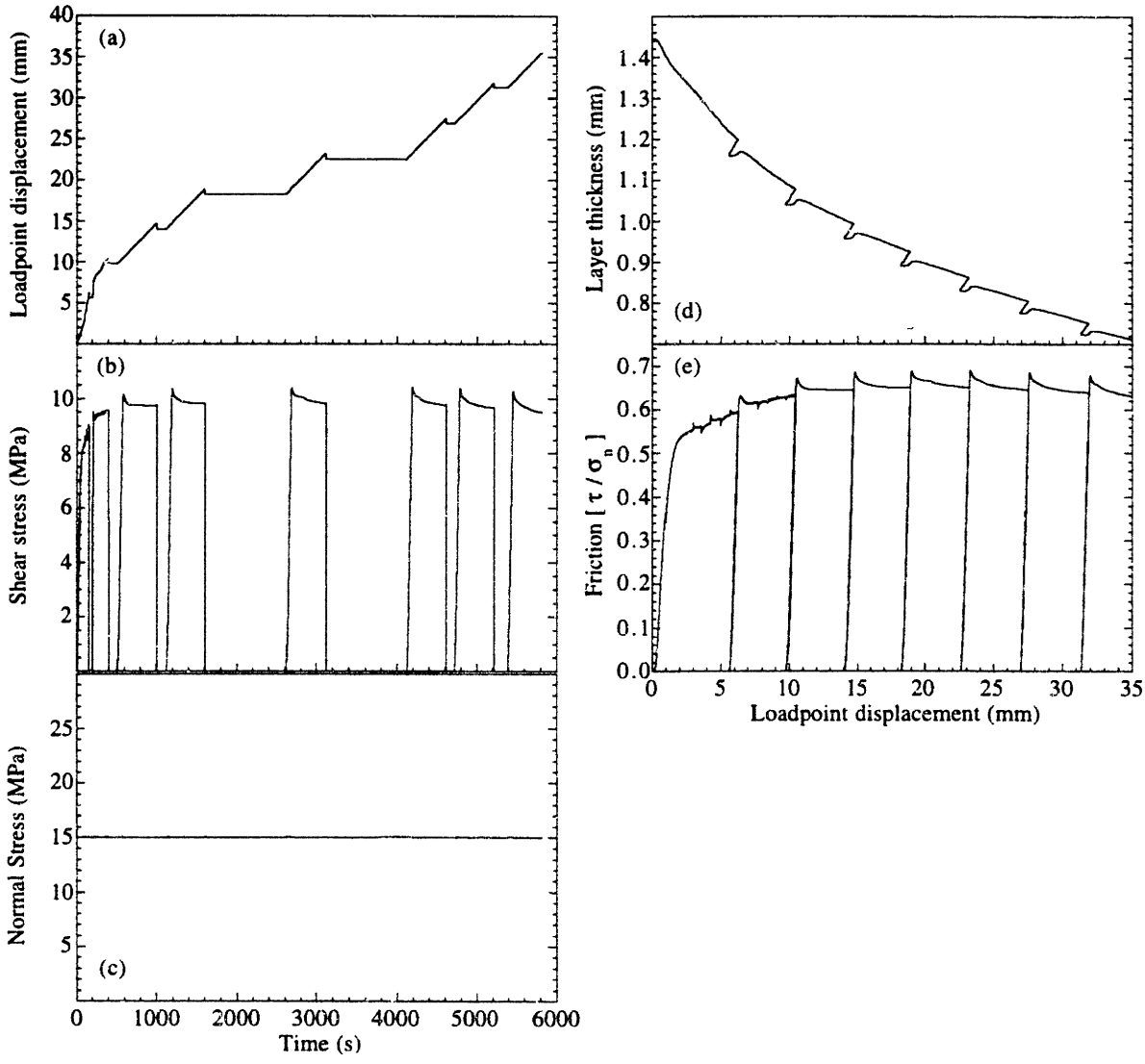

Experiment m233

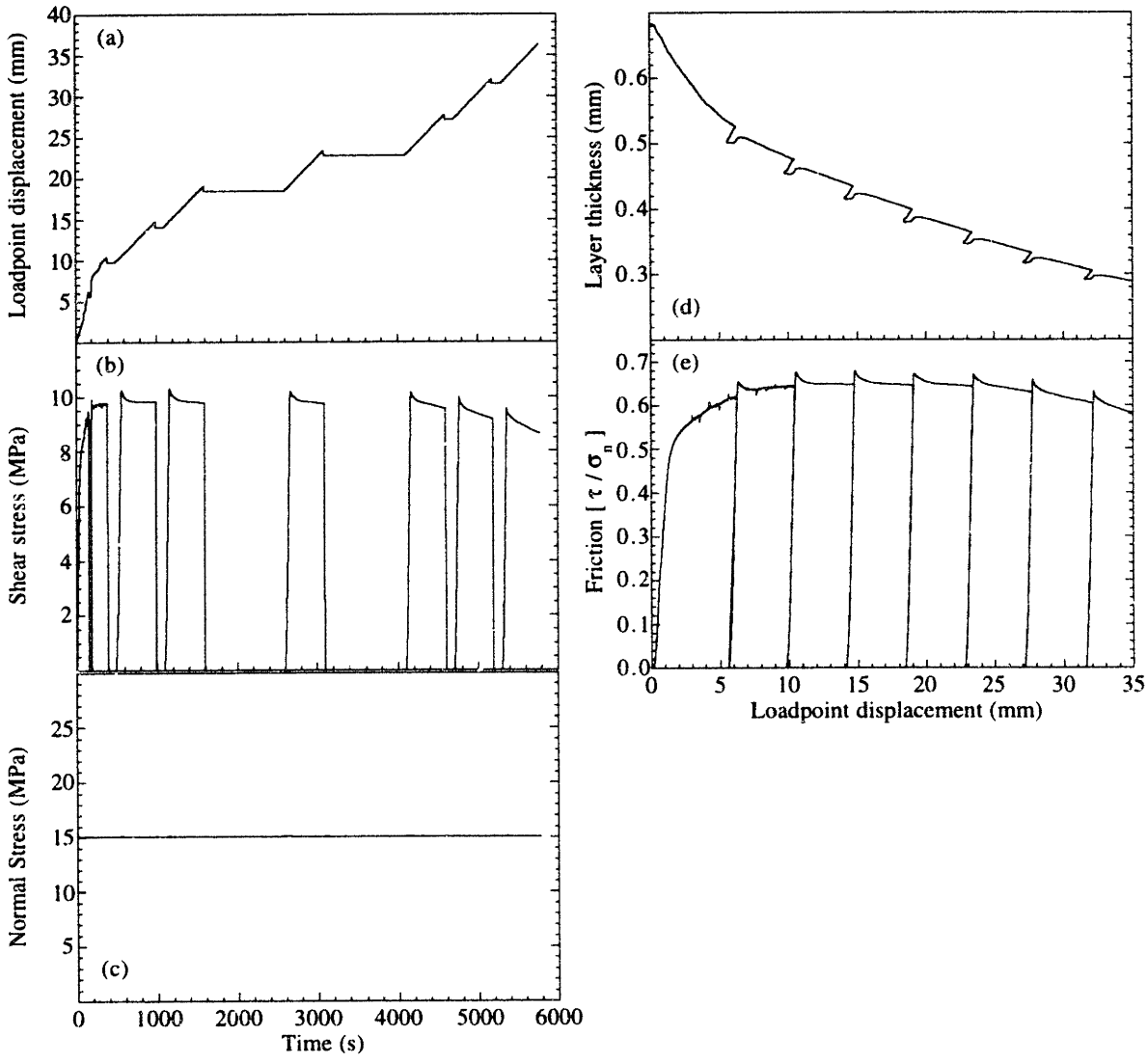

Experiment m235

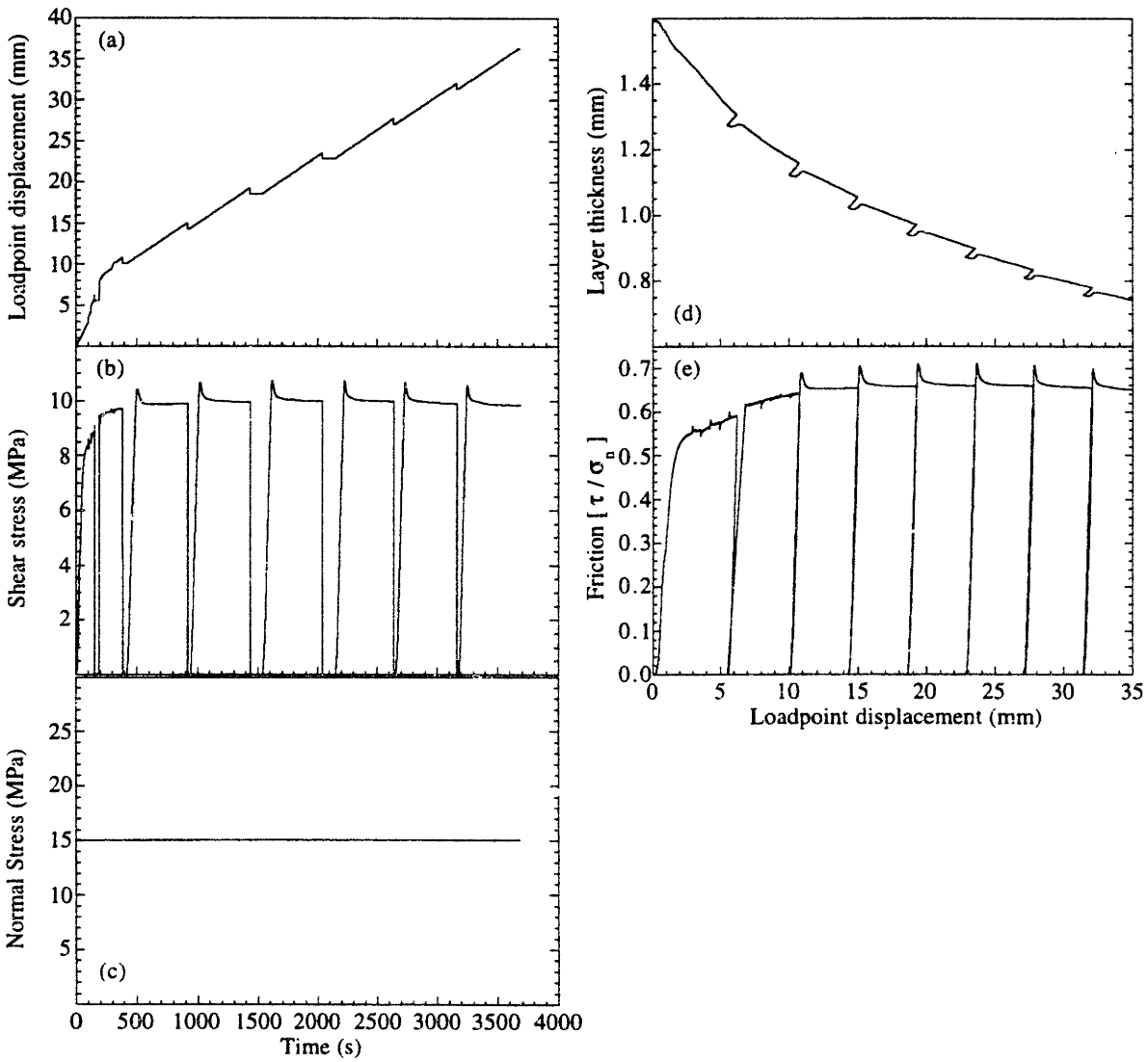

Experiment m236

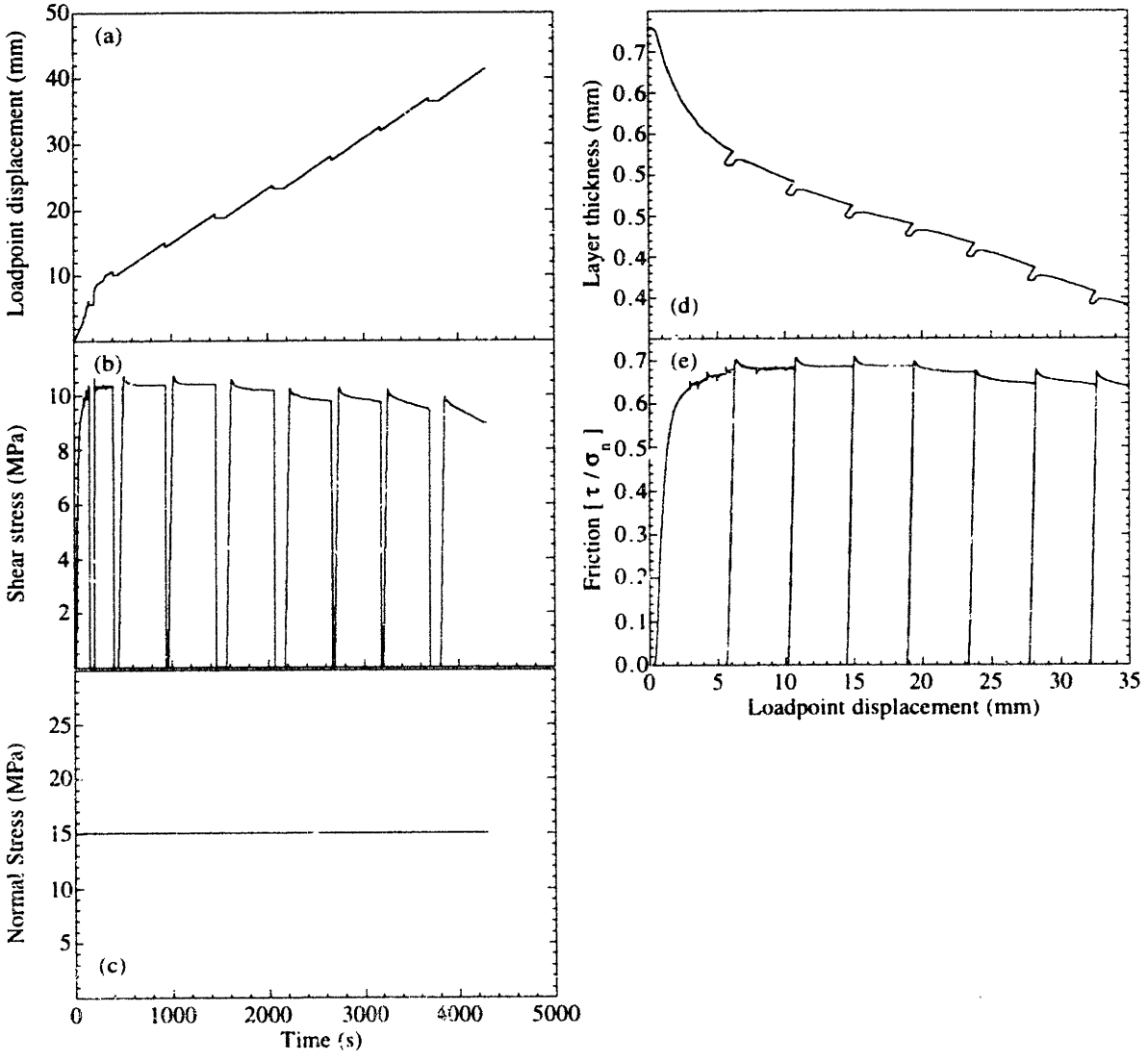

Experiment m244

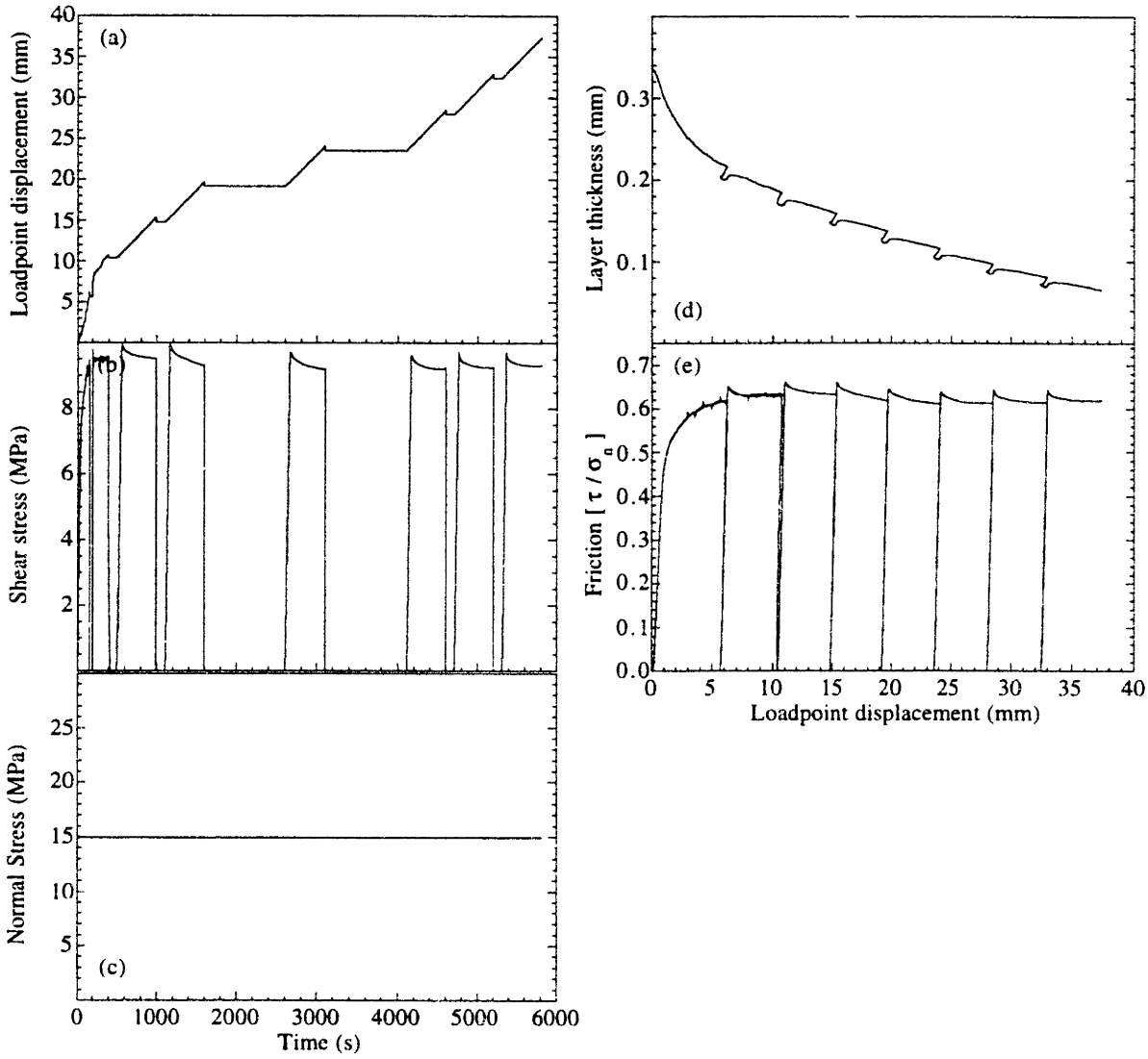

Experiment m246

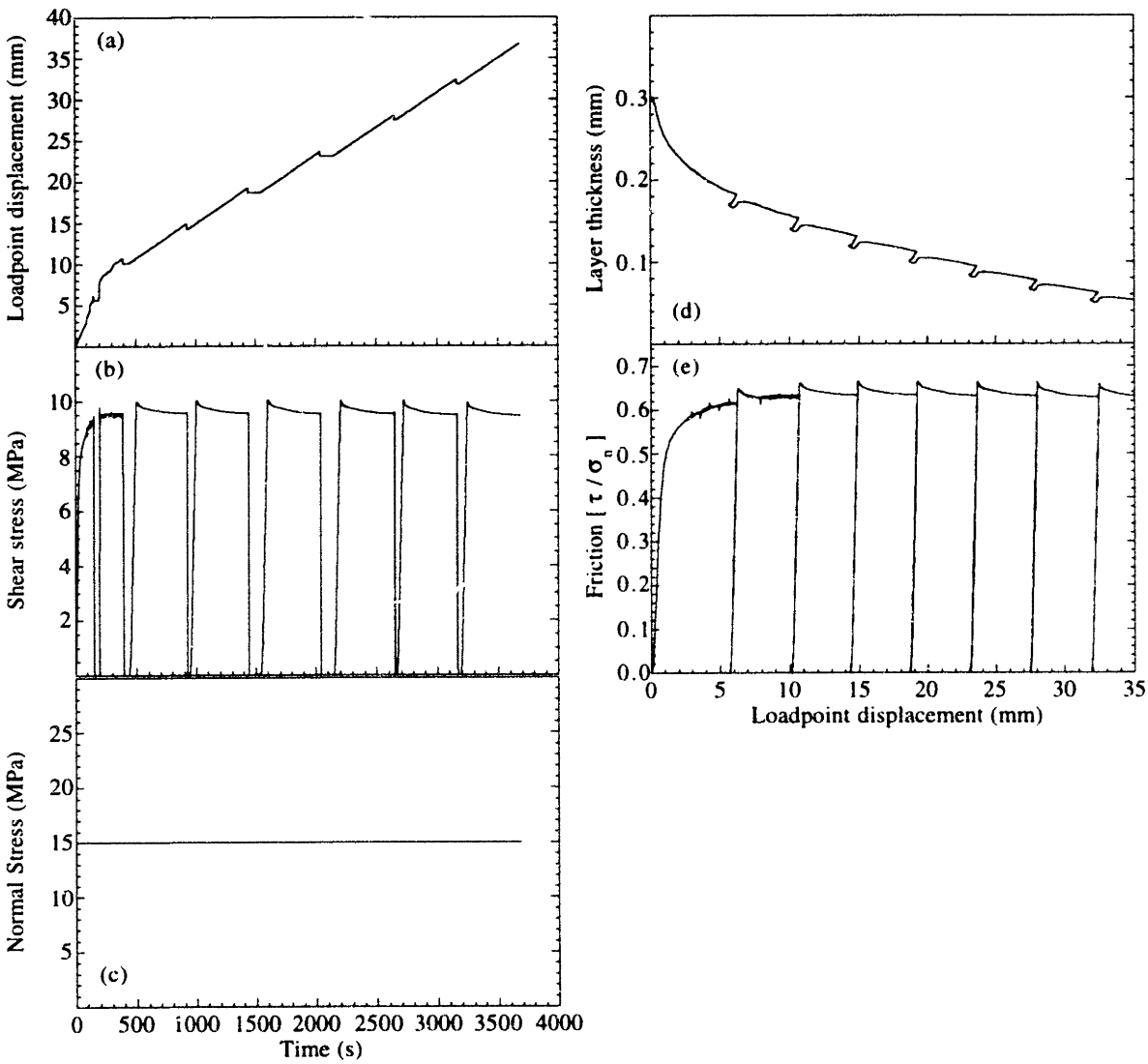

Experiment m247

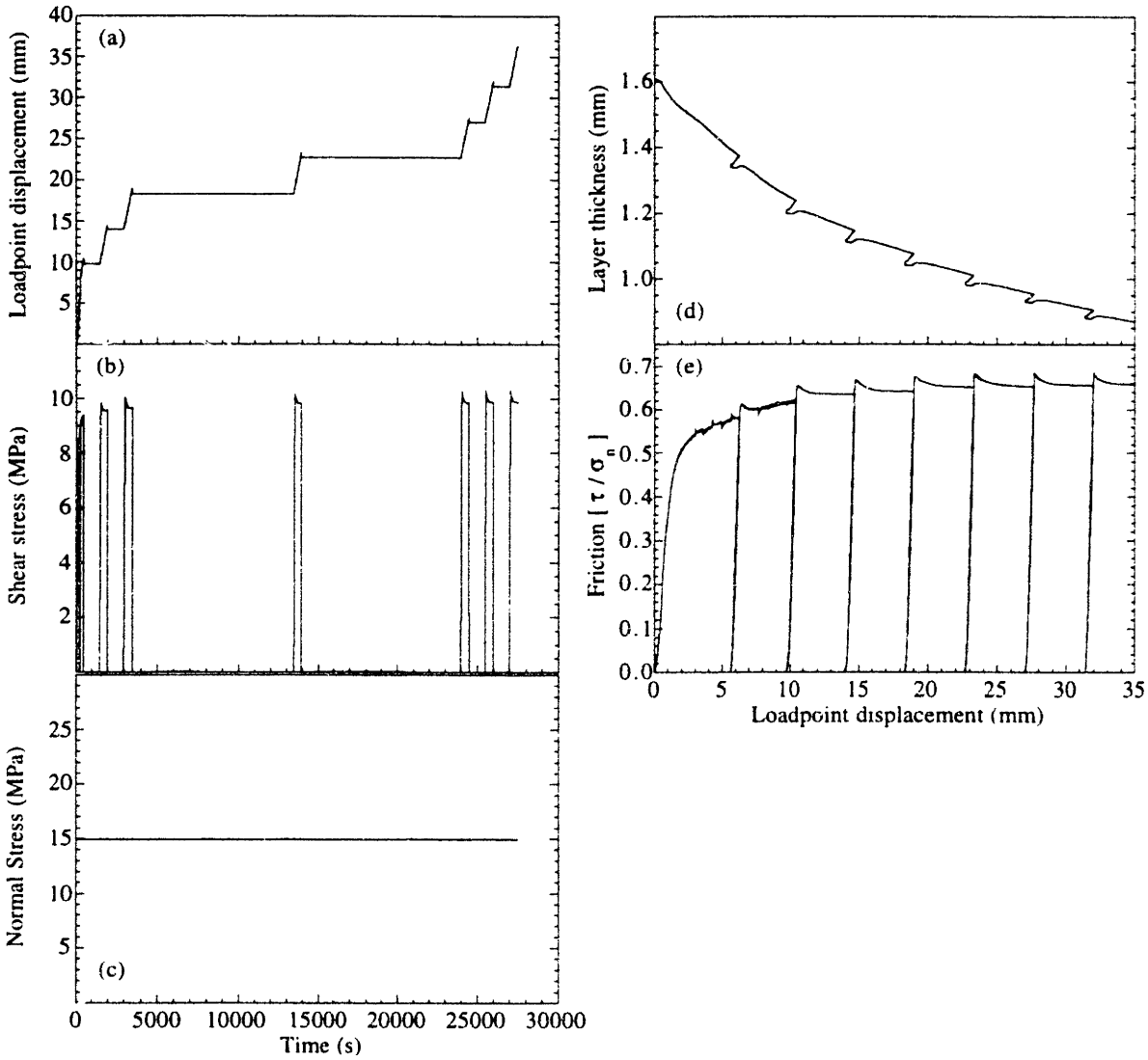

Experiment m248

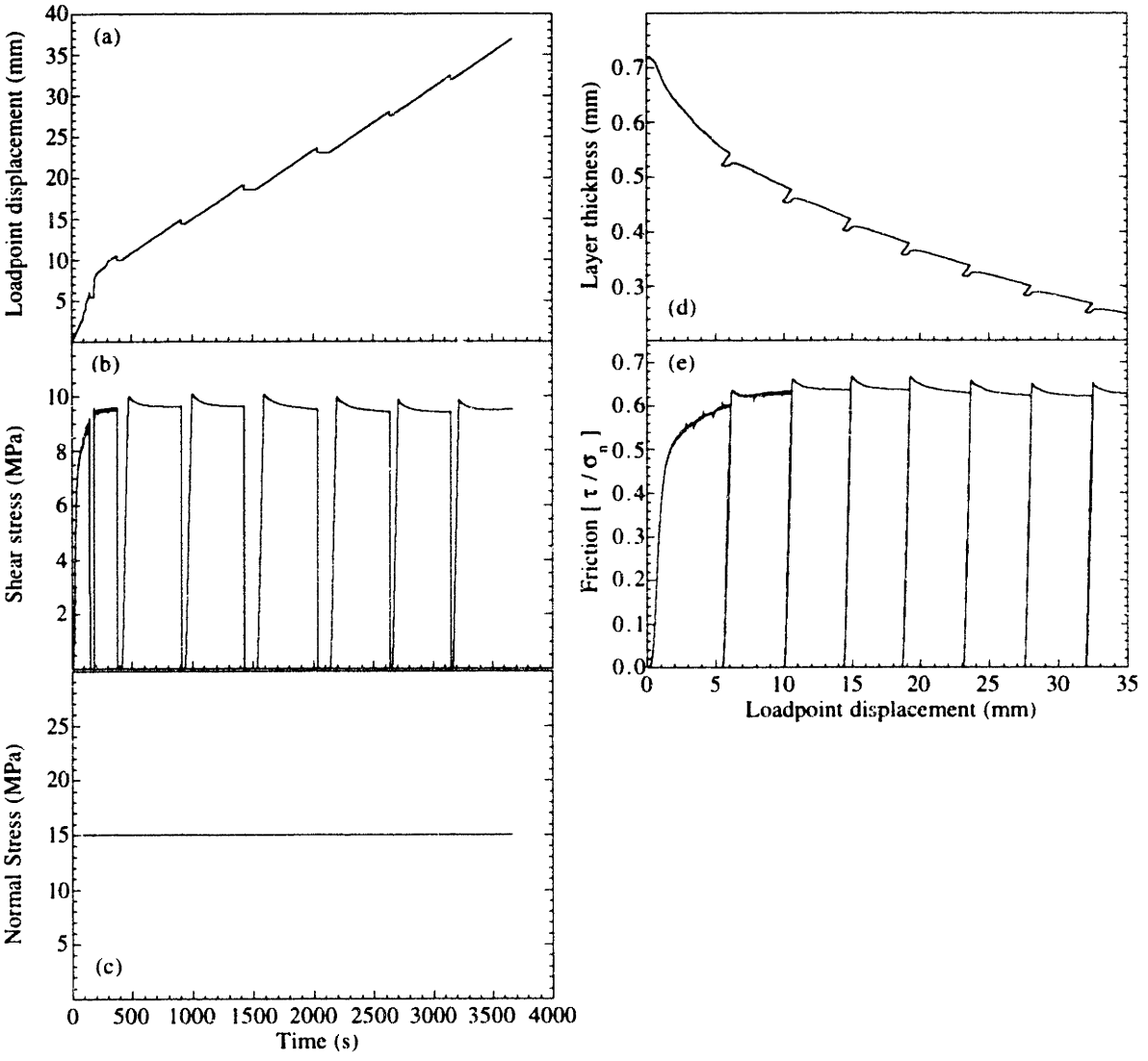

Experiment m249

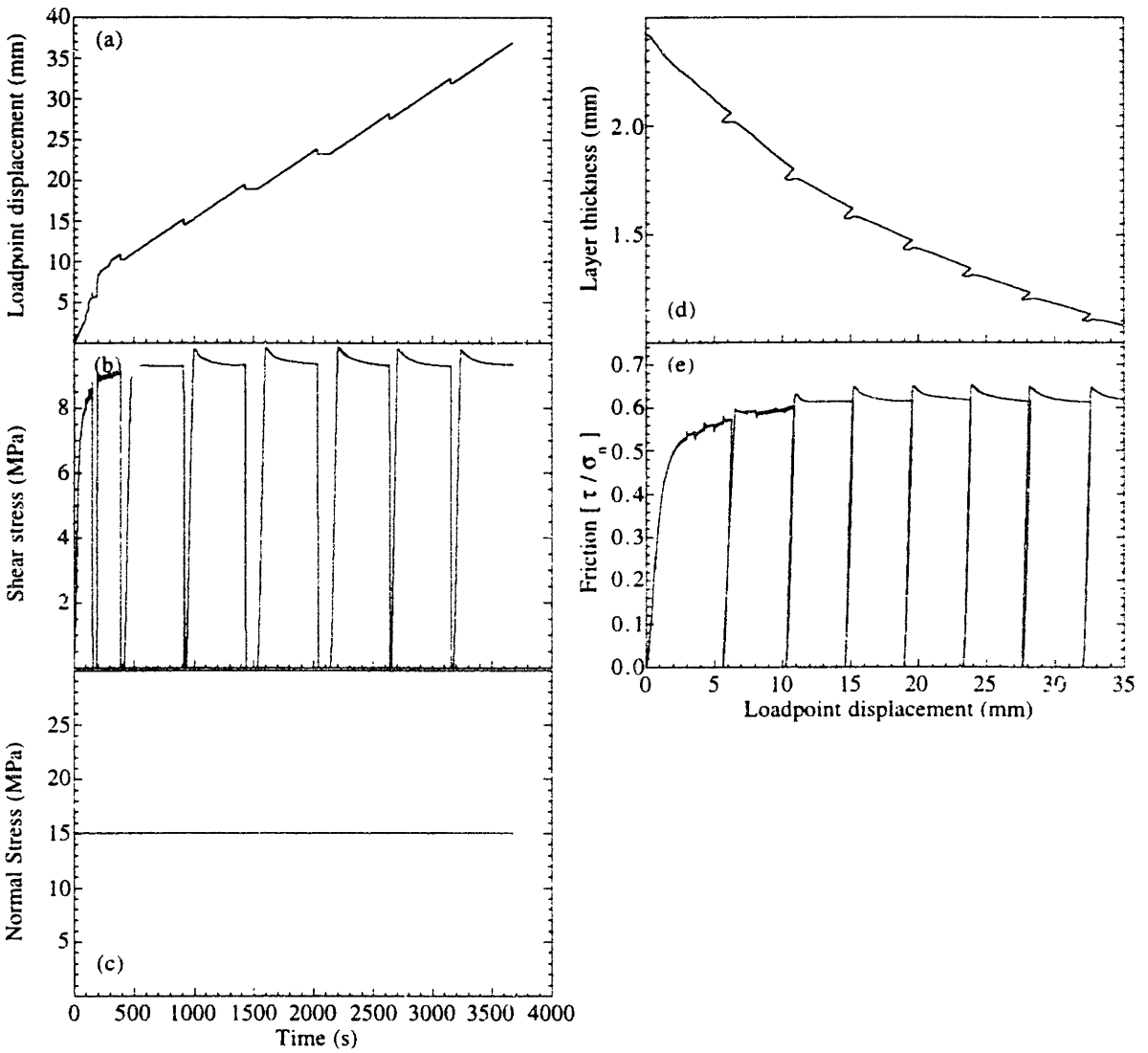

Experiment m250

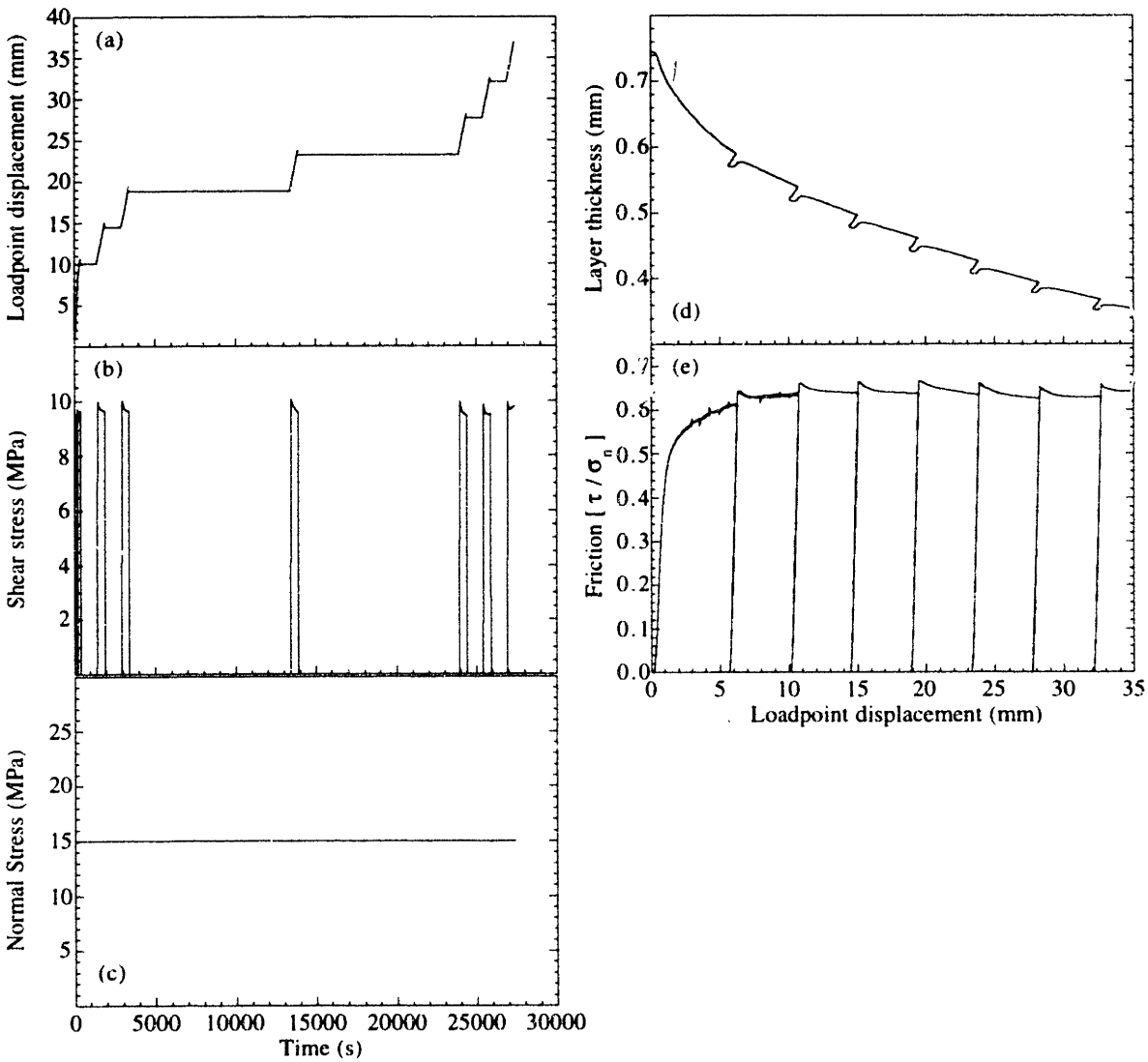

Experiment m251

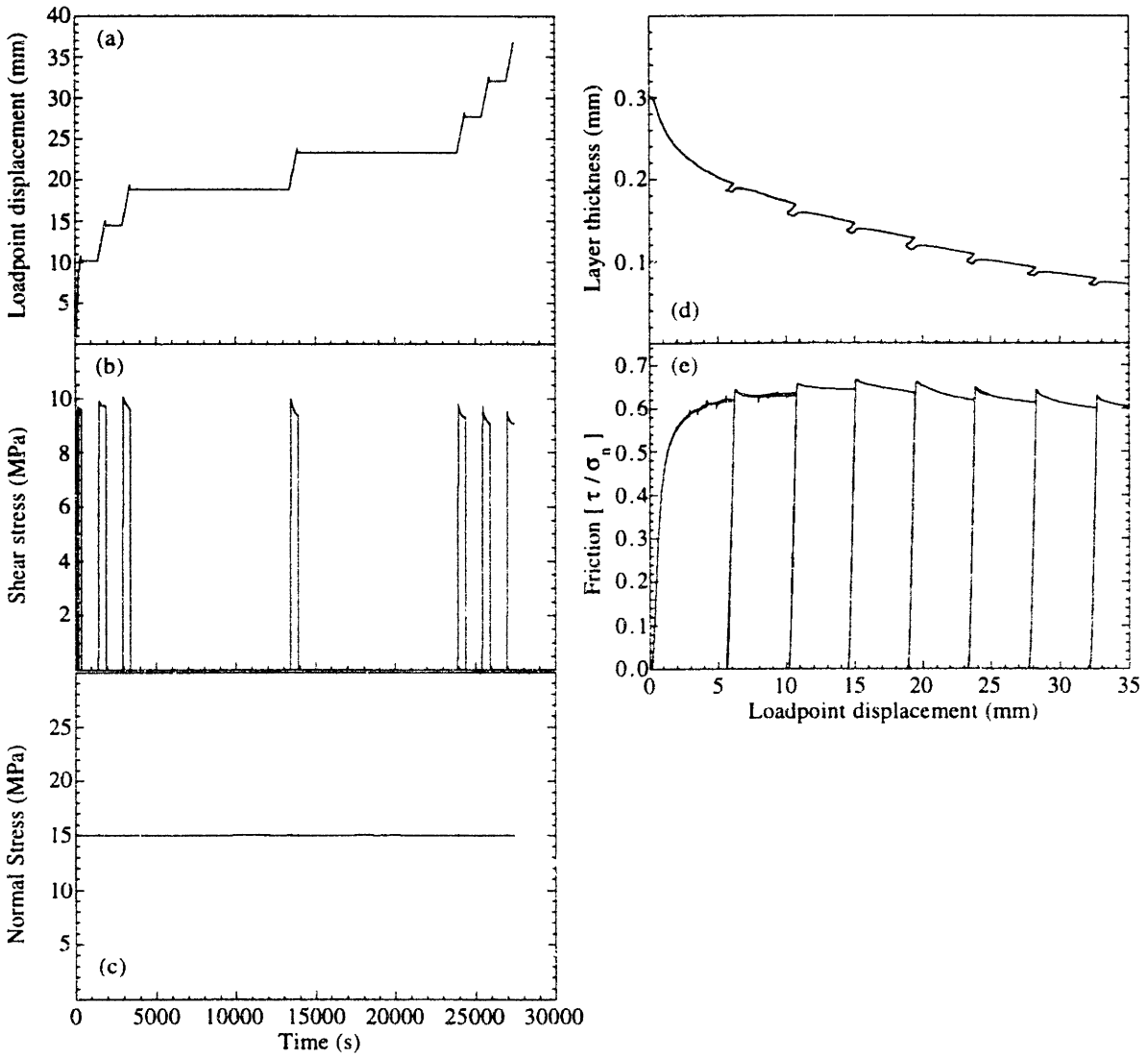

Experiment m262

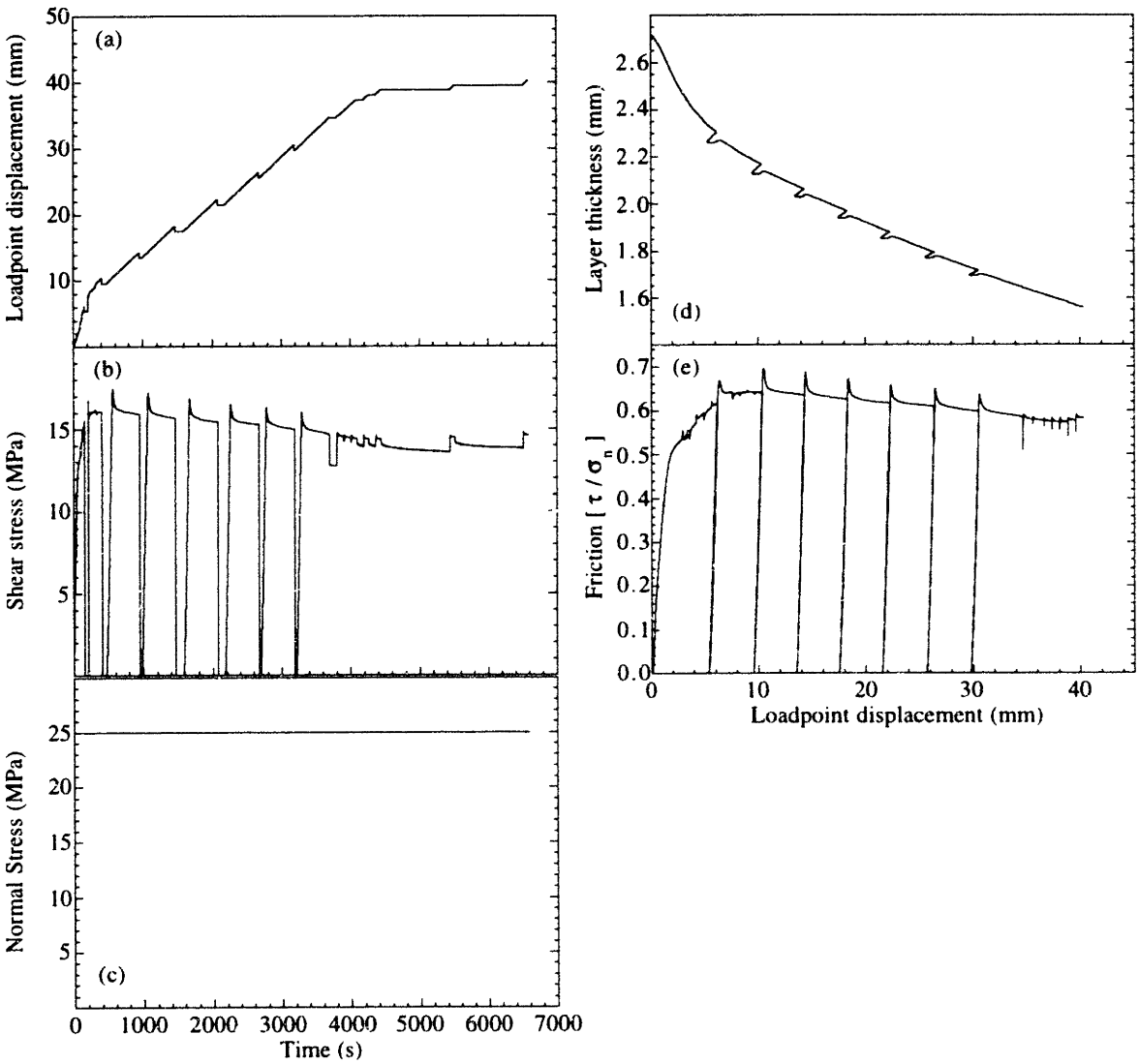

Experiment m262 (continued)

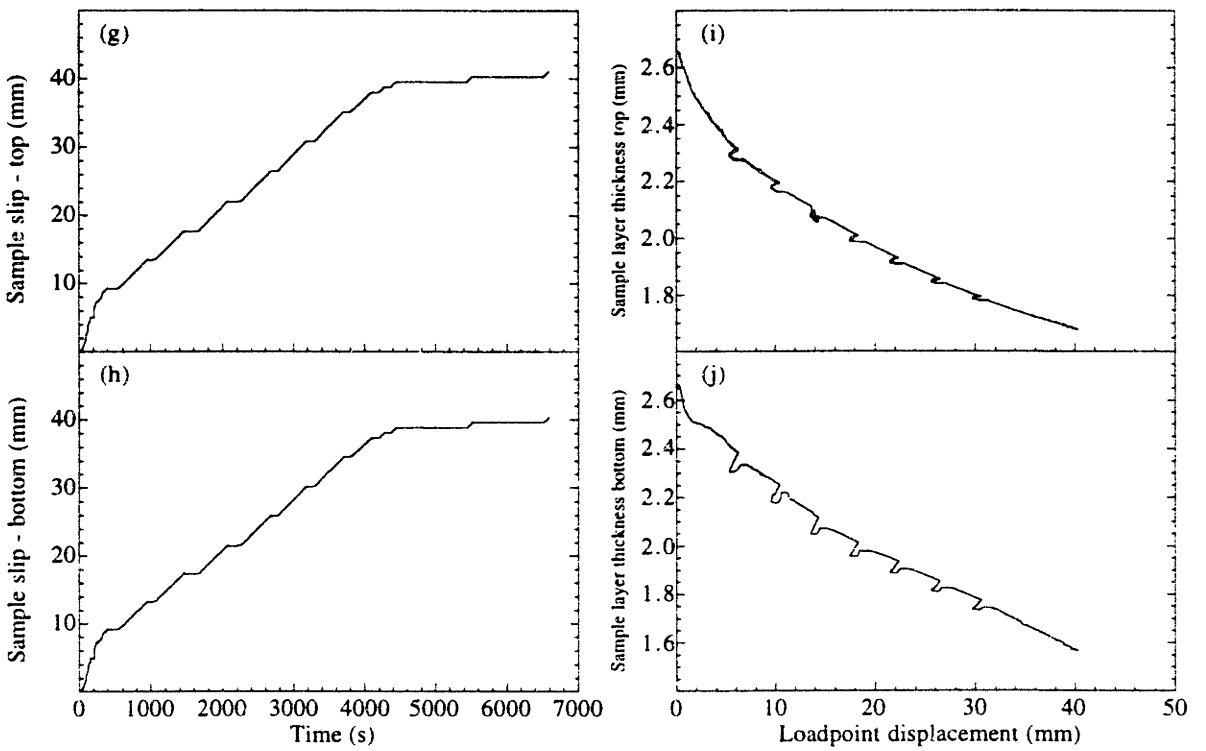

Experiment m263

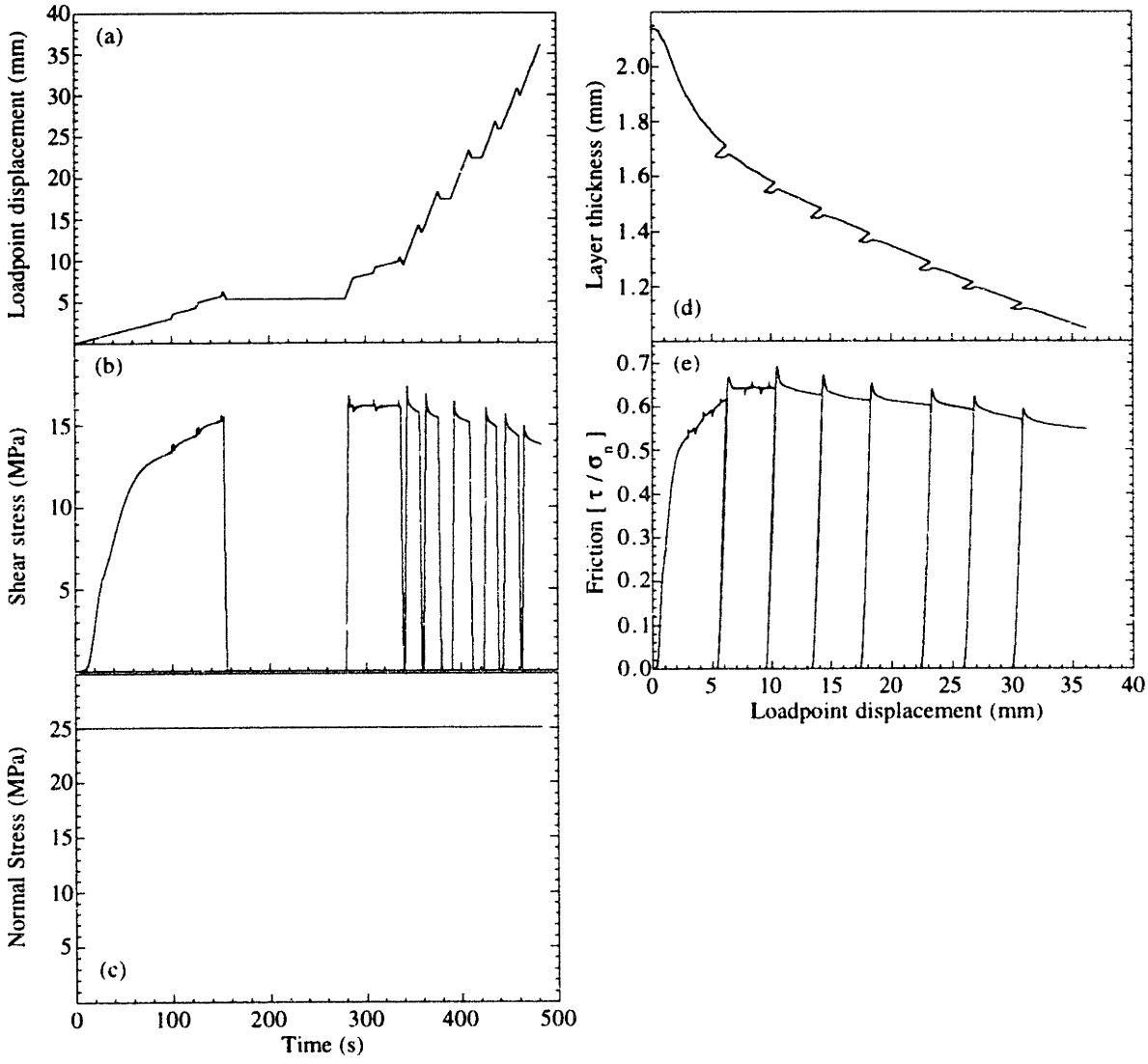

Experiment m263 (continued)

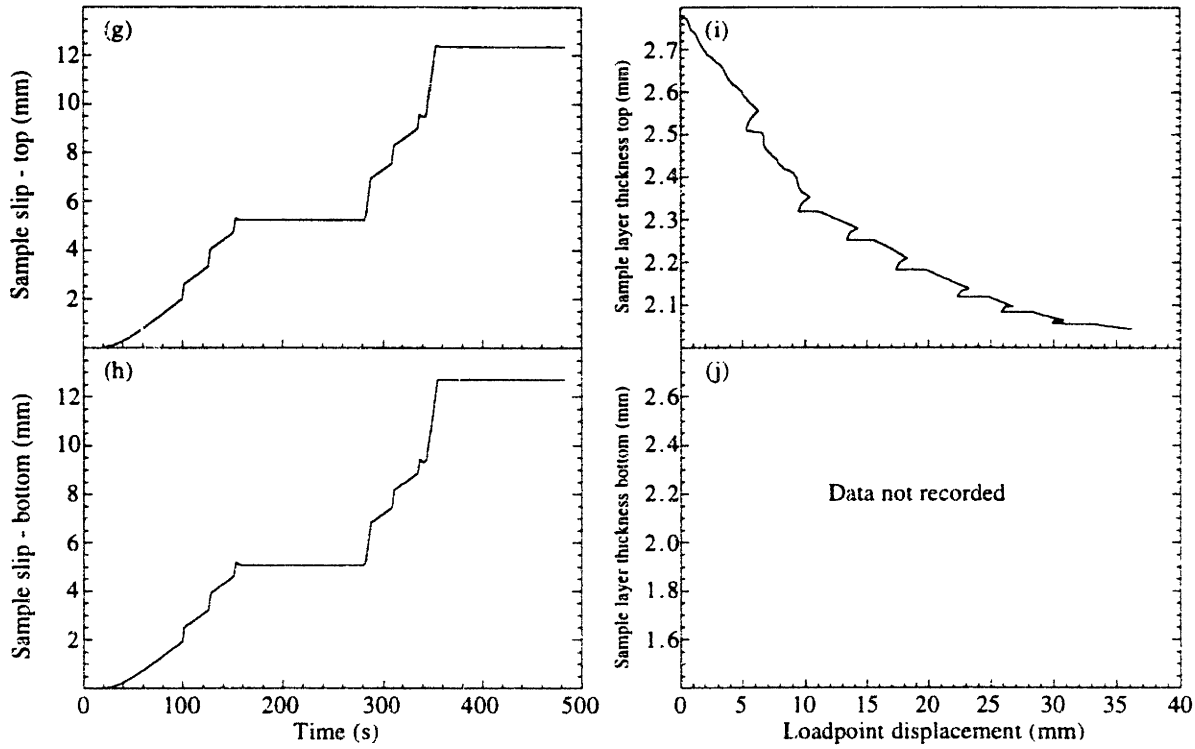

Experiment m264

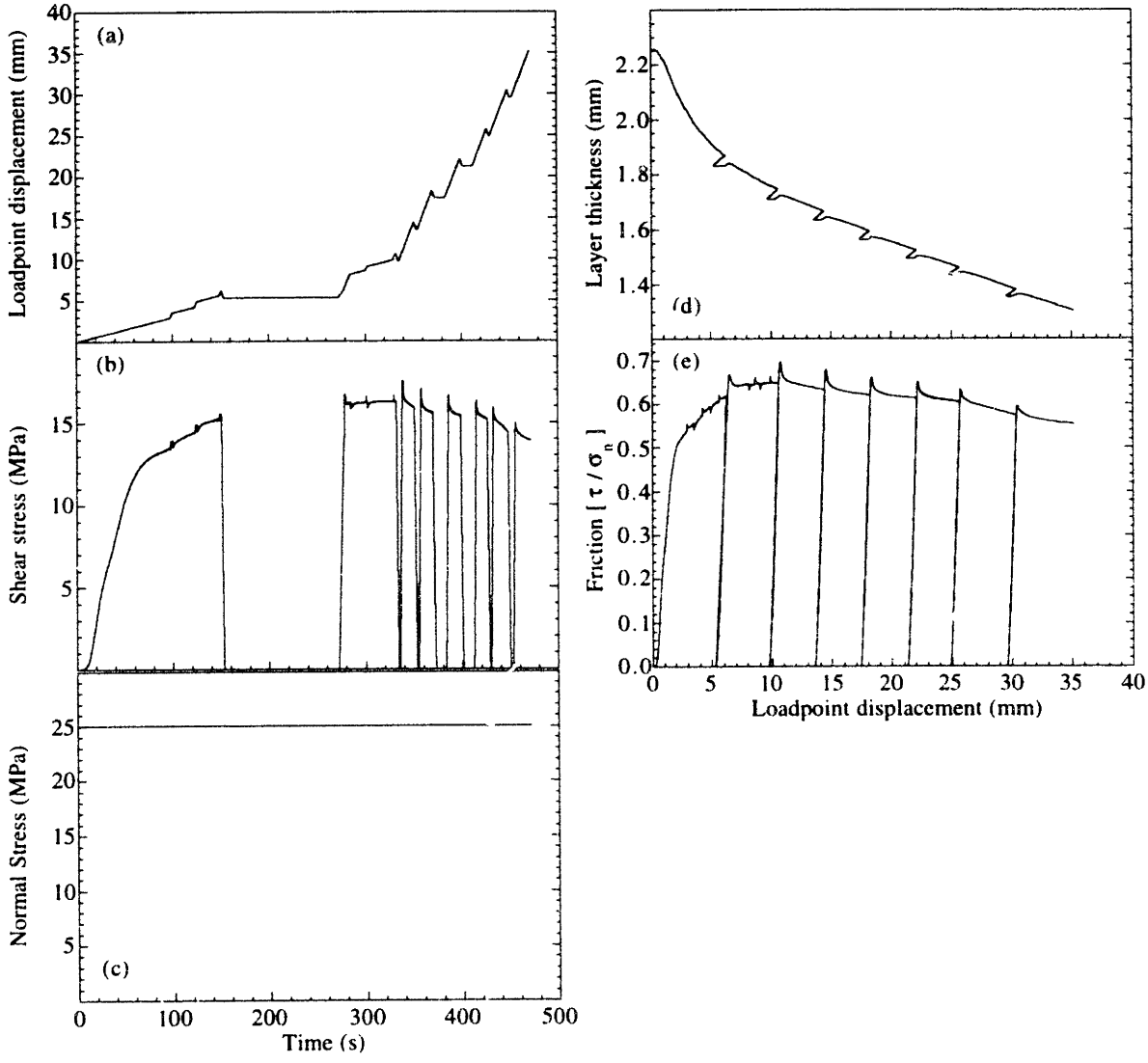

Experiment m264 (continued)

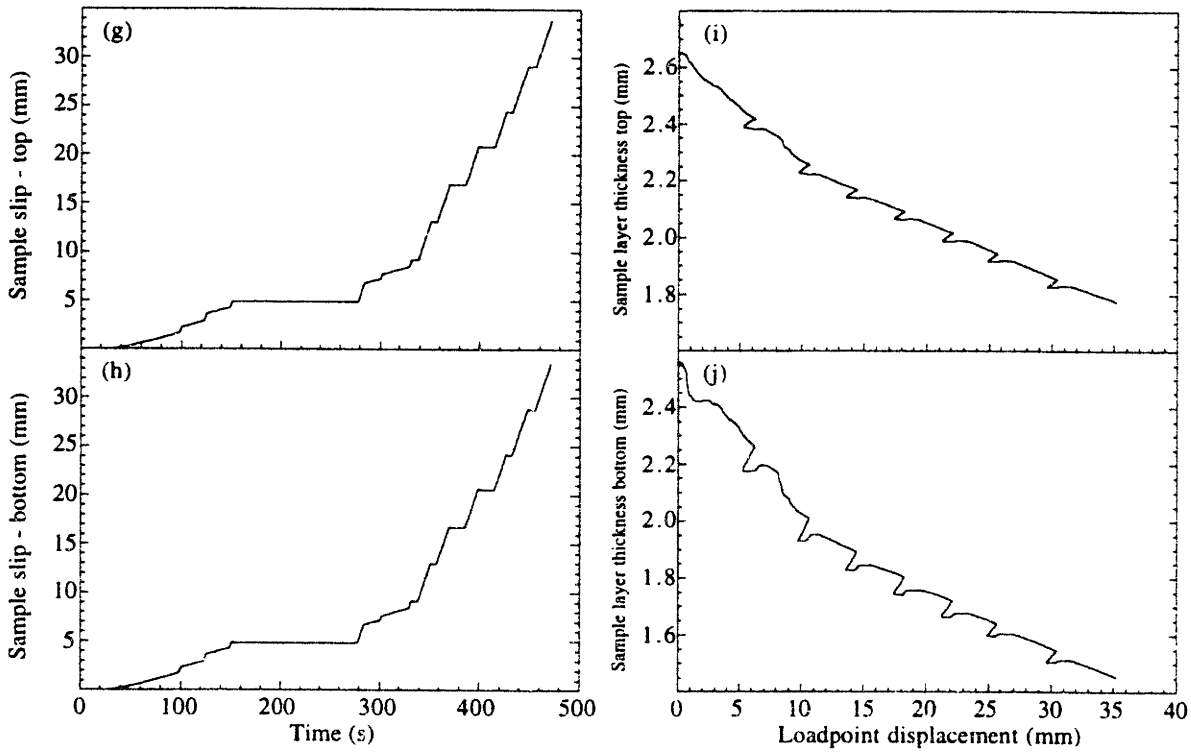

Experiment m265

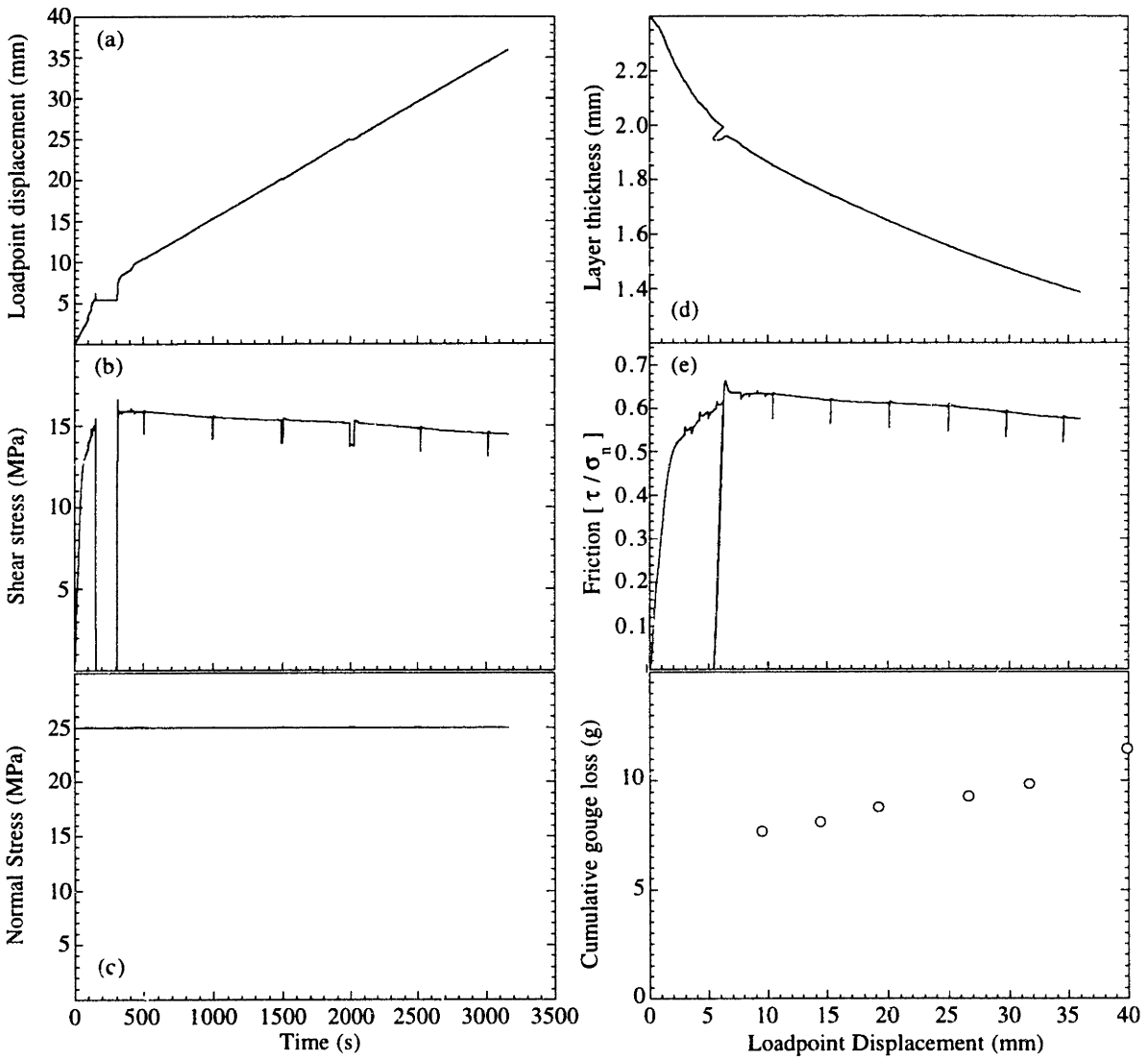

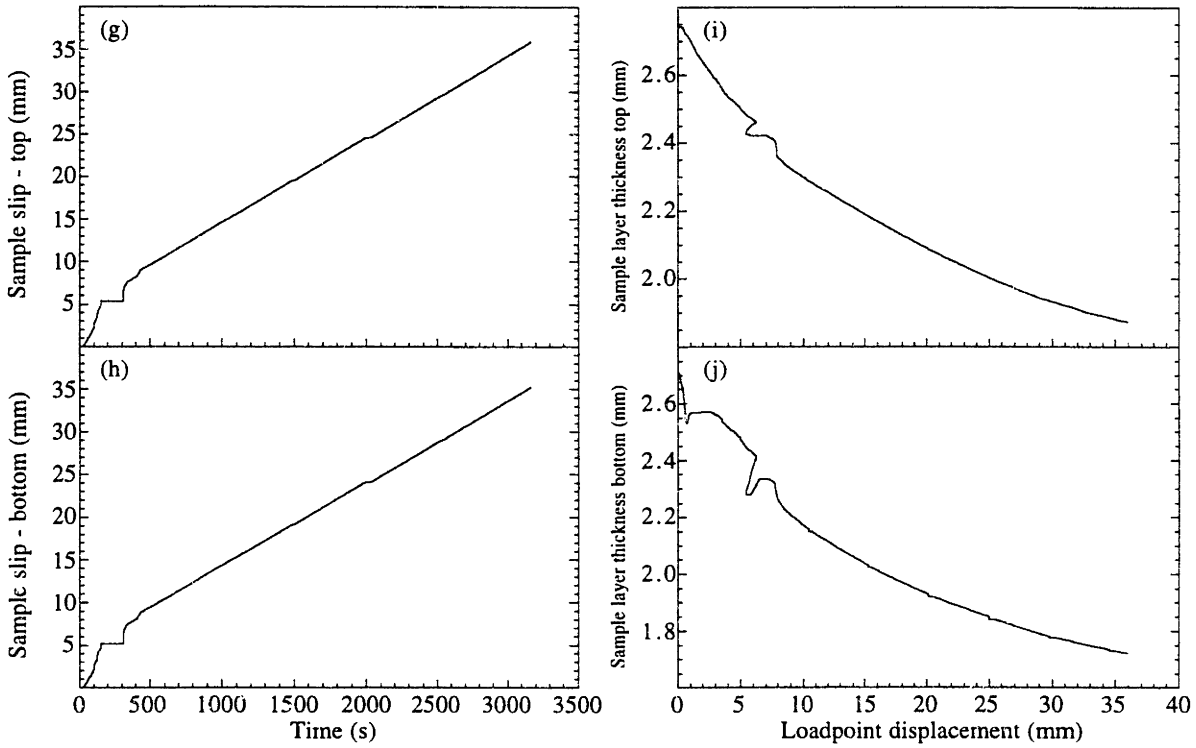
(g)
(h)
(i)
(j)
Sample slip - top (mm)
Sample slip - bottom (mm)
Sample layer thickness top (mm)
Sample layer thickness bottom (mm)
Time (s)
Loadpoint displacement (mm)

Experiment m266

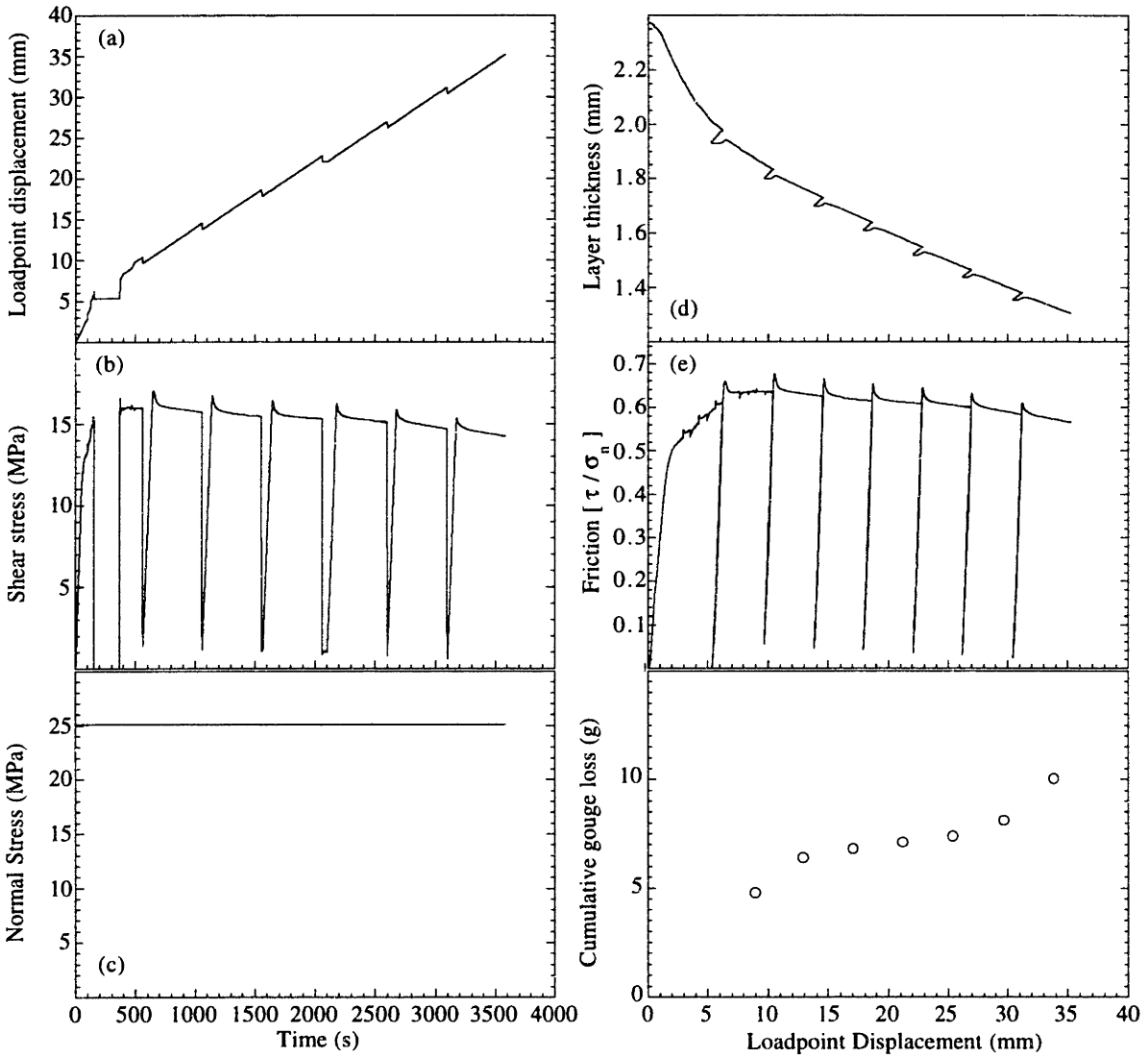

Experiment m266 (continued)

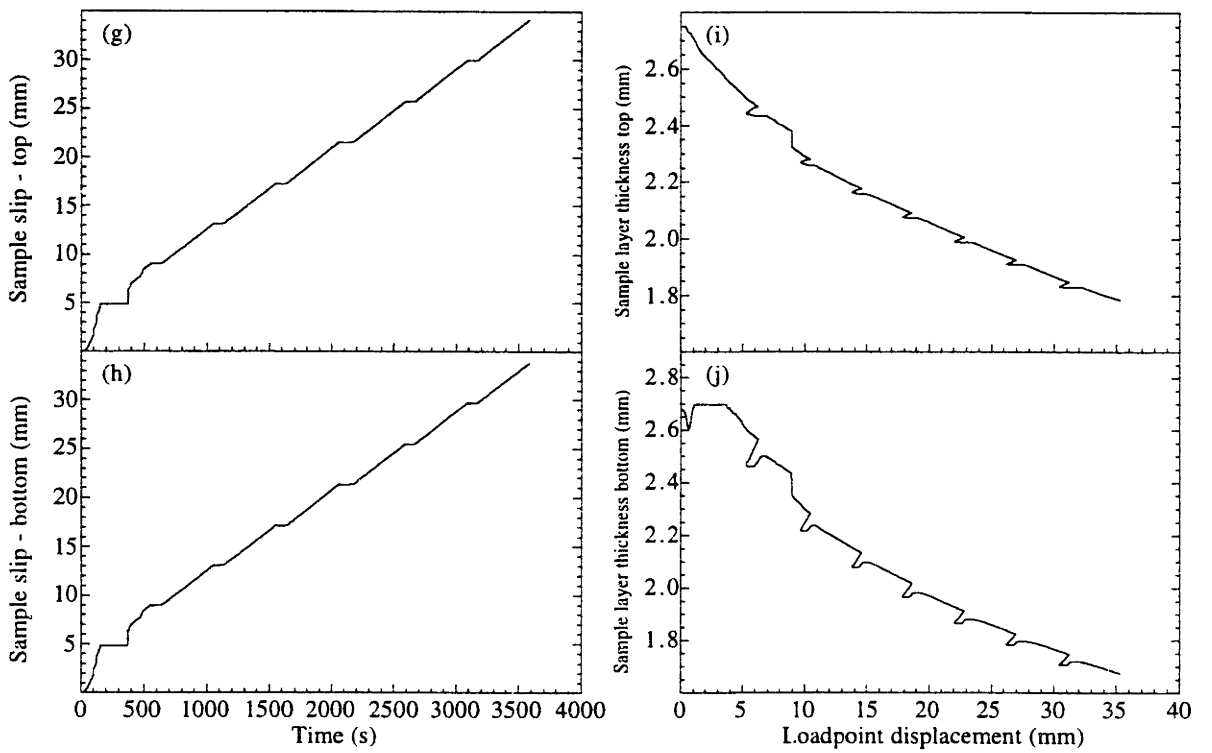

Experiment m267

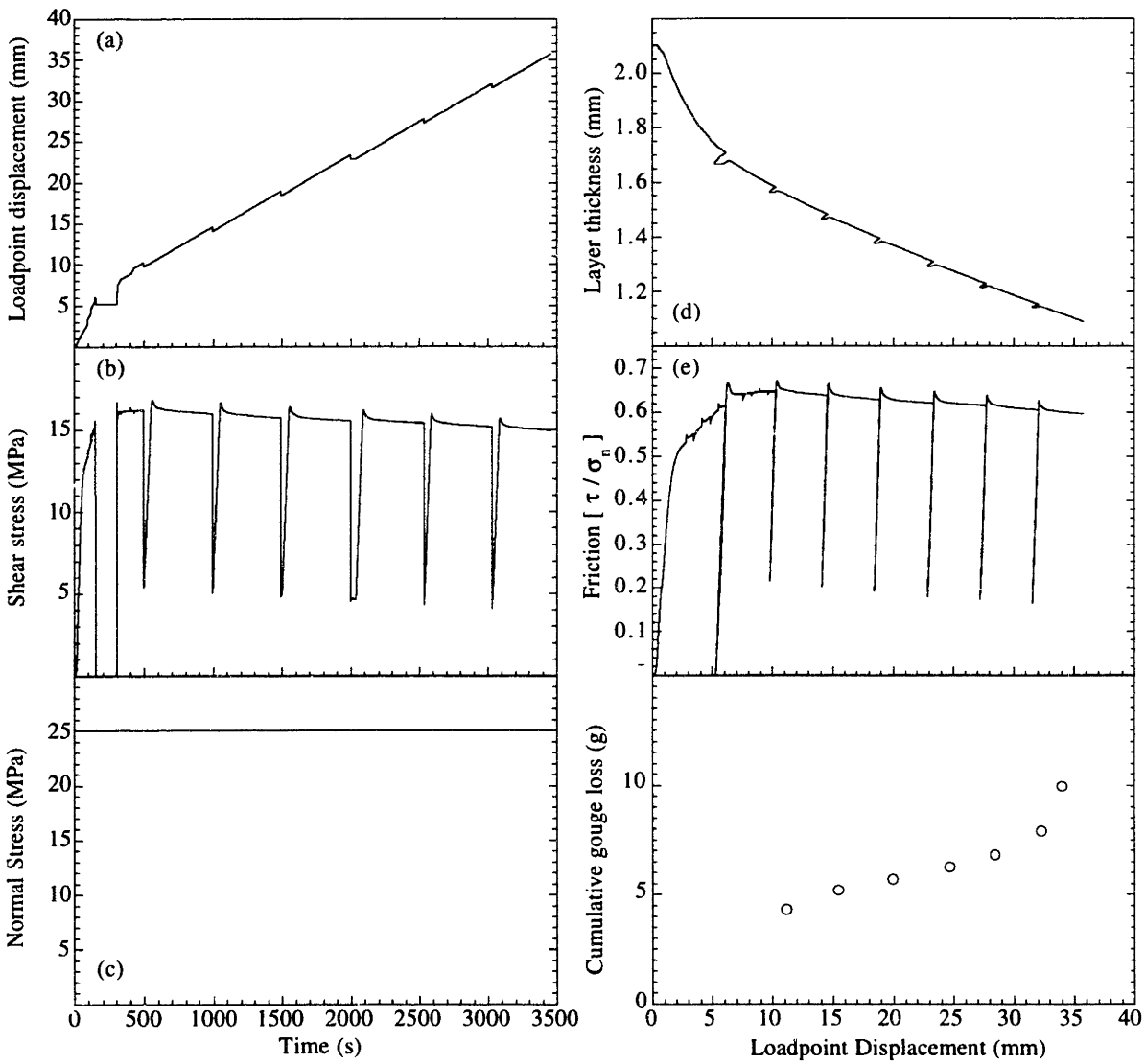

Experiment m267 (continued)

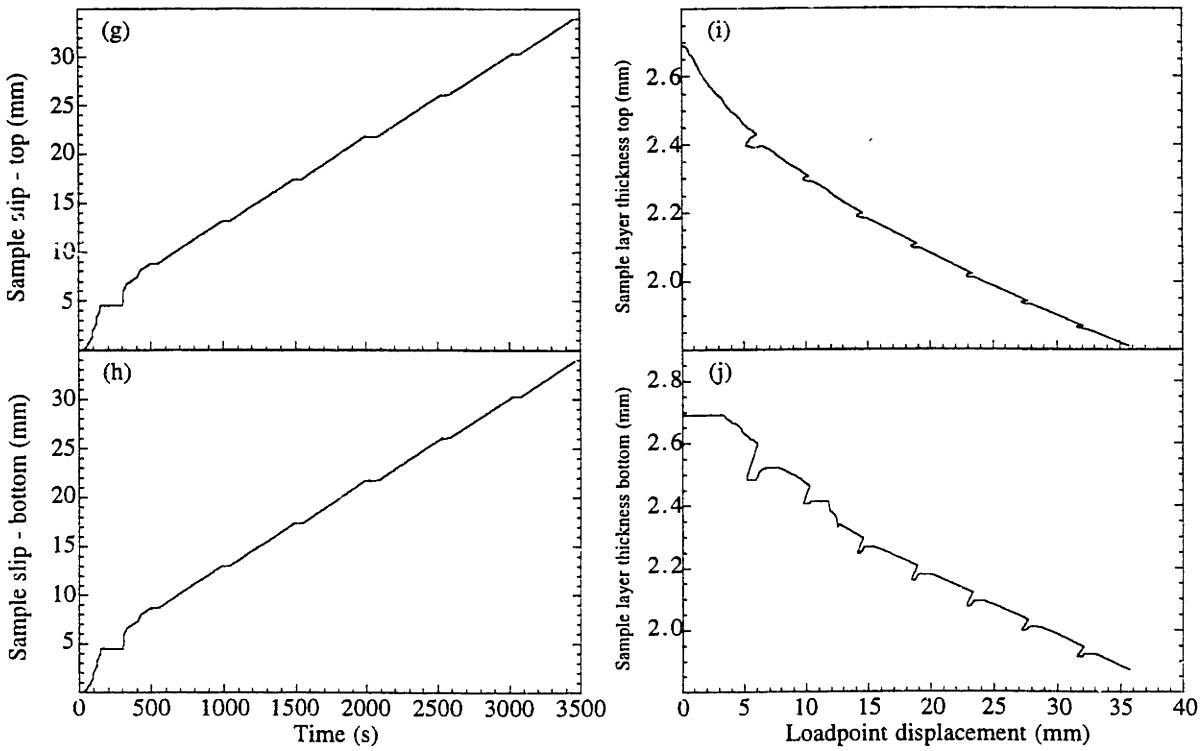

Experiment m282

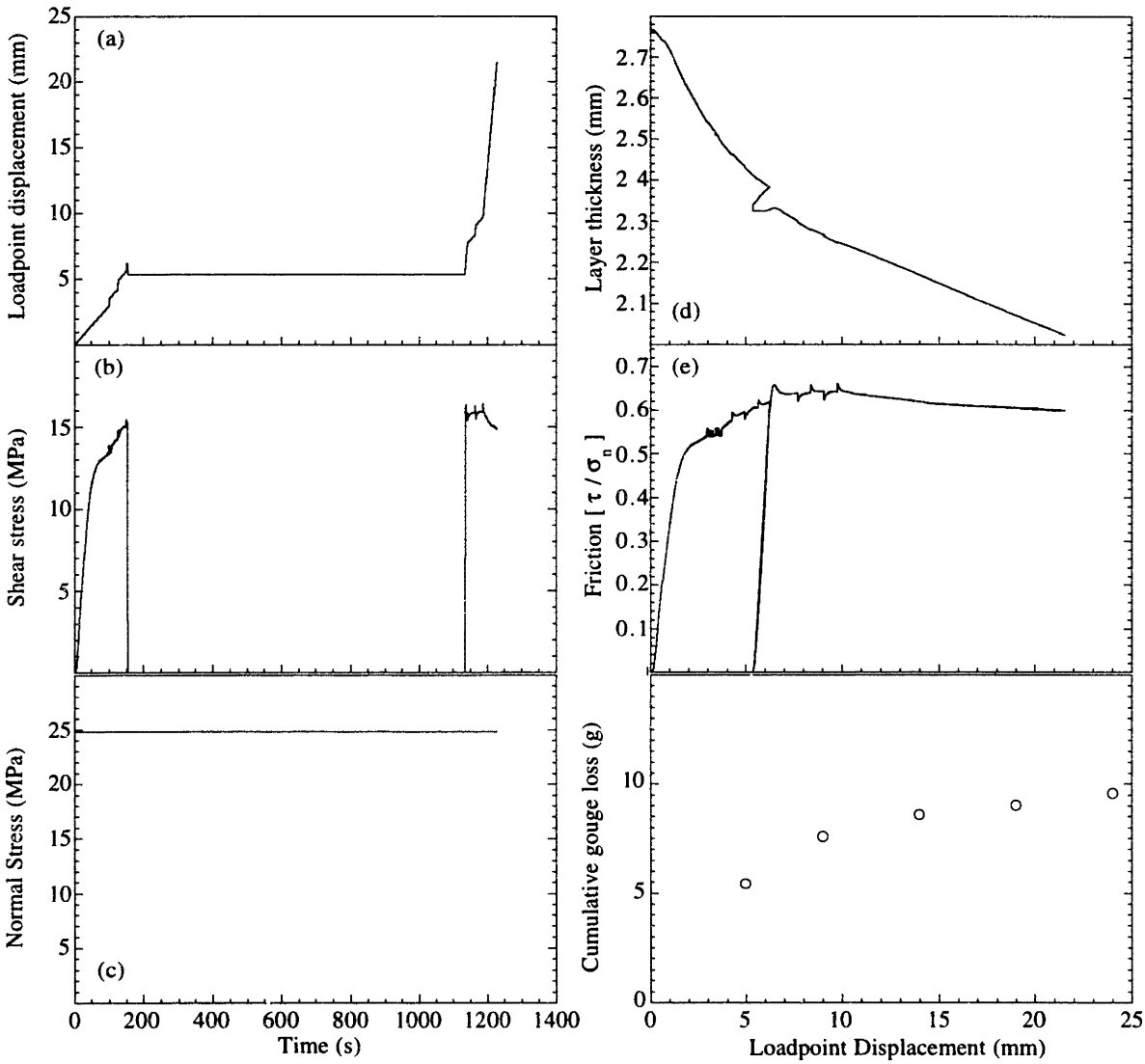

Experiment m282 (continued)

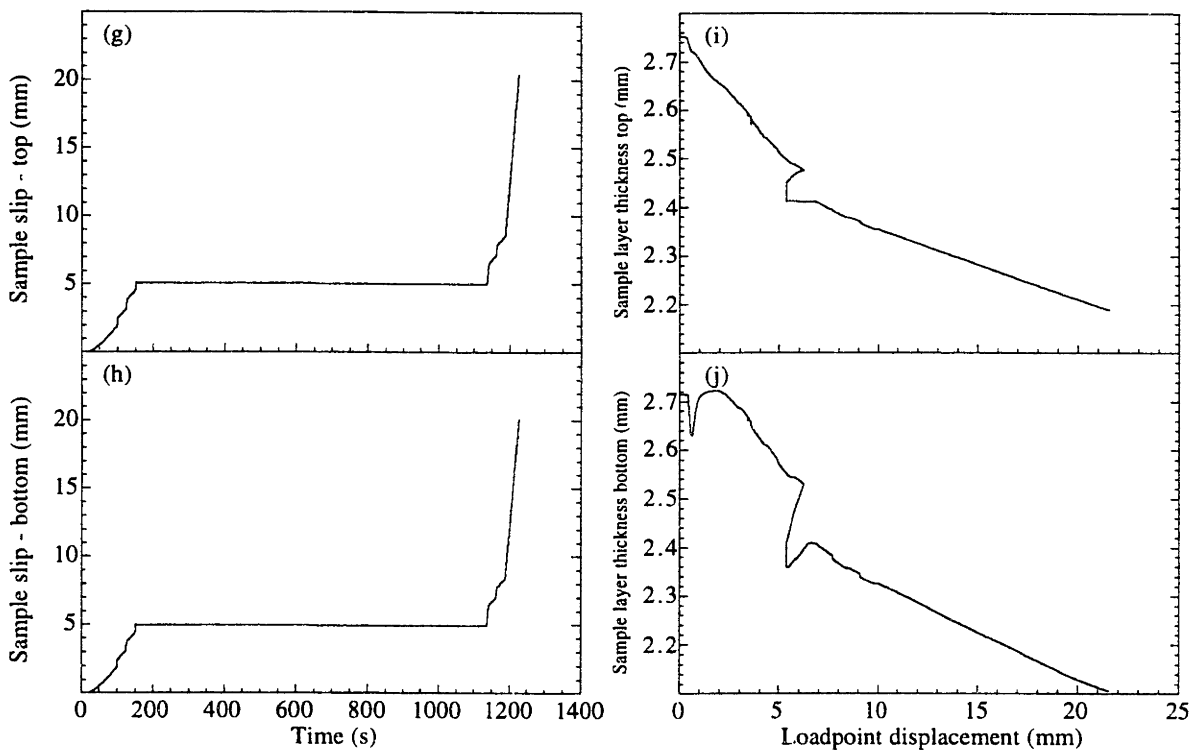

Experiment m283

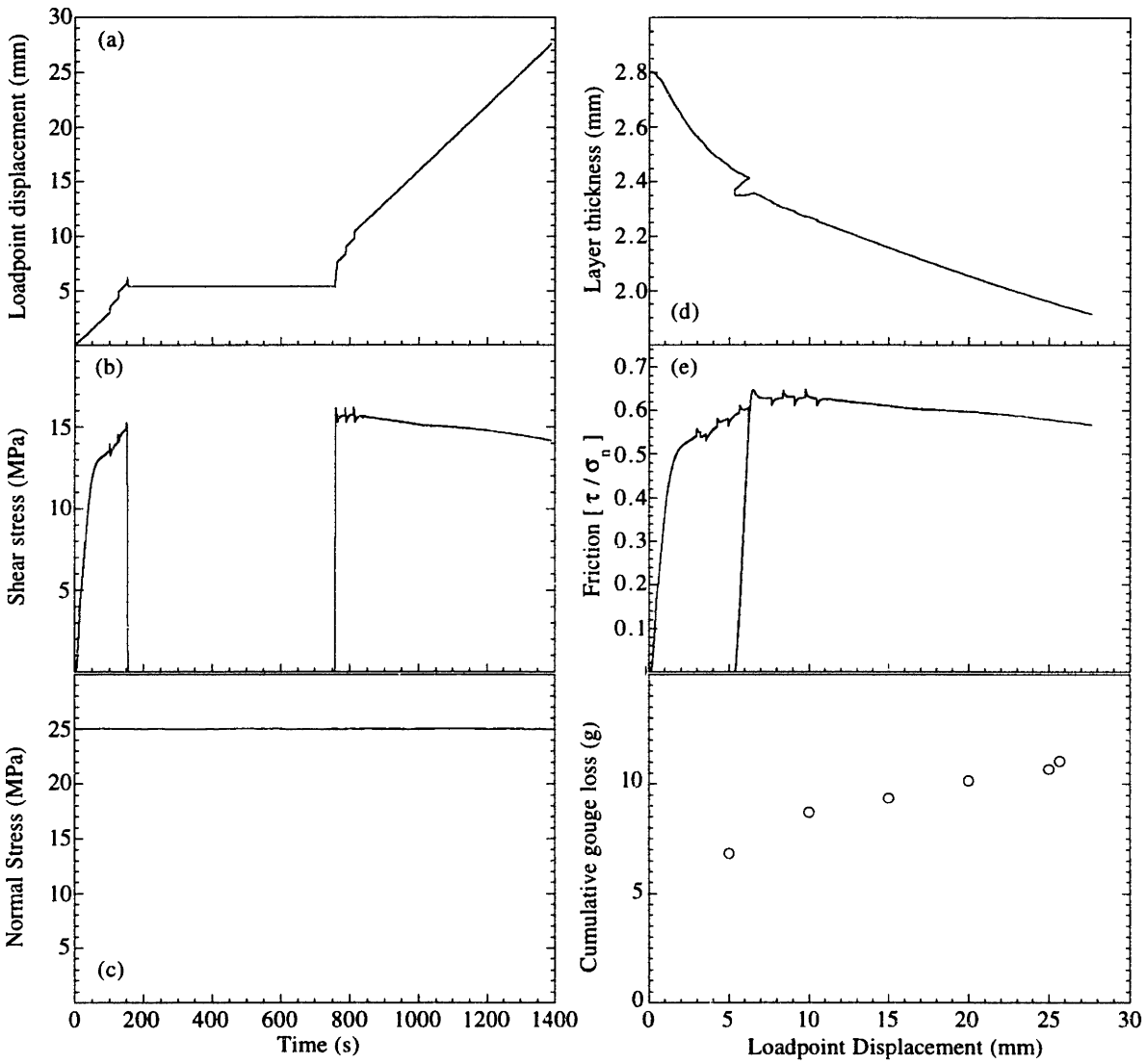

Experiment m283 (continued)

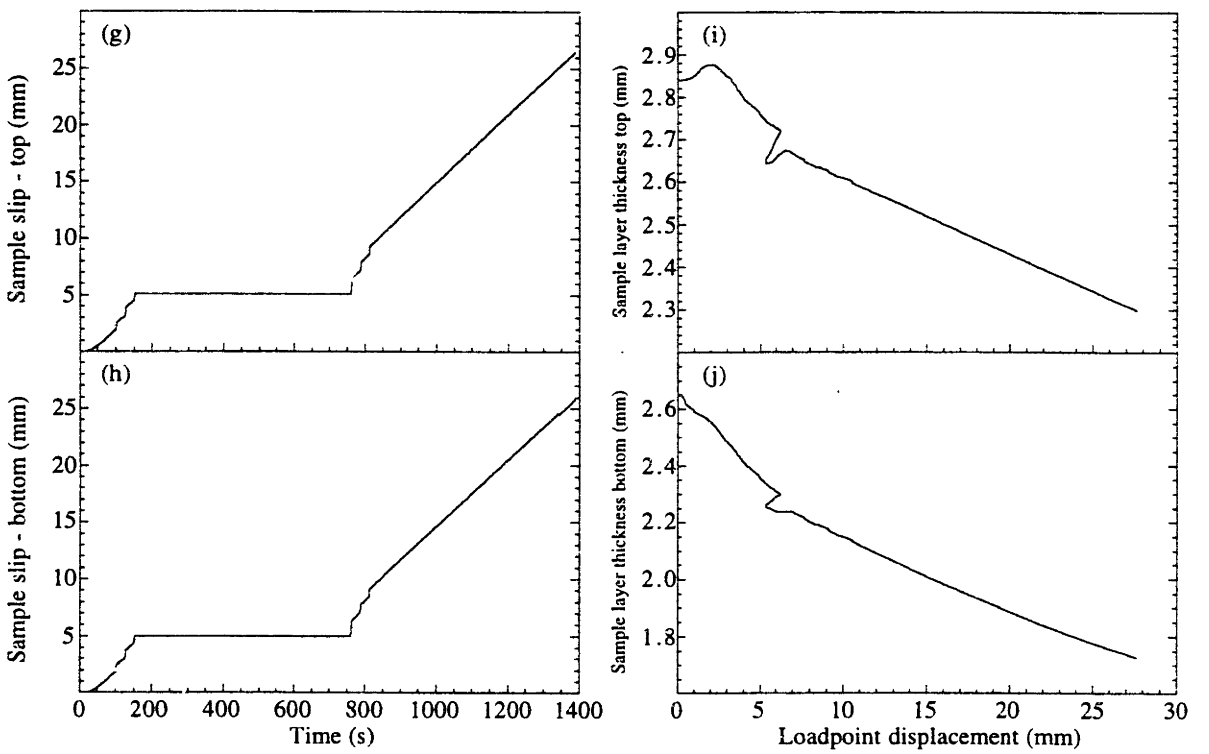

Experiment m284

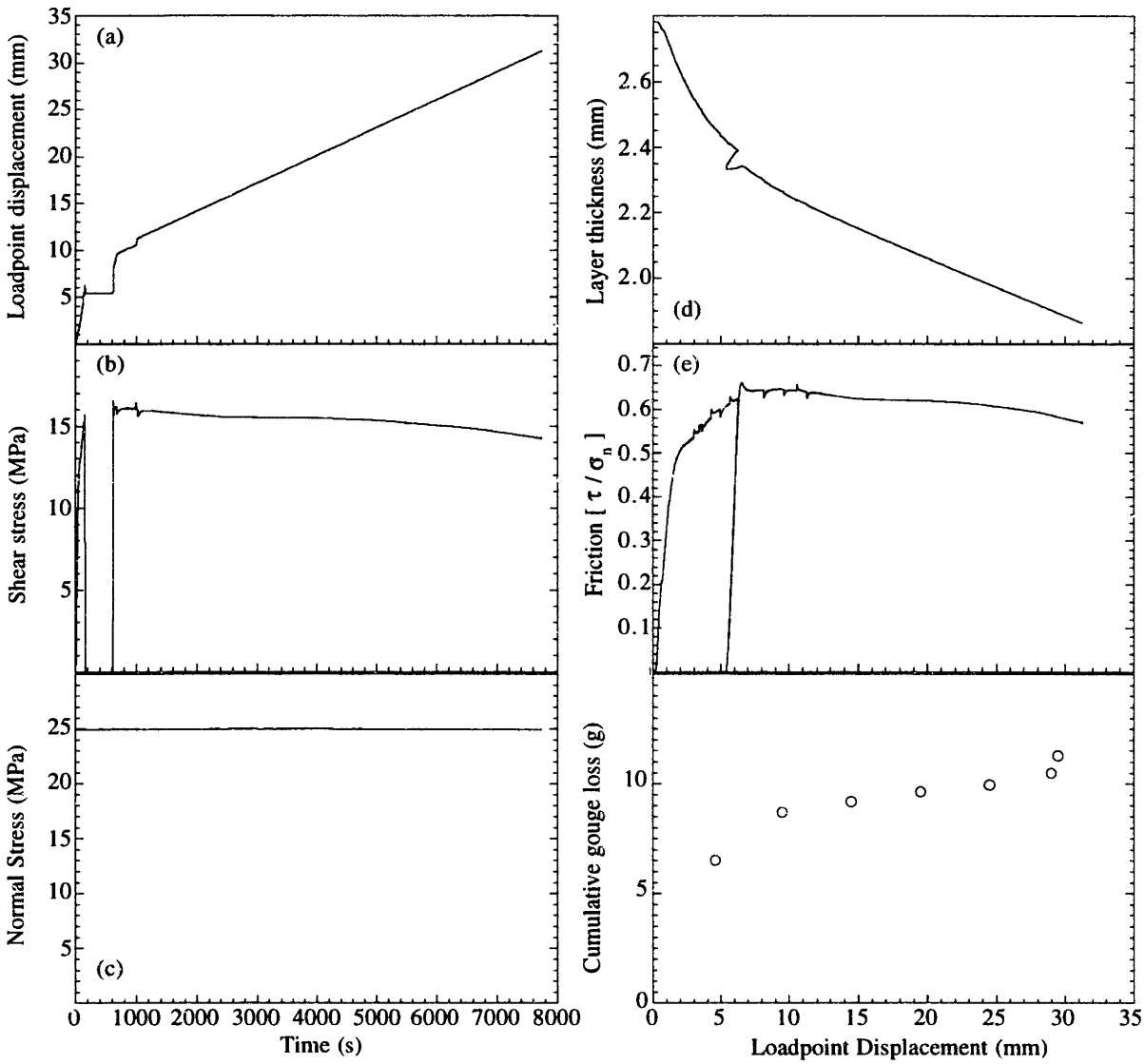

Experiment m284 (continued)

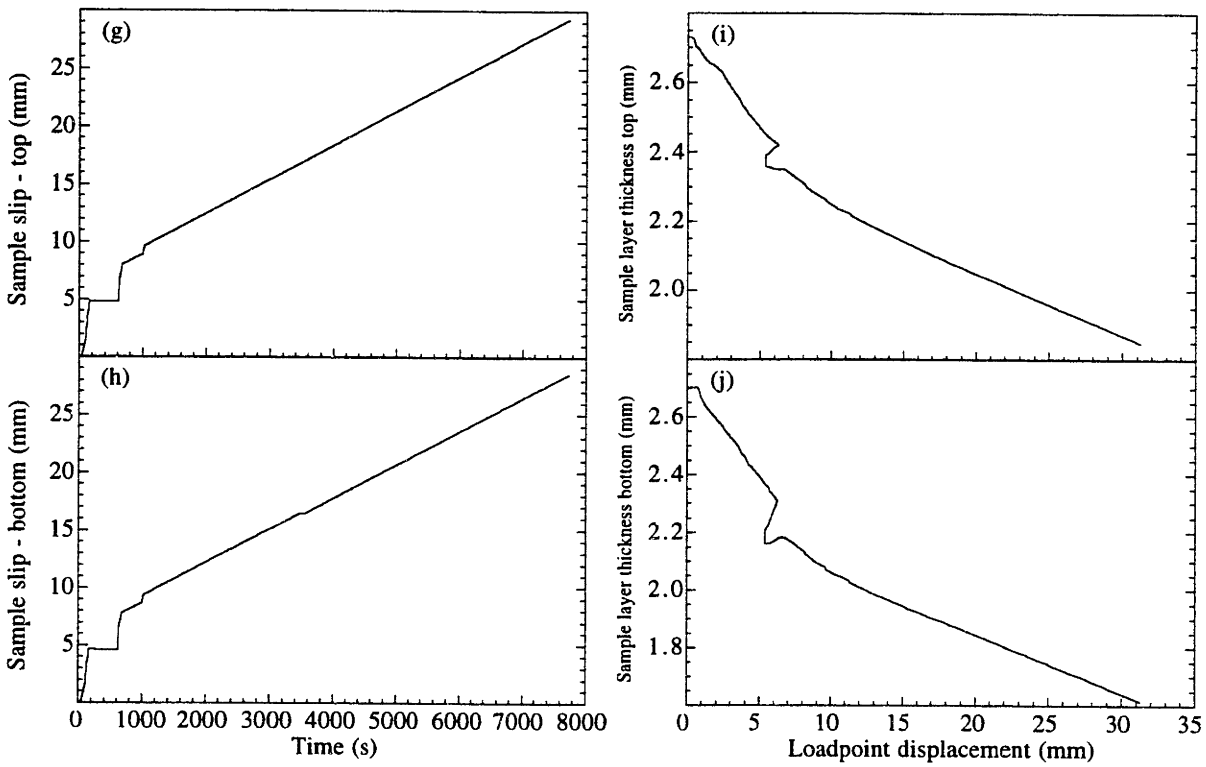

Experiment m295

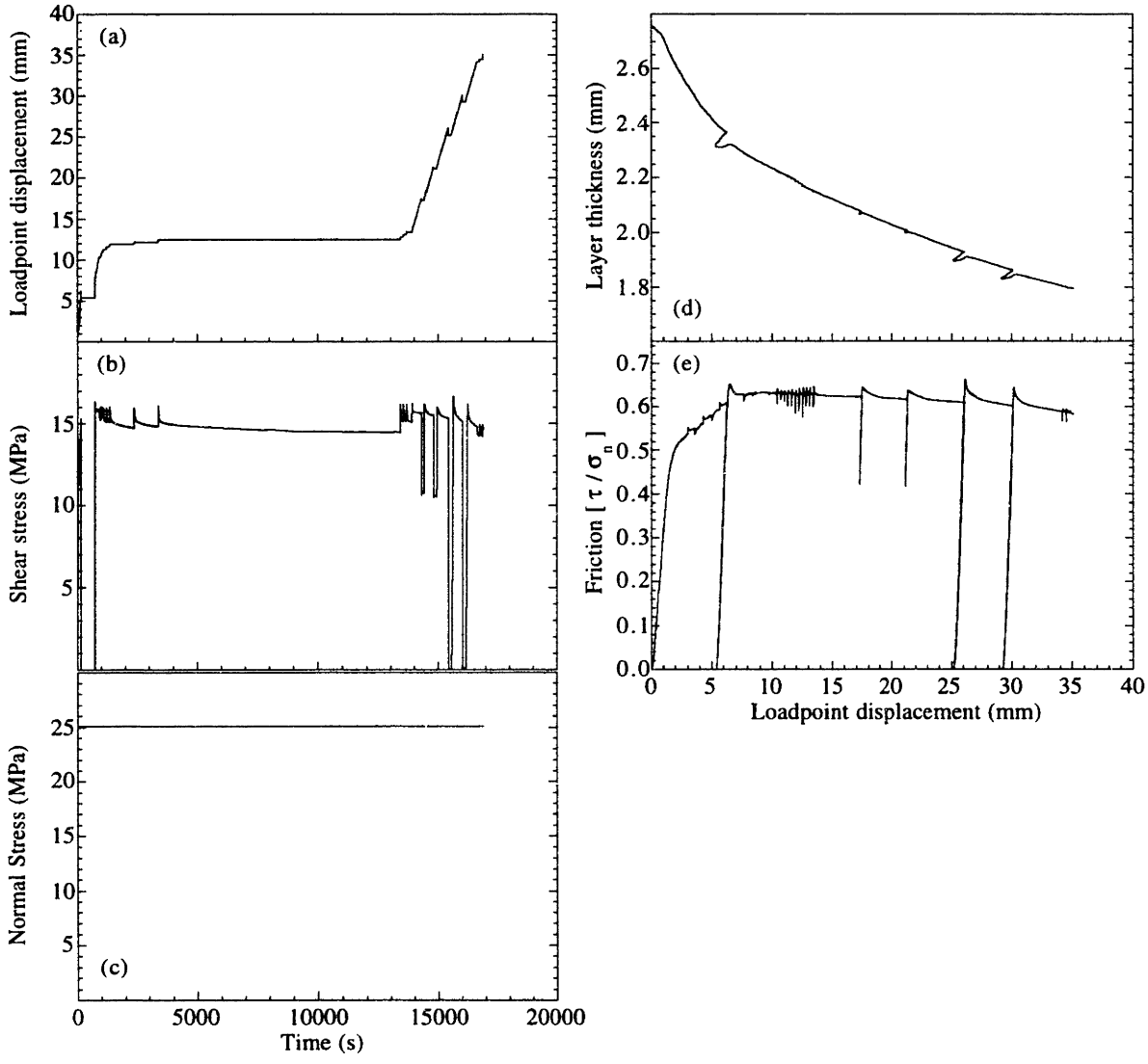

Experiment m295 (continued)

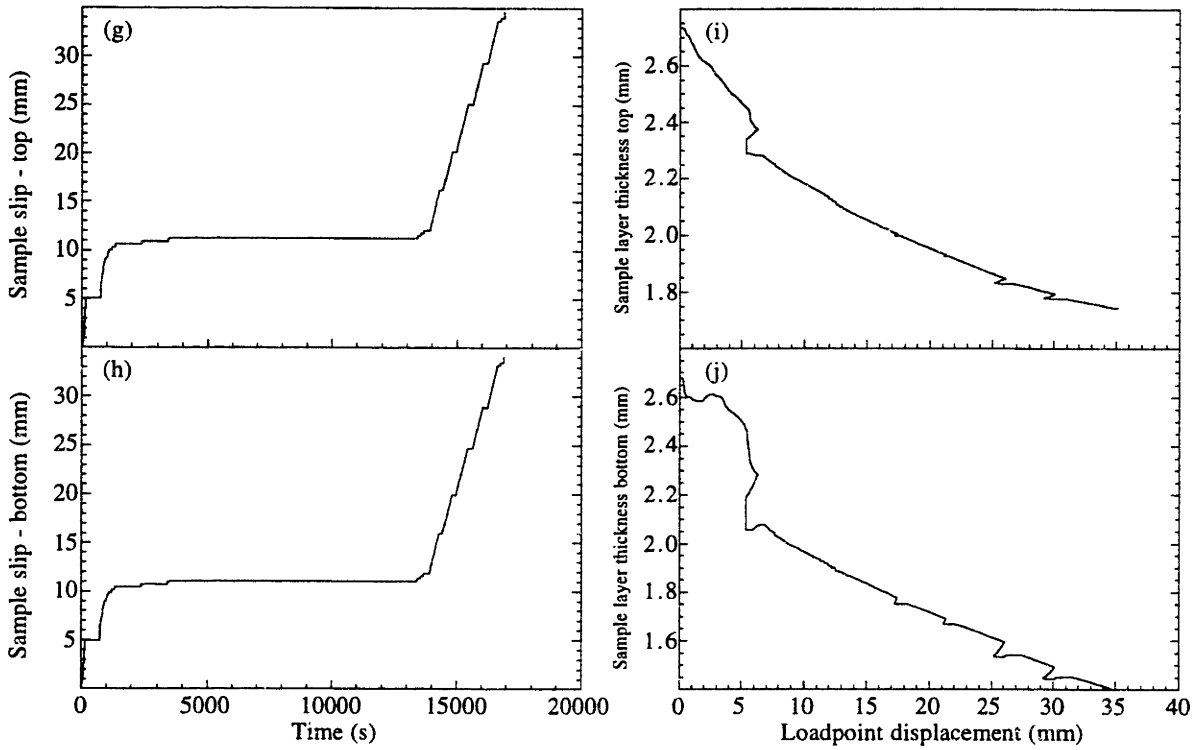

APPENDIX E

Data from triaxial tests on quartz gouge (Chapter 4)

The following figures show data from experiments performed on layers of quartz gouge, as described in Chapter 4 of this thesis. All experiments were conducted in a triaxial deformation apparatus under hydrothermal conditions. For all tests, shear was imposed by controlling the velocity of the loading piston. Confining pressure was maintained constant throughout each test. For a summary of experiment conditions Table 4.1 is reproduced on the following page.

The following figures show data from each experiment. The applied loading force and piston displacement were measured at the loadpoint. Confining and pore-fluid pressures were monitored using pressure transducers. Temperature was monitored by a thermocouple used to control the heating furnace. The thermocouple was located approximately 1-2 mm into the top of the sample (in the pore-fluid access port). Friction is determined from the shear and normal stresses (calculated from the applied axial load) and the applied pore-fluid pressure.

During the course of this study, major modifications were made to the testing apparatus and data recording system. This is reflected in the measurements that were recorded. For example, in the earlier tests (with lower identification numbers) pore-fluid pressure could not be recorded. In later tests, pore pressure was monitored.

a). Displacement of the loading piston. The slope of the data indicates the imposed loading rate.

b). Shear displacement resolved onto the sawcut surface.

c). Normal stress resolved onto the sawcut surface.

d). Shear stress resolved onto the sawcut surface.

e). Coefficient of friction determined as described above.

f). Pore-fluid pressure.

g). Temperature.

h). Confining pressure.

For reference, the Table 4.1 containing the summary information for the experiments shown in this Appendix is reproduced on the following page.

Experiment	Healing temperature (°C)	Deformation temperature (°C)	Time of healing at T_h (sec)	Experiment type
S01	636	230	3600	hold-slide
S02	636	636	3600	hold-slide
S03	636	636	10000	hold-slide
S04	636	636	300	hold-slide
S05	636	230	10000	hold-slide
S06	636	230	300	hold-slide
S07	636	636	0	hold-slide
S07L	636	636	60 and 600	slide-hold-slide
S08	230	230	0	hold-slide
S09L	636	636	600	slide-hold-slide
S10	450	250	3600	hold-slide
S11L	636	636	60	slide-hold-slide
S12	636	230	100000	hold-slide
S15	636	230	100000	hold-slide
S16	636	230	100000	hold-slide
S17	636	636	100000	hold-slide
S18	636	230	3600	hold-slide
S19L	636	636	600 and 6000	slide-hold-slide
S20	636	636	3600	hold-slide
S23	600	600	3600	hold-slide
S24	600	600	3600	hold-slide
S25	600	600	3600	hold-slide
S26	636	636	100000	hold-slide
S27	636	636	100000	hold-slide
S28	600	600	36000	hold-slide
S29	600	600	0	hold-slide
S30	600	600	0	hold-slide
S31	600	600	0	hold-slide
S32	600	600	3600	hold-slide
S33	636	230	36000	hold-slide
S34L	600	600	60000	slide-hold-slide
S35L	600	600	60 and 600	slide-hold-slide
S36L	450	450	6000	slide-hold-slide
S37L	450	450	60 and 600	slide-hold-slide
S38	600	600	100000	hold-slide
S39L	250	250	60, 600, 6000	slide-hold-slide
S42L	250	250	60, 600, 3000	slide-hold-slide
S43	350	350	3600	hold-slide
S43L	350	350	60 and 600	slide-hold-slide

Table E.1. Summary information from the experiments performed for this study. The primary variables include the temperature at which samples were deformed and the time that the samples were healed at the healing temperature.

Experiment_S01

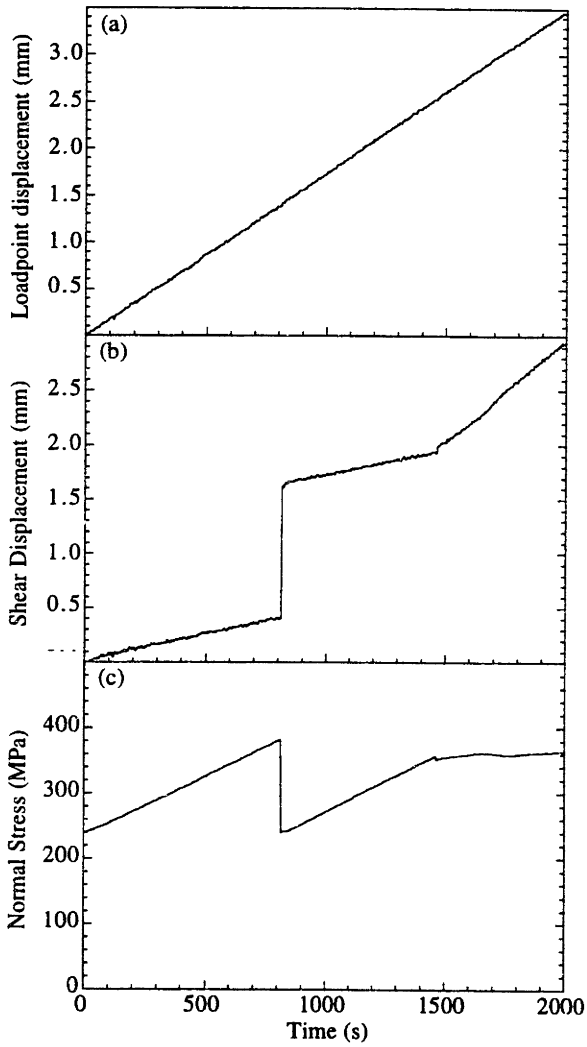

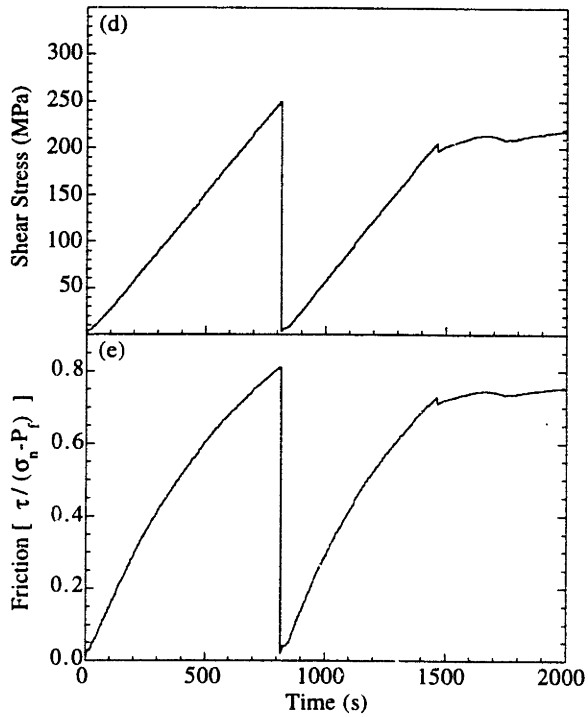

Experiment S02

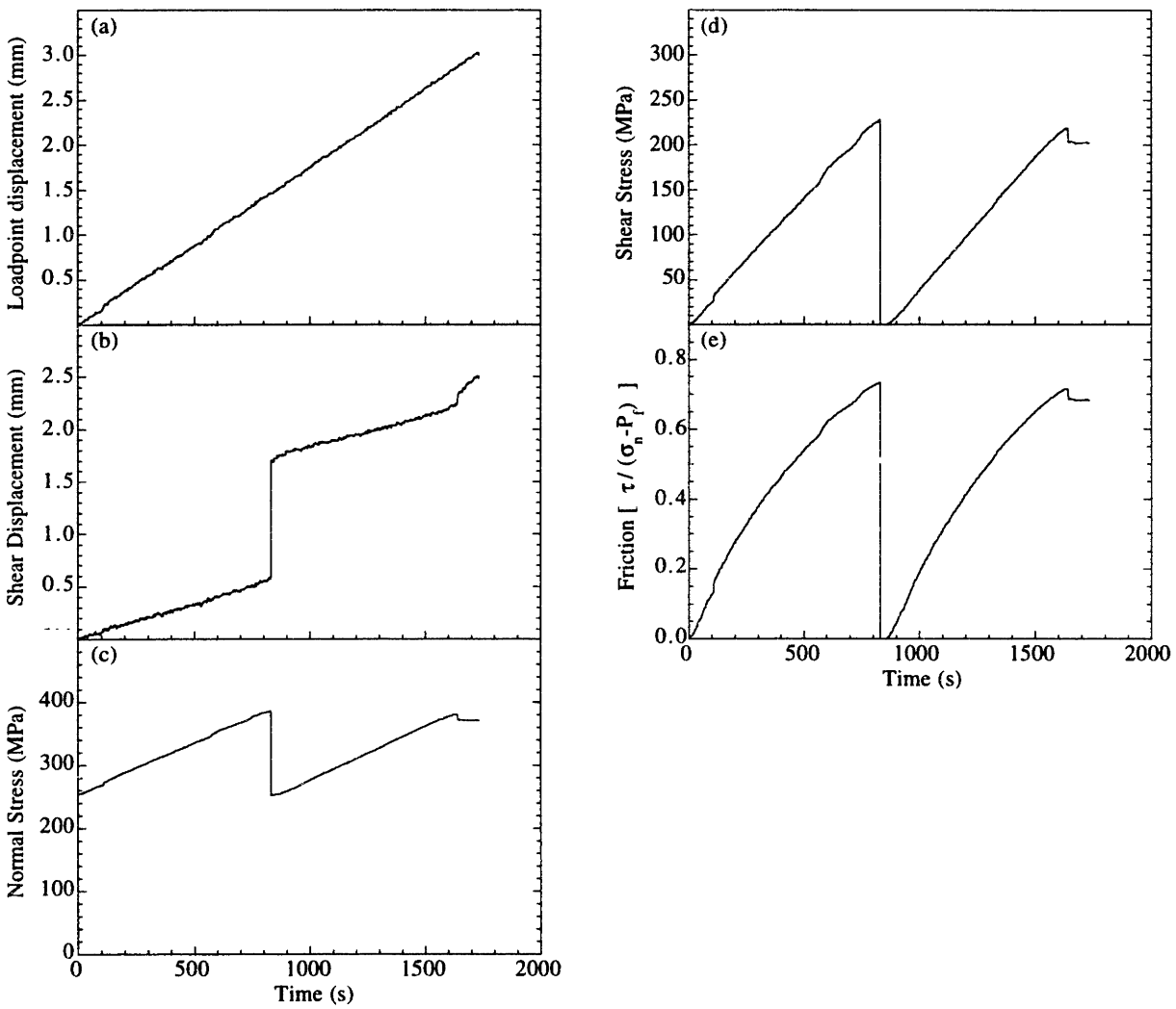

Experiment S03

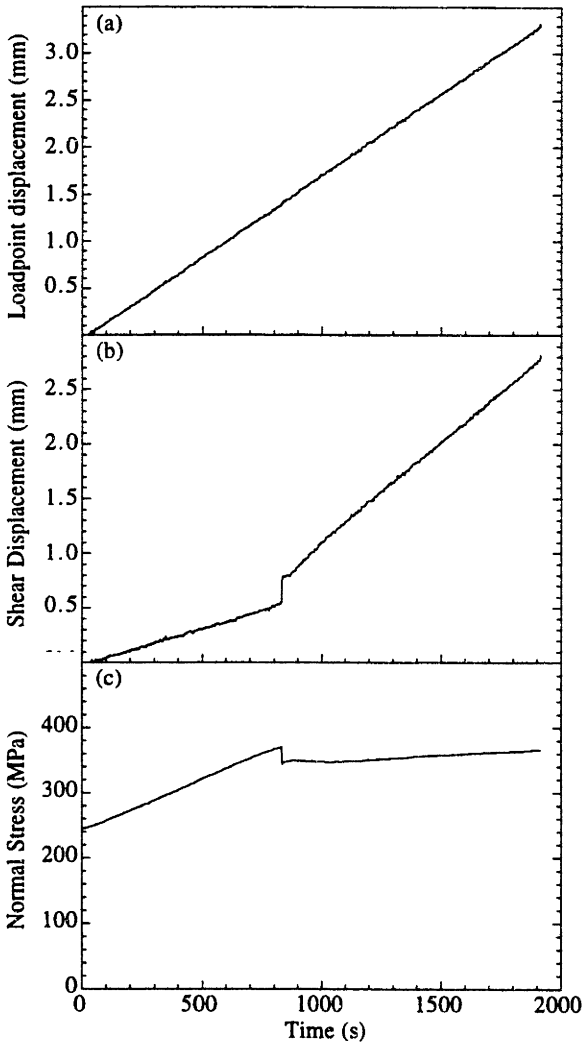

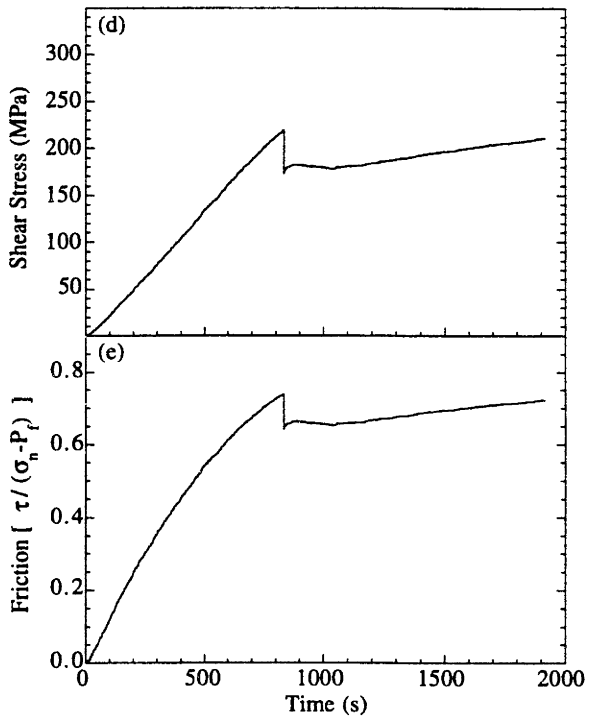

Experiment S04

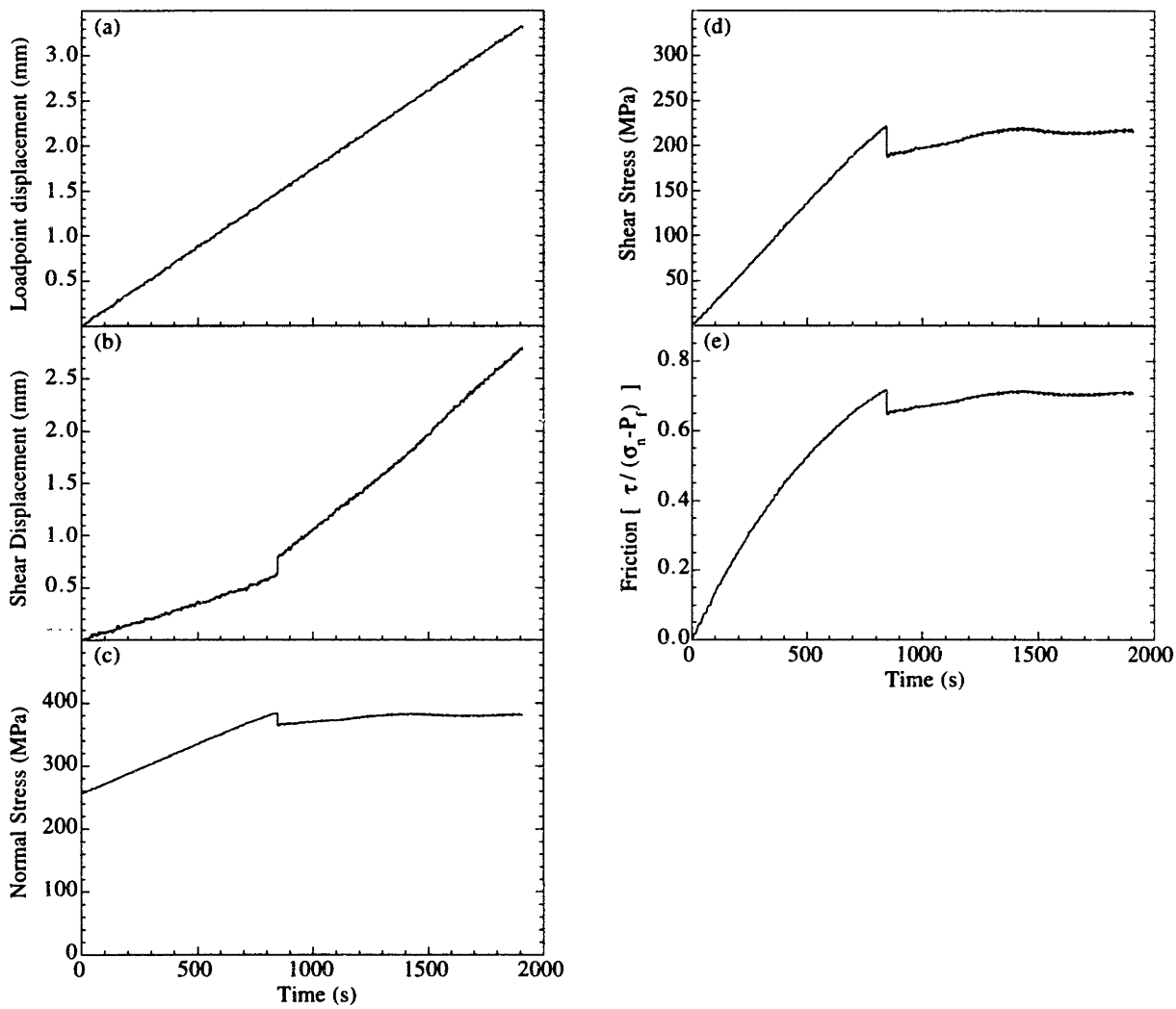

Experiment S05

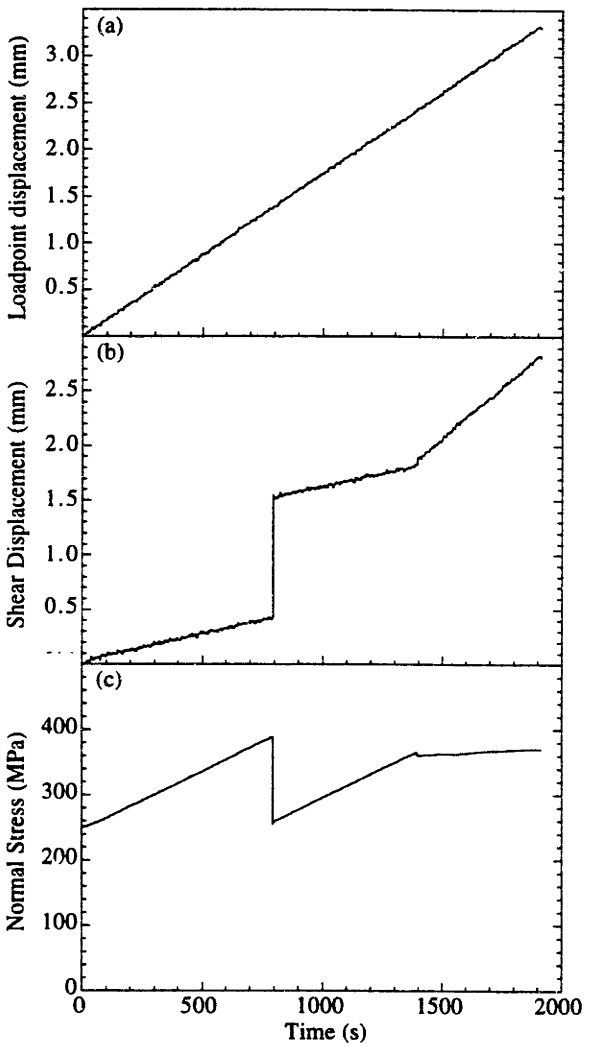

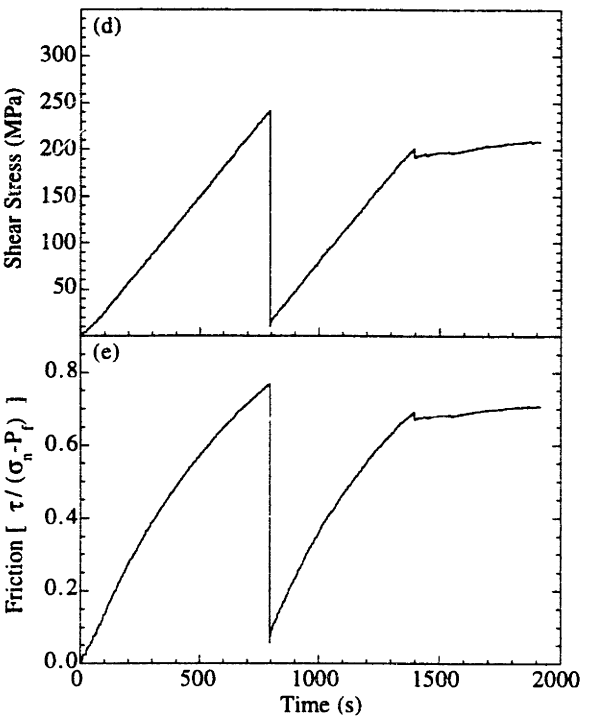

Experiment S06

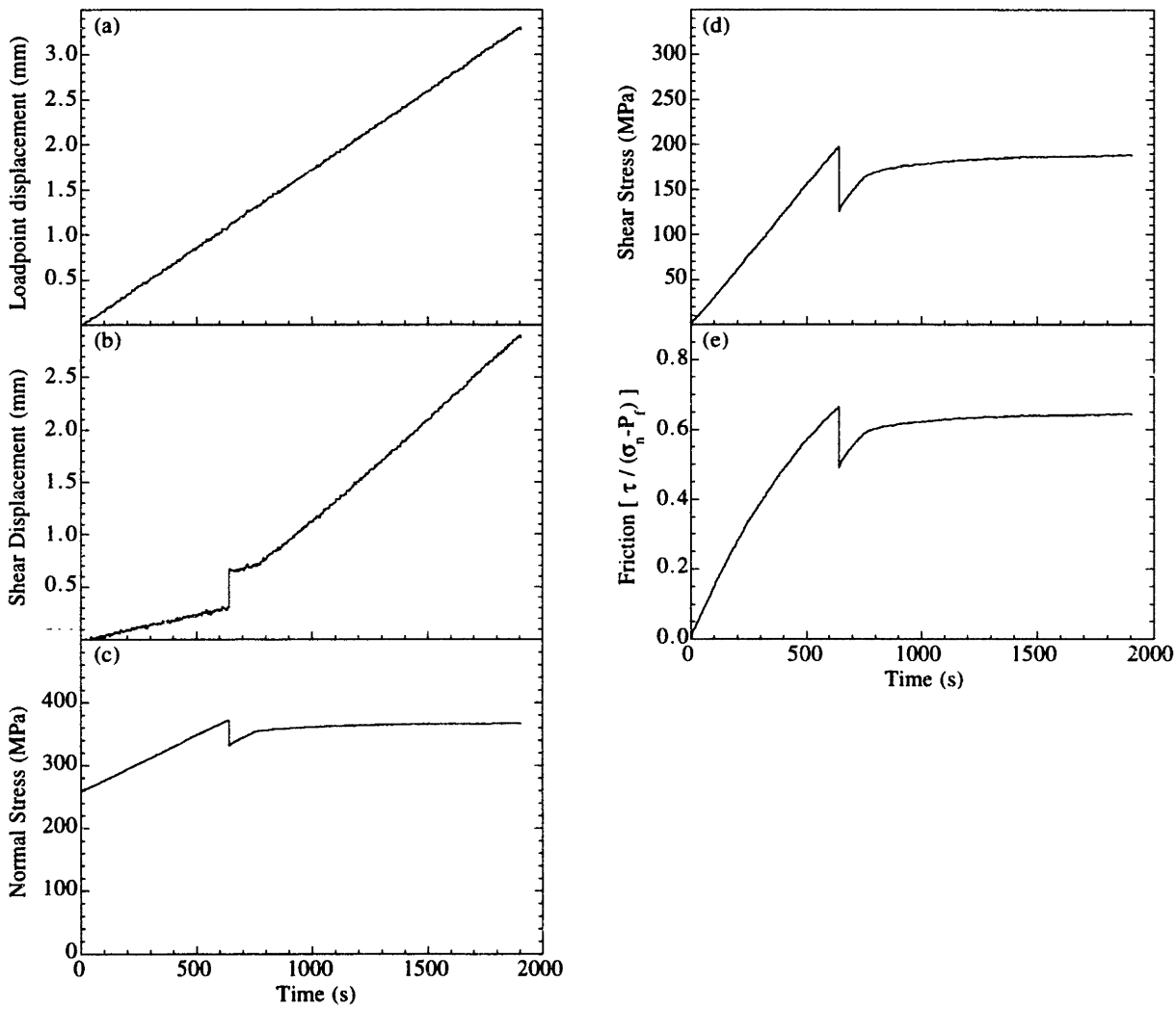

Experiment S07

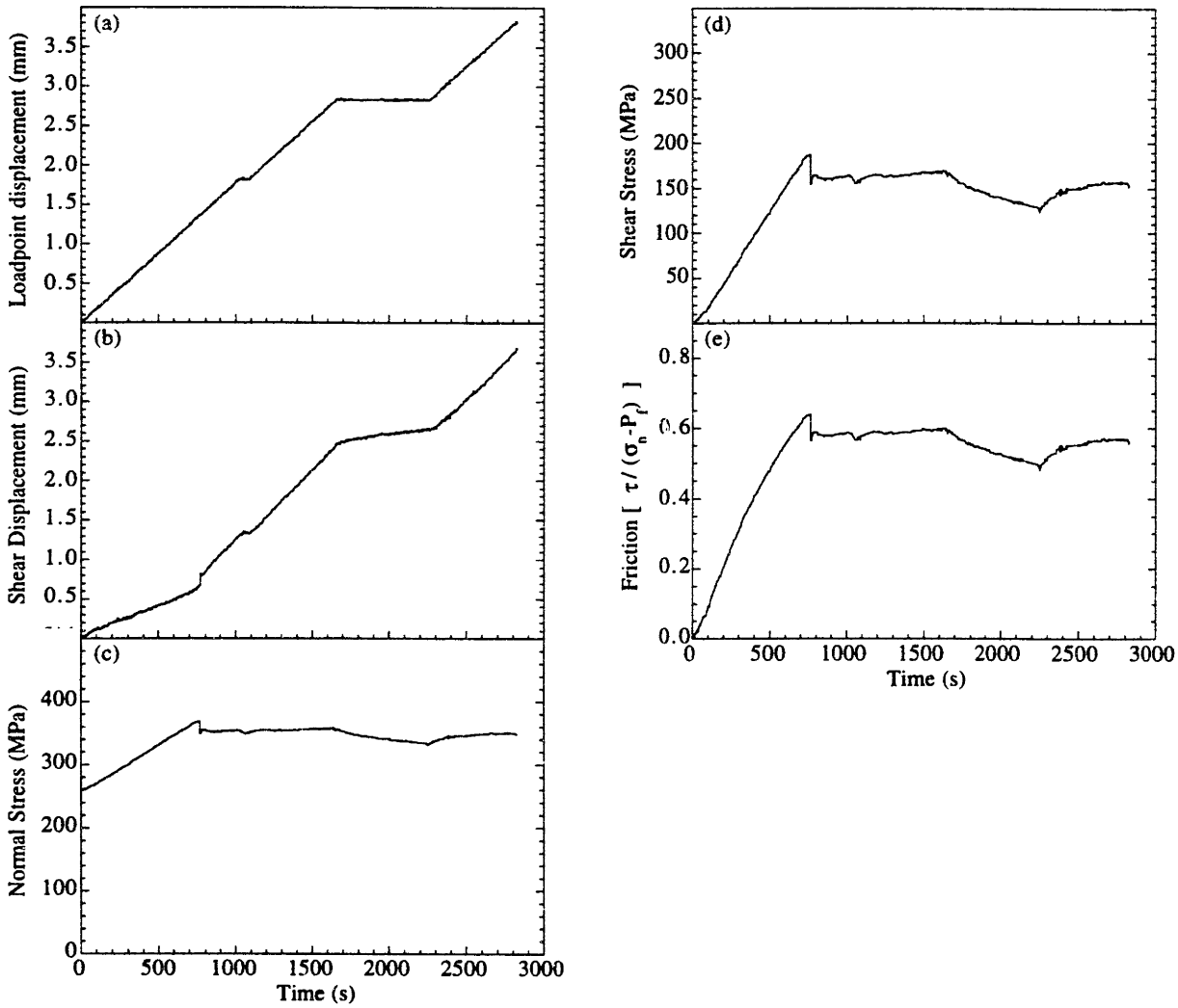

Experiment S08

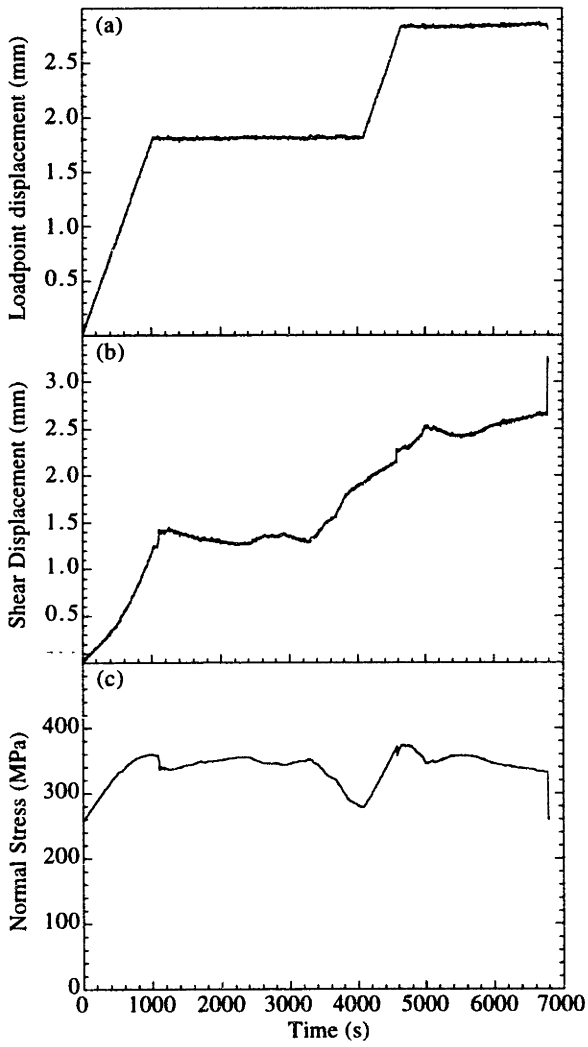

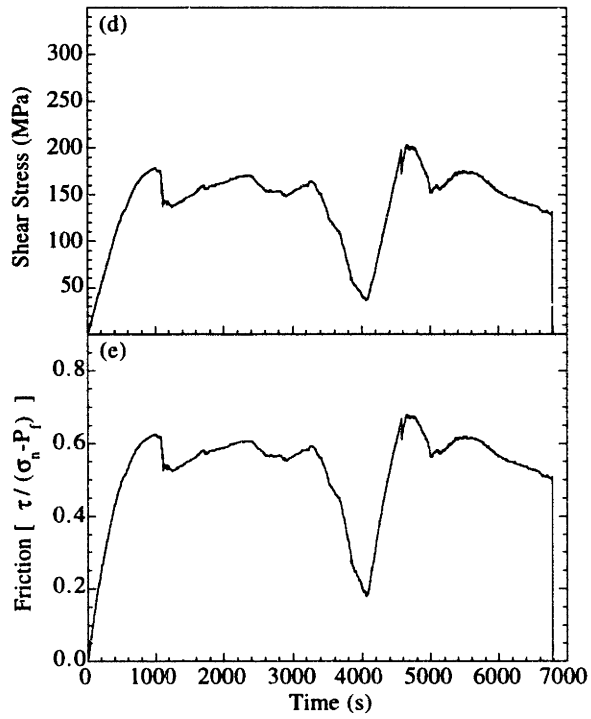

Experiment S09

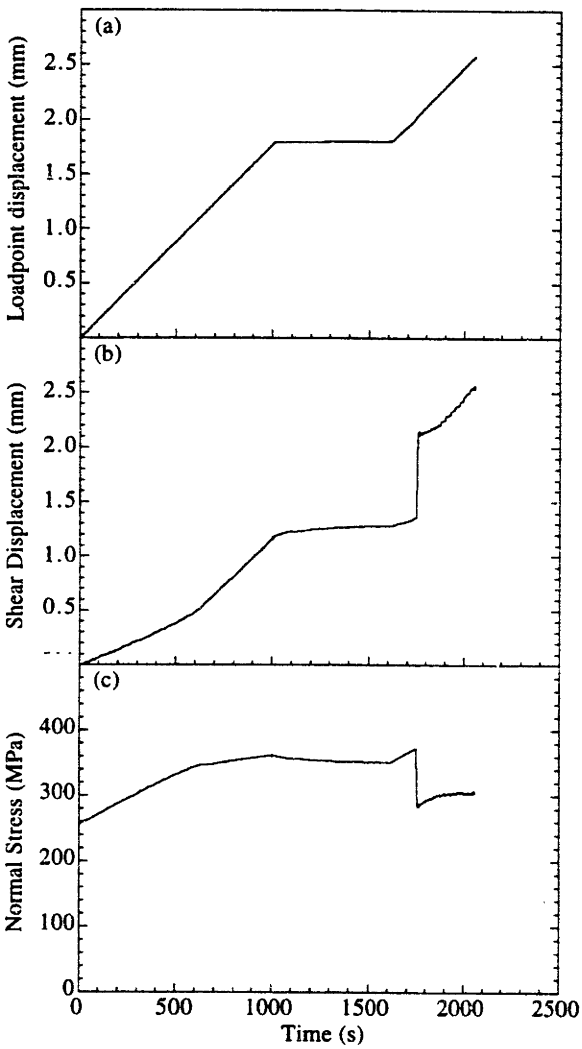

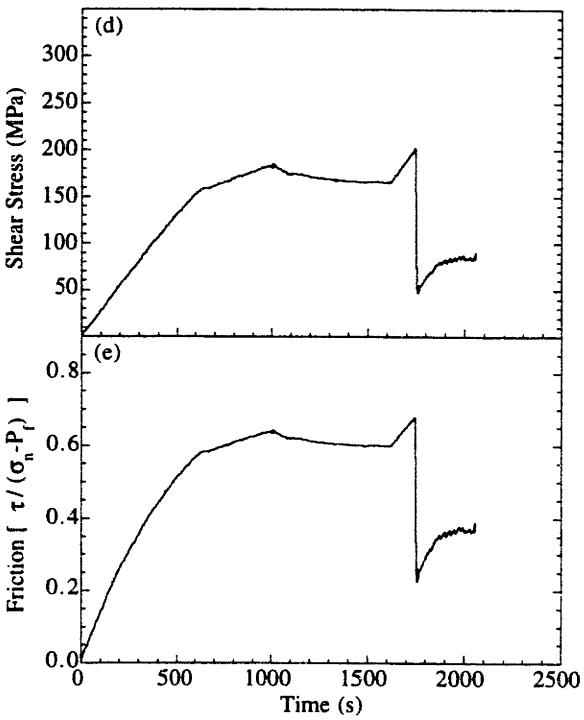

Experiment S10

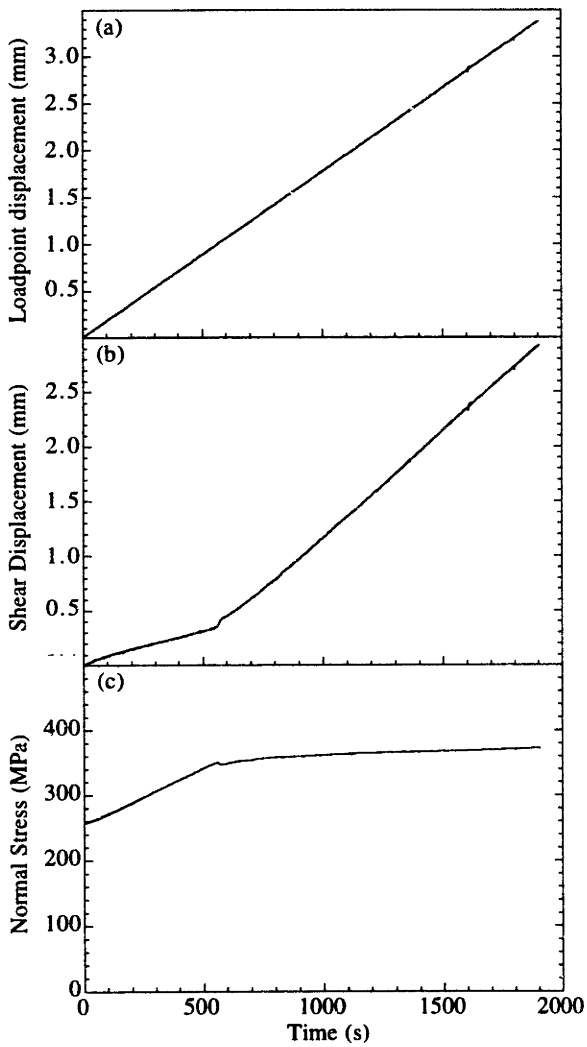

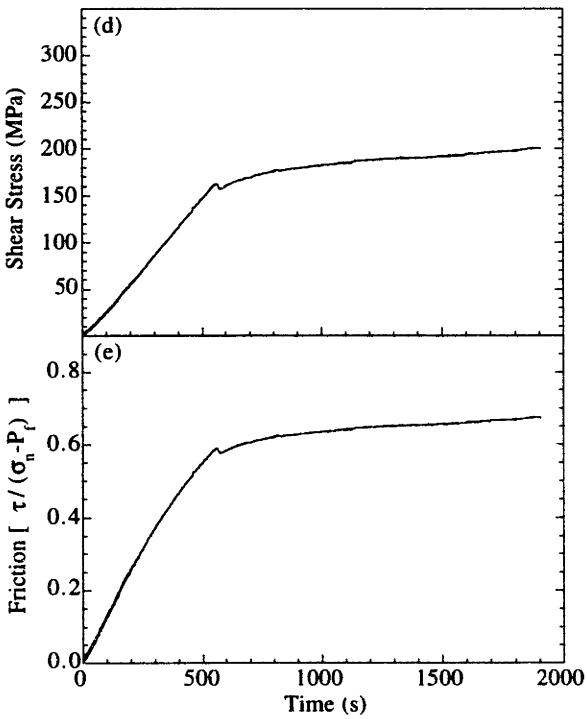

Experiment S12

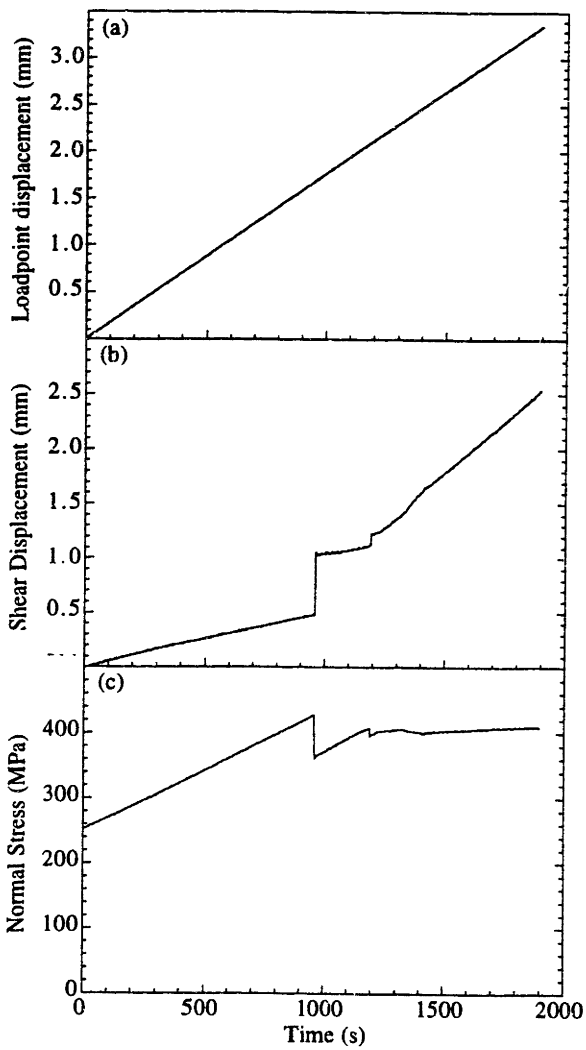

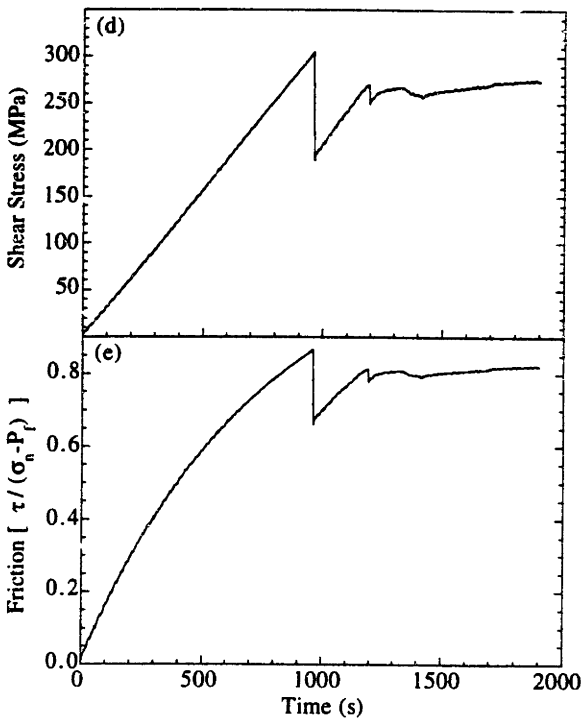

Experiment S15

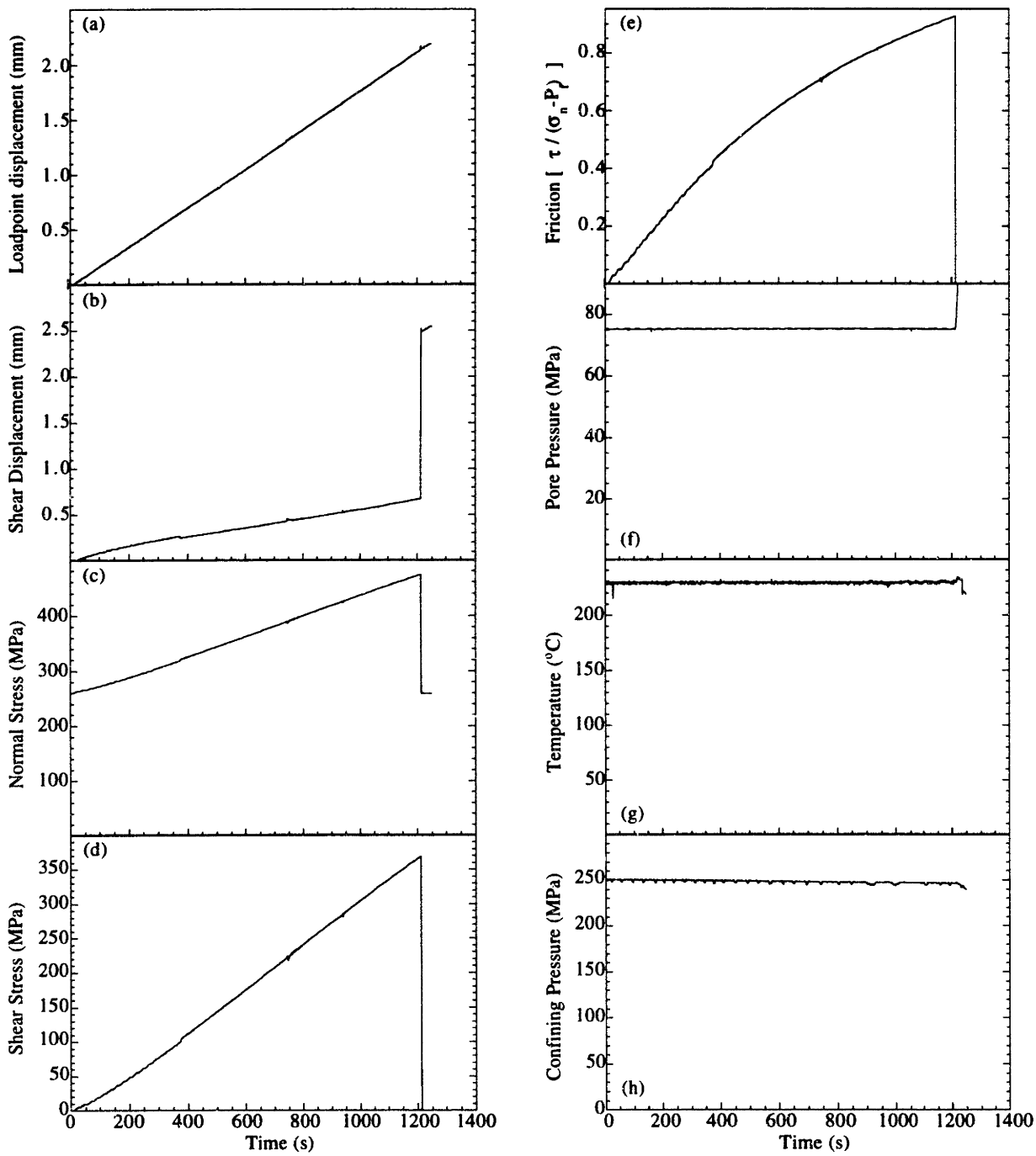

Experiment S16

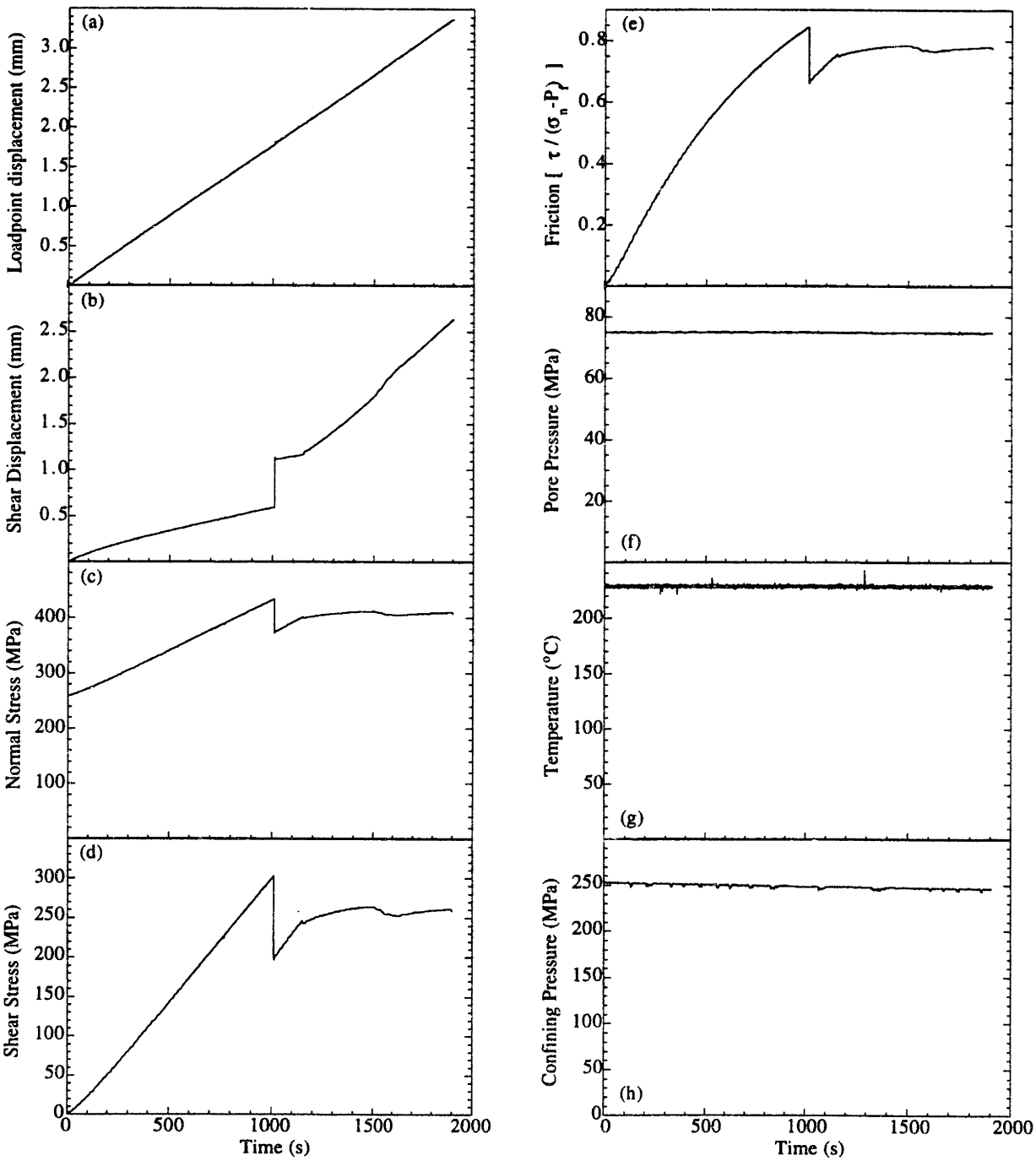

Experiment S17

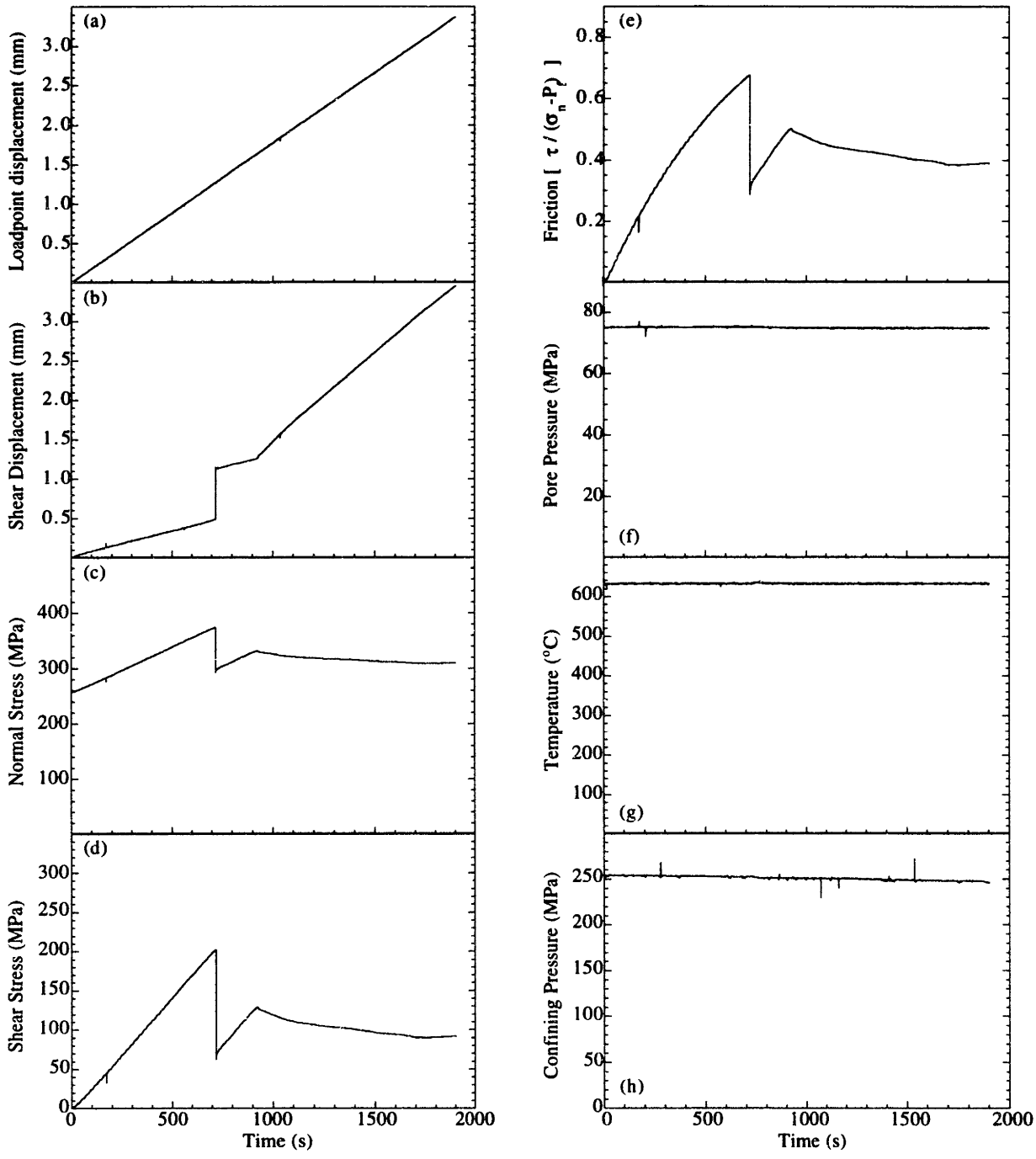

Experiment S18

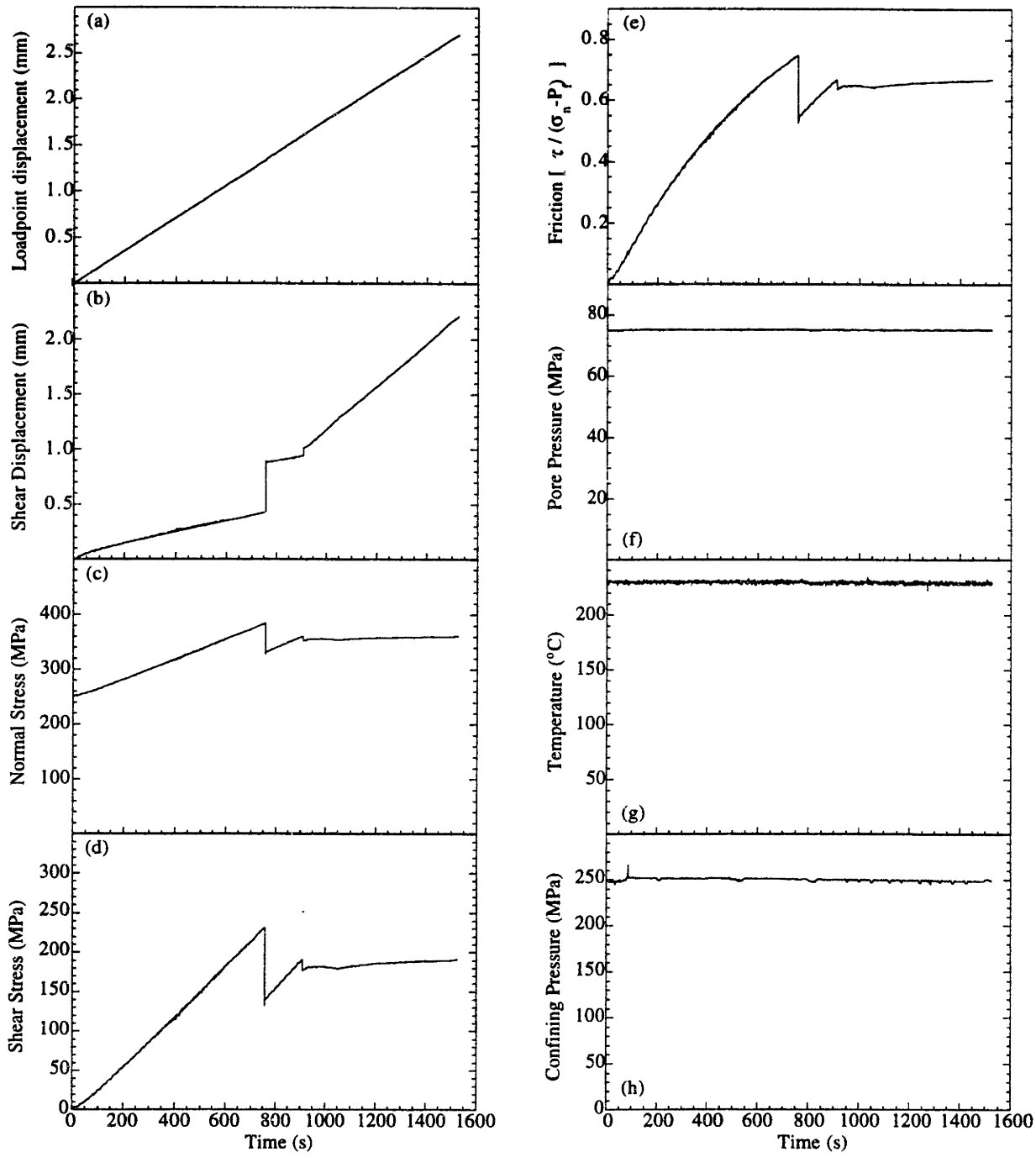

Experiment S19

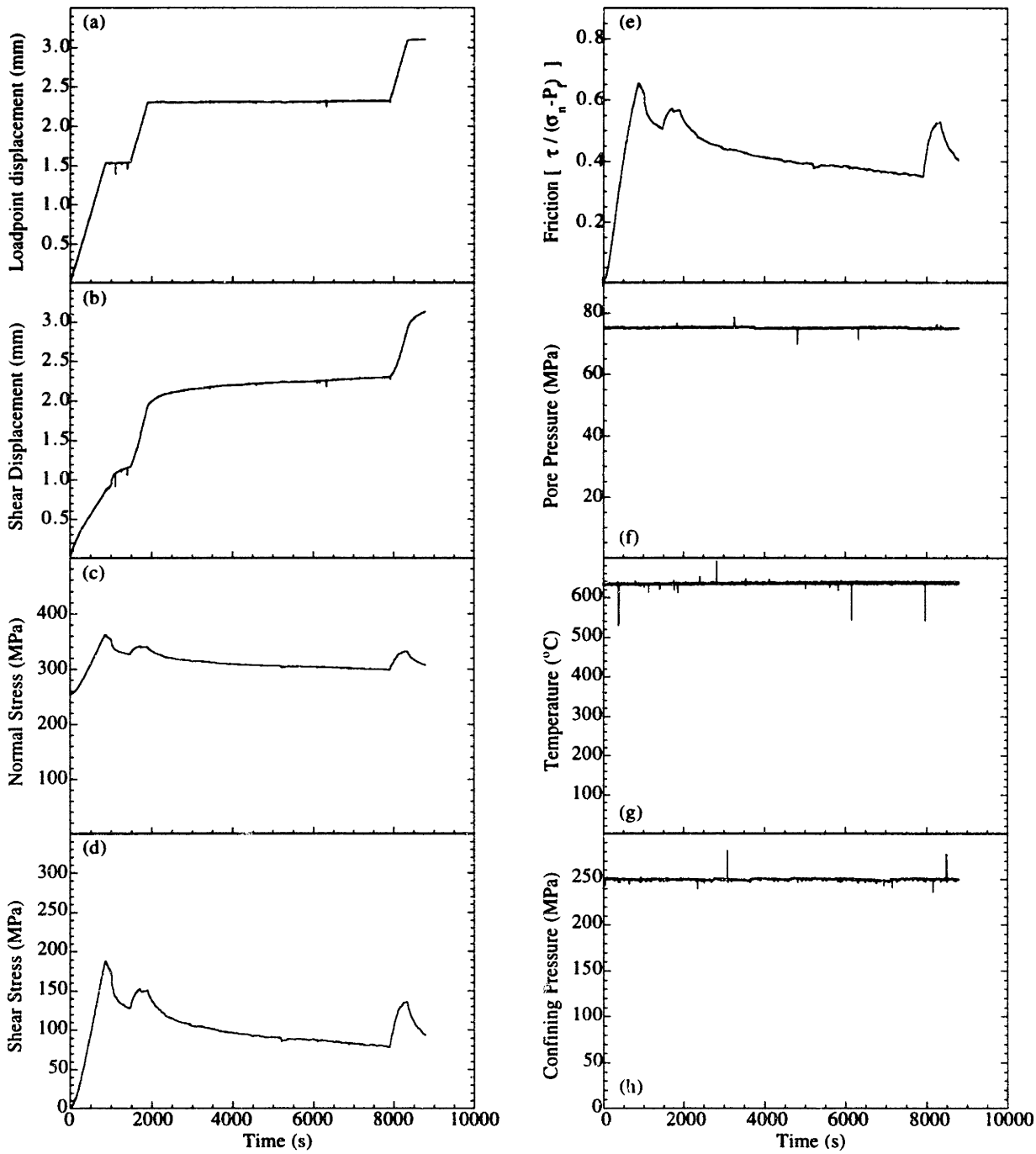

Experiment S26

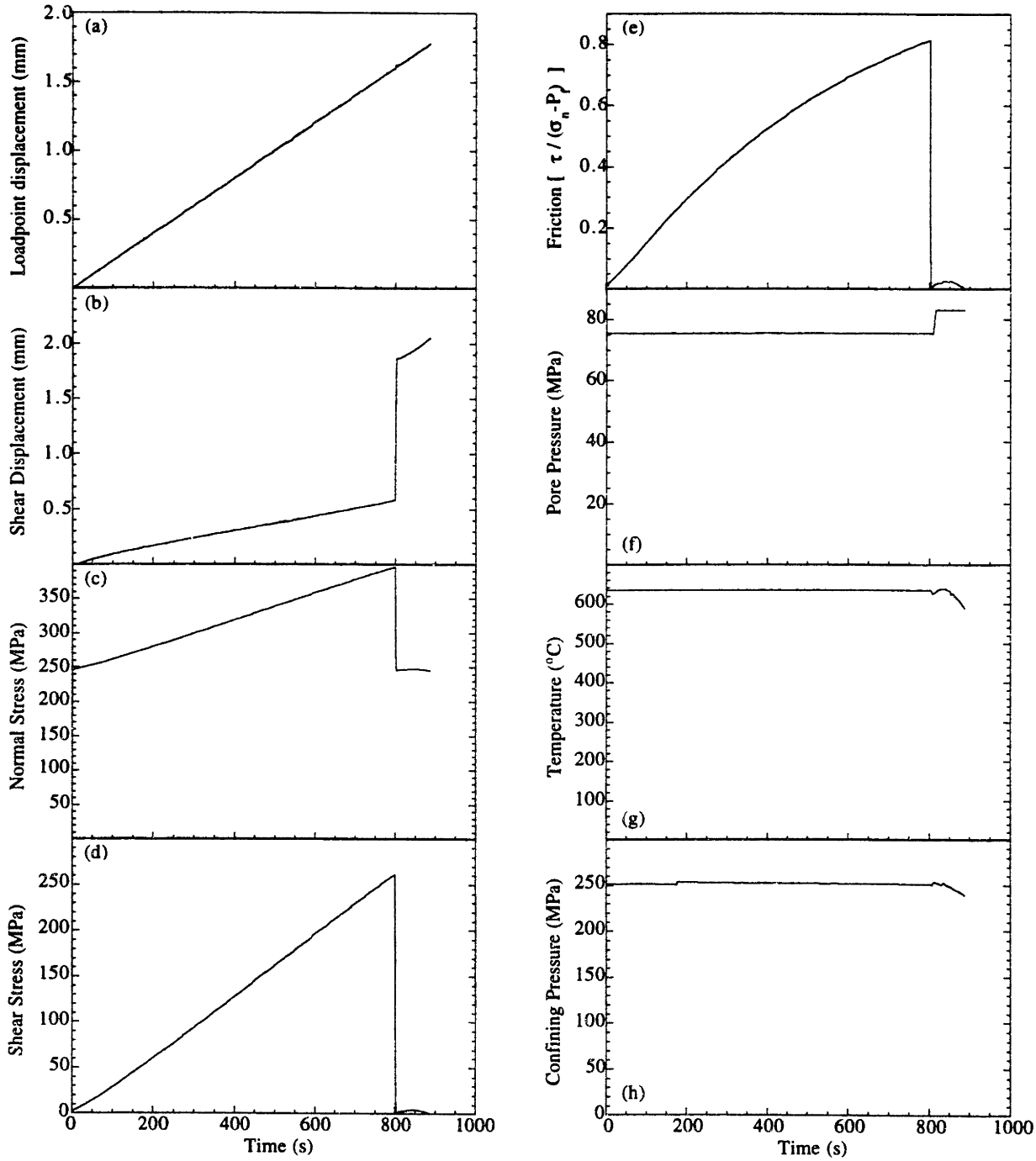

Experiment S28

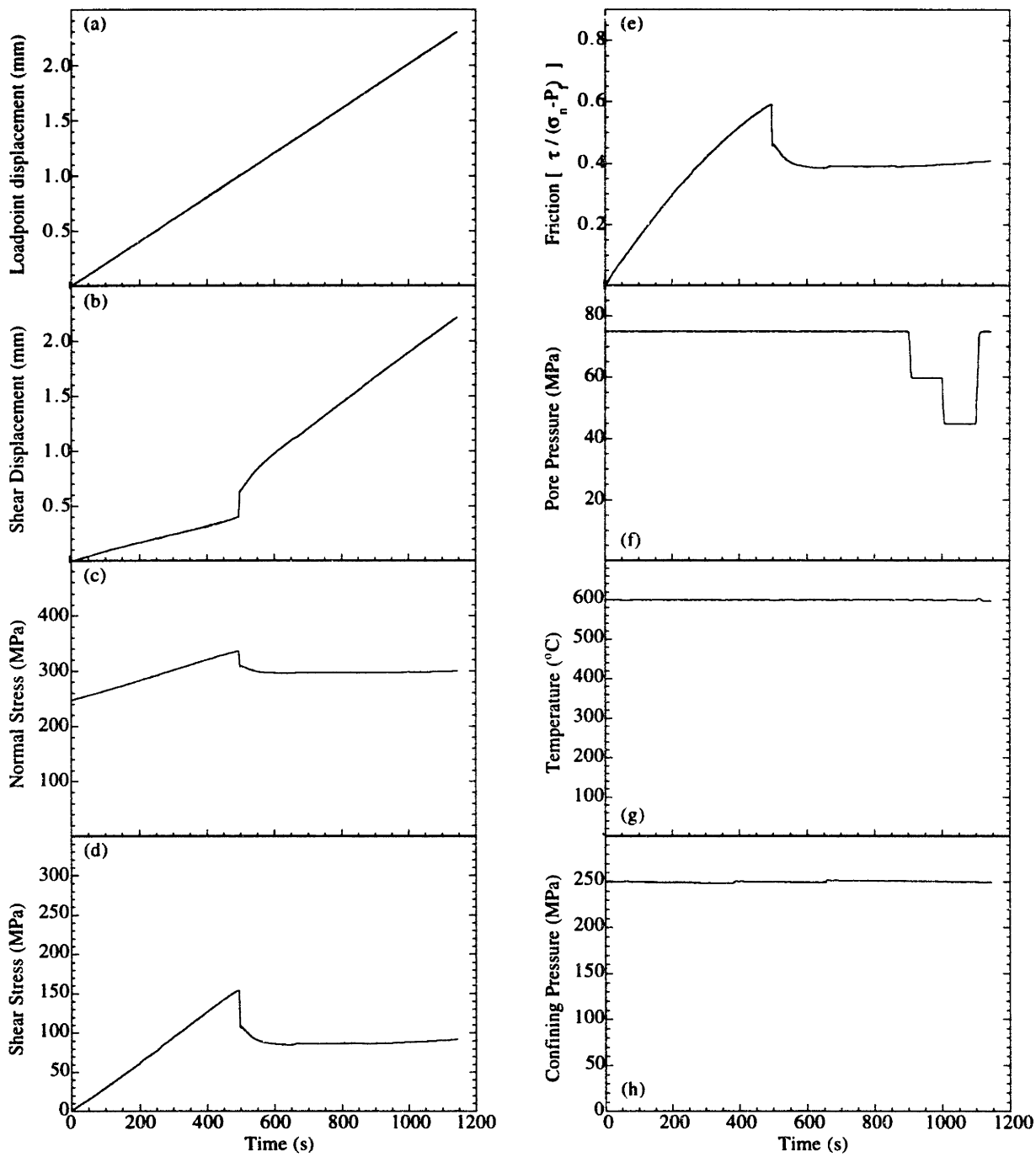

Experiment S29

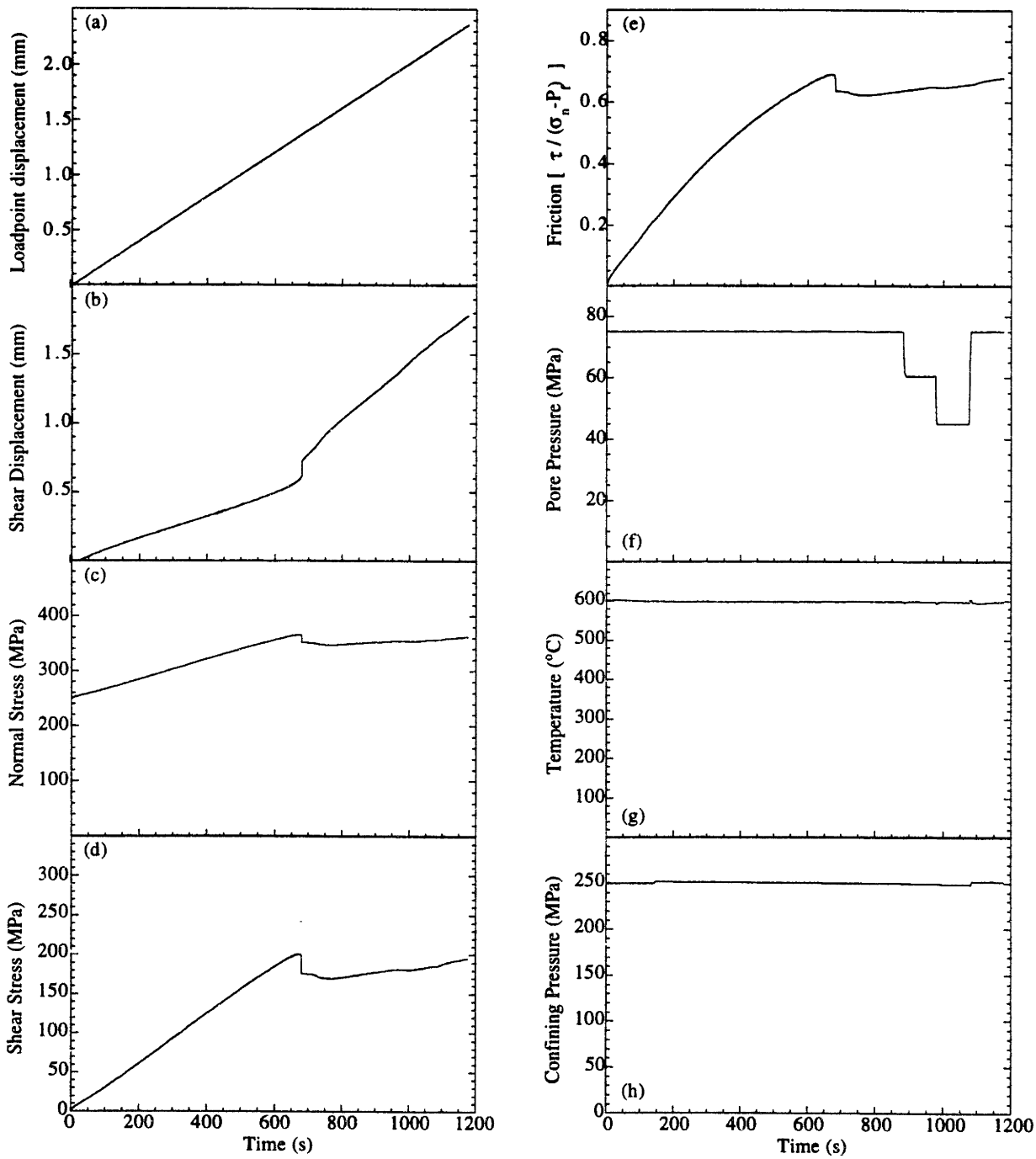

Experiment S30

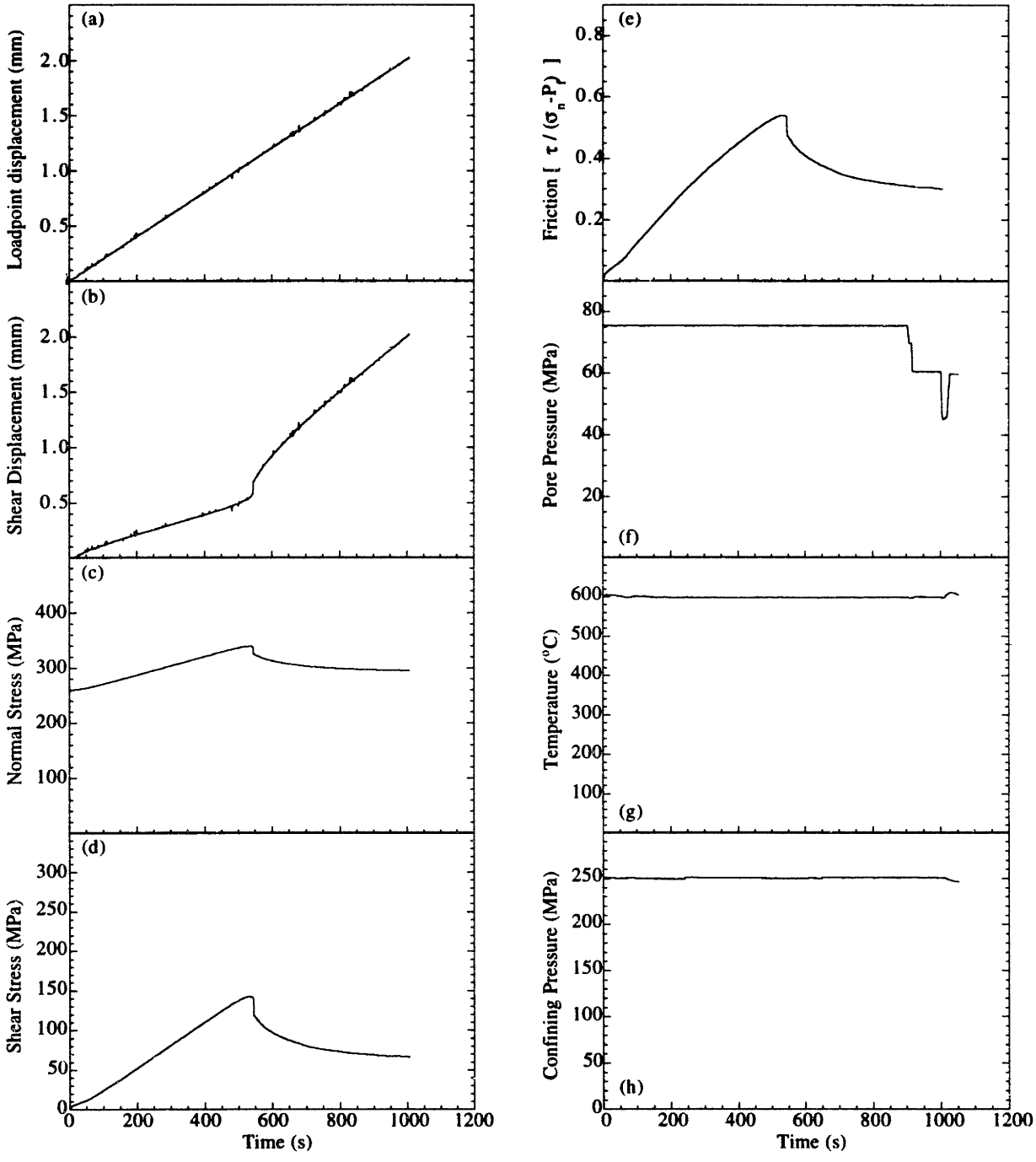

Experiment S31

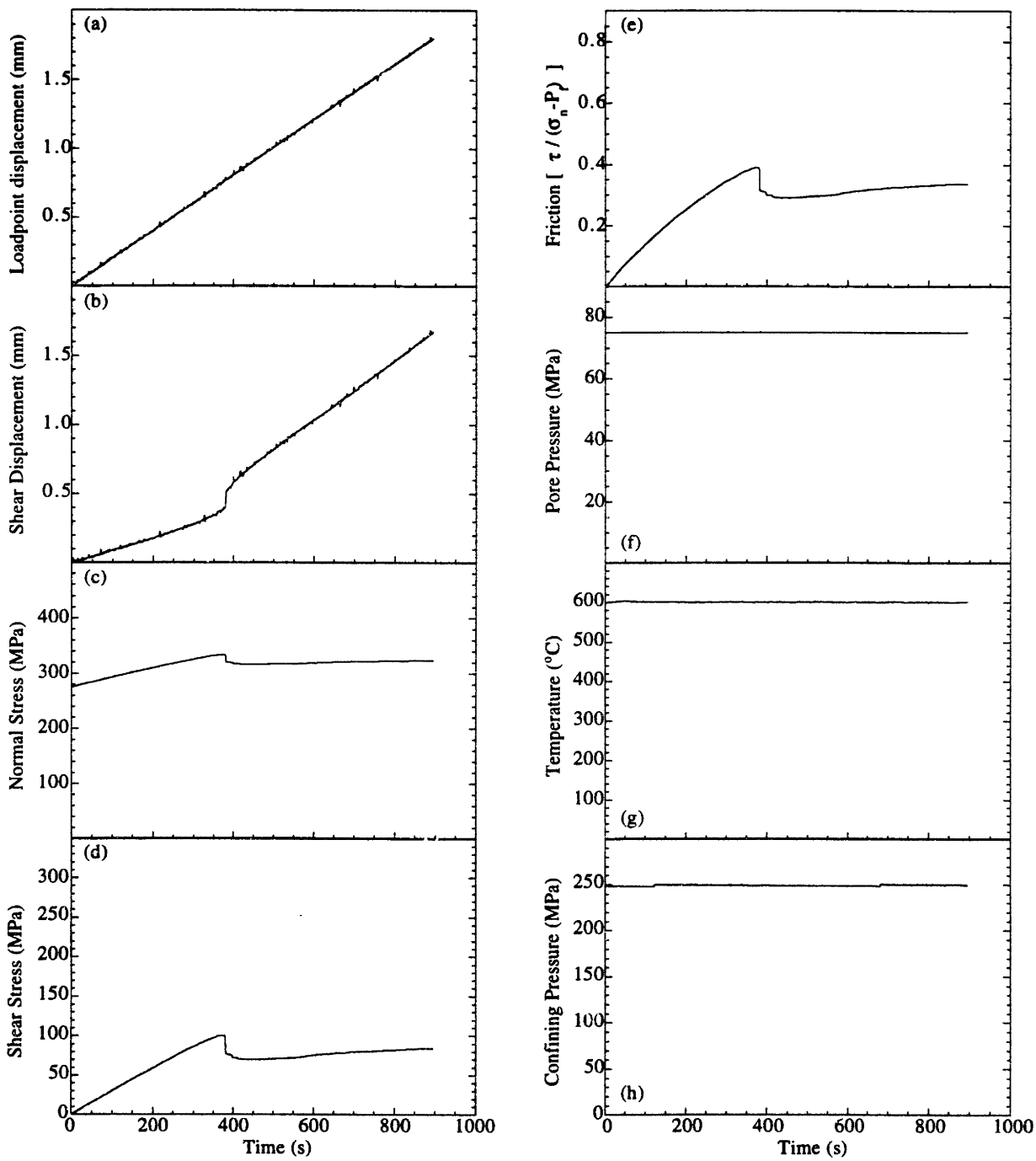

Experiment S32

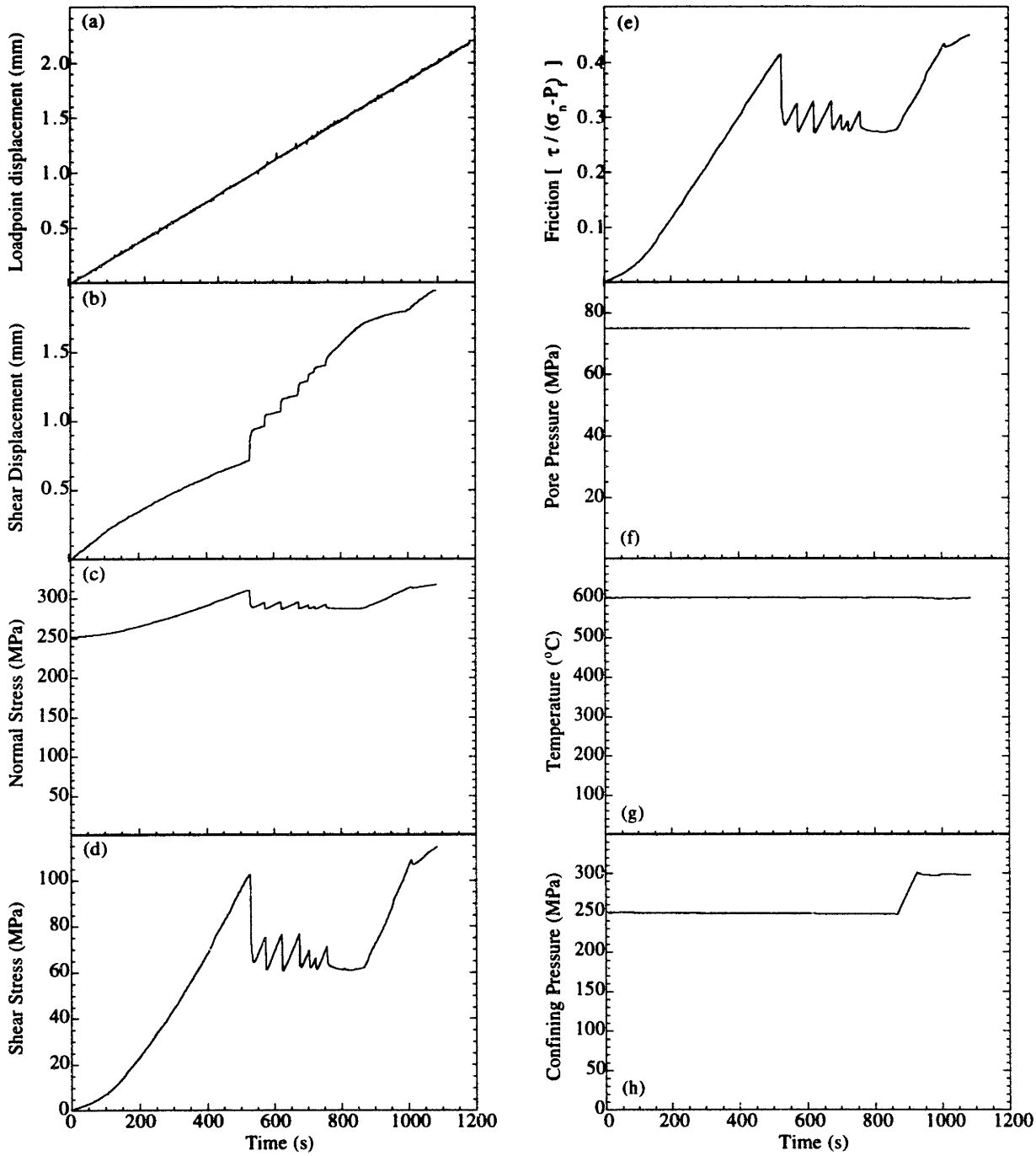

Experiment S33

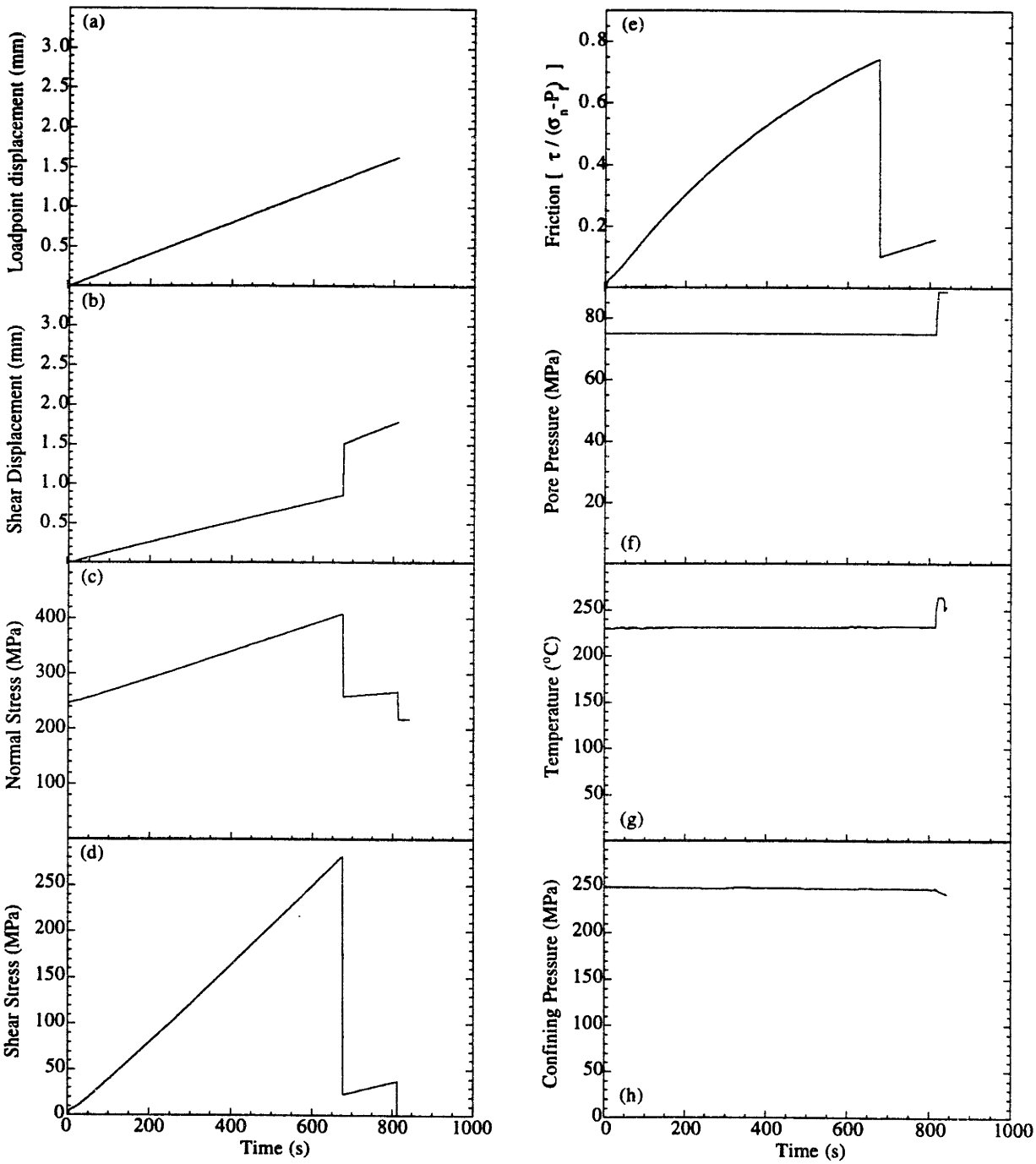

Experiment S35

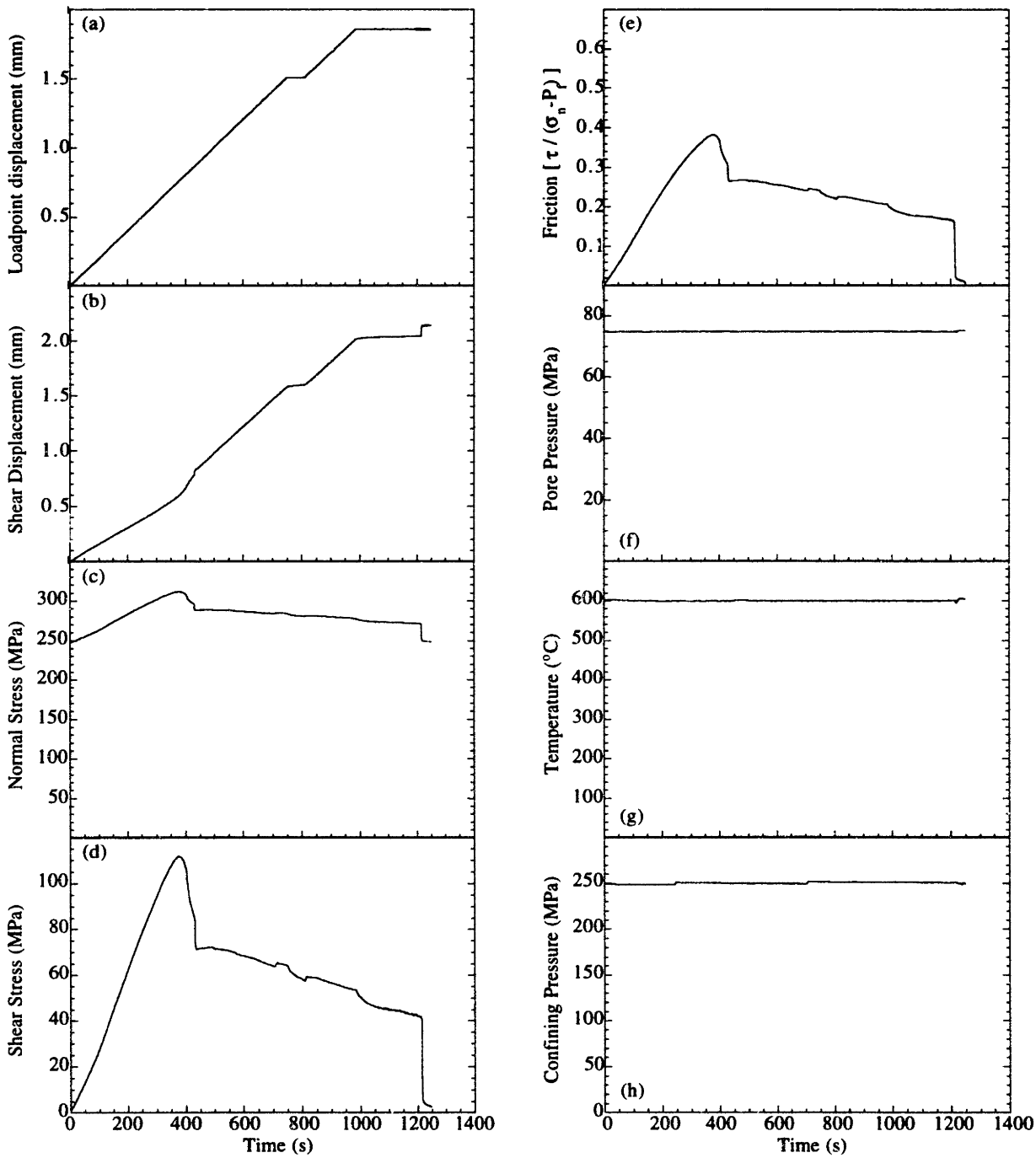

Experiment S36

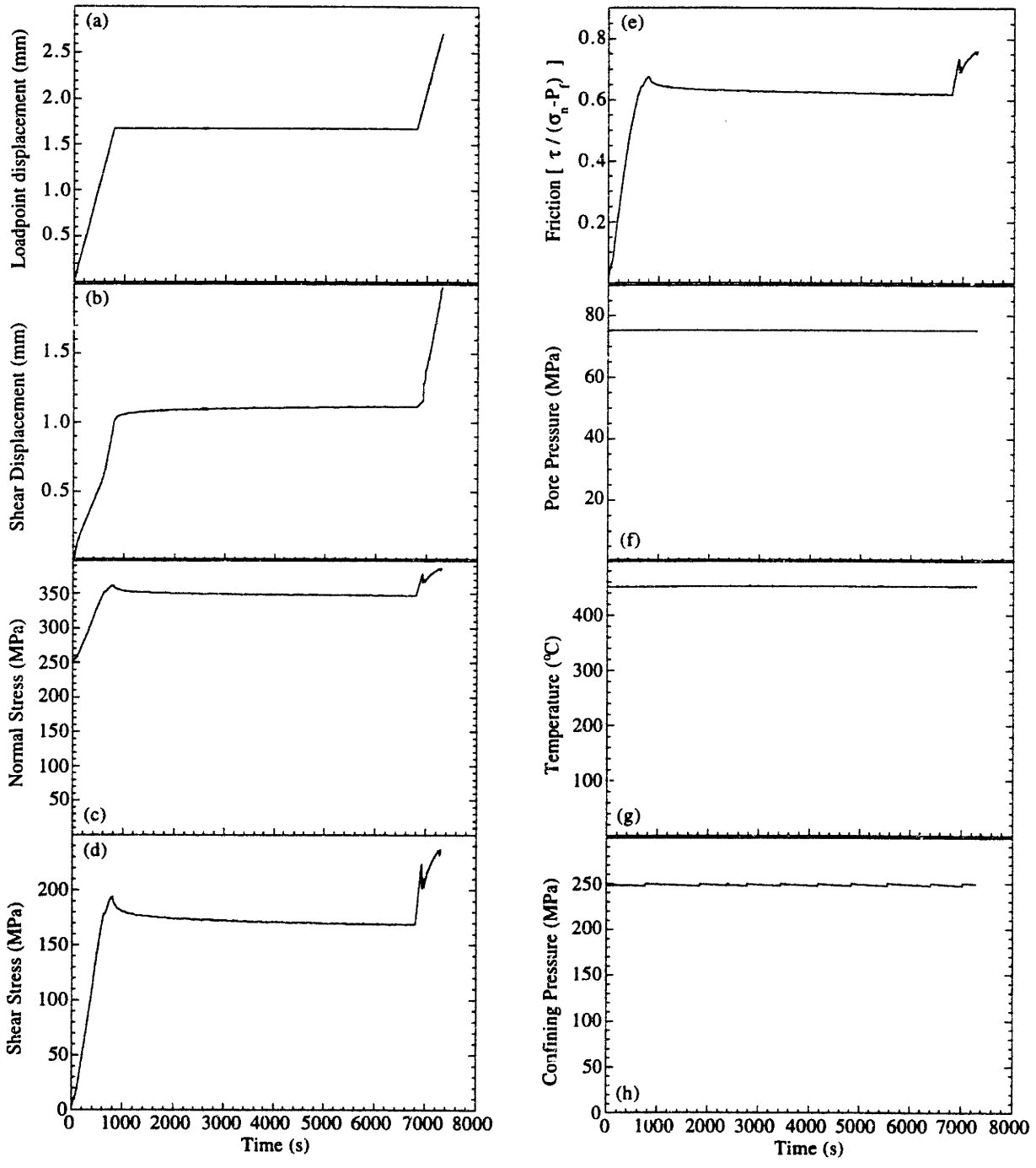

Experiment S37

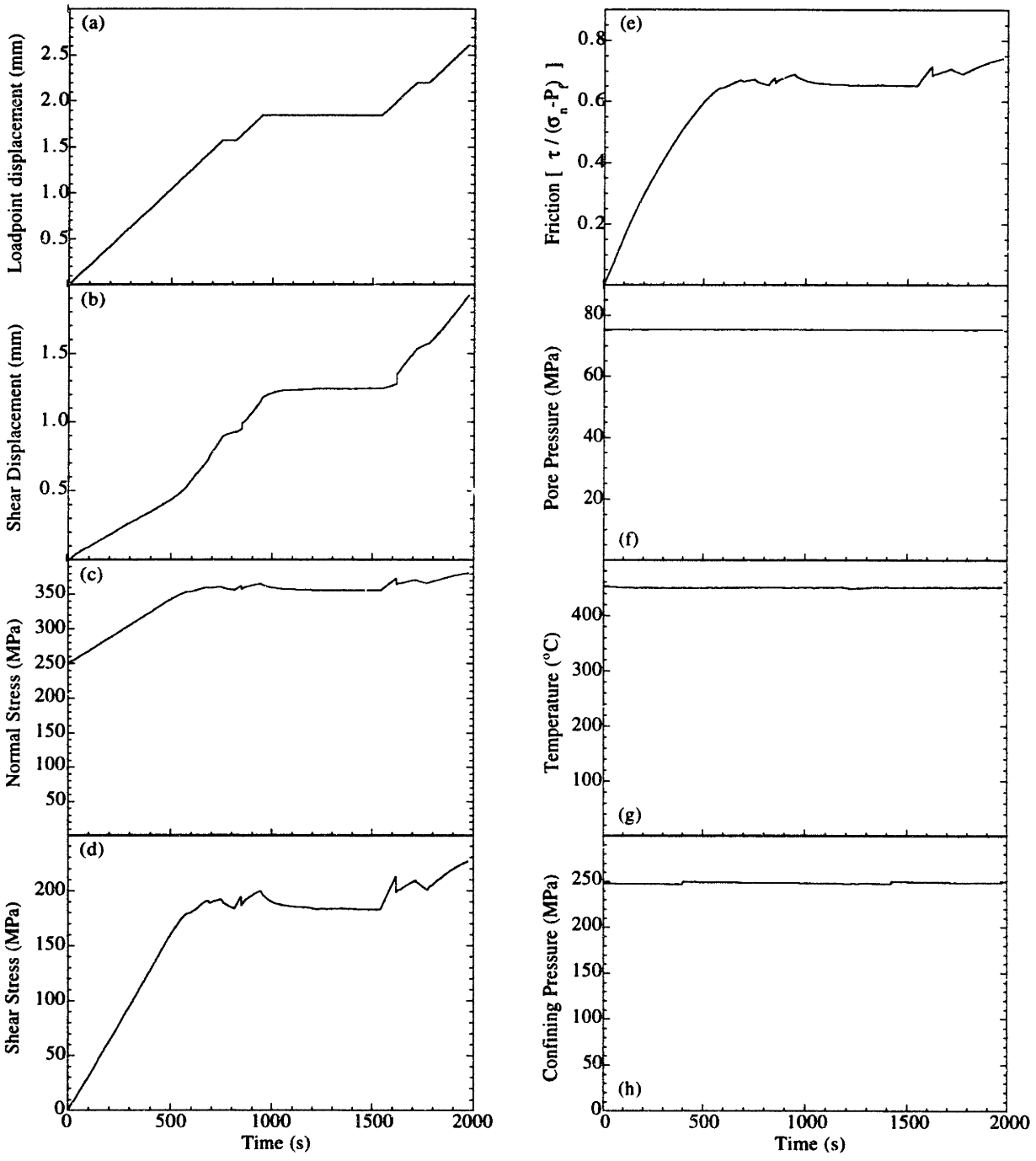

Experiment S38

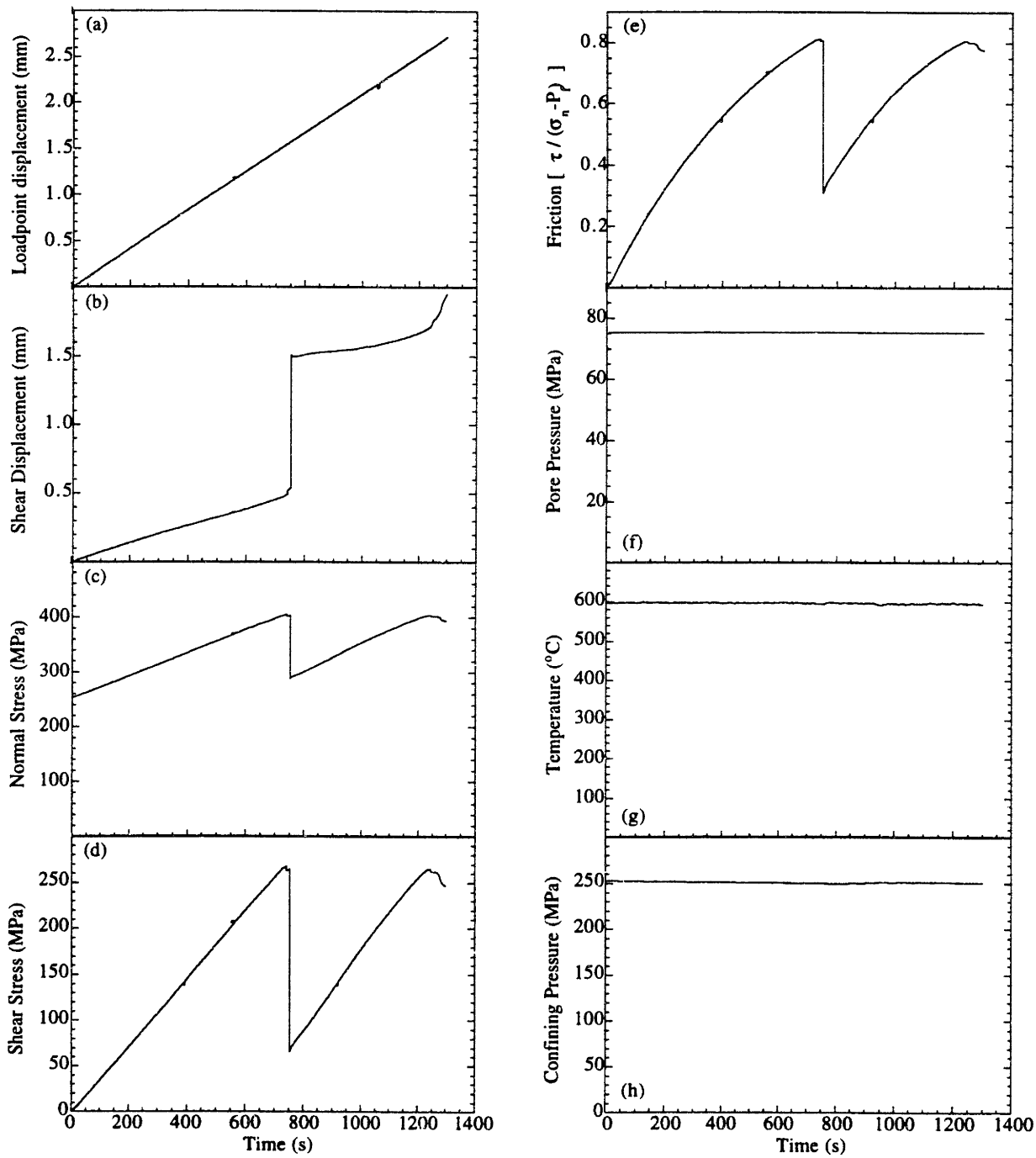

Experiment S39

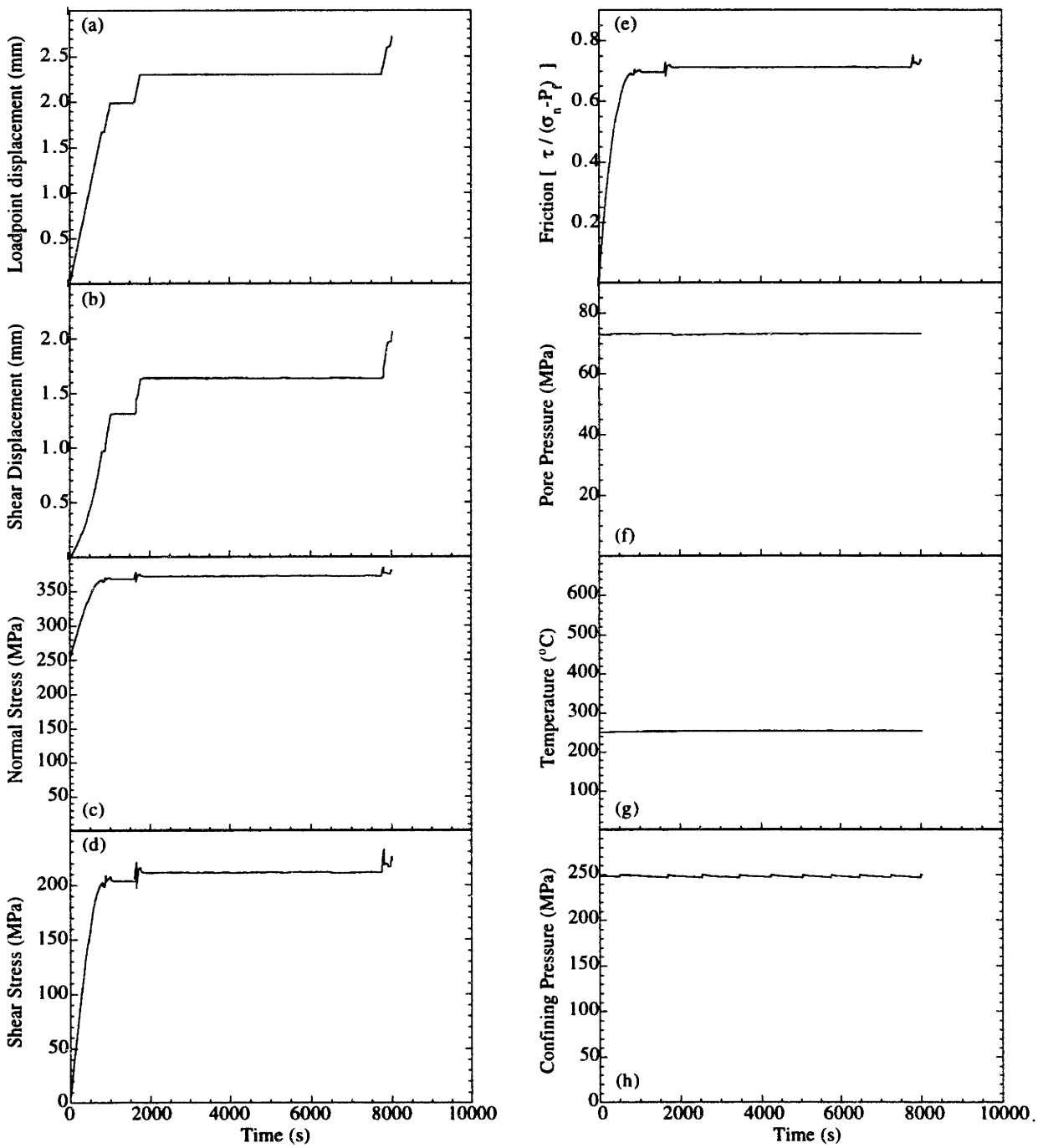

Experiment S42

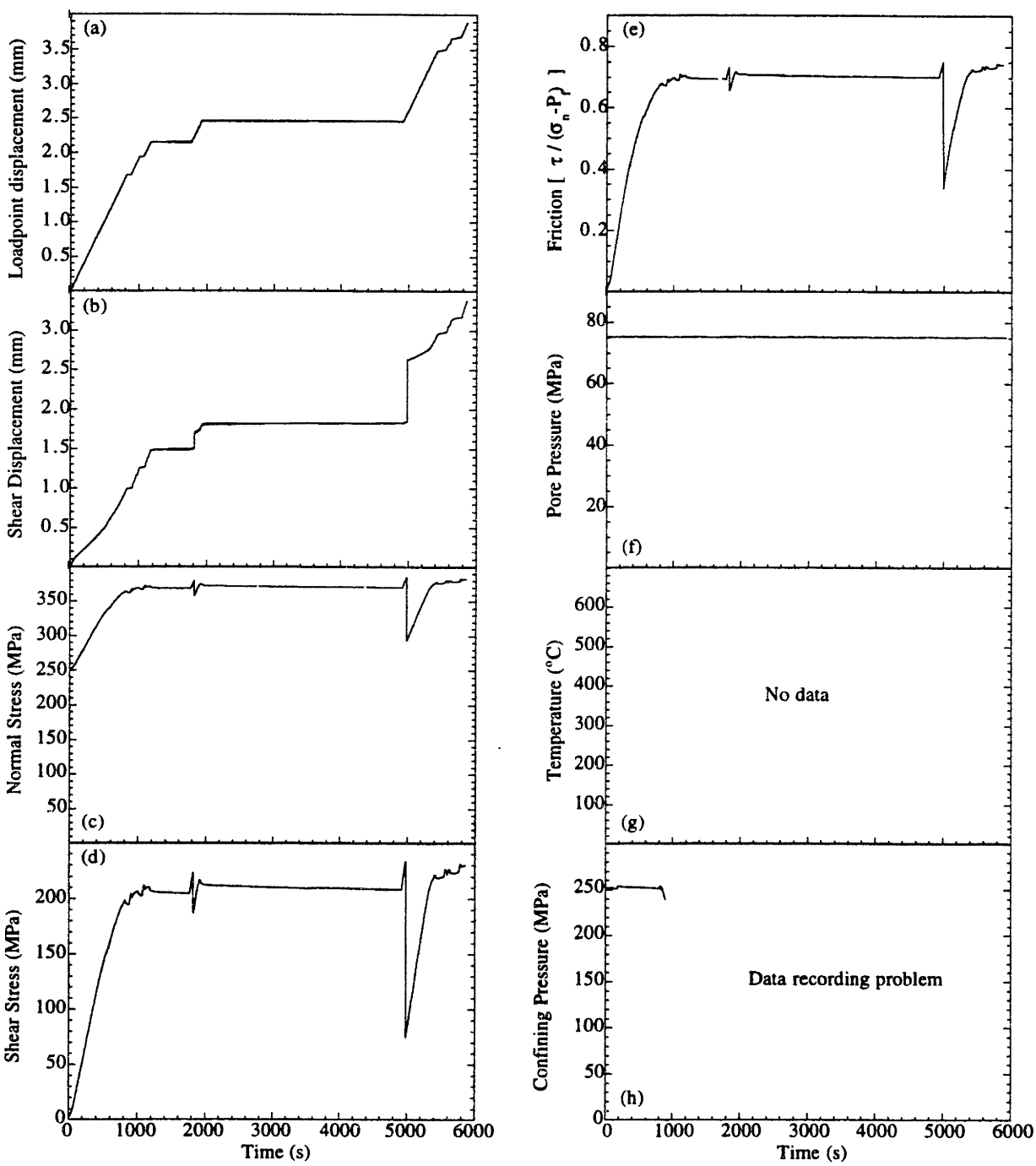

Experiment S43

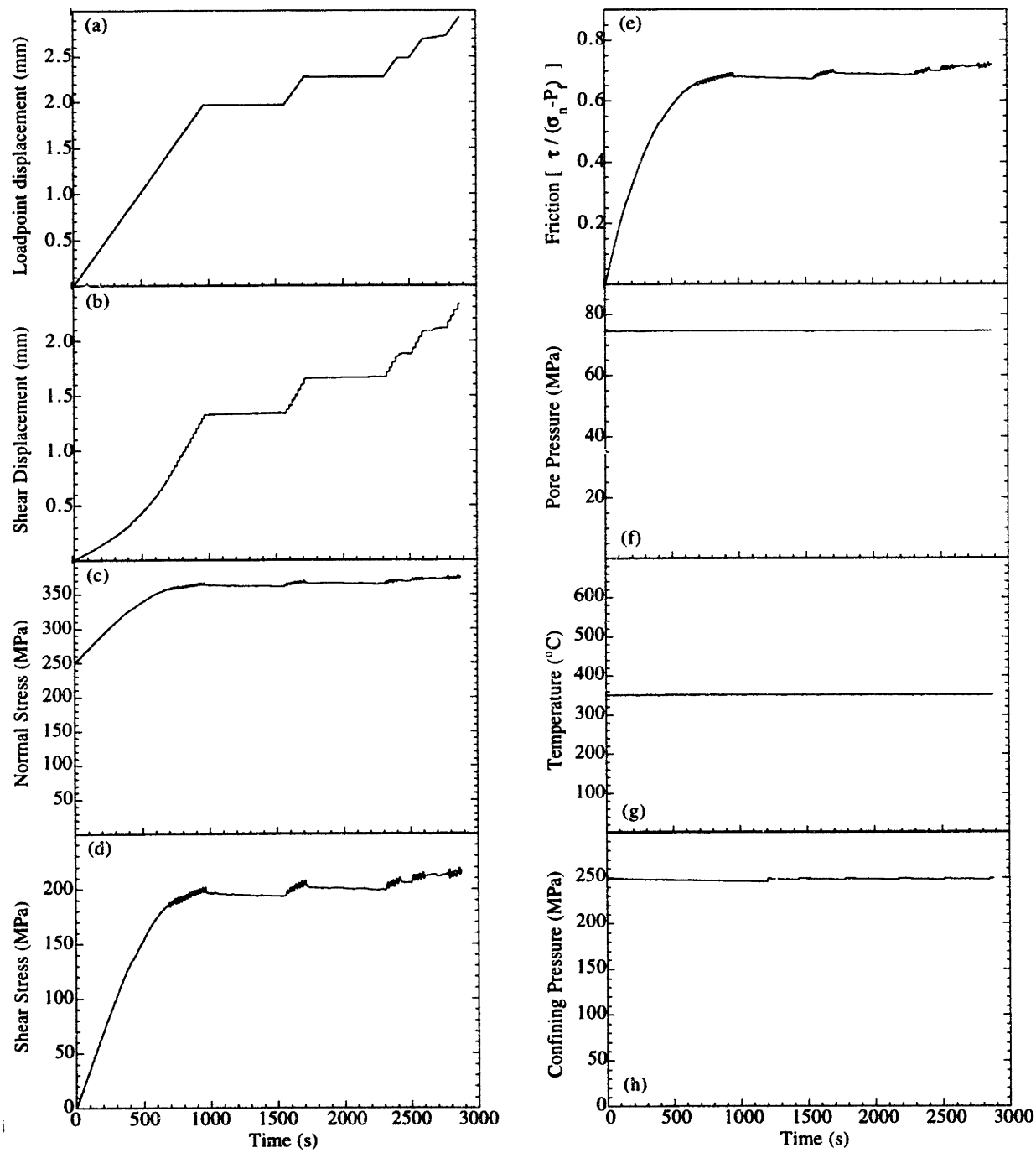

THESIS PROCESSING SLIP

FIXED FIELD: ill. _____ name _____

index _____ biblio _____

▶ COPIES: (Archives) Aero Dewey Eng Hum

(Lindgren) Music Rotch Science

TITLE VARIES: ▶☐ _____

_____

_____

NAME VARIES: ▶☐ Leslie _____

_____

IMPRINT: (COPYRIGHT) _____

_____

▶ COLLATION: _____

_____

▶ ADD: DEGREE: _____ ▶ DEPT.: _____

SUPERVISORS: _____

_____

_____ ___ _____

_____ ___ _____

_____ ___ _____

_____ ___ _____

_____ ___ _____

_____ ___ _____

_____ ___ _____

NOTES:

_____ cat'r date

page

▶ DEPT: _____

▶ YEAR: _____ ▶ DEGREE: _____

▶ NAME: _____

_____